

STRESS RELIEF CRACKING IN
CREEP RESISTING LOW ALLOY FERRITIC STEELS

by

ROBERT ANDREW TAIT

Churchill College, Cambridge

A dissertation submitted for the degree of
Doctor of Philosophy at the University of Cambridge.

July 1976.

ACKNOWLEDGEMENTS

The work described in this thesis was undertaken in the Department of Metallurgy and Materials Science at the University of Cambridge, between September 1970 and January 1974. The results obtained and the theories discussed in conjunction with them are original except where reference is made to the work of others. The thesis is not substantially the same as any that I have submitted for a degree or diploma or other qualification at any other University. Furthermore, no part of the thesis has already or is being concurrently submitted for any such degree, diploma or qualification.

I must acknowledge with gratitude and appreciation the help afforded me by friends and colleagues both in Cambridge and Kingston. In particular, thanks are due to my Supervisor, Dr.J.F.Knott, for his advice and unfailing encouragement, to Professor R.W.K.Honeycombe for the provision of laboratory facilities, to Drs. R.O.Ritchie, R.F.Smith and other fellow members of the Engineering Alloys Group, for their inspiration by example, to Messrs. R.Turkentine, S. Charter, D. Evans, P.Hull and D.Duke, for their guidance and assistance during all stages of the experimental work; also to Professor G.S.Kent, Dr.M.N.McMorris, Professor T.P.Hughes, Dr.P.N.Chin and all my colleagues at U.W.I., for their invaluable moral support during the writing of this thesis, to Mrs.D.McDonald who graciously consented to type the manuscript, to Miss J.Phillips and to many others, whose names do not appear, but who will never be anonymous to me. While in Cambridge, I was supported by the Science Research Council.

R. Tait.

R.A.Tait

SUMMARY

Early investigations of the phenomenon of Stress Relief Cracking in low alloy steels suggested that the observed failure along prior austenite grain boundaries was in large part promoted by the relative strengthening of the grains with respect to the grain boundaries, during the stress relieving heat treatment. In this respect, it was felt that certain Cr-Mo-V steels containing vanadium carbide should be particularly susceptible to this mode of failure, since $V_4 C_3$ is well known to confer very good creep strengthening in these low alloy steels. As a result of this work, it has been established that the above view is both inaccurate and misleading. Most of the experiments were performed on two samples of commercially produced $\frac{1}{2}Cr \frac{1}{2}Mo \frac{1}{4}V$ steel. One of these samples had proved to be susceptible to stress relief cracking during fabrication. Detailed observations of the austenitic grain growth and secondary hardening response of the two samples are described. The results facilitated the design of a series of high temperature hardness and tensile tests in which the separate effects of grain strengthening and grain size in promoting high temperature intergranular failure could be identified. In particular, it is observed that although both steels exhibit very similar strength characteristics, the effect of grain size in promoting low ductility in association with intergranular failure is

more marked in one steel than in the other. The steel in which a marked tendency towards stress relief cracking had been observed is seen to show low ductilities at high temperatures even in fine grain size specimens; suggesting that the state of the boundaries, independent of the strengthening effect, is an important factor in promoting high temperature intergranular failure. By using an anisothermal stress relaxation testing procedure, it was possible to identify precisely the conditions of stress, temperature and micro-structure under which stress relief cracking occurs. In particular, it was observed that the susceptible sample failed by nucleation controlled intergranular cavitation in association with a particular stress/strain-rate/temperature regime where the deformation process is rate controlled by the diffusion of carbon. Further experiments described in the latter part of the thesis examine the effect of purity in promoting intergranular failure both at low and high temperatures. The results suggest that the presence of impurities like phosphorus, which are known to segregate to prior austenite grain boundaries, may act to allow easier nucleation and growth of cavities during failure by intergranular cavitation. The conclusions of the thesis outline the mechanism of stress relief cracking and make discussion in terms of current theories of intergranular failure at high temperatures. Recommendations are made concerning both the assessment of susceptibility of steels to this mode of failure, as well as the adoption of safer stress relief procedures.

oh?

CONTENTS

	Page
ACKNOWLEDGEMENTS	
SUMMARY	
CONTENTS	
CHAPTER I	
A Review of the Problem of Stress Relief Cracking	1
1.1 Introduction	1
1.2 The Creep Resisting Properties of Low Alloy Steels	4
1.3 The Problem of Stress Relief Cracking in Low Alloy Steels	13
1.4 Brittleness of Metals at Elevated Temperatures	25
1.5 Summary	38
Figures 1 to 8.	
CHAPTER II	
The Approach to the Problem	41
2.1 Selection of Material	41
2.2 Austenite Grain Growth during Solution Treatment	43
2.3 Ambient Temperature Secondary Hardening Response as a Function of Solution Treatment	48
2.4 Observations of Hardening Behaviour at Elevated Temperatures through Hot Hardness Measurement	52
2.5 Conclusions	56
Figures 9 to 19.	
CHAPTER III	
The Uniaxial Tensile Mechanical Properties of Commercial 'susceptible' and 'non-susceptible' $\frac{1}{2}\text{Cr}$ $\frac{1}{2}\text{Mo}$ $\frac{1}{4}\text{V}$ Steel at Elevated Temperatures	58
3.1 Introduction	58
3.2 Experimental Details	59
3.3 The Effect of Prior Solution Treatment upon the Tensile Mechanical Properties of $\frac{1}{2}\text{Cr}$ $\frac{1}{2}\text{Mo}$ $\frac{1}{4}\text{V}$ Steel at Elevated Temperatures	62

	Page	
3.4	Observations of the Work Hardening Behaviour during Elevated Temperature Tensile Testing	66
3.5	The Effect of Prior Austenite Grain Size upon the Tensile Mechanical Properties at Elevated Temperatures	71
3.6	Fractographic Examination of Specimens Deformed at Temperatures of 400°C and above	76
3.7	Summary	81
	Figures 20 to 37	
 CHAPTER IV		
	Tensile Strain Rate Sensitivity Effects in Commercial 'susceptible' and 'non-susceptible' $\frac{1}{2}\text{Cr } \frac{1}{2}\text{Mo } \frac{1}{4}\text{V}$ Steel at Elevated Temperatures	83
4.1	Background	83
4.2	Experimental Results	85
4.3	Estimation of Strain Rate Sensitivity and Associated 'degree of instability' of Tensile Deformation	88
4.4	The Relationship between Elevated Temperature Flow Stress and Hot Hardness	92
4.5	Conclusions	94
	Figures 38 to 47.	
 CHAPTER V		
	The Anisothermal Stress Relaxation Behaviour of Commercial 'susceptible' and 'non-susceptible' $\frac{1}{2}\text{Cr } \frac{1}{2}\text{Mo } \frac{1}{4}\text{V}$ Steel	96
5.1	Introduction	96
5.2	Experimental	98
5.3	Anisothermal Stress Relaxation Behaviour of 'non-susceptible' Commercial $\frac{1}{2}\text{Cr } \frac{1}{2}\text{Mo } \frac{1}{4}\text{V}$ Steel	101
5.4	Anisothermal Stress Relaxation Behaviour of 'susceptible' Commercial $\frac{1}{2}\text{Cr } \frac{1}{2}\text{Mo } \frac{1}{4}\text{V}$ Steel	106
5.5	Discussion	108
5.6	Conclusions	112
	Figures 48 to 70.	

	Page
CHAPTER VI	
Intergranular Failure of Commercial 'susceptible' and 'non-susceptible' $\frac{1}{2}\text{Cr}$ $\frac{1}{2}\text{Mo}$ $\frac{1}{4}\text{V}$ Steel at Low Temperatures	114
6.1 Introduction	114
6.2 Estimation of Fracture Toughness at 77°K in as Quenched Material	115
6.3 Observations of Tensile Mechanical Properties of Tempered $\frac{1}{2}\text{Cr}$ $\frac{1}{2}\text{Mo}$ $\frac{1}{4}\text{V}$ Steel at 77°K	117
6.4 The Effect of Tempering at 350°C in Promoting Intergranular Failure in the Region of the Ductile-Brittle impact Transition Temperature	122
6.5 Conclusions	124
Figures 71 to 83.	
CHAPTER VII	
The Tensile Mechanical Properties of High Purity $\frac{1}{2}\text{Cr}$ $\frac{1}{2}\text{Mo}$ $\frac{1}{4}\text{V}$ and $2\frac{1}{4}\text{Cr}$ 1Mo Steels at Elevated Temperatures	126
7.1 Introduction	126
7.2 The Variation of Prior Austenite Grain Size and Secondary Hardening as a Function of Prior Solution Treatment	127
7.3 The Effect of Prior Solution Treatment on the Tensile Mechanical Properties of the High Purity Alloys at Elevated Temperatures	128
7.4 The Effect of Prior Austenite Grain Size upon the Tensile Mechanical Properties of the High Purity Samples at 500°C	131
7.5 Comparison of the Behaviour of Commercial and High Purity Materials	133
7.6 Conclusions	137
Figures 84 to 98.	

	Page
CHAPTER VIII	
Concluding Remarks	139
8.1 The Mechanism of Stress Relief Cracking in Cr-Mo-V Steels	139
8.2 The Significance of Current Theoretical Treat- ments of Intergranular Cavitation to the Under- standing of Stress Relief Cracking	142
8.3 The Possibility of Safer Thermal Stress Relief of Weld HAZ's	144
APPENDIX I	
The Relationship between Ultimate Tensile Strength and Work Hardening Behaviour	147
APPENDIX II	
An Approximate Relationship between Tensile Flow Stress and Vickers Pyramid Hardness at Elevated Temperatures	149
Figure 99.	
REFERENCES	151

CHAPTER I

A Review of the Problem of Stress Relief Cracking1.1 Introduction

The main theme of this thesis is the establishment of a precise definition of the factors that contribute to the stress relief cracking (SRC) of ferritic low alloy creep resisting steels, which occurs during the thermal stress relief of welded structures. In this class of steels, failure during such reheat treatment is observed¹ in the coarse grained heat affected zone (HAZ) around the weld. The cracking is generally found to be intergranular at prior austenite grain boundaries. Typical examples^{50,64} are shown in figure 1.

The rationale behind thermal stress relief is simply that as the temperature of the stressed region is raised, the flow or yield stress is lowered, so that the stress level is reduced through plastic flow. Intuitively, one might expect that in materials designed for use at elevated temperatures this reduction of flow stress will not be so marked, so that alternative modes of stress relaxation, for example the formation of cracks, may occur. That such stress relief cracking is not observed in plain carbon steels¹ is clear support for this idea. Consequently the most widely accepted explanation for the phenomenon of SRC is that the strength of the grains is maintained during the reheat treatment of a weld HAZ while that of the boundaries is reduced so that boundary failure occurs as a result of strain concentration in the boundaries under the action of the unrelieved residual

stress². Taken to its logical conclusion it would appear that this simple interpretation implies that all creep resisting alloys should suffer from SRC. That this is not the case emphasises the need for a more detailed appraisal of the phenomenon.

The following sections of this first chapter attempt to identify the major deficiencies of the above definition of SRC. In this respect it has been found necessary to examine critically the present understanding of creep resistance and elevated temperature brittleness in low alloy steels in order to locate SRC within the general context of elevated temperature deformation.

Basically, creep resistance is understood to involve two major components, viz:

- (i) creep strength
- (ii) creep ductility.

These components are usually described by the data derived in conventional, constant load or constant stress, tensile creep tests as:

- (i.) the stress required to produce a certain strain or cause failure in a given time;
- (ii) the strain or time required to cause failure at a certain stress.

The review of the following section of this chapter describes the way in which microstructural investigations of low alloy creep resisting steels have led many investigators to attribute the creep strength of these alloys to the production of a fine dispersion of alloy carbides. Furthermore, a close association between secondary hardening and the formation of a fine dispersion

of alloy carbides has led to the idea that the achievement of creep strength in these alloys may be understood in the same terms as the achievement of high strength at ambient temperatures.

The third section of this chapter discusses how this idea has been used to reinforce the simple definition of SRC. It further discusses the way in which SRC has been investigated as a problem of low creep ductility resulting from high creep strength, and goes on to illustrate how some inconsistencies of interpretation in these investigations have arisen because of the ambiguous definition of creep ductility in terms of rupture strain or rupture life. It is possible to envisage a situation (for example the creep testing of a superplastic alloy) in which the rupture life is low while the rupture strain is high. More precisely, SRC should always be understood as a problem of low rupture strain, because it occurs during stress relaxation at constant low levels of strain within a weld HAZ.

The fourth section examines the effect of this same ambiguity upon the development of a theoretical understanding of elevated temperature brittleness through intergranular cavitation. It would appear that most models employ the concept of creep ductility in terms of time to failure and further assume that this is directly proportional to the strain to failure. In this way the mode of unstable rupture in the final stages of failure is ignored by most treatments. Experimental evidence is reviewed in this section and suggests that in a strain controlled situation like SRC, consideration of the final unstable failure mode and the associated ductility during intergranular cavitation

should lead to a more consistent assessment of the ability of a particular alloy to resist extensive cracking during a thermal stress relief heat treatment, than that currently used.

1.2 The Creep Resisting Properties of Low Alloy Steels

It was not until the early 1950's that extensive investigations of the microstructure of commercial ferritic creep resisting steels could be attempted using electron microscopy. Smith and Nutting⁵ developed the direct carbon replica technique which was utilized by Baker and Nutting⁶ to carry out extensive investigations of microstructure and carbide morphology in commercial 2¼% Cr - 1% Mo creep resisting steel, and by Smith and Nutting⁷ to study the tempering of low alloy steels containing chromium, molybdenum and vanadium. Parallel work by Seal and Honeycombe⁸ provided convincing support for the relative importance of the major alloying elements (Cr, Mo, V) upon the tempering of this class of steels.

In particular, the formation of alloy carbides was recognised as being responsible for 'secondary hardening' of these steels during the tempering of specimens which had been austenitized and quenched. It was suggested⁹ that the hardening observed in molybdenum steels was due to the formation of molybdenum-rich zones (analogous with the formation of copper-rich zones in duralumin), but no zones were observed¹⁰ during a repeat of the investigations⁹.

It is now accepted that fine dispersions of $V_4C_3^*$ and Mo_2C^\dagger carbides are responsible for secondary hardening in vanadium and molybdenum bearing steels respectively. Both carbides allow some solubility of chromium[§], molybdenum or vanadium but in Cr - Mo - V steels, the main secondary hardening carbide is V_4C_3 which is formed coherent with the ferrite matrix in the early stages of precipitation¹⁹.

As the knowledge of the microstructure of ferritic low alloy creep resisting steels was being developed^{11,12,13,14}, so the relationship between heat treatment and the essential property of 'creep resistance' was receiving attention. The work of Glen^{15,16,17} in the 1950's made a serious attempt to rationalise the resistance to high temperature deformation of a wide variety of metals (mainly different types of steel) in terms of 'latent creep resistance'. By plotting strain rate against plastic strain (observed during a constant stress creep test) on a log-log plot, he illustrated that the strain rate tended towards a minimum and then increased towards the secondary creep rate value. The position and depth of the minimum appeared to be strongly stress, temperature and composition dependent. He postulated that the existence of the minimum was

* Vanadium forms a carbide which is basically VC, but the content of vanadium can be equivalent to V_4C_3 by the formation of a defect lattice⁹.

† Molybdenum carbide is usually Mo_2C but may also be Mo_6C ⁹.

§ Chromium forms basically two carbides - M_7C_3 and $M_{23}C_6$ both dissolving V and Mo with slightly higher solubility in the latter².

due to strain-age hardening, or a dislocation-induced precipitation hardening mechanism, and outlined the effect of composition by remarking:

" In general, it can be stated that whatever the original microstructural condition of an alloy, the same number of transitions in creep rate will be obtained. The amount of strain-age-hardening constituent available for precipitation during creep testing may however, vary greatly so that the latent creep resistance also varies depending upon the original microstructure of the alloy".

This work was not accompanied by any microstructural investigations so that the physical basis of the theories developed are in many places unclear. However, the observation that in many commercial alloys, structural changes can occur during creep testing which manifest themselves by the occurrence of transitions of creep rate, during which a deceleration of creep rate occurs, was clearly established. Furthermore it appears from the number of times that reference is made to this work, that it established in the minds of most of Glen's contemporaries the concept that creep resistance in metals involved the impeding of dislocation motion within the grains, i.e. that it was developed in much the same way as high strength at low temperatures. Little or no recognition was given at this stage to any loss of ductility. ←

By the beginning of the 1960's it had become accepted¹⁸ that the creep strength of a precipitation hardened alloy was largely dependent on the form, stability and distribution of the precipitated phase. The work of Buchi, Page and Sidey^{19,20} sought

to establish a direct correlation between microstructure and creep strength in 1% Cr - Mo - V steels. In particular, their results provided a correlation between the mean interparticle spacing of V_4C_3 and creep strength (i.e. stress required to produce a given strain), which could be used to make quantitative predictions concerning the optimum microstructural requirements for creep resistance in these steels. Their findings were criticised at the time by Barford and Day²¹ who showed that after replotting the data presented^{19,20}, factors such as particle diameter, grain boundary sliding and carbides other than V_4C_3 might play an important role during creep deformation. Nevertheless, this^{19,20} and other work²² did establish that a fine carbide dispersion in alloyed ferrite is a microstructure which exerts a controlling influence upon creep strength.

In their review, Woodhead and Quarrell²³ concluded that deformation at elevated temperatures is influenced primarily by the type and dispersion of carbide phases, and to a lesser extent by the solid solution strengthening of ferrite. With regard to the stability of the precipitated phase, Buchi, Page and Sidey¹⁹ suggested that a tempered upper bainitic structure contained a uniform and stable dispersion of fine vanadium carbide platelets, and should therefore provide excellent long term creep resistance. It became accepted^{22,24} that a tempered upper bainitic structure did provide better creep resistance than similarly tempered lower bainite, martensite or proeutectoid ferrite structures. Furthermore it appeared that a simple law of mixtures existed such that the creep strength of a given

material was increased with increased upper bainite content. A large body of experimental support for this proposition was given by Murphy and Branch²⁵ who presented creep rupture data on a number of casts of low-carbon Cr - Mo - V alloys plotting log (bainite content) versus stress to rupture in 10,000 hours at 575°C to show an apparently linear relation with rupture stress increasing constantly with upper bainite content. These data were later replotted by Barford and Willoughby⁴, with linear scales. In this way it appeared that increasing upper bainite content up to about 20% had a marked effect, but above 20% there was in fact little gain in strength. They⁴ extended their examination of published data with some of their own experimental results and were able to show that a 20% bainite structure optimised both strength and ductility during creep deformation. From micrographic evidence they showed that in specimens containing up to 20% bainite, failure was transgranular (with strains to fracture of about 5%) while in specimens containing slightly increased bainite contents (e.g. 23%) failure was intergranular (with strains to failure of about 4%). With increased bainite content the strain to failure decreased and intergranular cavitation cracking increased. Indeed the mixed upper and lower bainite matrix produced by oil quenching, showed very brittle behaviour associated with little opening of the intergranular cracks.

The implication that the effect of a fine dispersion of vanadium carbide in tempered upper bainite is to produce high creep strength through a precipitation hardening effect²² or a solute drag effect²⁶ is put in some doubt in a situation in which

only 20% volume fraction of the "better" transformation product may be as effective as 100%. Barford and Willoughby⁴ hypothesised that the role of the precipitate particles lay in the stabilisation of the fine cell dislocation structure rather than in the direct immobilisation of slip dislocations or by the provision of a high equilibrium solute content.

During the 1970's further measurements of carbide morphology and mechanisms of nucleation and growth have been made using Field Ion Microscopy^{27,28}. Much interest has been shown in the possibility of producing a fine, stable dispersion of alloy carbides during the isothermal decomposition of austenite^{29,30}. Recent work³¹ on commercial $\frac{1}{2}\%Cr$ $\frac{1}{2}\%Mo$ $\frac{1}{4}\%V$ would seem to suggest that it is possible, by encouraging the ferrite reaction at high temperature, to produce improvements in creep strengthening over that obtained from a mixed microstructure of tempered bainite and ferrite produced during air cooling. However, the precise role of the carbides during high temperature deformation still remains a matter of some conjecture.

The question of ductility during creep deformation is usually associated with the propensity of the material to fracture in an intergranular manner⁴. Glen¹⁶ observed that intergranular failure usually occurred during a 'transition in creep rate' (minimum creep rate) and proposed that the incidence of intergranular failure should increase as the metal hardens as a result of either strain hardening, strain age hardening or strain induced precipitation. This followed an earlier suggestion³², that intergranular failure with a low strain to fracture results when

the relative strength of the body of the grains compared with that of the grain boundary regions exceeds a critical value. No metallographic evidence of intergranular failure or details of grain size and phase distribution were given, but the idea that grain strengthening should lead to intergranular failure was clearly supported. The work of Stone and Murray³³ extended this view by illustrating the importance of solution treatment upon the subsequent ductility, of quenched and tempered material during creep deformation. In particular for Cr - Mo - V steels they showed that high solution treatment temperature gave rise to a very intense precipitation of vanadium carbide in the matrix during subsequent tempering. They also investigated the presence of precipitate free zones close to the prior austenite grain boundaries and were able to illustrate that high solution treatment was also accompanied by little or no denudation of the region adjacent to prior austenite grain boundaries. Conversely for a low solution treatment temperature they observed a less intense precipitation of vanadium carbide, and a considerable region in the vicinity of the grain boundaries which was denuded of precipitate. This latter microstructure was observed to give a considerably increased ductility. They hypothesised that the presence of the precipitate free zones allowed the region close to the boundaries to accommodate strain by plastic deformation rather than by boundary failure, and so when combined with a matrix which contains less intense fine scale precipitation (and is hence less hard) the balance between matrix and boundary strength is sufficient to allow the development of large strains to fracture.

There are two major complications to this argument. The first concerns the role of prior austenite grain size in promoting a change in ductility. Clearly the higher solution treatment temperature will also produce an increase in grain size over the lower solution treatment temperature. The second concerns the exact role of the precipitate free zone. Stone and Murray³³ attributed the improvement in rupture ductility of Cr - Mo - V steels by small additions of titanium to strengthening the denuded regions with a fine precipitate (not identified). Although this result may be confused if titanium acts as an austenite grain refiner it would appear that while a wide denuded zone is associated with good creep ductility, a narrow denuded zone is also associated with good creep ductility and with good rupture strength. As pointed out by McLean³⁴ this evidence suggests that there is little direct influence of precipitate free zone width upon creep ductility, at least in Cr - Mo - V steels.

The beneficial effects of small additions of titanium, often used as a deoxidant, have been observed by other workers^{35,36,37} but as yet no convincing explanation for them has been proposed. By contrast, the usual effect of aluminium, also used in deoxidation practice, is to cause a marked decrease in ductility³⁸. Strangely this deleterious effect of aluminium has often been attributed to the relatively fine grain size of aluminium-killed steels^{39,40} arising from the grain refining effect of aluminium nitride⁴¹. The work of Ratliff and Brown⁴² did, however, show that increasing the soluble aluminium above about 0.01% resulted in pronounced notch sensitivity and a marked reduction in creep

ductility.

The general effect of trace element additions upon creep ductility has recently become a subject of much interest. Work by Stone and Murray⁴³ studied low creep ductility in ferritic bolt steels and suggested that an increased susceptibility to temper-brittle fracture is associated with low creep ductility. More recently, Bruscato⁴⁴ showed that reduction of antimony content to 4 ppm, both arsenic and tin to 90 ppm and phosphorus to 70 ppm, imparted significant improvement to creep ductility of a 2½ Cr - 1 Mo weld metal, without influencing the rupture life, as shown in fig.2. Other work^{45,46} has involved the comparison of the creep rupture properties of two commercial Cr - Mo - V steels with steels of similar composition made from high purity material having lower contents of Co, Cu, S, P, As, Sb, Sn, O and N. The steels having low levels of trace elements gave at least twice the rupture lives of the commercial steels at the highest stresses, and an even greater difference at lower stresses. Rupture ductility was also greater in the steel with low trace element levels. The action of trace elements in reducing creep ductility is not fully understood, but as discussed in later sections, the explanation is generally made in terms of reduced resistance to cavity nucleation and subsequent growth along grain boundaries.

The preceding review summarises those aspects of creep resistance which have a direct bearing upon the development of an understanding of the phenomenon of SRC.

Briefly, the achievement of good creep resistance is understood firstly in terms of the restriction of plastic flow at

high temperatures and secondly in terms of the limitations of ductility which usually arise from the formation of cavities at grain boundaries. For the most part, these two aspects of creep resistance have been regarded as a direct extension of resistance to flow and fracture at ambient temperatures. Increasingly, however, it has become apparent that this approach is not entirely appropriate. The review of Argent et al⁴⁷ for example, suggests that fine distributions of niobium, vanadium, molybdenum and chromium carbide are capable of conferring short term creep strength at 600°C in ferritic steels. However, for long term exposure it is shown that it is the concentrations of vanadium and carbon in solution (which determine the number of vanadium-carbon pairs capable of providing pinning dislocation networks) that is most effective in maintaining creep strength. Currently the mechanisms by which cavities form and act to limit creep ductility is an extremely active area of investigation, as discussed later. Two important aspects of the state of the boundary, its strength relative to the matrix and the possibility of it being contaminated, have been shown to provide decreased ductility in association with cavity formation.

1.3 The Problem of Stress Relief Cracking in Low Alloy Steels

During the welding of a ferritic steel, the HAZ adjacent to the weld transforms to austenite, the grains close to the fusion zone attaining particularly high temperature and undergoing considerable growth. At the same time, carbides tend to dissolve, dissolution being more complete in the coarse

grained region because it attains a higher temperature. The HAZ is cooled rapidly by the cold parent metal and, as a result, re-precipitation of the alloy carbides is to some extent suppressed. Examination of the microstructure of simulated HAZ's in Cr-Mo-V steels has shown the structure to be bainitic containing fine carbide dispersions⁴⁸. Bentley⁴⁹ observed fine vanadium carbide precipitation in Cr - Mo - V steels which had been air cooled to produce a mixed ferrite/bainite microstructure in a weld HAZ simulated thermal cycle. Hardness measurements of welds in Cr - Mo - V castings by Jones⁵⁰ gave values of Vickers Hardness (20 kg load) of about 250 VHN for the HAZ region which would also seem to indicate a bainitic structure, from inspection of the data of Irvine⁵¹ shown in figure 3, for a carbon content of 0.1%.

It is fairly difficult to assess exactly the microstructure of the as welded HAZ in on-site welds since the thermal cycles experienced are in the first instance dependent upon the process used and also upon the geometry of the welded structure. The heat inputs used in submerged arc welding are greater than those used in shielded and gas metal arc techniques so that the cooling rates are lower. The welding of thicker sections allows more rapid removal of heat and consequently the rate of cooling is higher. There appears therefore to be little scope for the control of microstructure in thick section welds through cooling rate towards the achievement of the 20% upper bainite optimum content⁴ since upper limits must be placed on weld heat inputs in order to restrict excessive grain growth and associated brittleness of the HAZ⁵³.

The local expansion and contraction resulting from heating and cooling cycles of the welding operations, and the thermal shrinkage of the weld metal on cooling, create stresses in the weld metal and in the HAZ of the parent plate. The magnitude of the resultant strain field depends upon the section thickness (greater strain gradients usually being associated with greater section thickness). It has also been suggested⁵² that increased weld heat inputs which promote lower cooling rates further give rise to lower thermal gradients and hence lower levels of residual stress. It is generally assumed⁵⁴⁻⁵⁷ that the level of residual stress is of the order of the yield strength of the steel. Hence higher levels of residual stress may be accommodated by steels with higher yield strengths. These residual stresses may be relieved in welded components by application of an appropriate heat treatment.

The stress relieving practice which is generally applied to thick section weldments in low alloy ferritic creep resisting steels involves heating at the rate of about 50°C to 100°C per hour to a temperature in the region 690°C - 710°C, holding at this temperature for times up to 12 hours and then cooling to room temperature at the rate of about 50°C to 100°C per hour.

During the application of such a heat treatment to the weld HAZ of Cr - Mo - V steels, carbides are precipitated from the supersaturated solid solution in a manner similar to that which would occur in a normal tempering operation. The type and morphology of the carbide precipitates depend in detail

upon the composition of the parent plate and of the weld metal, and on the temperature of the stress relieving heat treatment. Many workers^{49,58,59} have observed that a stress relief heat treatment of welded low alloy steel results in increased precipitation of fine alloy carbides within the matrix of the weld HAZ. The occurrence of precipitate free zones adjacent to the grain boundaries has also been reported in some investigations^{59,60}, but not in a consistent manner. It would appear from the previous discussion concerning the interrelation of strength and ductility with reference to creep resistance that there are certain major aspects of the microstructure of weld HAZ of creep resisting ferritic low alloy steels that would lead one to expect a low creep ductility (viz coarse grained, intense fine precipitation, usually mixed upper-lower bainite matrix). It is then not surprising that the relief of stress in such regions by thermal methods is often achieved by the formation of cracks associated with low creep ductility rather than by plastic flow through creep deformation^{1,2}. However, the major area of investigation in this field has been concerned with the effect of steel composition in promoting susceptibility to stress relief cracking. The actual assessment of susceptibility has, in the main, been made by the employment of two types of test procedure

Firstly, there have been several varieties of restraint tests aimed at simulating the conditions existing in a real weld. Basically, the restraint sample, after welding, is subjected to differing thermal treatments, then examined and sectioned to determine the extent of cracking. Typical tests of this type are

the tube and plate test used by Younger and Baker⁶¹, the restrained circular patch test⁶² and the testing of restrained longitudinal welds in tubular specimens⁶³. Meitzner⁶⁴ used several different restraint tests and concluded that the Lehigh Test was the most severe and the most reproducible. This general type of test is very useful in providing some degree of differentiation between various welding processes, stress relieving heat treatments, weld geometry and parent plate composition so that the engineer may assess the suitability of a given steel, welding conditions and geometry for a particular structural situation. However, reproducibility is a major problem, and clearly it is very difficult to assess exactly the conditions (stress, temperature and time) under which any cracks are formed.

The work of Nakamura et al.⁶³ involved a large experimental programme using the tubular restraint specimens, designed to investigate the effect of composition upon susceptibility to SRC. Clearly this approach has its merits, since wherever practical most engineers would choose to reduce the problem by selection of a non-susceptible material rather than by total reliance upon design, welding and heat treatment specifications which may or may not counteract the effects of stress concentration, levels of stress and development of susceptible microstructures. The major result of the survey of many different composition combinations was the proposal that susceptibility to SRC may be described by the following equation:

$$\Delta G = \%Cr + 3.3 \%Mo + 8.1 \%V - 2 \dots \quad (1.1)$$

such that:

TABLE I

Comparison of Cracking Susceptibility Index, ΔG , with Observed Behaviour

Steel	Predicted Cracking Susceptibility (ΔG)	Verdict	Observed Behaviour	Reference
A517F (0.54Mo-0.54Cr-0.07V)	0.89	crack	badly cracked	59
A517J (0.04Cr-0.57Mo)	-0.08	borderline	borderline	59
C-Mn Steels	-2	safe	not susceptible	58
$\frac{1}{2}$ Mo-B	-0.5	safe	susceptible	58
$\frac{1}{2}$ Cr-Mo-V	2.5	crack	susceptible	58
1Cr-Mo	0.5	crack	not susceptible	58
2 $\frac{1}{2}$ Cr-Mo	3.4	crack	borderline	58,65
5Cr-Mo	4.5	crack	not susceptible	58
9Cr-Mo	9.7	crack	not susceptible	58
C-Mn-0.2%Mo-0.04%V	-1	safe	cracked	66
C-Mn-0.25%Mo-0.15%V	0.1	borderline	cracked	66
$\frac{1}{2}$ Cr- $\frac{1}{2}$ Mo-V	>0.5	crack	cracked	67
1Cr-1Mo-0.35V	5.2	crack	cracked	67,68

(facing p.18)

$\Delta G > 0$ indicates susceptible material

$\Delta G < 0$ indicates non-susceptible material

Clearly, emphasis is placed upon the importance of alloy carbide forming elements, though the authors did note that there appeared to be a detrimental effect of B, S and Cu which they attributed to the possibility of these elements promoting hot cracking before reheating. The above equation has been applied¹ to various results of investigations reported in the literature, as shown in Table I. It can be seen that the work of the engineer in specifying the welding of creep resisting low alloy steels must still involve a great deal of attention to the conditions of the weld, since the predictive capability of the above equation appears to be somewhat erratic. Some more recent Japanese work³⁶ of a similar nature has produced a more comprehensive relationship:

$$\Delta G = \%Cr + \%Cu + 2 \%Mo + 10 \%V + 7 \%Nb + 5 \%Ti - 2 \dots (1.2)$$

within the range $\%C > 0.1$ and $\%Cr < 1.5$

once again:

$\Delta G > 0$ indicates susceptible material

$\Delta G < 0$ indicates non-susceptible material

Both of the above relationships place high significance upon the vanadium contents, and it would seem that even small amounts are associated with a susceptible composition. The presence of chromium in both relationships, and titanium in the latter would seem to be at variance with most reported work in which increasing chromium tends to reduce susceptibility and even remove it⁵⁸ and in which usually small additions of titanium³⁷ are found to impart considerable reduction in the level of cracking.

The second type of test measures the time to failure of specimens held under various conditions of mechanical loading at elevated temperatures. In most cases the specimens have been heat treated in a manner which closely simulates the weld thermal cycle of a HAZ. Meitzner et al.⁵⁹ employed notched and smooth tensile specimens, which had been heat treated in a Gleeble weld thermal cycle simulation device, in a stress relaxation test in which the specimen was placed in position in the tensile testing machine, heated rapidly to the test temperature, strained until a predetermined stress level was achieved, then allowed to deform, at temperature under conditions of zero crosshead velocity. Earlier, Murray⁵⁸ had employed the same technique. By plotting the time to failure versus the test temperature, these authors produced "C" curve diagrams such as that shown in figure 4.

which allowed direct comparison between various steels in terms of the distance of the 'fracture nose' from the ordinate.

This type of data leads naturally to the idea that one way to avoid cracking during stress relief is to heat the structure at a rate which allows the 'nose' to be missed. For certain highly susceptible alloys this is clearly impossible. For example, Murray⁵⁸ showed that $\frac{1}{2}\text{Cr } \frac{1}{2}\text{Mo } \frac{1}{4}\text{V}$ fractured in less than one minute at 650°C , while Meitzner⁵⁹ showed that for A517F the 'nose' came close to touching the ordinate at around 565°C . Nevertheless, several authors have proposed that higher rates of heating to the stress-relief temperature result in lower risks of stress relief cracking^{49,69,70,71}. It has been

suggested^{49,72} that slow heating rates allow precipitation of carbides to occur at a lower temperature. It is surmised that this leads to a condition of higher creep strength and associated loss of ductility during stress relief, so that cracking occurs. For fast heating rates it is proposed that appreciable precipitation is avoided at the lower temperatures so the stress may be relieved without cracking. On the other hand, it has been demonstrated⁶⁷ that widely differing heating rates (30 and 300°C/h) can still result in cracking of $\frac{1}{2}\text{Cr } \frac{1}{2}\text{Mo } \frac{1}{4}\text{V}$ steel plate and pipe materials of 80mm thickness. Whatever, the interpretation it seems that the way in which the 'C' curves were generated (in terms of heating rates) is so far removed from the situation which pertains during practical stress relieving operations as described on page 15 that their use to determine optimum heating rates is incapable of accuracy. Furthermore, as observed^{48,49}, the possibility of autotempering during cooling of the as welded region is fairly high so that it would seem that variations of heating rate during the reheat treatment cycle offer little scope for varying the intensity of precipitation, and clearly there is always the danger of causing a seriously increased stress level due to differential heating effects which arise during the rapid heating of thick-section welds. Finally, the assessment of ductility through rupture life measurement ignores the fact that SRC of weld HAZ's always occurs at low strain.

A recent variant of this type of test is one in which fatigue cracked, three point notched bend specimens are

held at temperature, under conditions of constant load. Isothermal plots of initial stress field intensity (k_{Ii}) versus time to failure are then presented^{73,74} which illustrate difference in susceptibility between various steels in terms of the value of k_{Ii} to cause failure at a given temperature. Saunders⁷³ extended the applicability of such data by estimating the size of defects which could be expected to cause failure in a given time at a particular temperature. Although it is important to try to place the study of stress relief cracking on a more quantitative basis, particularly from the aspect of defect tolerance levels during stress relief, subsequent work³⁷ has suggested that the levels of resolution and reproducibility of the assessment of SRC in these investigations does not exceed those attained by any of the previous work. It has been suggested^{1,73} that loading conditions of stress relaxation under constant strain rather than the presently used constant load conditions would more closely simulate the situation existing within a weld HAZ.

It has been indirectly proposed by Boniszewski and Eaton⁷⁵ that these limits of resolution and reproducibility experienced in attempts to assess the susceptibility of a particular class of steels may be explained in terms of apparently minor cast to cast variations. Often in one set of experiments a particular composition appears to be susceptible whilst in another (for nominally similar conditions) it appears to be safe. Even the case of $\frac{1}{2}\text{Cr}$ $\frac{1}{2}\text{Mo}$ $\frac{1}{4}\text{V}$ is cast in some doubt when one considers that almost every test finds it to be extremely

susceptible, and yet there are very many service welds in this material which have been stress relieved and subjected to creep operating conditions without any sign of premature failure. In an earlier discussion⁷⁶ Boniszewski remarked:

"In reheat cracking* the failure occurs at grain boundaries but intergranular strengthening is blamed for this. There are steels, the high temperature strength of which is almost as high ($2\frac{1}{4}\text{Cr} - 1\text{Mo}$) or higher ($6\text{Cr}-1\text{Mn}-1\text{Mo}-\text{W}-\text{V}-\text{Ti}$, $12\text{Cr} - 1\text{Mo}(\text{W}) - \text{V} - \text{Nb}$) than that of $\text{Cr} - \text{Mo} - \text{V}$ steel, but they are less ($2\frac{1}{4}\text{Cr} - 1\text{Mo}$) or even not at all susceptible to reheat cracking. Therefore instead of thinking about lowering the intragranular strength, we should aim at improving the resistance of grain boundaries to creep rupture".

It is clear from subsequent work⁷⁵ that in particular Boniszewski was referring to the effect of trace elements, in the context of resistance of grain boundaries to creep failure. In this latter work⁷⁵ a detailed examination of the fracture surfaces of weld stress relief cracks in $\frac{1}{2}\text{Cr} \frac{1}{2}\text{Mo} \frac{1}{4}\text{V}$ steam pipe was made using scanning and transmission electron fractography. It was shown that the intergranular fracture facets were covered with small cavities, each of which was associated with particles of V_4C_3 , 200 - 600 Å in diameter which indicated the possibility of heterogeneous cavity nucleation (as discussed in the next section).

*An alternative term for stress relief cracking.

However, in their discussion they remarked that strong effects of thermal faceting were observed in cavities and on crack faces, which were interpreted as indicating that impurity segregation to grain boundaries might promote premature creep rupture. As already mentioned, the detrimental effects of certain trace element additions upon creep rupture ductility has been widely reported. With respect to SRC it has been shown^{77,78} that higher levels of impurity elements (e.g. P) and trace elements (e.g. Cu, As, Sb and Sn) can markedly increase the susceptibility of Cr - Mo - V steels. In a study of the effect of the sum total of residual elements⁸³, it was found that increasing the total contents of (P + Cu + Sn + Sb + As) resulted in a marked increase in the degree of cracking. Earlier work⁴⁹ demonstrated that a $\frac{1}{2}\text{Cr}$ $\frac{1}{2}\text{Mo}$ $\frac{1}{4}\text{V}$ steel containing 0.2%Cu and 0.3%Sn failed more rapidly during stress relaxation testing than when containing 0.1%Cu and 0.2%Sn.

Metallurgically, three major factors have been identified as contributing to the likelihood of failure within a weld HAZ during thermal stress relieving:

- (i) The presence of an intense distribution of fine alloy carbide (usually V_4C_3) precipitates within the HAZ matrix, and along prior austenite boundaries.
- (ii) The presence of a largely bainitic (mixed upper and lower) microstructure contained within large prior austenite grains of the HAZ.
- (iii) The possibility of grain boundary contamination by minor trace elements.

Chemically, the effect of basic composition is some-

what ill-defined though it does appear that elements such as vanadium and molybdenum are usually present in steels which exhibit this type of failure, while high chromium contents and small additions of niobium, titanium or zirconium appear to produce beneficial reductions in the extent of cracking. It is noted at this stage that all six of the above mentioned elements show a fairly strong tendency to form fine dispersions of alloy carbides and in this respect the beneficial effects of titanium and zirconium on rupture ductility may be explained by postulating³³ that the supposed TiC and ZrC precipitates effectively bind carbon and minimise V_4C_3 formation. However, by the same token, other effects of composition⁴² remain unexplained unless, as pointed out⁷⁵, it is assumed that some impurities promote the formation of V_4C_3 particles, on grain boundaries, of a size critical for cavity formation.

One possible reason for the present incompleteness in the understanding of the phenomenon of SRC is the dichotomy of requirements which exists between welding engineers and alloy developers. On the one hand the engineer would like to know simply whether a steel is susceptible or non-susceptible, while on the other the alloy developers have been largely interested in the way in which a specific alloying addition affects the engineers' measure of susceptibility. As a result very little of the work produced has attempted to investigate systematically microstructural variables such as -

- (a) prior austenite grain size;
- (b) matrix form and stability;

(c) impurity content.

For example, although the failed regions of a stress relieved HAZ have been shown generally to fall close to the fusion boundary (figure 1), where the grains are coarse, no attempt has been made to show if there is a lower limit to grain size below which such failure either does not occur, or is ameliorated. There appears to be little data upon the grain coarsening characteristics of the Cr - Mo - V class of steels. While it is desirable that the engineer should have some means of assessing the suitability of a particular steel in a particular welding situation it is clear that the tests so far used offer only limited scope for assessing realistically the conditions of time, temperature and composition under which failure occurs.

1.4 Brittleness of Metals at Elevated Temperatures

As discussed in the previous sections an important aspect of creep resistance in metals, is the resistance to the development of intergranular cavitation . The appearance of brittleness during elevated temperature exposure of metals is generally observed during tensile testing (i.e. constant load, constant stress, constant strain or constant strain-rate creep tests) in the temperature range $0.3T_m$ to $0.9T_m$, and is associated with a change in fracture mode from transgranular to intergranular. An early attempt³² to rationalise this problem involved the concept of equicohesive temperature illustrated schematically in figure 5, which shows the strengths of grains and grain boundaries as a function of temperature. Above a temperature, the equicohesive

temperature, the grain boundary apparently becomes strength limiting.

In the context of SRC, it has been proposed⁴⁹ that either increasing the strength of the grains by the formation of an intense distribution of fine V_4C_3 precipitate, or lowering the strength of the boundary, through contamination, or both, may reduce the equicohesive temperature and thereby increase the tendency for intergranular failure.

In fact, the creep strength of the matrix is not considered specifically in any theoretical treatment of intergranular failure, although frequent reference is made to the importance of this property in determining whether a local stress concentration may be relaxed⁸⁰. Observations of the form of intergranular failure have identified two basic modes of crack formation⁸². The first involves cracking at grain boundary triple junctions, commonly called w-type voids, which seems to be favoured by higher stresses, while the second has been recognised as the formation of cavities or r-type voids on grain boundaries which are approximately normal to the applied stress, and is usually associated with conditions of low stress. The two types of cracking are frequently observed to occur together⁸² and it is now considered by some workers⁸³ that the classification is artificial. Nevertheless, a large amount of work has been devoted to consideration of the existence of the so called Stroh-McLean transition^{81,82,84} during which a change over of the dominant mode is thought to occur.

The development of a theoretical understanding of

cavitation has generally described three stages in the promotion of final failure:

- (a) nucleation of cavities
- (b) growth of cavities
- (c) unstable fracture.

Most attention has been given to the first two stages, but as yet no theory has successfully incorporated all three stages to allow reliable prediction of the widely used parameter of rupture life. Treatments of nucleation have involved both homogeneous and heterogeneous mechanisms. Briefly, the former mechanism originally proposed by Greenwood⁸⁵⁻⁸⁸ involves the agglomeration of lattice vacancies under the action of the applied stress on to grain boundaries. Later experimental work^{89,92} suggested that homogeneous nucleation was highly improbable. Since then, as discussed by Perry⁸¹ all models have assumed nucleation to be heterogeneous, involving the presence of grain boundary ledges or particles and based on a combination of stress and grain boundary sliding.

Two general types of mechanism have been invoked to explain heterogeneous nucleation⁸¹. The first concerns the formation of nuclei in association with steps or ledges in grain boundaries, which have been supposed to result from the intersection of slip traces or sub-grain boundaries with the grain boundary⁹³. Chen and Machlin^{94,95} pointed out that any discontinuity on a sliding boundary could be expected to generate sufficient concentration of stress to cause a void to nucleate. Alternatively, local break-down of grain boundary adhesion

associated with precipitates or impurity particles (possibly of low adhesion with the matrix) can produce void nuclei^{96,97,98}. The evidence for the first case rests on metallographic observations of cavitation⁹⁵ and also on the ability to induce cavities to form on boundaries at 45° to the applied stress, by predeforming to produce suitable steps⁹⁹. In the second case, association of cavities with particles in grain boundaries has been observed by a number of authors^{98,100}. Removal of such particles is observed to increase ductility at elevated temperatures. This latter effect has also been associated with grain boundary migration¹⁰¹ in copper, in which extended creep ductility was thought to result because migration destroyed boundary jogs, thereby preventing nucleation.

With regard to low alloy steels, association of voids with carbide particles on prior austenite grain boundaries in bainitic steel has been observed^{75,102}. The former observations have already been discussed, the latter were made on specimens which had been creep tested at 550°C and a stress of 232 MNm^{-2} . The cavities occurred on prior austenite grain boundaries in proximity to one or more large carbide particles and in areas containing fewer dislocations and much less fine precipitate than found in the bainitic matrix (which appears to be at variance with the observations³³ concerning precipitate free zones). No evidence of facetting on the surfaces of the cavities was found, and this was attributed to the lower temperature of formation of cavities, no mention being made of impurity interaction or differing conditions of stress application. Nucleation and growth

of cavities were widespread and continuous throughout the creep tests on grain surfaces subjected to both shear and normal components of stress. These observations are in agreement with conclusions of Perry⁸¹ who in his review summarised that experiments have shown that grain boundary sliding with a net stress across the grain boundary is an essential feature in the nucleation of cavities during creep, and that cavitation begins at the beginning of the creep test and is continuous throughout the duration of the test.

The transition to the growth stage is generally felt to be dependent upon the stability of the growing nucleus. Below a certain size the void requires an input of energy for continued growth, while above that size stable growth will occur. McLean¹⁰⁴ considered nucleation as the problem of growing a hole to radius of curvature r_c given by:

$$r_c = \frac{2\gamma}{\sigma} \quad \dots \quad (1.3)$$

where γ is the surface energy per unit area, and σ is the stress acting upon the hole. For $r < r_c$ the hole is thermodynamically unstable and may collapse. McLean estimated that a local stress concentration of 100 - 1000 is needed to produce a stable hole. The pile-up model of Smith and Barnby¹⁰⁵ suggested that the stresses generated by a dislocation pile-up at a discontinuity such as a grain boundary particle should be sufficient to allow the conditions for nucleation to be met frequently in practice.

The treatment of the stage of stable cavity growth has received the most attention both theoretically and experimentally. It is the easiest stage to observe. Nevertheless,

there still exists a great deal of uncertainty with regard to the relative importance of the various models. As stated previously, all of the theories assume a stable matrix in the sense that the properties of the grain are time independent. Earlier theories also assumed that the stress remained constant up to fracture, though some authors have now attempted to refine the models by estimating the increase of stress in the region of the void which results as the cavity volume increases. As with nucleation two basic approaches to the phenomenon have been developed, one involving vacancy flow, in which the difference in chemical potential of atoms at a region of high stress in the cavity (e.g. the periphery along the boundary) and of those at lower stress in the boundary causes a net influx of vacancies and hence cavity growth. The other envisages growth resulting from continued sliding and associated strain controlled enlargement of the void.

The work of Greenwood⁸⁵⁻⁸⁸ already cited in connection with nucleation, had envisaged continued growth also occurring by vacancy condensation, at the high temperatures and low strain rates involved. A model for growth by vacancy accretion by Balluffi and Seigle¹⁰⁶ considered vacancies flowing to the voids from the transverse boundaries. It predicted that no transverse void growth should occur under compressive stress, which was confirmed during compressive creep of magnesium¹⁰⁷ and recently in uranium dioxide¹⁰⁸. The work of Hull and Rimmer¹¹⁴ studied the creep of copper under both tensile stress (σ) and hydrostatic stress (P). They developed an analytical model which allowed calculation of the growth rate of cavities on the basis of

vacancy condensation on 'non-wetting' particles, and assuming that the cavity remained spherical, they showed that the rate of increase of radius (r) was given by:

$$\frac{dr}{dt} = \frac{D_g \delta z \Omega (\sigma - P)}{2kT a r} \quad \dots \quad (1.4)$$

where σ, P, r as defined above
 D_g grain boundary diffusion coefficient
 δz effective grain boundary width
 a cavity spacing
 Ω atomic volume
 k, T usual meaning

The rupture time was then calculated by integrating the above equation and assuming that final separation occurs when $r = \frac{a}{2}$, giving

$$t_r = \frac{kT a^3}{4D_g \delta z \Omega (\sigma - P)} \quad \dots \quad (1.5)$$

Further modifications¹¹⁰⁻¹¹⁶ of the original analysis have refined the treatment to deal with continuous nucleation of voids, increase of stress in the vicinity of the voids and details of void geometry and spacing. The recent treatment by Raj and Ashby¹¹⁶ is particularly comprehensive, dealing with variables such as grain size, precipitate size, precipitate distribution, void type, continuous nucleation on sliding and non-sliding boundaries and applied strain rate. They apply classical nucleation and growth concepts to predict the existence of ductility minima by calculating rupture life as a function of temperature, for the various conditions described above.

This model is summarised schematically in figure 6. The strongest

experimental support for growth by vacancy condensation comes from work in which the application of hydrostatic stress, to achieve the condition $\sigma = P$, inhibits cavitation. Ratcliff and Greenwood¹⁰³ showed that further cavitation in magnesium was completely suppressed by the application of hydrostatic pressure, no matter what stage the creep process had reached.

These experiments¹⁰³ are not universally accepted as critical evidence for vacancy growth. In the opinion of Machlin¹¹⁸ for example, the experiments only show that a net stress difference across the boundaries is necessary to prevent re-cohesion. A further objection relates to the temperature dependence of growth rate. According to Raj and Ashby's analysis¹¹⁶, as the temperature increases, the stress required to maintain a given strain rate falls in such a way that the growth rate increases. Observations that the area of visible voids at a particular strain was independent of temperature (in the range of 650° - 900°C) have been reported¹¹⁹. Further, examples of linear increase of void volume with strain have been reported^{120,121} which would seem to indicate that grain boundary sliding may contribute directly to void growth. The review of Perry⁸¹ summarises the large amount of experimental evidence concerning the study of void shapes¹²², angular distribution of cavity containing boundaries¹²³, variations of grain size¹²⁴ and the effect of stress reversals¹²⁵ which has been presented in support of the contention that void growth is to a large extent controlled by the extent of grain boundary sliding and associated deformation processes. This effect has largely been ignored in theories of growth by vacancy

control. The analysis of Raj and Ashby¹¹⁶ incorporates boundary sliding merely to account for an increase in the stress level acting upon a void which is understood to grow only by vacancy condensation.

A further criticism^{120,126} of vacancy control arises from the observation that the diffusion coefficient is only slightly affected by alloying, whereas creep and cavitation rates can change markedly. It would appear that deformation due to vacancy controlled void growth is most likely to be important at low stresses^{108,114,127}.

It is doubtful that any one mechanism of growth operates individually. The situation is more likely to be one in which several modes involving crack propagation from void apices, tearing between voids, internal necking with enhanced intercavity sliding, grain boundary sliding and vacancy condensation are possible, of which one or more may dominate under a given set of conditions.

The final stage at which the growth becomes unstable is the least investigated and understood. In all of the calculations of rupture life from theoretical growth laws it is assumed that final fracture occurs when the area fraction of voids in a specimen reaches some specified value. Generally no account of stress intensification or plastic instability is made. In a detailed analysis of grain boundary sliding and diffusional creep¹²⁸ it was shown how the stress upon a boundary is redistributed when diffusional accommodation is allowed. In the light of this observation it was commented¹²⁸ that:

" It is not generally realised that standard elastic solutions such as those for an elastic crack, are not applicable to problems of grain boundary sliding at high temperatures (when diffusion is possible) because of this redistribution of stress".

Such considerations would tend to place in doubt the analysis of Williams¹²⁹ which treated the opening produced during the growth of a wedge crack, as shown in figure 7, allowing final failure to occur when the crack tip opening displacement attained a critical level.

Recent work¹³⁰ has shown that the final failure mode and associated ductility, during hot fracture of an industrial copper-base alloy, changes with grain size (figure 8). At fine grain sizes (<100 μm) they¹³⁰ propose an 'intergranular void sheet' mechanism, which is essentially based upon the analysis of McClintock¹³¹ dealing with the growth of voids in the context of ductile fracture. For coarse grain sizes the stress to cause unstable intergranular crack propagation is influenced by the crack length, but it appears that caution is necessary in applying simple linear elastic fracture mechanics concepts. With regard to this latter point, other work¹³⁶ has recently shown that the rupture stress of a 20Cr - 35Ni alloy which was fractured in an intergranular manner at 700°C could be related to the length of the largest crack through the relation:

$$\sigma c^n = \text{constant} \quad \dots \quad (1.6)$$

where σ = rupture stress
 c = largest crack length

with $n = 0.55(\pm 0.07, 95\% \text{ confidence limit})$

This result was interpreted as showing that the Griffith criterion, $\sigma\sqrt{c} = \text{constant}$, is a good description of the relationship between rupture stress and crack length. Incidentally, it is notable that the grain size of the material used in this investigation was of the order of $40 \mu\text{m}$, which according to the previous classification¹³⁰ should fail by the ductile coalescence of voids. Measurements of the area fraction of voids at fracture were also reported¹³² which exhibited a clear stress dependence, being approximately inversely proportional to rupture stress.

Another aspect of cavitation, is that which occurs during superplastic deformation. This is dealt with now because it clearly shows the inadequacy of present theories of intergranular failure with particular reference to the way in which the final fracture is ignored. Micrograin superplastic flow characteristically occurs at low flow stress and usually results in high tensile ductility with little internal void formation^{133,134}. However, some alloys of copper, notably those containing zinc¹³⁵ or aluminium¹³⁶, and some iron-carbon alloys¹³⁷ have been found to cavitate at either grain or interphase boundaries during superplastic deformation. In recent work¹³⁸ observations of cavitation at grain and phase boundaries during superplastic flow of an aluminium bronze were made which showed a gradual development of voids with increased strain, which behaviour was suggested to be consistent with nucleation by grain boundary sliding as observed in creep. However, the occurrence of cavitation was not observed to promote a serious loss of ductility (values in excess of 200%

elongation were reported in specimens for which the extent of cavitation was greatest), which suggests that during superplastic deformation cavity interlinkage by internal necking is inhibited in much the same way that the rate of external necking is reduced¹³³. This contention is supported by the observation¹³⁸ that elongations greater than 700% failed to produce complete failure in specimens of aluminium bronze deformed at a strain rate which corresponded to a maximum strain rate sensitivity of the flow stress. Cavities increased in frequency as the strain rate was increased above this value. Final fracture at lower strain rates took place by gentle necking until point separation occurred. Final fracture at greater strain rates never achieved 100% reduction in area but instead resulted from the continued nucleation and growth of the cavities and interlinkage by internal necking between them.

Even though certain evidence apparently supporting the critical area fraction of voids criterion for final fracture is still being produced¹³⁹, it is clear that, at least, for conditions of extreme brittleness and extreme ductility of metals at elevated temperature (i.e. those of greatest engineering interest), it is not appropriate. Moreover, there is little theoretical justification for it. It is in this context that the recent theory of intergranular fracture at elevated temperatures according to Raj and Ashby¹¹⁶ has been criticised¹⁴⁴.

With regard to the interpretation of SRC in terms of current views of intergranular failure, there are several major difficulties. Not least among these is the fact that there is little reported data giving details of the conditions under

which the cracks, or cavities, are formed. As already discussed the derivation of the 'C' curves has been somewhat artificial, and the accompanying metallography has generally concentrated upon the matrix, rather than the cavities. During these studies it has, however, been shown that the matrix is by no means stable. Fractographic studies^{75,102} have shown the close association of vanadium carbide particles with cavities formed in low alloy Cr - Mo - V steels at elevated temperatures. Since these precipitates are generally formed coherent with the matrix, the condition of 'non-wetting' particles for the nucleation of creep cavities required by most of the aforementioned theories does not appear to be met.

On the other hand several factors which could contribute to the phenomenon have been identified or underlined. The first of these is clearly grain size. Most observations and predictions agree that a coarse grain size is effective in reducing ductility during intergranular failure. Grain boundary migration, clearly very difficult in the case of prior austenite grain boundaries in bainitic or martensitic steels, is usually associated with increased resistance to cavitation failure. Grain boundary irregularities in the form of ledges or precipitates are required as sites for heterogeneous nucleation. Transformation products such as bainite or martensite are well known to cause considerable surface relief effects, so it seems plausible to assume that prior austenite grain boundaries will be similarly rumped after transformation. The existence of grain boundary precipitates is well established. Lastly is the

effect of purity. The lack of cavitation reported in pure aluminium⁹⁰ is taken by many workers to indicate that all cavitation phenomenon in commercial alloys may be based on the segregation of impurities to the grain boundaries.

1.5 Summary

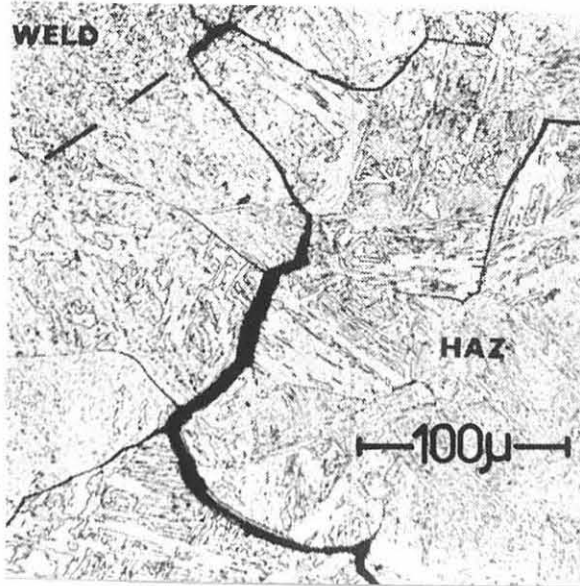
Stress relief cracking in low alloy ferritic creep resisting steels is understood essentially as a problem of low creep ductility, involving unstable intergranular crack growth at low strains. Although the previous work on SRC has failed to elucidate precisely the conditions under which crack growth occurs, it is usually assumed to be promoted by the creep strengthening of the grains during the formation of a fine dispersion of alloy carbides. In Cr - Mo - V steels, the formation of V_4C_3 is seen to be particularly important in this respect. For the most part, the assessment of susceptibility to SRC has been concerned with the effect of composition and it appears that although the above assumption may represent a necessary condition, it is not sufficient to provide reliable prediction of the occurrence of SRC in a particular steel sample.

In terms of the formation of intergranular cavitation, SRC may be understood as a problem involving the rapid onset of the final stage of unstable crack growth. None of the theoretical treatments currently available is able to deal with this stage satisfactorily. Indeed, it is ignored by most, since it is understood to contribute only a small fraction of the estimated rupture life. However, experimental observations of intergranular

cavitation immediately prior to final failure show that it is possible to develop large strains to failure during this final stage of rupture. It appears that the major controlling factors in the process are the grain size, the stability of tensile deformation and the grain boundary cleanliness. It is possible that these three factors may not be independent. Clearly, a definition describing SRC as a problem of reduced rupture life is insensitive to the effects of these factors and the importance of this is underlined by considering that even though the levels of residual stress within a weld HAZ may be of the order of the yield strength of the steel, the levels of residual strain will be low (say 0.5%). *In this way, although measured rupture strains of 0.2% and 2% may represent the difference between susceptible and non-susceptible material, the difference in measured rupture lives at this level of strain will be negligible.*

The investigation described in the following pages was carried out to examine some of these points in detail. Chapter two discusses a series of preliminary experiments made on two samples of commercial $\frac{1}{2}\text{Cr } \frac{1}{2}\text{Mo } \frac{1}{4}\text{V}$ steel which were designed to investigate the extent of grain strengthening at elevated temperatures in this material. Chapter three describes the tensile mechanical properties of these samples as a function of temperature, and prior austenite grain size. The work described in chapter four examines the effect of stability of tensile deformation in promoting low ductility during failure of the commercial samples by intergranular cavitation. Chapter five describes a series of experiments where the conditions under

which failure occurs during a stress relief heat treatment are clearly established. The sixth and seventh chapters examine the effect of sample purity upon the strength of the grain boundaries. The final chapter discusses the observations in terms of currently accepted theories of intergranular failure, and goes on to make recommendations towards realistic test procedures for assessment of susceptibility to SRC, as well as possible practical routes for the avoidance of SRC.



(a)



(b)

Figure 1. (a) HAZ cracking in A517F (Ref. 64)
(b) HAZ cracking in $\frac{1}{2}\text{Cr } \frac{1}{2}\text{Mo } \frac{1}{4}\text{V}$ (Ref. 50)
(N.B. A517F composition is basically 0.5%Cr 0.5%Mo 0.1%V)

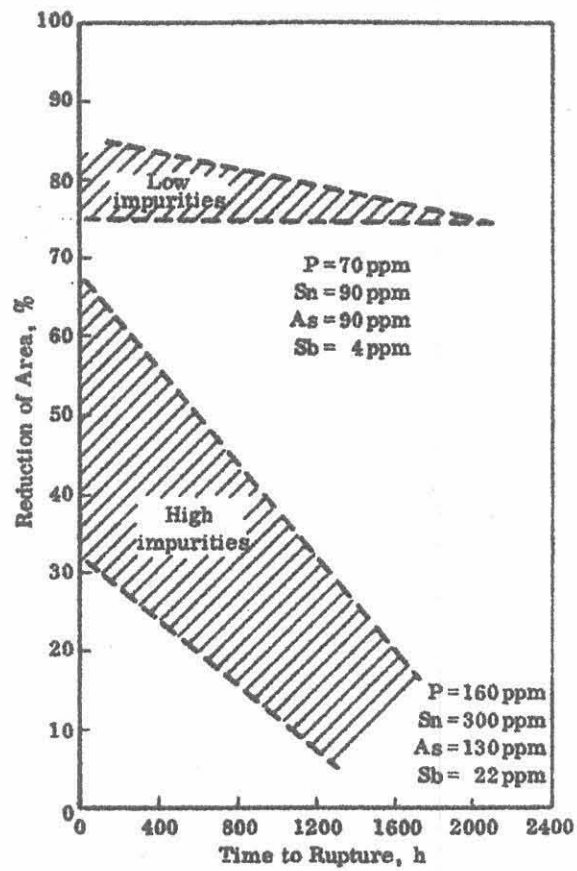


Figure 2. Effect of P, Sn, As and Sb on creep rupture ductility of post weld heat treated $2\frac{1}{4}$ Cr-1Mo weld metal at 566°C. (Bruscato, 44)

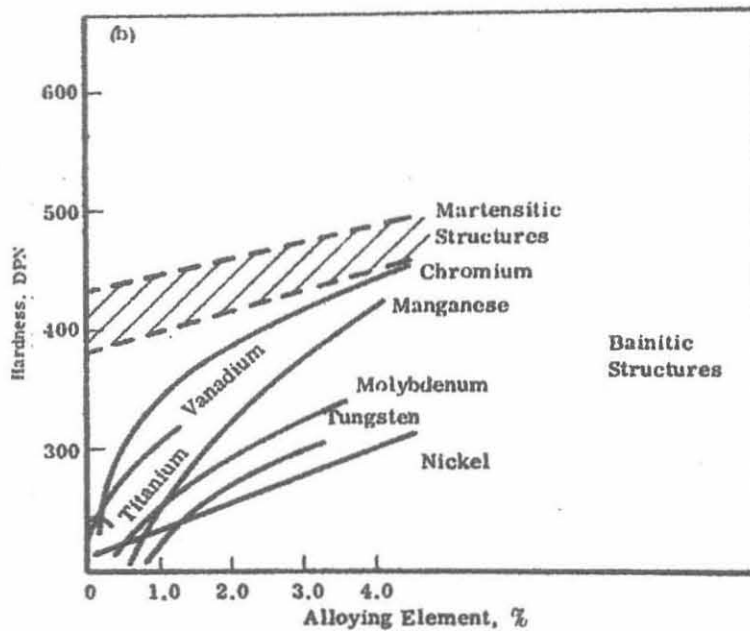
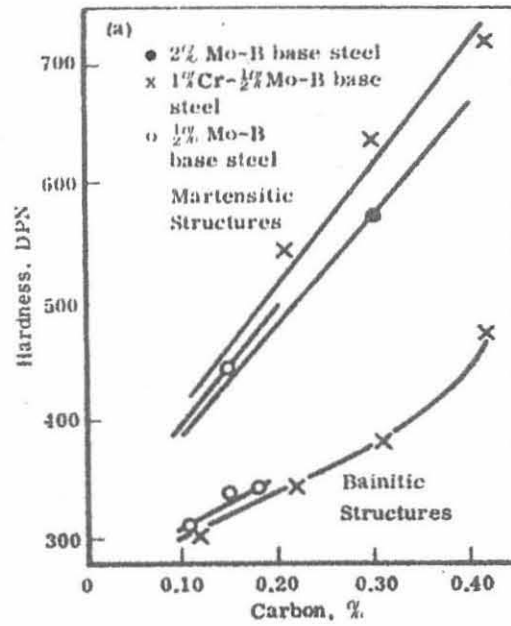


Figure 3. Effect of carbon and alloy additions on bainite and martensite hardness (51)

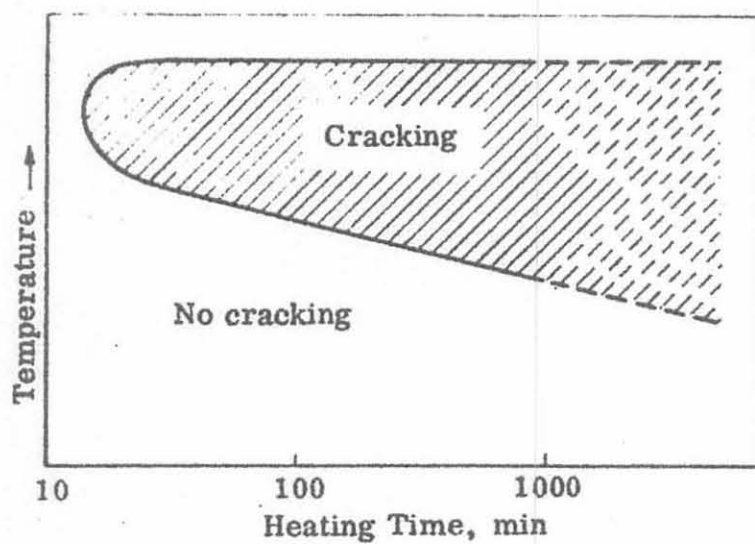


Figure 4. Schematic representation in time-temperature co-ordinates of the occurrence of cracking during stress relieving of weld HAZ microstructures.

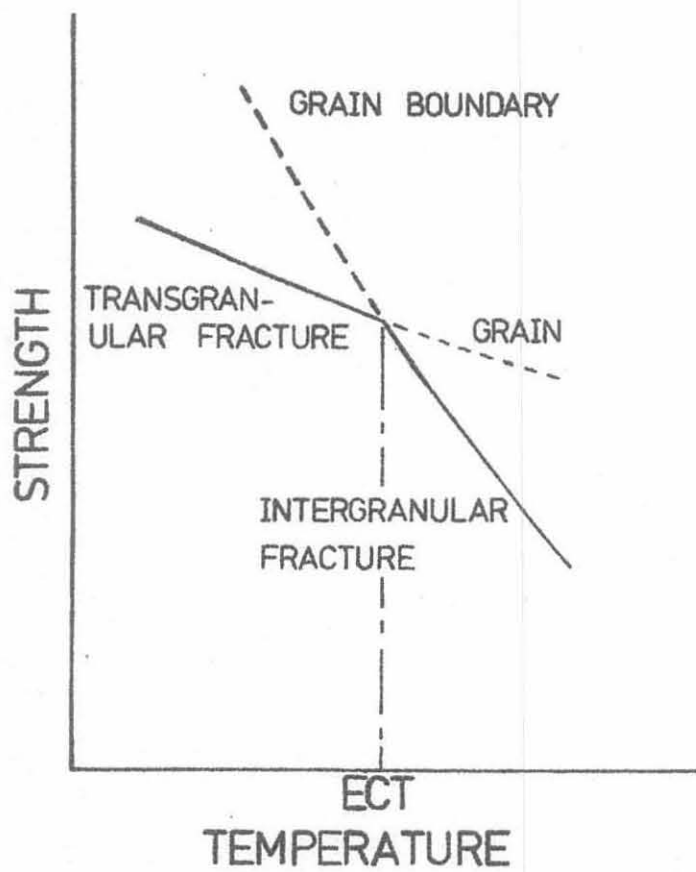


Figure 5. Schematic illustration of the concept of equicohesive temperature.

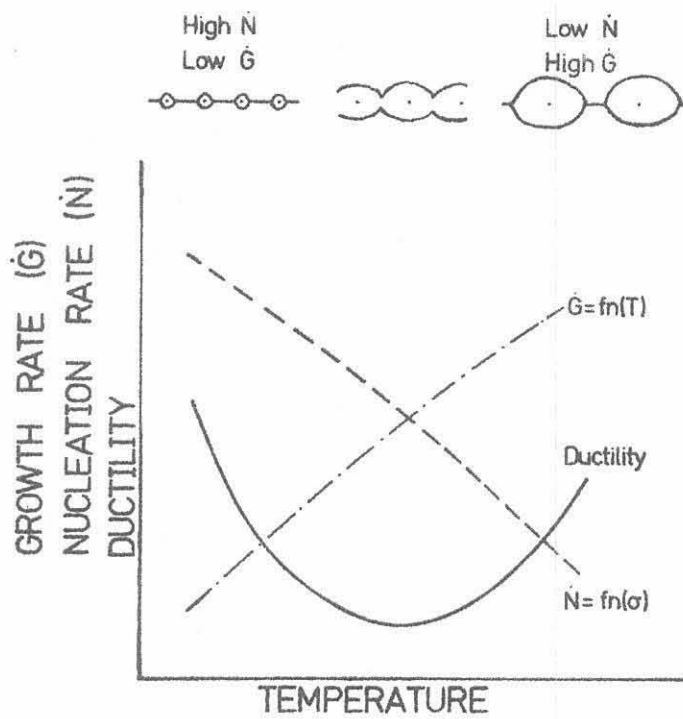
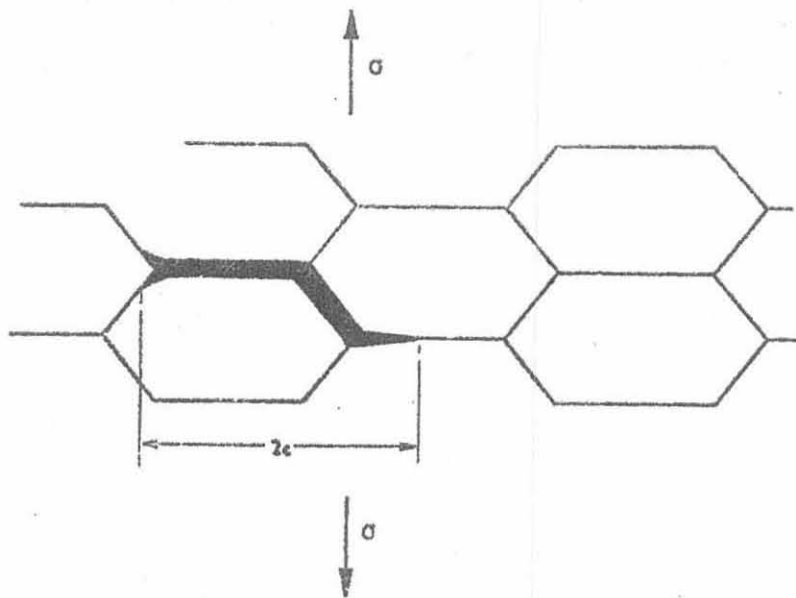
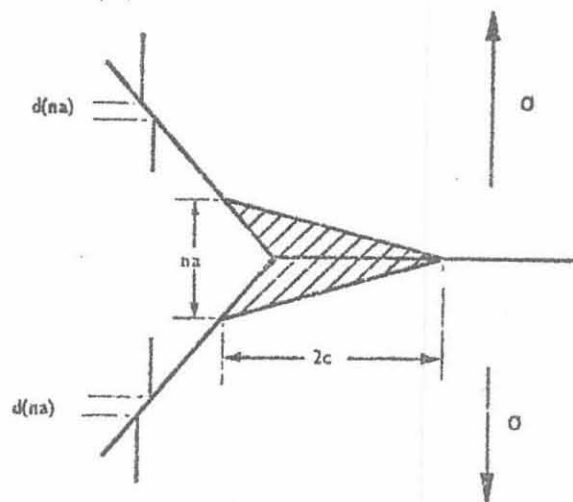


Figure 6. Schematic illustration of the model used by Raj and Ashby¹¹⁶ to predict the existence of a ductility minimum during failure by intergranular cavitation.



(a)



(b)

Figure 7. (a) Typical wedge crack.

(b) Model used (Williams, 129), in which crack length, $2c$ depends upon the amount of sliding, and final failure occurs essentially at a 'critical' crack length.

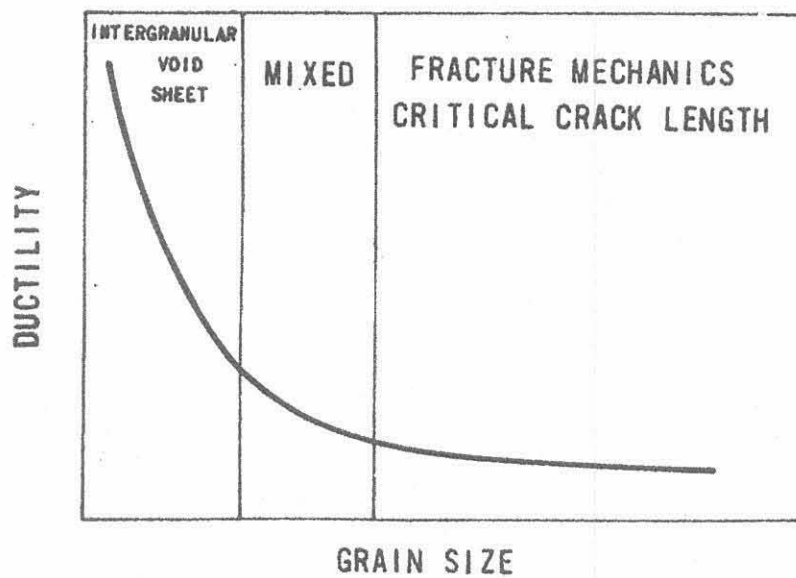


Figure 8. Schematic illustration of the effect of grain size upon the failure mode and ductility during intergranular cavitation at elevated temperature. (Ref. 130)

CHAPTER II

The Approach to the Problem2.1 Selection of Material

From the discussion of the previous chapter it is apparent that the occurrence of stress relief cracking in low alloy steels is frequently associated with the presence of vanadium in the alloy composition. In particular, the widely used material $\frac{1}{2}\text{Cr } \frac{1}{2}\text{Mo } \frac{1}{4}\text{V}$ is often described as being inherently susceptible. It was decided to confine the investigation mainly to this material in order to ascertain the reasons for its apparent ability to appear susceptible in some instances and safe in others. Accordingly, two samples of steam pipe material were obtained, one from Messrs C.A.Parsons and Sons, and one from the C.E.G.B. In service these pipes had proved to be respectively non-susceptible and susceptible to stress relief cracking. Further materials examined were high purity $\frac{1}{2}\text{Cr } \frac{1}{2}\text{Mo } \frac{1}{4}\text{V}$ and high purity $2\frac{1}{4}\text{Cr } 1\text{Mo}$ provided by Mr.H.Tipler of the N.P.L.

The chemical composition of each of these materials was determined by wet analysis and is shown in Table II. The commercial materials are labelled (A) (Non-susceptible) and (B) (Susceptible).

Following the work of Nakamura et al.⁶³ values of ΔG , the 'susceptibility index', were calculated for each of the above compositions from the relationship -

$$\Delta G = \%Cr + 3.3 \%Mo + 8.1 \%V - 2 \quad (1.1)$$

The results are shown in Table III.

TABLE IIChemical Analysis of Alloys Used (wt%)

Alloy	Element																		
	C	Cr	Mo	V	S	P	As	Sb	Sn	Cu	Pb	N	O	Ni	Mn	Si	Ti	Nb	Al
A	0.12	0.39	0.52	0.22	0.012	0.016	0.013	<	0.010	0.059	<	*	*	0.055	0.55	0.24	-	-	-
B	0.13	0.54	0.61	0.24	0.011	0.017	0.030	0.006	0.016	0.130	<	*	*	0.062	0.62	0.27	-	-	-
H.P. $\frac{1}{2}$ Cr $\frac{1}{2}$ Mo $\frac{1}{4}$ V	0.11	0.39	0.50	0.26	0.004	0.009	0.003	0.001	0.003	0.003	<	0.001	<	*	*	<	*	*	-
H.P. $2\frac{1}{4}$ Cr 1Mo	0.14	2.12	1.07	-	0.003	0.006	0.001	<	<	0.004	<	*	*	<	<	<	*	*	-

< indicates content is less than the quoted figure

- indicates not detected

* indicates not analysed

TABLE III

Values of susceptibility index, ΔG for above alloys

<u>Alloy</u>	<u>ΔG</u>
A	1.89
B	2.50
H.P. $\frac{1}{2}\text{Cr}$ $\frac{1}{2}\text{Mo}$ $\frac{1}{4}\text{V}$	2.15
H.P. $2\frac{1}{4}\text{Cr}$ 1Mo	3.65

Since positive values of ΔG are taken to indicate susceptible material, it would appear that all of the above materials should exhibit SRC. With regard to the possible effect of trace elements, previous work⁷⁷ has suggested that a measure of the total percentage of (P + Cu + Sn + Sb + As) gives some indication of the cracking tendency of the material. The figures for the materials used in this investigation are shown below in Table IV.

TABLE IV

Total content of certain trace elements

<u>Alloy</u>	<u>wt % (P + Cu + Sn + Sb + As)</u>
A	0.101
B	0.199
H.P. $\frac{1}{2}\text{Cr}$ $\frac{1}{2}\text{Mo}$ $\frac{1}{4}\text{V}$	0.019
H.P. $2\frac{1}{4}\text{Cr}$ 1Mo	0.014

It would appear that this approach could give a better classification of susceptibility to SRC. Other work⁴⁴ which is summarised in figure 2 would seem to indicate that both of the commercial alloys should be susceptible with respect to contents of phosphorus, arsenic and antimony with marginal safety with

respect to Tin while the pure metals would appear to be safe in all respects except that of antimony which appears marginal.

No details of deoxidation practice used in the manufacture of the pipes were available. It is notable that no Ti, Nb or Al could be detected in either sample. Lastly, it is apparent that among the $\frac{1}{2}\text{Cr}$ $\frac{1}{2}\text{Mo}$ $\frac{1}{4}\text{V}$ samples the carbon content is more or less the same, while it is slightly increased in the $2\frac{1}{4}\text{Cr}$ 1Mo sample.

2.2 Austenite Grain Growth during Solution Treatment

The initial part of the investigation was conducted using the commercially produced samples. Results obtained on the high purity samples are presented later on. As discussed in the previous chapter the importance of grain size in promoting low creep ductility has been realised for some time, but little quantitative assessment of its effect in promoting SRC has been reported. Since the problem is generally associated with failure along prior austenite grain boundaries it is this grain size that is of primary interest in the present investigation. Previous work¹⁴¹⁻¹⁴⁴ has been mainly concerned with austenite grain refinement as it relates to the production of a fine ferrite grain size in plain carbon-manganese steels. Basically, the production of a fine austenite grain size is considered to be promoted by the existence of fine precipitate particles on the grain boundaries which remain stable, and thereby effect a pinning action upon the boundary, through their restricted solubility in austenite at the solution treatment temperature employed.

Carbide* forming elements such as vanadium, zirconium, niobium and titanium together with nitride formers such as aluminium are recognised to be effective in this respect.

The elements niobium and titanium (in the form $M(CN)$) appear to be most effective in preventing grain growth at temperatures up to about 1150°C . Aluminium, in the nitride form is recognised as being able to inhibit grain growth at temperatures up to about 1050°C . In the oxide form aluminium is ineffective as is zirconium. Although vanadium carbonitride is recognised by most workers in the field of austenite grain growth as being an effective grain refiner at temperatures up to about 1100°C , it has been reported³ that varying the solution treatment temperature of vanadium-containing steels does not alter the magnitude of the precipitation of vanadium carbide during subsequent tempering, which has been understood to imply that there is no significant difference in the amount of solution during austenitisation¹⁴⁵. This latter observation is not borne out in the present work as is discussed in the next section.

The solution treatments employed in the investigation of SRC have generally taken the form of simulated weld thermal cycles. However, in this work it was decided to study grain size as a controlled experimental variable and as such it was felt that

* There has been some discussion¹⁴¹ concerning the possibility that nitrides of these elements may in fact be particles responsible for austenite grain refinement. Since they are generally isomorphous with the carbides, and mutual solubility of carbon or nitrogen may occur in either species, the particles are often referred to as carbonitrides $M(CN)$.

standard forms of heat treatment would allow a more reproducible variation in grain size. In the first instance a 'single' solution treatment was studied, in which specimens were heated for one hour at the solution treatment temperature (in the range 1000°C to 1300°C). Then a second series of 'double' solution treatments was investigated in which the specimen was given a one hour exposure to a temperature in the range 1050°C to 1200°C followed immediately, without intermediate cooling, by a 1000°C soak, for one hour. It was anticipated that this latter heat treatment might establish whether any vanadium carbide taken into solution during high temperature austenitisation could be reprecipitated at the lower temperature.

Disc specimens (10mm dia., 1mm thick) from each of the samples were encapsulated in sealed silica glass tube, into which a small partial pressure of dry argon had been admitted after evacuation to 10^{-4} Torr. Heat treatments as described were then carried out in horizontal tube furnaces, after which the specimens were water quenched. The specimens were then mounted and prepared for optical examination and grain size measurement. Initially, the etch used was the picric acid etch with additions of CuCl_2 and a wetting agent, which has been used by several workers^{144,146} to reveal the prior austenite grain boundaries. However it was found that a procedure involving the use of a 10% Nital etch, in a re-polish, re-etch sequence, provided quicker and more consistent revealing of the boundaries. Examples of coarse and fine grain sizes are illustrated in figure 9.

The grain size was measured using a circular intercept

method on a Zeiss Neophot metallurgical microscope upon which a field of view of known magnification was projected onto a ground glass screen, with a circle of known diameter superimposed upon it. It was possible to arrange the magnification so that the number of boundaries intersecting the circle (as shown schematically in figure 10) was in the range 20 - 30. A close approximation to the mean linear intercept was then calculated using the equation:

$$\bar{d} = \frac{2\pi r}{M \times n} \quad \dots \quad (2.1)$$

The percentage difference between this estimate of mean linear intercept and one determined using the projected straight line is given by the equation:

$$\% \Delta \bar{d} = \left(1 - \frac{n}{\pi} \sin \frac{\pi}{n} \right) \times 100 \quad \dots \quad (2.2)$$

In equations (2.1) and (2.2)

\bar{d} = mean linear intercept

r = circle radius

M = magnification of field of view

n = number of intercepts

Equation (2.2) indicates that percentage difference is less than 1.00% for $20 < n < 30$. Considering that this method proved to be considerably less fatiguing and therefore allowed a greater number of boundaries to be counted (about 200 for each specimen), the results are probably more accurate than comparable conventional mean linear intercept value determinations (generally involving about 30 to 50 boundaries per specimen). The results of the

grain size measurements from the commercially produced alloys are shown in figure 11. It is immediately apparent that alloy B (the susceptible material) achieves a greater extent of grain growth than alloy A, for equivalent heat treatment. Furthermore within the range of scatter (one standard deviation) the effect of double solution treatment does not markedly change the observed grain size for a given material. The mean values, as plotted, suggest that some grain refinement occurs, for the higher initial solution treatment temperature. The reasons for this difference in grain growth characteristics were not investigated in detail. The compositions of the steels do not suggest that any of the grain refining elements mentioned previously is present in one steel to a greater extent than in the other. The samples were supplied in the "fully heat-treated" condition, which probably implies that they were solution treated in the region 950°C to 1000°C , normalised and tempered in the region 650°C to 700°C . Further, both samples were taken from extruded seamless pipes having the same nominal dimensions of 250mm I.D. 80mm wall thickness, so that their respective thermo-mechanical history would appear to be nominally similar. However, it is not known in detail what the effects of prior treatment are, upon the austenite grain growth characteristics of this type of steel. McMahon¹⁴⁷ has suggested that austenite grain size achieved in certain steels is strongly dependent upon the prior austenite grain size resulting from previous thermo-mechanical heat treatment.

Whatever the reason for the difference, it is felt that the presently adopted scheme of applying a standardised heat

treatment to the as received material, leads one to suspect that a coarser range of grain size might reasonably be expected within the heat affected zone of material B over that in material A.

2.3 Ambient Temperature Secondary Hardening Response as a Function of Solution Treatment

In view of the observations reported in the previous chapter, that the precipitation of vanadium carbide in Cr - Mo - V steels is mainly responsible for the secondary hardening effect observed during tempering, as well as for the promotion of creep strengthening, it was felt that the important question of degree of solution of vanadium carbide during austenitisation might be resolved by detailed observation of the secondary hardening response of the materials A and B, in conjunction with the range of single and double solution treatments reported in the previous section. It was at this stage that standardisation of the heat treatment procedure immediately following austenitisation had to be considered. As described previously, the heat affected zone structure in Cr - Mo - V thick-section welds is generally of a mixed upper-lower bainite type which results in a room temperature hardness in the range 230 to 280 VPN.

Inspection of the isothermal transformation diagram for $\frac{1}{2}\text{Cr} \frac{1}{2}\text{Mo} \frac{1}{4}\text{V}$ steels³¹, as shown in figure 12, illustrate the presence of pronounced pearlite and bainite transformation noses. It was felt therefore that the conventional air cool or oil quench treatments used in previous work to simulate heat affected zone structures might in fact mask the effects of

solution treatment upon the secondary hardening characteristics; firstly through the possibility of auto-tempering during cooling, and secondly through the formation of a wide range of transformation products each with differing initial hardness during tempering. Accordingly it was decided that a water quench would be used after austenitisation in order to produce a largely martensitic matrix. Initial hardness values in the range 390 - 410 VPN were measured.

The specimens used in the hardening response investigation were cut from the as received samples with dimensions approximately 5mm×5mm×1mm. For initial solution treatment, batches of specimens were sealed in silica glass tubes with a partial pressure of dry argon. After solution treatment and water quenching*, each specimen was lightly ground on wet silicon carbide grinding papers and the value of initial Vickers Hardness determined. Not less than six indentations were made for each determination, and it was found that the standard deviation for a particular measure was usually within 1% of the mean value quoted.

Tempering treatments were carried out at 625°C using a molten tin bath. This temperature was chosen in the light of previous work^{148,149,150} which suggested that peak hardness in vanadium bearing steels occurs after about one hour at 625°C, during the tempering of a martensitic matrix. Of particular interest is the work of Tanino and Nishida¹⁵¹ in which the

*

Care was taken to ensure that the silica capsules were broken outside the water bath in order to ensure uniformity of quench rate for each batch.

effect of tempering temperature on the hardness of quenched and tempered vanadium steels containing about 0.17%C and a range of vanadium contents were studied. The results¹⁵¹ are summarised in figure 13 which shows that variation of vanadium contents within the range 0 to 0.53% produced significant changes in the value of secondary hardening peak without altering its position with respect to temperature. Detailed electron microscopy accompanying this work showed that the number of fine vanadium carbide particles, precipitated at a particular tempering temperature, increased with increasing vanadium contents. The evidence of the importance of vanadium carbide itself and the degree of precipitation, in the process of secondary hardening is therefore clearly established.

In the present investigation, individual specimens from a particular solution treatment batch were tempered at 625°C for times ranging from 2 to 120 minutes after which they were water quenched. The specimens were then lightly ground and the hardness of each one was determined as before. In order to offset the effects of variable initial hardness the results are presented as hardness change, in which the change in hardness of each individual specimen is presented, as a function of the length of time of tempering treatment. Figure 14 compares the effect of single solution treatment upon the hardening response of the two commercial materials. It would appear that for both steels the intensity of hardening is increased with increasing solution treatment temperature.

In terms of the work of Tanino¹⁵¹ the implication

would appear to be obviously that increasing the solution treatment temperature does increase the degree of solution of vanadium carbide. This is evidenced by the increased intensity of peak hardness, which has previously been correlated with the degree of precipitation of vanadium carbide from a supersaturated matrix, during tempering.

To further investigate the possible effects of austenitisation treatment upon the degree of solution of vanadium carbide, batches of specimens which had been subjected to a range of double solution treatments were investigated as before. The results of hardness change as a function of length of time of tempering treatment are presented in figure 15. The upper and lower bound single solution treatment results are plotted for comparison. It would appear that the degree of supersaturation of the material prior to tempering may be reduced by a double solution treatment. Presumably some of the vanadium carbide taken into solution at the higher temperature is reprecipitated in the austenite at the lower temperature. Clearly the precipitate formed in the austenite could not be expected to form part of the fine distribution produced during tempering (i.e. that which has been closely associated with intensity of secondary hardening). Hence the observed reduction of secondary hardening as a result of double solution treatment is indicative of a reduced degree of solution of V_4C_3 in austenite.

It is apparent that the simple double solution treatments used were not completely effective in reducing the degree of supersaturation prior to tempering. Nevertheless,

taken in conjunction with the austenite grain coarsening results, discussed in the previous section, it would appear that this approach offers a clear opportunity for distinguishing between the two variables of grain strength and grain size during intergranular failure at elevated temperatures. After all, in the context of the understanding of SRC already discussed, it cannot now be argued that material B proved to be susceptible in service while material A did not, simply in terms of secondary hardening effects as they relate to creep strength of the grains (see for example the work of Bentley⁴⁹), because it is apparent that under these controlled conditions the two materials behave in an ostensibly very similar manner during secondary hardening. This latter point is reinforced in the next section.

2.4 Observations of Hardening Behaviour at Elevated Temperatures through Hot Hardness Measurement

Although the hardness measurement involves a complex non-uniform strain field, the possibility of direct correlation with flow properties as assessed through tensile testing has been quite well established by the work of Tabor¹⁵². The technique of elevated temperature hardness measurement has been used by several workers¹⁵³⁻¹⁵⁶ in the investigation of the effects of composition variation and phase changes upon elevated temperature flow properties. Recently, a hot micro-hardness machine was built in Cambridge and used to determine the flow properties of inclusions in steel at temperatures used in hot rolling practice¹⁵⁷.

This machine was designed to overcome some of the difficulties which have been encountered by other workers. In

particular a dual furnace arrangement was incorporated in order that the indenter temperature was maintained at the same level as that of the specimen. Also, the testing chamber was constructed so that measurements could be made under conditions of high pressure inert or reducing atmospheres. In view of the emphasis laid upon the relative strengths of grains and grain boundaries by many workers in the interpretation of SRC it was felt that the use of micro-hardness testing at elevated temperatures, in specimens of each of the sample materials which had been heat treated to give a wide range of grain sizes, might clarify the issue to some extent.

The experiment was designed to test the following assumptions which are frequently invoked during discussions of SRC, viz:

- (i) That the hardening behaviour of the material at elevated temperatures bears a direct relationship to that observed at ambient temperatures after equivalent high temperature exposure.
- (ii) That the hardening behaviour observed at ambient temperatures in steels containing non-equilibrium transformation products is not greatly affected by the presence of prior austenite grain boundaries, such that any deviation from the first condition may be attributed to the contribution made by these grain boundaries at elevated temperatures.

The second assumption involves the idea that creep strength is intimately associated with the formation of a fine

distribution of vanadium carbide precipitates within the matrix in much the same way as in the promotion of the secondary hardening effect.

The specimens used in the hot micro-hardness testing machine were cylindrical having dimensions 8mm diameter \times 8mm long. These were cut and machined from the as received samples and then sealed in silica glass capsules, as before, prior to solution treatment. Three batches of specimens from each of the samples were solution treated at: 1300°C (50h) + 1000°C (1h) + W.Q.
1200°C (1h) + 1000°C (1h) + W.Q.
1000°C (1h) + W.Q.

respectively. These treatments produced grain size variation as shown in Table V.

TABLE V

Prior Austenite Grain Size Measurement in Hot Hardness

Specimens

Solution Treatment	Prior Austenite Grain Size (μ m)		
	A	B	Material
1000°C (1h) + W.Q.	25.2	72.3	
1200°C (1h) + 1000°C(1h) + W.Q.	138.0	202.4	
1300°C (50h)+ 1000°C(1h) + W.Q.	~680	~700	

The weight used during the elevated temperature micro-hardness testing was 550gm. Typical indentations produced in material A at 625°C are shown in figure 16. It can be seen that in the coarse grained material the indentation does not impinge upon or even approach a grain boundary, in the

intermediate grain size material it is possible that it may lie on one or two boundaries and in the fine grain material the indentation is approximately 10 - 12 grain diameters across.

The hardness testing was performed isothermally. The furnace system allowed very rapid rates of specimen heating to be achieved so that the results may be considered as directly comparable with the secondary hardening observations made at ambient temperature after isothermal tempering. Figure 17 illustrates the hardening response of the three batches of material A at various temperatures. Figure 18 shows equivalent results for material B. It is immediately apparent that there is no direct comparison with the hardening peaks shown in figures 14 and 15 even in the very coarse grained specimens. The flat elevated temperature hardening response shown here, is very similar to that reported³ in a similar investigation which employed tensile testing rather than micro-hardness.

To make further comparison of the elevated and ambient temperature response of the materials the change in hardness after an exposure of one hour at temperature was plotted against temperature as shown in figure 19a for sample A, and figure 19b for sample B. In order to justify the two assumptions outlined previously, it would be expected that even if the fine and intermediate grain size specimens failed to illustrate hardening peaks at about 625°C (like those shown in figure 13) then the very coarse grained material should. It may be argued that at temperatures in excess of about 550°C the coarser grained specimens do achieve a slightly reduced change of hardness over that

observed in the fine grained specimens, but the fact that this difference increases with increased temperature and is greater in the finer grained material A, would suggest that it results from an increased contribution of indentation strain due to grain boundary sliding with increased temperature, rather than through any matrix hardening effect. It is noted that hardening peaks for plain carbon steels tested at about 300°C have been observed¹⁵⁷.

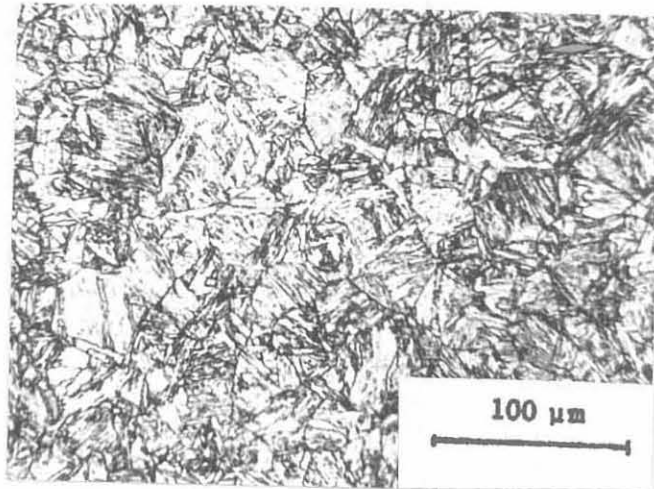
2.5 Conclusions

The preliminary work described in this chapter was particularly concerned with the major assumptions which are made regarding the assessment of susceptibility of a particular steel to the problem of stress relief cracking. As such, the work and therefore the conclusions derived were directed mainly towards the commercial samples A (non-susceptible) and B (susceptible).

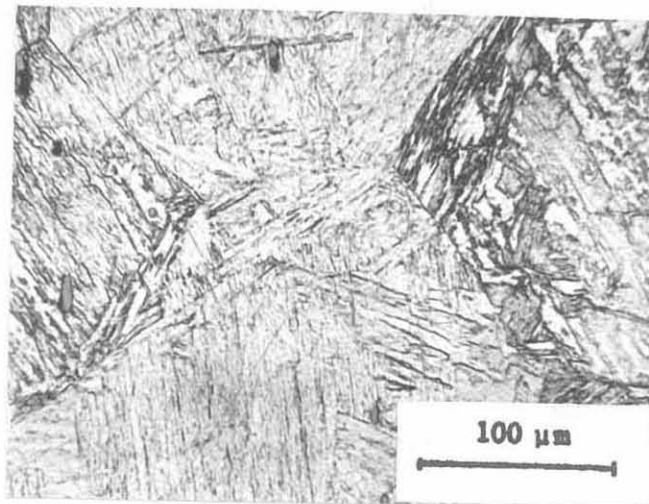
In the first instance it was shown that assessment of susceptibility by simple inspection of steel composition is unreliable in respect of major alloy contents, but would seem to show some consistency in terms of trace element analysis. Secondly, it was found that the austenite grain coarsening characteristics of the commercial samples were significantly different. No convincing explanation of the effect could be found in terms of composition and it was considered that it may have resulted from differing thermo-mechanical history. The observations of hardening response at ambient temperatures following elevated temperature tempering have shown that the

degree of solution of vanadium carbide within austenite is increased as the solution temperature is increased. Further, it would appear that vanadium carbide may be brought out of austenite solution during the lower temperature exposure of a double solution treatment. The hardening intensity during the secondary hardening of a double solution treated specimen closely approaches that of a single solution treated specimen which was heated at a temperature corresponding to the lower temperature of the double solution treatment. In this latter respect it was also observed that the austenite grain size of the double solution treated specimen was close to that of a single solution treated specimen which had been heated at a temperature corresponding to the upper temperature of the double solution treatment. The difference in hardening response observed at ambient temperatures could not justify assessment of the materials A and B as susceptible or non-susceptible in terms of differing intensity of secondary hardening. Finally, the observations of hardening behaviour at elevated temperatures failed to justify any direct relationship between secondary hardening as observed at ambient temperatures and matrix or grain hardening at elevated temperatures.

It would appear that the grain strengthening argument for stress relief cracking must be modified to include a grain size component. The next chapter describes a series of tensile tests performed upon the materials A and B in order to examine in greater detail the possible interactions of the above variables upon their deformation and fracture behaviour in the range of temperatures from ambient to 700°C.



(a)



(b)

Figure 9. Typical fine and coarse grained microstructures.

(a) Sample A solution treated at 1000°C for one hour.

(b) Sample B solution treated at 1200°C for one hour.

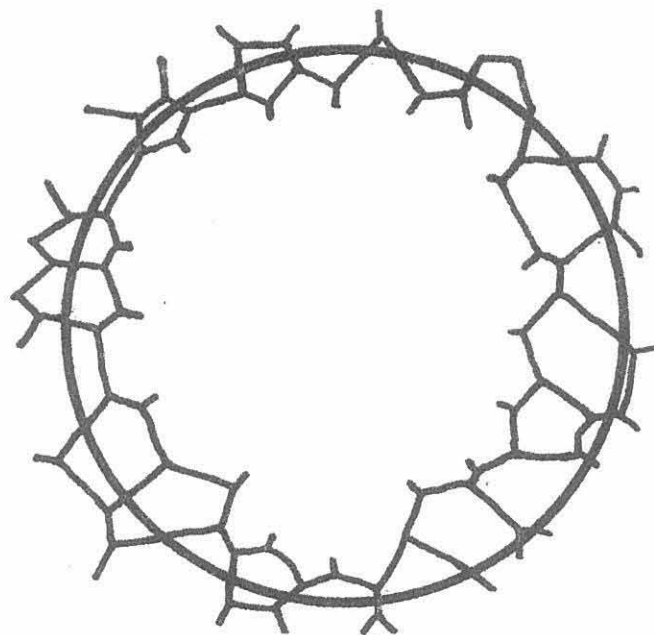


Figure 10. Schematic representation of circular intercept grain size measure.
In this diagram $n = 25$.

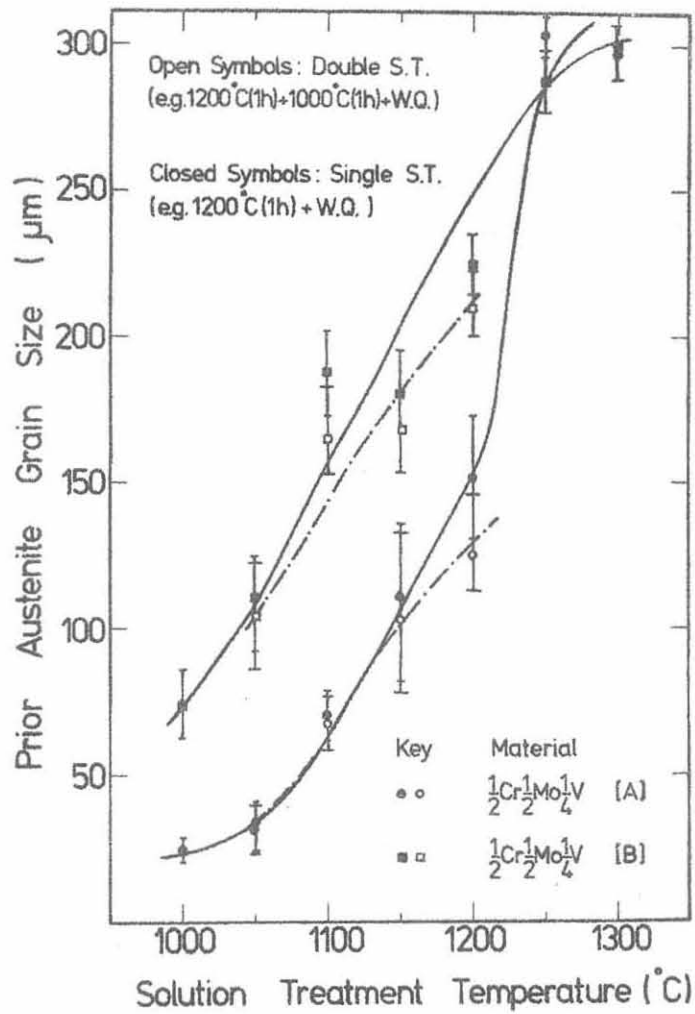


Figure 11. Austenite grain size for various solution treatments.

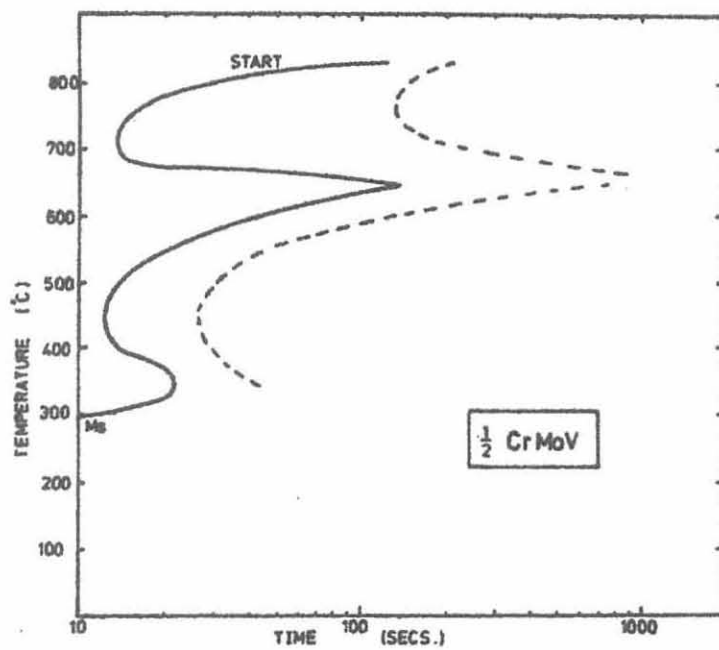


Figure 12. Isothermal Transformation diagram
for $\frac{1}{2}\text{Cr} \frac{1}{2}\text{Mo} \frac{1}{4}\text{V}$ (Dunlop 31)

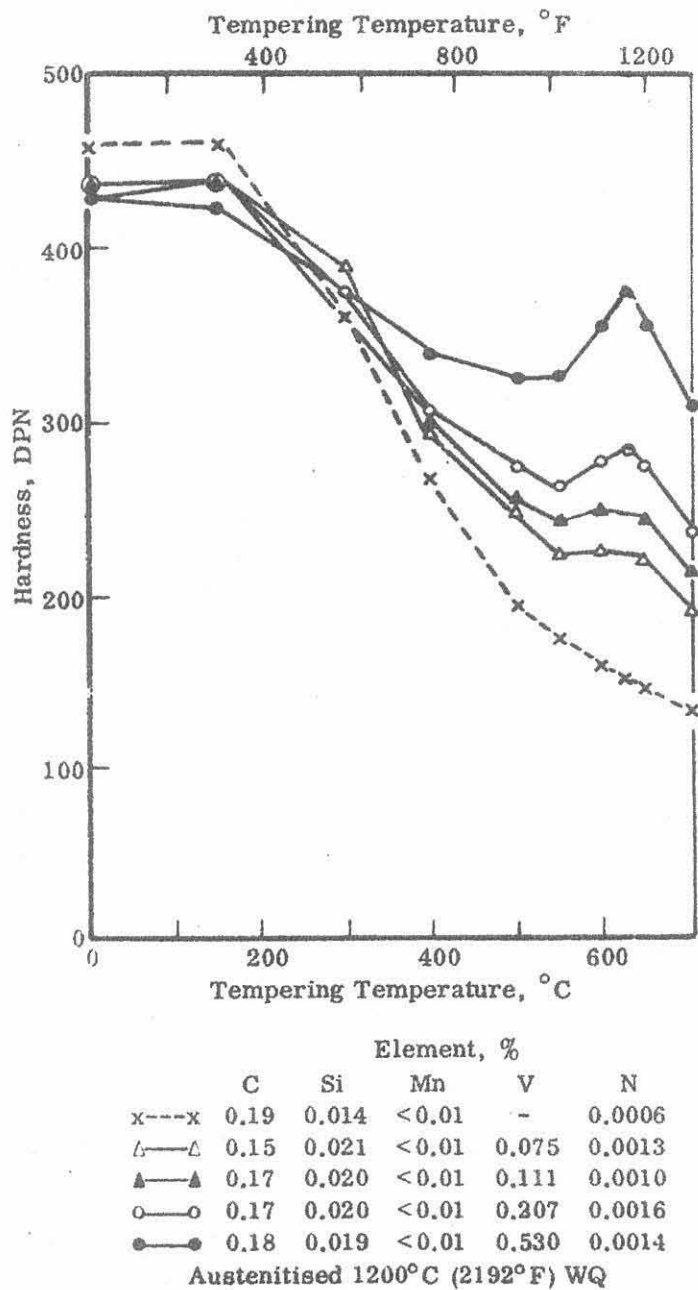
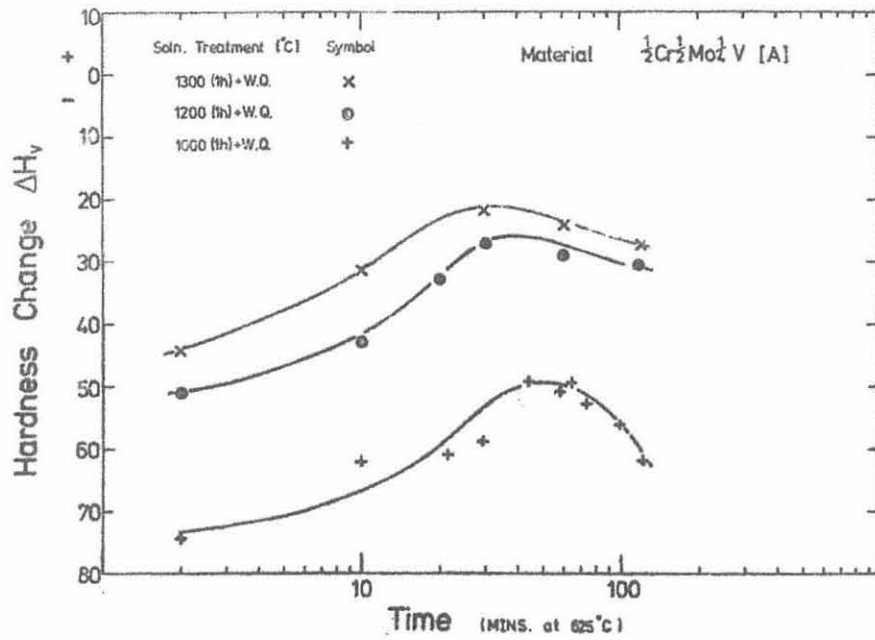
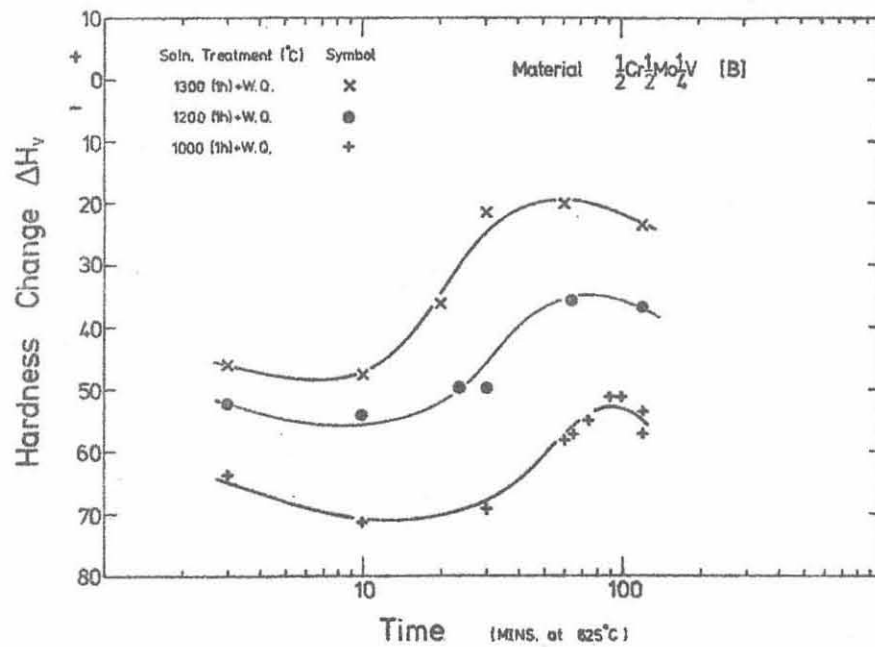


Figure 13. Effect of tempering temperature on hardness of quenched and tempered vanadium steels. (Ref. 151).



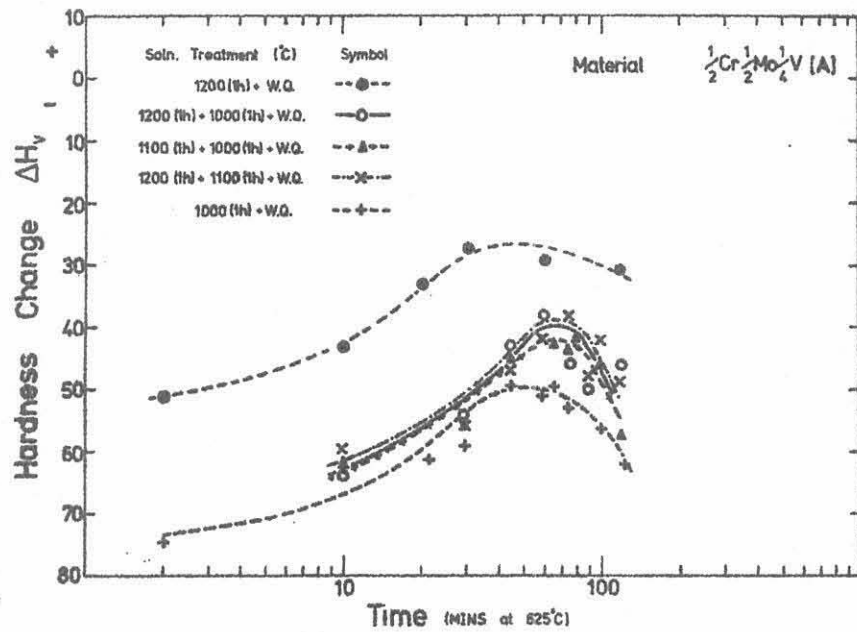
(a)



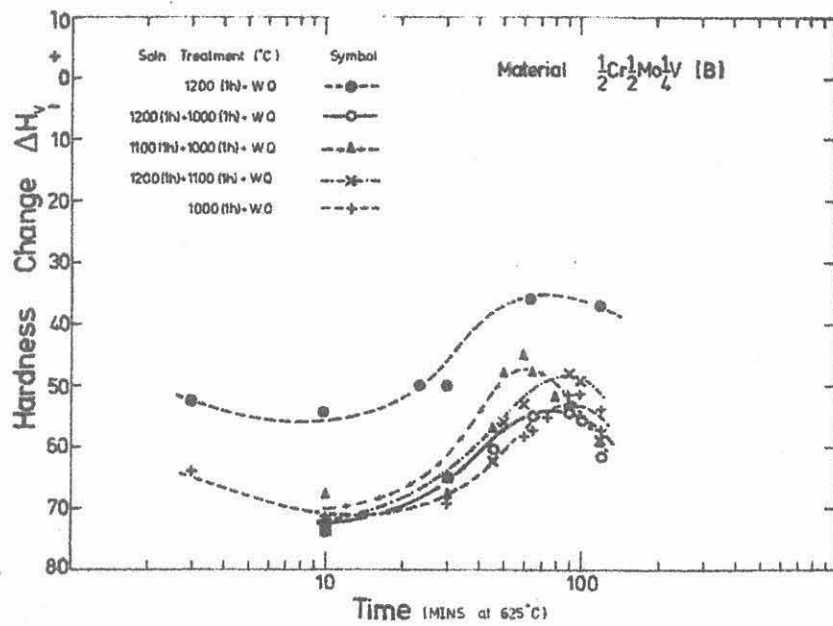
(b)

Figure 14. Secondary hardening response of commercial steels after single solution treatment.

- (a) $\frac{1}{2}\text{Cr}\frac{1}{2}\text{Mo}\frac{1}{4}\text{V}$ A
- (b) $\frac{1}{2}\text{Cr}\frac{1}{2}\text{Mo}\frac{1}{4}\text{V}$ B

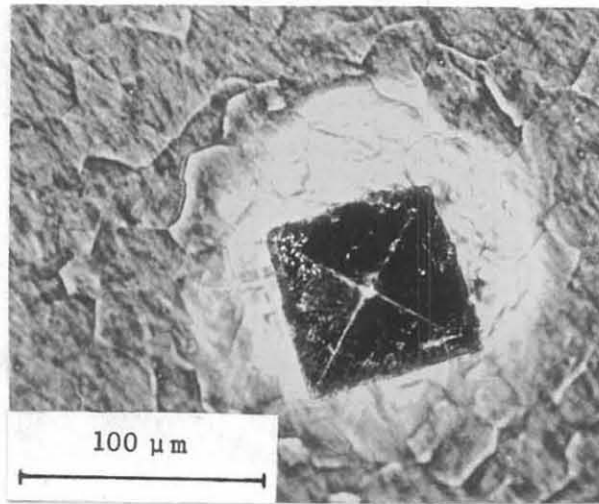


(a)

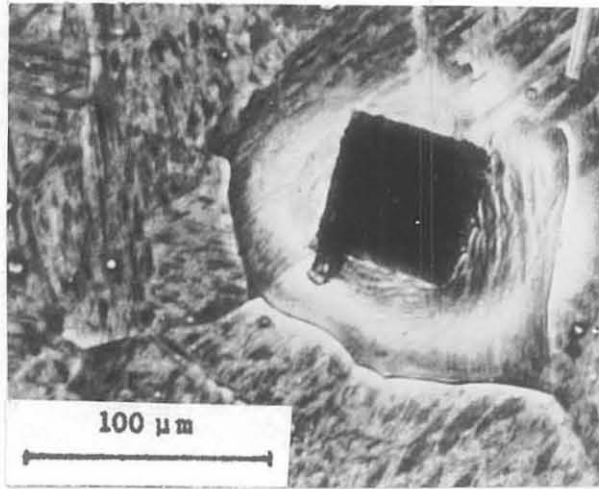


(b)

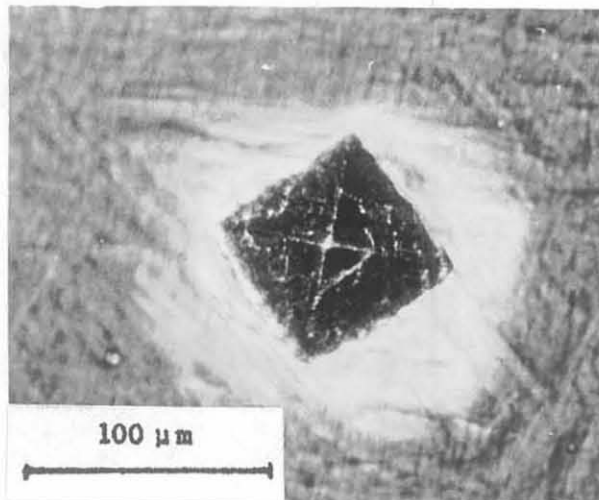
Figure 15. Secondary hardening response of commercial steels after double solution treatment.
 (a) $\frac{1}{2}\text{Cr}\frac{1}{2}\text{Mo}\frac{1}{4}\text{V}$ A
 (b) $\frac{1}{2}\text{Cr}\frac{1}{2}\text{Mo}\frac{1}{4}\text{V}$ B



(a)



(b)



(c)

Figure 16. Typical hardness indentations made at 625°C in material A.

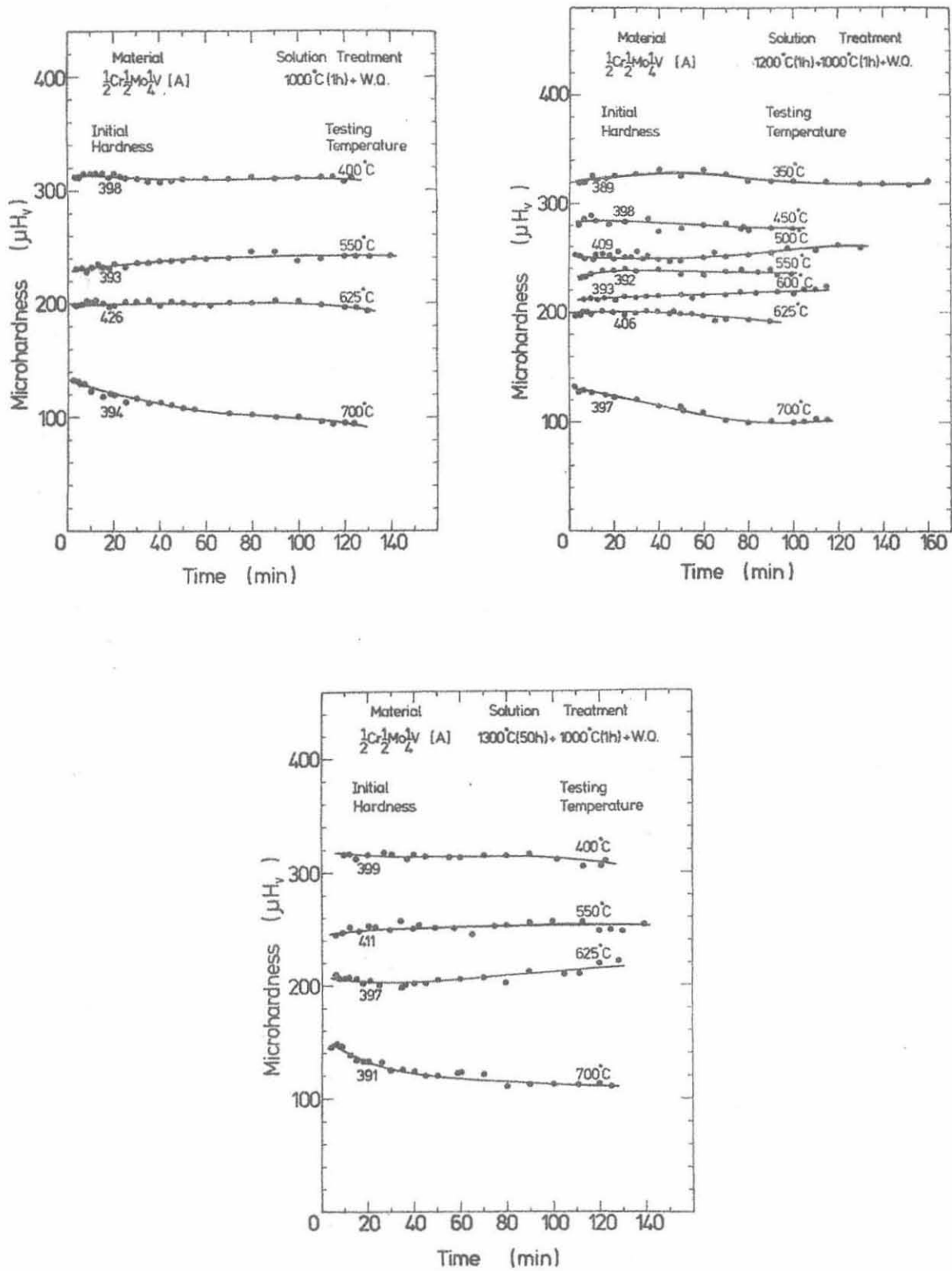


Figure 17. Elevated temperature hardness of specimens of sample A for various solution treatments.

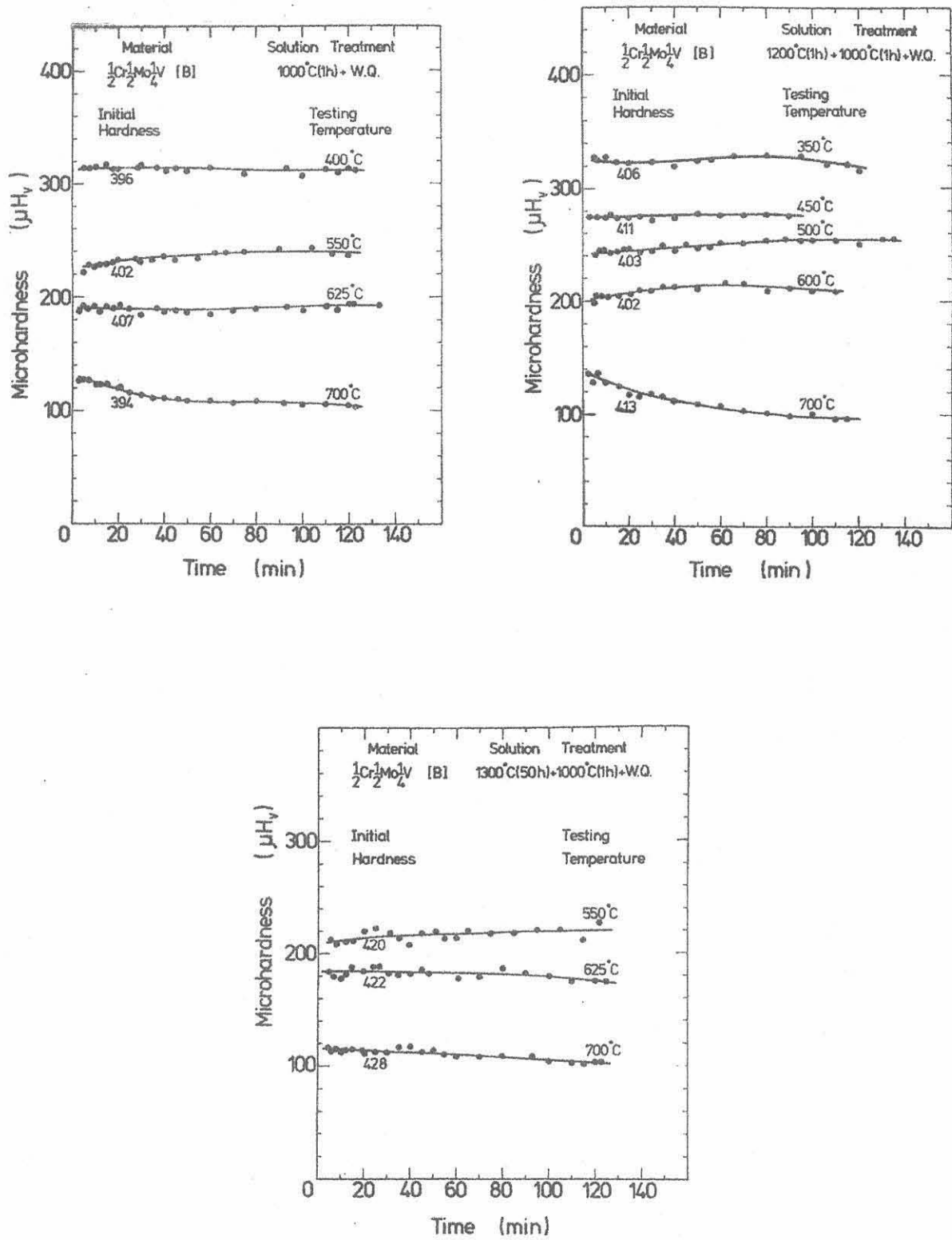
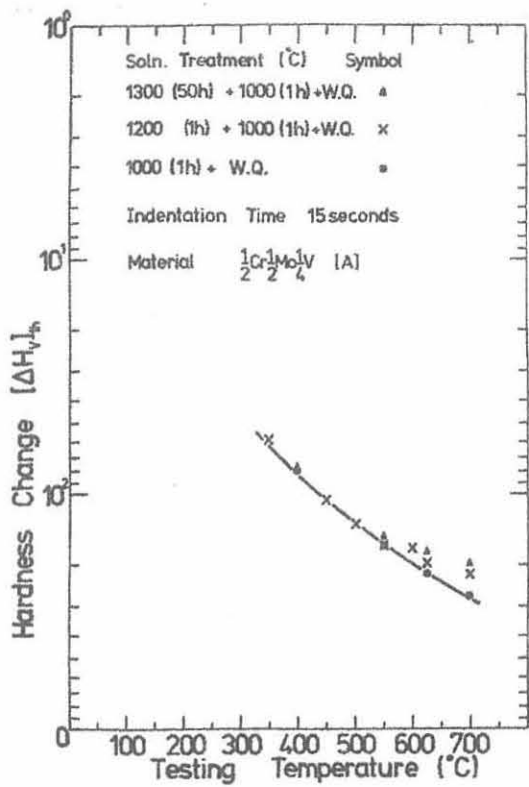
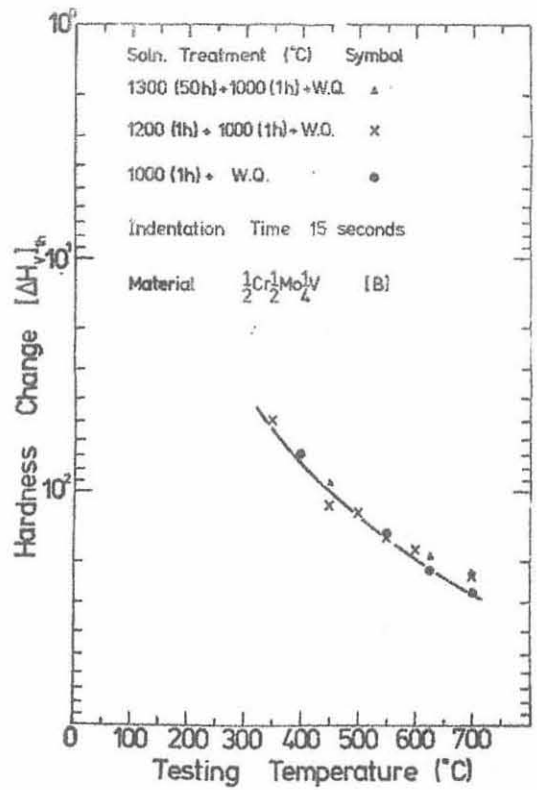


Figure 18. Elevated temperature hardness of specimens of sample B for various solution treatments.



(a)



(b)

Figure 19. Isochronal elevated temperature micro-hardness for samples A and B.

(a) $\frac{1}{2}\text{Cr}\frac{1}{2}\text{Mo}\frac{1}{4}\text{V}$ A

(b) $\frac{1}{2}\text{Cr}\frac{1}{2}\text{Mo}\frac{1}{4}\text{V}$ B

CHAPTER III

The Uniaxial Tensile Mechanical Properties of Commercial
'susceptible' and 'non-susceptible' $\frac{1}{2}\text{Cr}$ $\frac{1}{2}\text{Mo}$ $\frac{1}{4}\text{V}$ Steel
at Elevated Temperatures

3.1 Introduction

The tensile test enjoys its wide popularity for the evaluation of mechanical properties because the stress-state of uniaxial tension is particularly simple. In chapter two it was shown that the assessment of susceptibility to SRC through the measurement of flow properties at ambient and elevated temperatures, as observed during hardness testing, was inconclusive. In this chapter, work is described which attempts to relate the elevated temperature flow and ductility properties of the two commercial steels as observed during uniaxial tensile testing, with their respective susceptibilities to SRC. In this regard, particular attention is paid to the loss of ductility associated with failure by intergranular cavitation.

Stress fields associated with inhomogeneities, such as necking, void opening and Luders Band propagation during tensile deformation at ambient temperatures have been fairly well documented¹⁵⁸⁻¹⁶⁰. At elevated temperatures extra consideration needs to be paid to the importance of applied strain rate, and the way in which it affects the flow and ductility properties. The importance of strain rate sensitivity (see figure 20) at elevated temperatures was first clearly indicated by Nadai and Manjoine¹⁶¹. More detailed discussion of the assessment and effects of strain rate sensitivity within the present investigation is presented in chapter four. There

theoretical work¹⁶² is mentioned in which the main conclusion is that the problems of tensile plastic instability (necking) and tensile fracture behaviour in materials with low strain rate sensitivities, impose severe restrictions on the characterisation of deformation behaviour through tensile testing, since it is not generally possible to obtain reliable results on the steady state stress at a given strain rate.

It would appear that such difficulties and complications connected with the hot tensile test, essentially reduce any direct association between deformation and final failure behaviour to the level of a qualitative comparison. Previous work on low alloy steels, employing high temperature tensile tests¹⁶³ and stress relaxation tests at constant heating rates⁵⁴, have failed to produce an agreed mechanical parameter to characterise stress relief cracking. However, these results may well be inconclusive because there was:

- (a) inadequate appreciation of the limitations of the various forms of tensile test; and
- (b) no attempt to reduce the number of microstructural variables through controlled heat treatment.

It was with these two points in mind that the following programme of tensile testing was undertaken.

3.2 Experimental Details

Hounsfield No.13 double shouldered tensile specimens were machined from the samples of steam pipe. In view of the size of the programme involving approximately 500 tensile specimens, it

was decided to perform batch solution heat treatments in a specially constructed 316 stainless steel vacuum furnace*. The furnace design allowed the control thermocouple to be located inside the chamber adjacent to the specimen heating area. Heating was achieved by the use of 'Crusilite' † furnace elements which were placed above and below the chamber, transverse to its longitudinal axis. A procedure of trial and error in the positioning of the eight elements, finally allowed the achievement of a hot zone region about 100 mm long with a temperature variation within $\pm 2^{\circ}\text{C}$ at 1000°C , and $\pm 4^{\circ}\text{C}$ at 1200°C . The temperature control was effected by the use of a West-Guardian 30 Amp proportional controller.

The furnace was heated to the required temperature, the specimens loaded, and the chamber evacuated. Then, dry high purity argon was admitted and the system was re-evacuated. This flushing procedure was repeated three or four times at the beginning and periodically during the course of the heat treatment. Double solution treatments (as described in chapter two) were carried out without removing the specimens from the chamber, simply by readjusting the control temperature level. The lower temperature in these instances was only achieved after about 5 to 10 minutes. Before water quenching the vacuum system was closed off and argon admitted. The flow of argon was allowed to continue even while the door was opened and the specimens removed. In this way

* The assistance of the Engineering Department, University of Cambridge and the Welding Institute in performing the welding and final machining of this chamber is gratefully acknowledged.

† Tradename of the Morganite Electroheat Co.Ltd.

oxidation was kept to a minimum and rapid specimen removal and quenching rates were achieved.

Tensile testing at elevated temperatures was carried out using a MAND screw driven testing machine. A specially constructed 'suitcase-type' furnace was employed as shown in the general view of the experimental arrangement in figure 21. 'Crusilite' elements were also used in this furnace and power control was effected by an SKL 12 Amp proportional controller. As shown in figure 22 both the control and temperature monitoring thermocouples were located adjacent to the specimen during a test. The collet type hounsfield grips were machined from Nimonic 80 A. The arrangement, as shown, allowed specimen heating rates of the order of 80°C per minute to be achieved. Temperature was maintained to within $\pm 1^{\circ}\text{C}$ along the gauge length of the specimen and within $\pm 2^{\circ}\text{C}$ of the control level for the duration of the test.

The MAND screw driven testing machine employs a continuously variable speed motor to drive a single loading screw. Crosshead motion was measured indirectly by electrically monitoring the movement of the screw and feeding the signal to a chart recorder, the chart drive of which was activated in direct response to this signal from the screw movement monitoring system. The signal from the load cell was fed to the pen drive system such that a record of load against crosshead movement was produced directly for each test. All of the tests were carried out in air.

3.3 The Effect of Prior Solution Treatment upon the Tensile Mechanical Properties of $\frac{1}{2}\text{Cr}$ $\frac{1}{2}\text{Mo}$ $\frac{1}{4}\text{V}$ at Elevated Temperatures

Tensile tests were carried out in an attempt to examine the hypothesis that the degree of precipitation of vanadium carbide (as controlled by appropriate solution treatment) should bear a direct relation with the promotion of intergranular failure through a grain strengthening effect. Batches of tensile specimens from both samples A and B were solution treated as follows;

- (i) 1200°C (1h) + W.Q.
- (ii) 1200°C (1h) + 1000°C (1h) + W.A.
- (iii) 1000°C (1h) + W.Q.

All specimens were examined for distortion after quenching and those found to be distortion free were cleaned with emery paper along the gauge length, and hardness measurements were then made on one end. Any specimen having an as quenched hardness outside the range 390 - 410 VPN was rejected. Tensile tests were carried out as described in section 3.2 at a nominal strain rate of $7.5 \times 10^{-4} \text{ min}^{-1}$. In a few instances the test was stopped immediately prior to final failure, and the specimen broken open in liquid nitrogen in order to allow direct examination of cavitated boundaries.

Figure 23 compares the tensile mechanical properties of the two samples after single solution treatment at 1200°C.

Several points are apparent:

- (a) The observed values of flow stress as a function of temperature are similar for both samples.
- (b) There is a marked drop in observed ductility for both

samples above 450°C.

- (c) This latter effect would appear to be rather more severe in sample B which exhibits a reduction of area of 10% at 450°C, as against 43% for sample A, followed by more or less complete loss of ductility for temperatures above 500°C.
- (d) Two other ductility minima appear at temperatures of about 150°C and 350°C respectively. These latter minima are not as severe as that occurring above 450°C.

Figure 24 compares the tensile mechanical properties of both samples after single solution treatment at 1000°C, for testing temperatures in the region 250°C to 700°C. It would appear that:

- (a) The values of flow stress as a function of temperature are similar to those observed in specimens which had been single solution treated at 1200°C.
- (b) Values of percentage elongation to failure for both samples in this condition of prior solution treatment, show troughs in the region of 350°C and above 450°C.
- (c) The ductility of sample A in this condition of prior solution treatment is significantly improved with respect to that observed after single solution treatment at 1200°C.
- (d) The ductility of sample B in this condition of prior solution treatment though improved is still low in the temperature region 500°C to 600°C.

- (e) The form of the ductility behaviour of both samples above 450°C is more clearly trough-like in appearance.

Figure 25 compares the tensile mechanical properties of samples A and B after double solution treatment at 1200°C for one hour plus 1000°C for one hour. As shown in chapter two this condition of prior solution treatment allows the attainment of a prior austenite grain size, similar to that observed after single solution treatment at 1200°C combined with a degree of supersaturation of alloy carbide similar to that observed after single solution treatment at 1000°C . The main points to be noted are that:

- (a) The observed levels of flow stress are similar to those achieved in the tensile tests discussed previously.
- (b) For the range of temperatures investigated there appears to be a marked reduction of ductility above 450°C .
- (c) The form of the ductility behaviour of both samples more closely approximates to that of the specimens which had been single solution treated at 1200°C , in that there is no marked trough effect above 450°C .

This latter point is emphasised by figure 26 which compares the percentage elongation to failure of specimens after prior solution treatment at 1200°C with those after prior solution at 1200°C plus 1000°C . Clearly, the double solution treatment has imparted an improved tensile ductility at temperatures of 450°C and above. As shown in section 3.6 the failure mode in this temperature region, for all of the tests performed,

was by intergranular cavitation along prior austenite grain boundaries.

In summary, these observations have shown that:

- (i) For temperatures in excess of 250°C there are two ductility troughs at about 350°C and above 450°C .
- (ii) The most severe loss of ductility associated with failure by intergranular cavitation occurred above 450°C in specimens which had been single solution treated at 1200°C for one hour.
- (iii) The improvement in ductility above 450°C in specimens subject to solution treatments at
 - (a) 1000°C for one hour, and
 - (b) 1200°C (1h) plus 1000°C (1h)was not associated with any marked reduction in the levels of flow stress.
- (iv) In the context of stress relief cracking the evidence so far presented does not allow clear differentiation between sample A (non-susceptible) and sample B (susceptible) in terms of their relative susceptibilities.

The following sub-sections examine more closely the way in which the factors of flow stress, work hardening behaviour and prior austenite grain size act to promote reduced ductilities during the failure of $\frac{1}{2}\text{Cr } \frac{1}{2}\text{Mo } \frac{1}{4}\text{V}$ by intergranular cavitation.

3.4 Observations of the Work Hardening Behaviour during Elevated Temperature Tensile Testing

In the introduction to this chapter it was mentioned that the problem of tensile instability imposes severe restrictions upon the characterisation of deformation behaviour through tensile testing because of the loss of ductility which results after the onset of strain localisation and neck formation. In the present study, attention was directed towards the possible effects of such behaviour in promoting low ductility in association with unstable final failure by intergranular cavitation. An attempt to assess the extent of this behaviour was made, in the first instance, through a simple analysis of work hardening behaviour of samples A and B in the various conditions of prior solution treatment, as a function of temperature. The combined effects of strain-rate hardening and work hardening are discussed in chapter four.

The load-deflection records made during tensile testing were transformed to true stress-true strain and plotted on a log-log basis, as shown in figure 27. Least squares analysis of the above data for each specimen, allowed curve fitting of the stress-strain response according to the expression:

$$\sigma_t = \sigma_o \epsilon_t^n \quad (3.1)$$

where:

σ_t = applied true stress

ϵ_t = true strain

σ_o = extrapolated flow stress at 100% true strain

n = work hardening exponent.

In this way, values of σ_o and n were generated as a function of

temperature, for each sample in the various conditions of prior solution treatment.

Figure 28 compares the measured temperature dependence of σ_0 and n for samples A and B in three conditions of prior solution treatment. The correlation coefficients for each of the least squares determinations of n were in excess of 0.9900, many were in excess of 0.9990.

However, to further establish the limits of validity for these parameters over the range of temperatures investigated, the values of n and σ_0 for a particular test were used to calculate a value for the U.T.S. according to:

$$\text{U.T.S.} = \frac{\sigma_0 n^n}{\exp(n)} \quad (3.2)$$

The derivation of equation (3.2) is given in Appendix I. The value of U.T.S. thus calculated was then compared with the experimentally measured value as shown in figure 29. The lines drawn through the points are the best straight lines estimated through least squares analysis. The equations of these lines are:
For sample A:

$$\begin{aligned} (\text{Calc.U.T.S.}) &= 1.007053 (\text{Exp.U.T.S.}) + 18.91 \text{ MN m}^{-2} & (3.3) \\ &(\text{correlation coefficient } r = 0.998105) \end{aligned}$$

For sample B:

$$\begin{aligned} (\text{Calc.U.T.S.}) &= 1.032722 (\text{Exp.U.T.S.}) - 2.72 \text{ MN m}^{-2} & (3.4) \\ &(\text{correlation coefficient } r = 0.998426) \end{aligned}$$

In the context of the general limitations of tensile data the results of figure 29 and equations (3.3) and (3.4) provide some confidence for qualitative discussion of the temperature dependence

of σ_0 and n shown in figure 28.

The first observation to be drawn from figure 28 concerns the temperature variation of σ_0 in the samples. For sample A it is apparent that values of σ_0 measured in specimens which had been subject to differing solution treatments, converge at temperatures above about 350°C. If the value of σ_0 is taken as a measure of the general stress level achieved within a tensile specimen this observation may be interpreted as further support in the argument to refute the hypothesis that variation in ductility bears a direct relation to the elevated temperature flow stress. Furthermore, the form of σ_0 versus temperature is similar to that of hot hardness in that there does not appear to be any evidence of a 'secondary hardening' peak.

The results for sample B differ in that, as temperature is increased, the σ_0 -temperature curve for specimens which had been single solution treated at 1200°C remains below the curves for specimens which had been subjected to the other solution treatments. At first sight, this evidence would appear to be totally contrary to any form of strengthening argument in promoting reduced ductility. It must be regarded in the light of possible deformation mechanisms at elevated temperatures. Consider first, the relationship between n and σ_0 , as shown in figure 27. It may be understood that, as the slope, n , of the straight line is reduced, so the value of the intercept, σ_0 , will be similarly reduced. It is clear from figure 28(b) that the n values for the specimens which had been solution treated at 1200°C for one hour are lower than n values for other specimens of sample B.

At ambient temperatures when plastic deformation of metals occurs largely by dislocation glide mechanisms the value of n reflects the extent which the stress required to cause continued plastic deformation is increased as the glide process becomes impeded (at increased strain) through a variety of possible strain hardening mechanisms involving dislocation-dislocation interactions, dislocation-precipitate interactions and dislocation-boundary interactions. In this way a low value of n measured under these conditions of deformation is indicative of a reduced resistance to dislocation motion within the matrix grains, since a given stress increment will produce a larger strain increment. As the temperature is increased, other mechanisms of deformation play an increasingly important role. The work of Ashby and his co-workers^{167,168,169} in developing the concept of 'deformation mechanism maps' is extremely important in this context. It is clear from the theoretical treatment by Crossman and Ashby¹⁶⁹ that deformation mechanisms like diffusional creep, grain boundary sliding and dislocation creep which predominate at increased temperatures are rather more viscous in nature than dislocation glide. During the deformation of a perfectly viscous material, the stress required for continued deformation does not increase with increased strain, but remains constant for a constant applied strain rate. Under these conditions, n would be zero. It seems reasonable to suppose therefore that a decrease in the value of the work hardening exponent at elevated temperatures is associated with an increase in the viscous components which are contributing to the deformation process.

A clear feature of the temperature response of the work hardening exponent in both samples is the occurrence of two troughs. The magnitude of these troughs is greatest in specimens of sample B which had received the single solution treatment at 1200°C for one hour. The position of these troughs appears to be very similar to the ductility troughs discussed previously. In the case of the lower temperature, the correlation is understandable in the context of the observed failure mode of the plastic growth and coalescence of voids in association with large inclusions¹⁶⁰. For the upper temperature, at which the failure mode was intergranular cavitation, the importance of the temperature response of the work hardening exponent needs to be discussed in terms of the way in which it reflects changes in deformation mode which promote the onset of intergranular failure. In this respect it seems most reasonable to continue the 'weakest link' argument developed previously. It would appear that in this temperature region, deformation by dislocation glide become increasingly difficult with respect to the more viscous modes. In view of the conditions of temperature, stress and strain rate imposed, it is reasonable to suppose that grain boundary sliding (see ref. 168) will take preference.

As discussed in chapter one, boundary sliding is recognised as a necessary prerequisite of intergranular cavitation. It is noted that the above argument concerning the temperature response of the work hardening exponent has implied that deformation by dislocation glide is impeded. The measured stress levels are not increased since it is proposed that other deformation

mechanisms are operative, with grain boundary sliding predominating at the higher temperatures.

In summary, examination of the work hardening behaviour of the samples A and B suggests that a reduction of the work hardening exponent, n , occurs in the region of the ductility trough associated with unstable failure by intergranular cavitation. It would appear that such reduction is greatest in sample B, after single solution treatment at 1200°C . This observation has been briefly discussed in terms of the way in which it reflects the possible relationship between operative deformation modes in the promotion of unstable failure by intergranular cavitation. In chapter four further discussion is made concerning the reduction of the stability of tensile deformation associated with reduced n values and the way in which this factor may be associated with reduced ductility during unstable failure by intergranular cavitation.

3.5 The Effect of Prior Austenite Grain Size upon the Tensile Mechanical Properties at Elevated Temperatures

The work described in this section was carried out in an attempt to examine the effects of prior austenite grain size, independent of the carbide supersaturation effects presented previously.

The approach to the achievement of this condition has been discussed at length in chapter two. There it was shown how by the use of a double solution treatment, a similar degree of solution of vanadium carbide could be achieved in specimens having a range of prior austenite grain sizes. Accordingly,

batches of tensile specimens were solution treated in the following manner:

- (i) 1200°C (1h) + 1000°C (1h) + W.Q.
- (ii) 1150°C (1h) + 1000°C (1h) + W.Q.
- (iii) 1100°C (1h) + 1000°C (1h) + W.Q.
- (iv) 1050°C (1h) + 1000°C (1h) + W.C.
- (v) 1000°C (1h) + W.Q.

The grain size variation achieved in both samples A and B has been summarised in figure 11. Tensile tests were carried out at a strain rate of $7.5 \times 10^{-4} \text{ min}^{-1}$ and restricted to the temperatures of 500°C and 550°C, since the previous series of tests had indicated that these conditions were favourable to the promotion of failure through intergranular cavitation. Figure 30 compares the tensile mechanical properties of samples A and B as a function of prior austenite grain size at the temperatures of 500°C and 550°C.

It appears that at both temperatures the flow stress levels are slightly lower in sample B than in sample A. However, the ductility of sample B is, for the range of grain size investigated, lower than that of sample A, though this effect is more marked at 500°C than at 550°C. Examination of the response of the various flow stress parameters and values of work hardening exponent to variation in grain size is restricted mainly to the 550°C data. At 500°C, this response is ostensibly independent of grain size for all of the above measures in both samples. While at 550°C, particularly for sample B, both the flow stress parameters and the work hardening exponent are seen to increase

with increase of prior austenite grain size. In an investigation of the relationship between 0.1% flow stress and grain size under conditions in which grain boundary sliding was the dominant mode of deformation¹⁷⁰, a similar increase of flow stress with increased grain size was observed, and was attributed to a reduced contribution from grain boundary sliding due to the reduced amount of grain boundary area.

In the present work this same conclusion is further supported by the behaviour of the work hardening exponent at 550°C, particularly in sample B, which is seen to show an apparent increase with increase of prior austenite grain size. This observation, taken in conjunction with the observations and discussion of the previous section, suggests a decreased contribution to the overall deformation at 550°C through a viscous mechanism like grain boundary sliding, as the prior austenite grain size is increased. At 500°C it would appear that for the testing conditions employed, the contribution to the deformation process through the grain size dependent, grain boundary sliding is low. The response of the work hardening exponent as a function of grain size in sample A at 550°C differs in two major respects from that of sample B. Firstly, in the region where the grain size ranges for samples A and B overlap, the values for sample A appears to be consistently above those of sample B. Secondly, it would appear that for the finer grain size specimens of sample A the work hardening exponent increases with decreased grain size. These observations, taken in conjunction with the differences of ductility - grain size responses of the samples, point to the possible

influence which deformation behaviour imposes upon the development of failure by intergranular cavitation, in these materials.

Consider the region of overlap of the grain size ranges. The increased values of work hardening exponent for sample A may be taken as indicative of an increased contribution to flow through dislocation glide. This implies that stress intensification at boundaries caused through grain boundary sliding is either reduced through reduced grain boundary sliding or more easily relaxed through matrix deformation by dislocation glide or both. This behaviour is reflected by the increased ductility of sample A at 550°C. Notice that this interpretation has not invoked the concept of increased grain strength in promoting reduced ductility. If anything, the evidence would suggest that the more ductile sample A is stronger than sample B. Instead, attention has been directed towards the way in which various operative deformation modes may contribute to the process of unstable failure by the growth of intergranular cavities.

Most important for consideration in this latter respect is the fine grained region of sample A. It may be supposed that, consistent with the previously developed argument, a continuous decrease of grain size should be accompanied by a continuous increase of the contribution to deformation through grain boundary sliding. The observed response of the 0.2% proof stress at fine grain sizes would seem to support this contention¹⁷⁰. The observed increase of the work hardening exponent in this region would appear at first to be contrary to this view. However, it may be envisaged that as the fine grained body deforms through

grain boundary sliding, accommodation of the strain required to maintain grain compatibility will be gained through matrix deformation. The achievement of this accommodation will depend essentially upon the resistance to the growth of cavities (by whatever mechanism). This growth might be expected to depend upon four major factors:

- (a) temperature (for diffusion controlled growth)
- (b) grain size (which may control the magnitude of stress concentration due to sliding)
- (c) boundary purity (which may reduce growth by mechanical failure)
- (d) deformation mechanism (which may allow plastic growth)

The third of these factors is discussed in more detail in chapter seven. As discussed in chapter one, diffusion controlled growth is most likely to dominate under conditions of high temperature, low stress and low strain rate. The effect of the second factor in fine grained material is crucial, since it allows significant strain to be achieved without the large stress intensification associated with a long boundary¹²⁹. Furthermore, it has been recognised⁸¹ that triple points provide barriers to continued cavity growth, so that a fine grained specimen would be expected to be inherently tougher than a coarse grained specimen.

Taken in conjunction with the condition requiring grain compatibility, it is clear that the first three factors act together to place importance upon the final factor concerning deformation mechanism, particularly in the context of a fine grained specimen. It is proposed therefore, that the observed increase of work

hardening exponent in fine grained specimens of sample A reflects the tendency of the material in this condition to exhibit increased matrix deformation in an attempt to maintain grain compatibility in the face of a large contribution to the strain through grain boundary sliding. The observed increase of ductility in sample A, with decreased grain size is therefore not simply associated with the lowering of the observed flow stress but more importantly with a change of deformation behaviour which itself causes a change in the conditions promoting unstable failure by intergranular cavitation. This situation is similar to that observed by Fleck et al¹³⁰ for the hot ductility behaviour of an industrial copper based alloy (figure 7).

The presentation of the tensile mechanical properties of the two samples in this manner has allowed some insight to be gained in regard to the possible reasons for the observed susceptibility of sample B to stress relief cracking. Clearly, the importance of prior austenite grain size has been underlined. Furthermore, the ideas of grain strengthening discussed in chapter one have been modified to give a more realistic interpretation of the close association between deformation and ductility during unstable failure by intergranular cavitation.

3.6 Fractographic Examination of Specimens Deformed at Temperatures of 400°C and above

This section describes the main features of the failure mode associated with the observed tensile ductility minima above 400°C. Brief discussion is made of the applicability of currently accepted theories of failure by intergranular cavitation to these

observations.

Figure 31 illustrates the situation within the necked region of a specimen of sample B (solution treated at 1200°C for one hour) after deformation at 400°C just prior to final failure. The primary mode of failure is clearly the plastic growth and coalescence of voids, presumably formed around large inclusions. Closer examination reveals the formation of an intergranular cavity to the right of the main region of ductile failure. Figure 32 illustrates this cavity at higher magnification, which shows that the growth was associated with marked plastic deformation of the matrix and that it occurred on a boundary close to 45° to the tensile axis. The ductility of sample B under these conditions was 43% reduction of area.

Figure 33 illustrates cavitated boundaries in sample B (after prior solution treatment at 1200°C for one hour) formed during deformation at 450°C and 700°C. The ductility of sample B at these temperatures was respectively 10% reduction of area and less than 0.2%. Those photographs marked (a), (b) and (c) were taken during examination of a specimen which had been broken open in liquid nitrogen after having been deformed to a stage immediately prior to final failure at 450°C. At low magnification, these cavitated boundaries appear smooth in both cases. However, at higher magnification it is clear the surfaces are in fact pitted with very small voids. An estimate of the mean linear radius of these voids gave:

$$\bar{r}_{450} = 0.17 \mu\text{m}$$

$$\bar{r}_{700} = 0.30 \mu\text{m}$$

Figure 34 illustrates cavitated boundaries in sample A (after prior solution treatment at 1200°C for one hour) formed during deformation at 500°C and 700°C. The ductility of sample A at these temperatures was respectively 7% reduction of area and 2% reduction of area. The failure mode in all specimens of sample A tested below 500°C was by the plastic growth and coalescence of voids like that shown in figure 31. It is notable in this respect that the ductility of sample A in this condition, at 450°C was 43% reduction of area (Cf. 10% for sample B).

Examination of figure 34 suggests that the cavitated boundaries formed at 500°C are smooth. There appears to be some evidence of voids near the large inclusion in the centre of micrograph 34(c), but this does not appear to be wide spread. The boundaries formed at 700°C are clearly covered with large voids. The mean linear radius of these latter voids was estimated to be:

$$\bar{r}_{700} = 3.20 \mu\text{m}$$

As discussed in chapter one, the nucleation of cavities upon boundaries during high temperature tensile deformation occurs heterogeneously in association with grain boundary particles or ledges. It is essentially stress controlled such that a nucleus becomes stable when it has reached a critical size given by an equation like (1.3):

$$r_c = \frac{2\gamma}{\sigma} \quad (1.3)$$

It can be seen that for a high applied stress (at low temperature), or low surface energy, the critical nucleus size should be reduced. According to most theoretical treatments, discussed in chapter one, the growth of a stable nucleus is diffusion controlled such that

higher rates of growth might be expected to occur at high temperatures. The final failure is thought to occur when the growing cavities cover a certain area fraction of the grain boundaries. This is the basis of the model developed by Raj and Ashby¹¹⁶ to predict a minimum ductility (rupture life) at an optimum condition of nucleation and growth. This model was represented schematically in figure 6.

For sample A, figure 34, it would appear that the situation outlined in figure 6 is roughly adhered to. In this respect, it may be argued that the ostensibly smooth appearance of the facets formed at 500°C is due to the fact that the numerous nuclei are too small and finely spaced to be resolved by the scanning electron microscope. However, for those cavitated boundaries formed at 700°C, fewer nuclei have been produced, but they have grown sufficiently to be clearly visible during microscopic examination. The ductility behaviour of sample A (single solution treated at 1200°C) is quite clearly trough like in the temperature region 500°C to 700°C, as shown in figure 28.

For sample B, figure 33, the situation is clearly quite different. To begin with the ductility behaviour, illustrated in figure 28 does not show any minimum. The ductility of sample B (single solution treated at 1200°C) is vanishingly small for all temperatures above 500°C. The size of the voids on the cavitated boundaries formed at 450°C is only slightly lower than that of those formed at 700°C. This observation suggests that the nucleation of the voids in this temperature region remains relatively high even when the stress is low. Furthermore,

the fact that voids on the boundaries of the specimen deformed at 450°C are resolvable by SEM* suggests that the rate of growth at this relatively low temperature was in fact high.

It is tempting to relate this modified state of affairs to a lowering of the surface energy term of equation (1.3) due to the increased impurity content of sample B^{75,102}. In this way, the nucleation of cavities would become more highly dependent upon surface energy and therefore less temperature dependent. If high rates of nucleation are maintained at high temperatures then ductility would remain at a low level, as observed. This situation is illustrated schematically in figure 35. The cavitation observed to occur at 400°C in sample B may be taken as further evidence of the relative ease of cavity nucleation in this sample. However it would appear that the mode of growth (at 45° to the applied tensile stress) is influenced to a greater degree by the plastic deformation of the surrounding matrix regions.

Examination of the intergranular cavitation which occurs in fine grained sample A (after prior solution treatment at 1000°C for one hour) at 700°C indicates that much of the opening of cavities prior to final failure is also associated with deformation of the surrounding matrix regions. This situation is illustrated in figure 36. It is clear that a large contribution to the strain to final failure in specimens of sample A in this condition is due to the opening of the large number of cavitated boundaries prior to final failure. As explained on page 75 this condition arises partly because of the way in which the increased

* Scanning Electron Microscopy

number of triple points in a fine grained material act to provide barriers to continued cavity growth⁸¹. Figure 37 compares the cavitation behaviour of samples A and B at 600°C (both after prior solution treatment at 1000°C for one hour). The ductilities were respectively 24% and 2% reduction of area. The grain size of sample B in this condition is coarser than that of sample A. This cavitation in sample B, more closely approximates to that observed during the failure of the coarse grained specimens, as does the ductility.

No detailed quantitative metallography of the fracture surfaces of the double solution treated specimens was made. However, reasonable explanation for the observed ductility improvement in these specimens over that observed in specimens which had been single solution treated at 1200°C (figure 27), will probably involve a change in the density of suitable cavity nucleation sites as well as the temperature dependence of the nucleation rate. This is so since there was no significant difference in either grain size or flow stress level.

3.7 Summary

The work described in this chapter has established:

- (i) That the ductility of commercial $\frac{1}{2}\text{Cr}$ $\frac{1}{2}\text{Mo}$ $\frac{1}{4}\text{V}$ steel during unstable tensile failure by intergranular cavitation, does not bear a direct relation with the observed levels of flow stress.
- (ii) That for grain sizes of less than 100 μm , the prior austenite grain size of commercial $\frac{1}{2}\text{Cr}$ $\frac{1}{2}\text{Mo}$ $\frac{1}{4}\text{V}$ steel exerts a significant influence upon the ductility

during unstable tensile failure by intergranular cavitation.

Furthermore, the results have suggested:

- (i) That variation of the degree of supersaturation of vanadium carbide achieved in these commercial samples prior to testing did not **cause** any marked change in elevated temperature flow stress.
- (ii) That the stability of tensile deformation as assessed through work hardening behaviour is low in the region of the ductility minima associated with unstable failure by intergranular cavitation.
- (iii) That a fine prior austenite grain size inhibits intergranular cavity propagation rather than initiation, such that the ductility of the material in this condition reflects its ability to resist unstable strain localisation of the intercavity regions during final failure.
- (iv) That the ductility of coarse prior austenite grain size material is largely dependent upon the conditions which promote the nucleation of intergranular cavities. Finally it would appear that the susceptibility of

sample B to SRC is:

- (i) The result of its achieving a larger prior austenite grain size than that of sample A after equivalent solution treatment.
- (ii) The result of its prior austenite grain boundary structure providing more suitable sites for the easy nucleation of intergranular cavities, than that of sample A, after equivalent solution treatment.

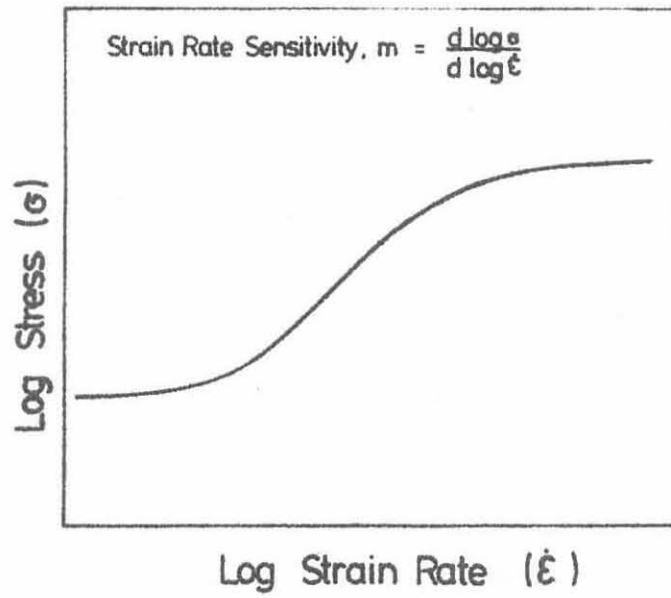


Figure 20. Schematic plot of flow stress as a function of strain rate, showing a maximum of slope at intermediate values of strain rate.

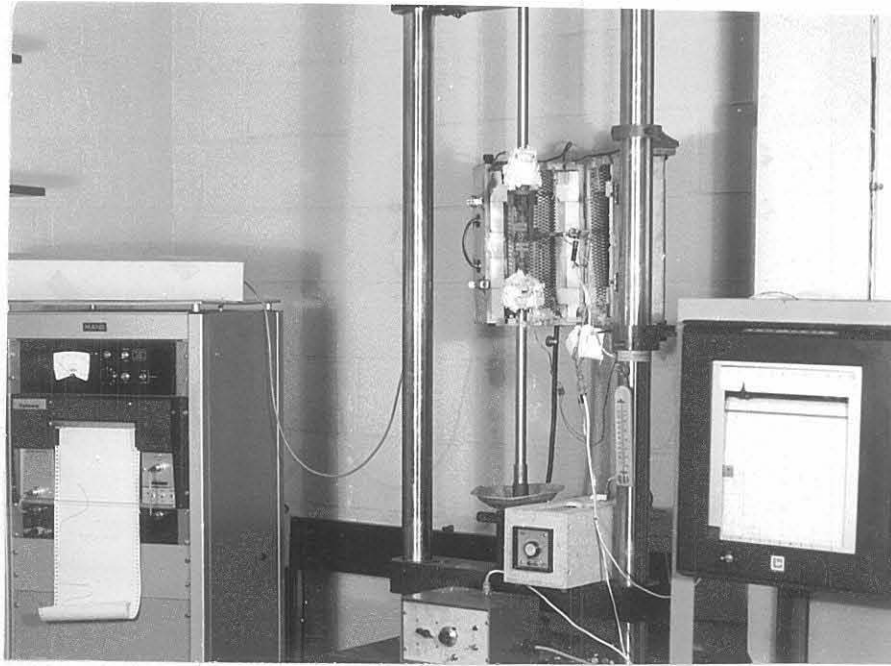


Figure 21. General view of experimental rig
used for rising load tensile testing.

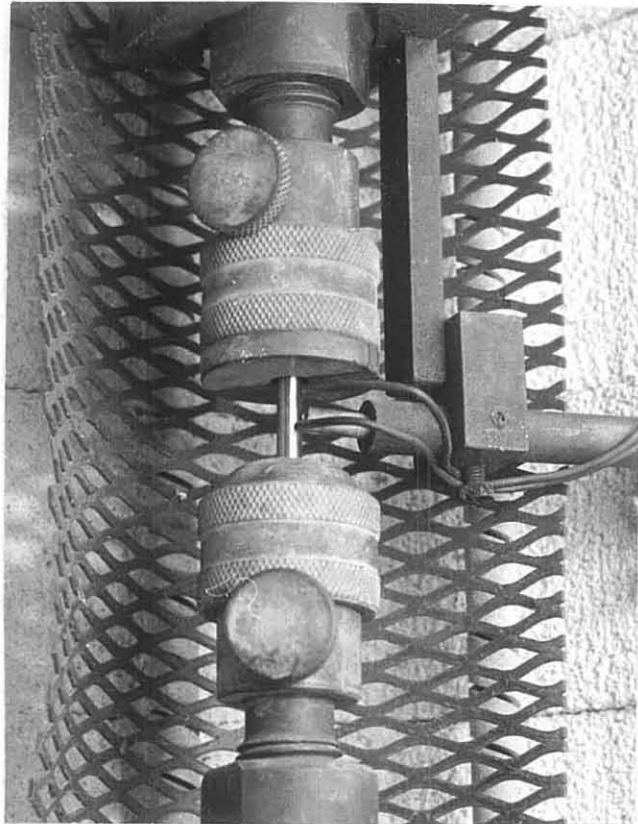
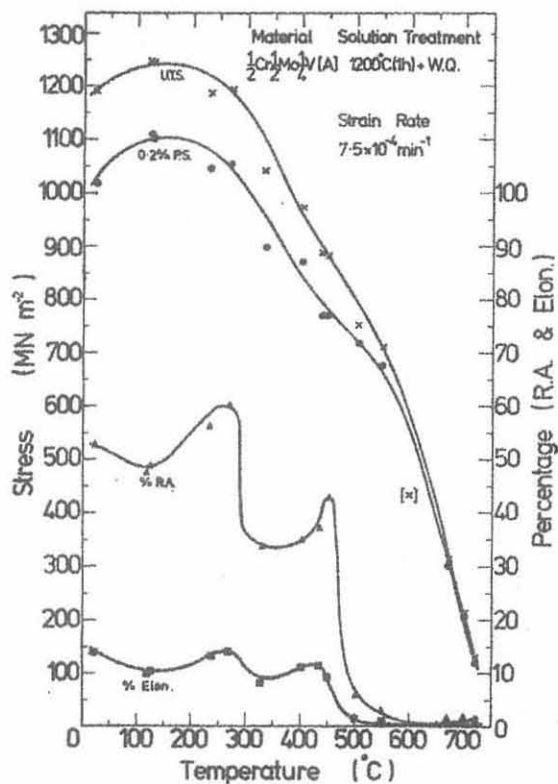
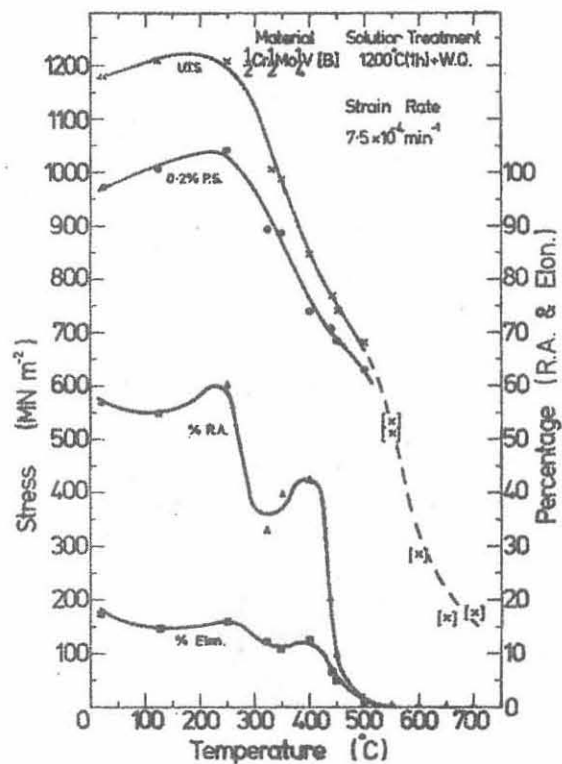


Figure 22. Location of measuring thermocouples
above and below the control thermocouple.

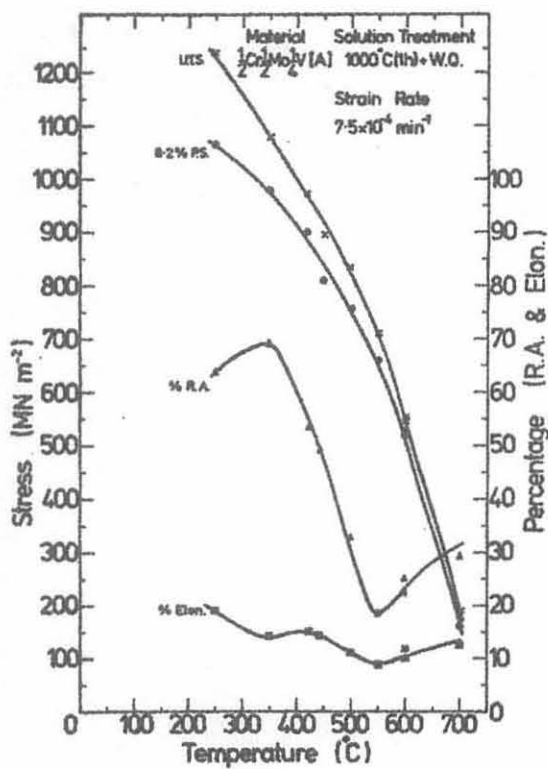


(a)

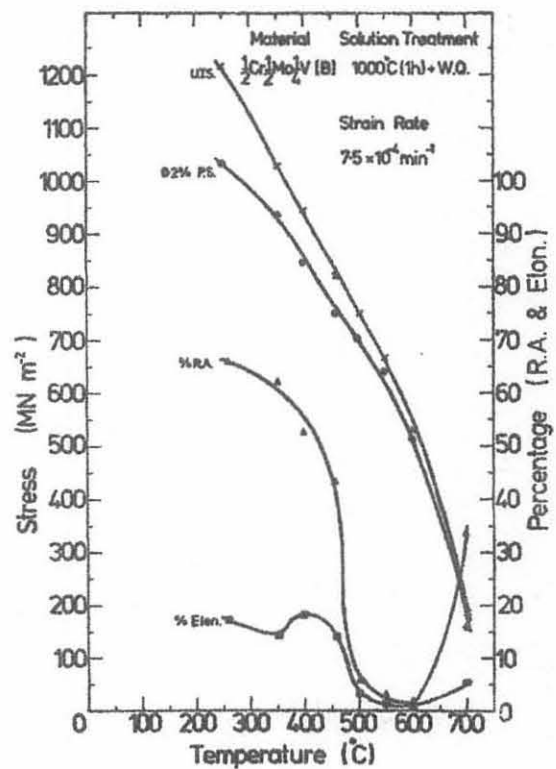


(b)

Figure 23. (a) Tensile mechanical properties of $\frac{1}{2}\text{Cr}|\frac{1}{2}\text{Mo}|\frac{1}{4}\text{V}$ A
 (b) Tensile mechanical properties of $\frac{1}{2}\text{Cr}|\frac{1}{2}\text{Mo}|\frac{1}{4}\text{V}$ B
 after single solution treatment at 1200°C for
 one hour, as a function of temperature.

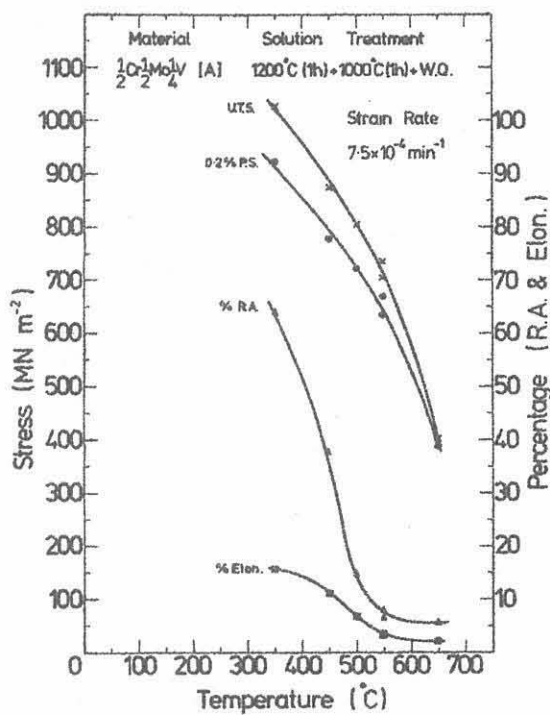


(a)

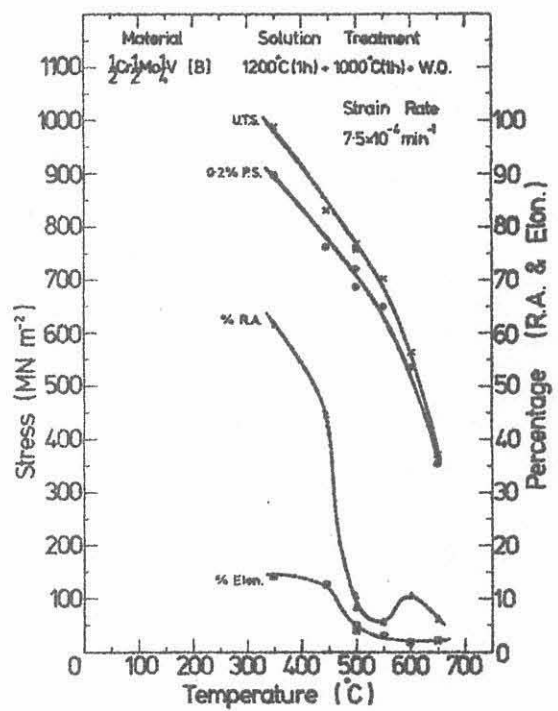


(b)

Figure 24. (a) Tensile mechanical properties of $\frac{1}{2}\text{Co}/\frac{1}{2}\text{Mo}/\frac{1}{4}\text{V}$ A
 (b) Tensile mechanical properties of $\frac{1}{2}\text{Co}/\frac{1}{2}\text{Mo}/\frac{1}{4}\text{V}$ B
 after single solution treatment at 1000°C for
 one hour, as a function of temperature.

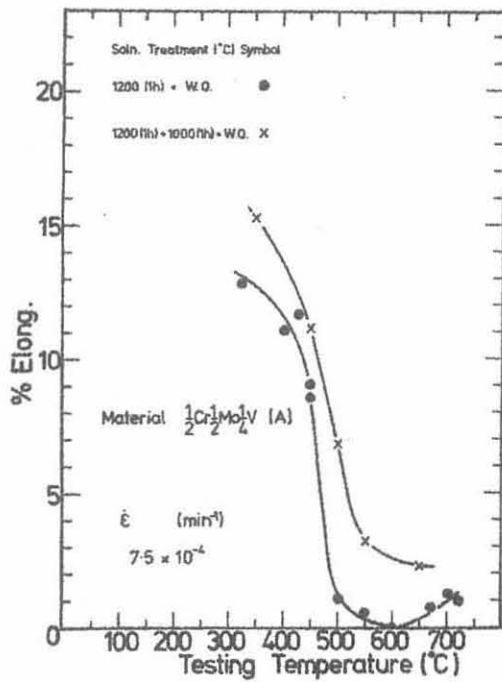


(a)

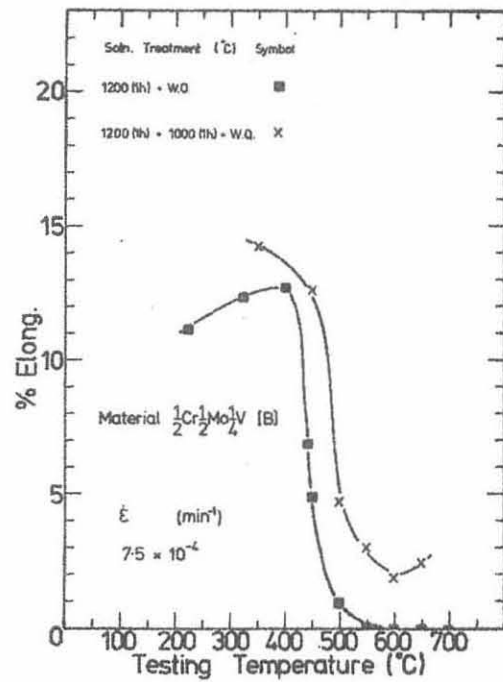


(b)

Figure 25. (a) Tensile mechanical properties of $\frac{1}{2}\frac{1}{2}\frac{1}{4}$ A
 (b) Tensile mechanical properties of $\frac{1}{2}\frac{1}{2}\frac{1}{4}$ B
 after double solution treatment at 1200°C for
 one hour plus 1000°C for one hour, as a function
 of temperature.



(a)



(b)

Figure 26. Ductility improvement in samples A and B after double solution treatment.

(a) $\frac{1}{2}\text{Cr} \frac{1}{2}\text{Mo} \frac{1}{4}\text{V}$ A

(b) $\frac{1}{2}\text{Cr} \frac{1}{2}\text{Mo} \frac{1}{4}\text{V}$ B

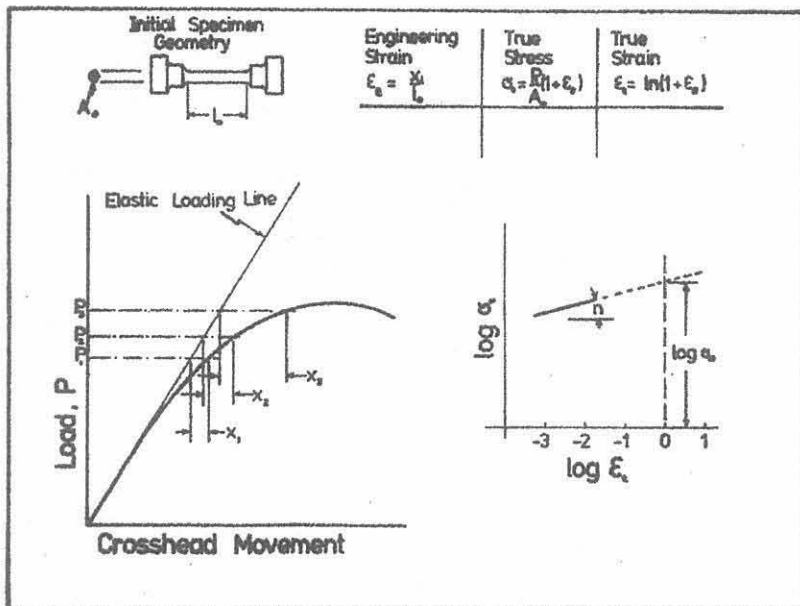
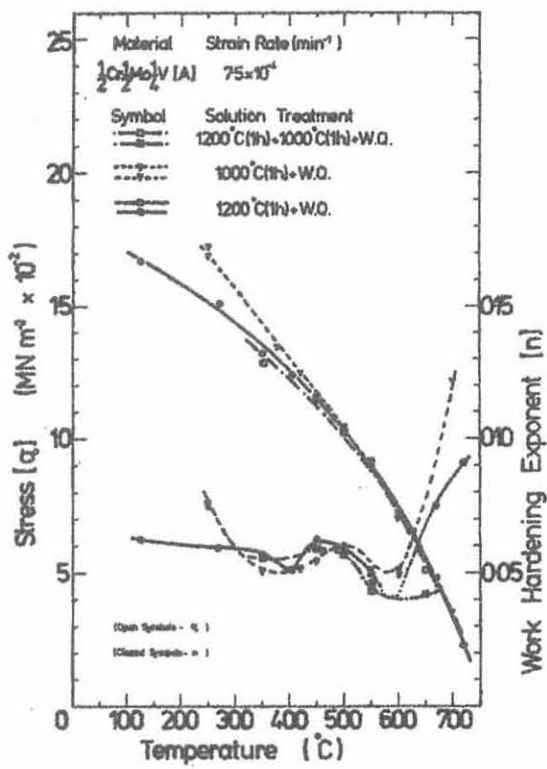
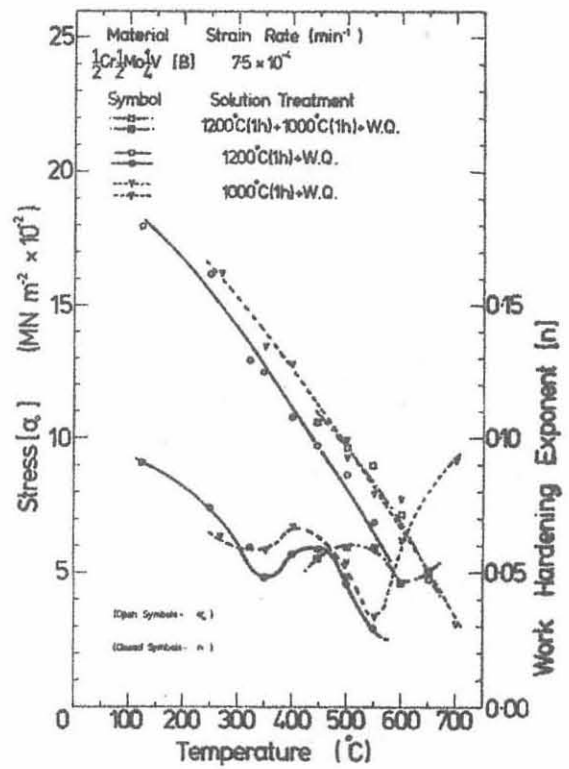


Figure 27. Schematic illustration of method used to transform load-deflection plot on to a log-log plot of true stress versus true strain, in order to evaluate σ_0 and n according to $\sigma_t = \sigma_0 \epsilon_t^n$.



(a)

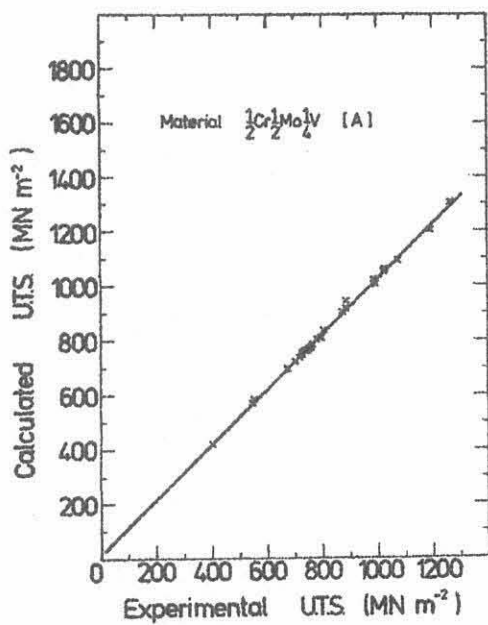


(b)

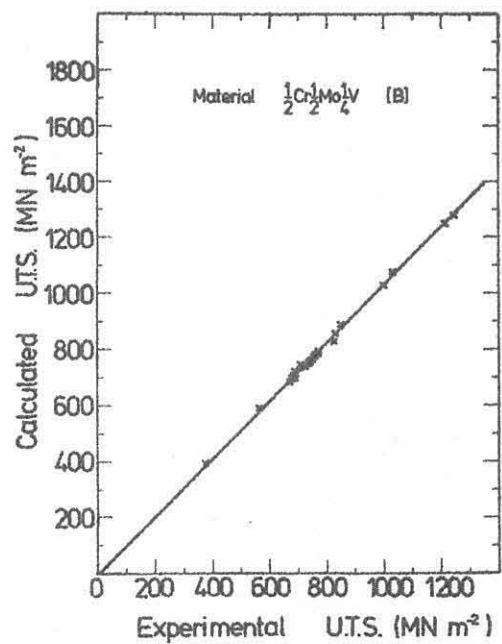
Figure 28. Temperature dependence of σ_0 and n for samples A and B in various conditions of solution treatment.

(a) $\frac{1}{2}\text{Cr}|\frac{1}{2}\text{Mo}|\frac{1}{4}\text{V}$ A

(b) $\frac{1}{2}\text{Cr}|\frac{1}{2}\text{Mo}|\frac{1}{4}\text{V}$ B



(a)

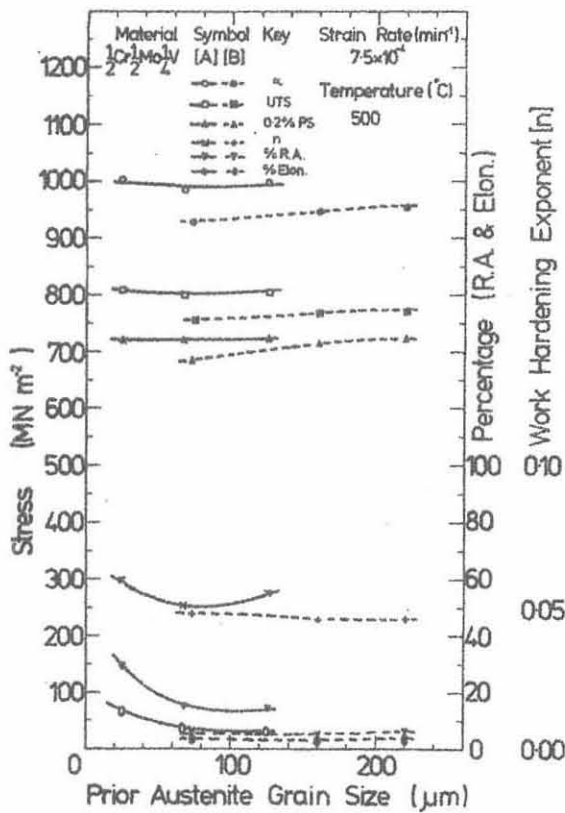


(b)

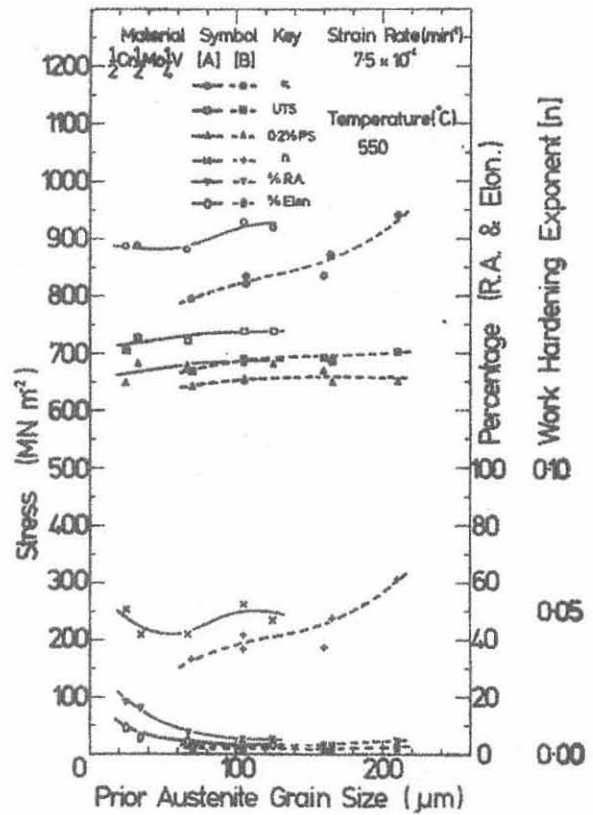
Figure 29. Comparison of experimental values of UTS with those calculated from values of σ_0 and n .

(a) $\frac{1}{2}\text{Cr}\frac{1}{2}\text{Mo}\frac{1}{4}\text{V}$ A

(b) $\frac{1}{2}\text{Cr}\frac{1}{2}\text{Mo}\frac{1}{4}\text{V}$ B



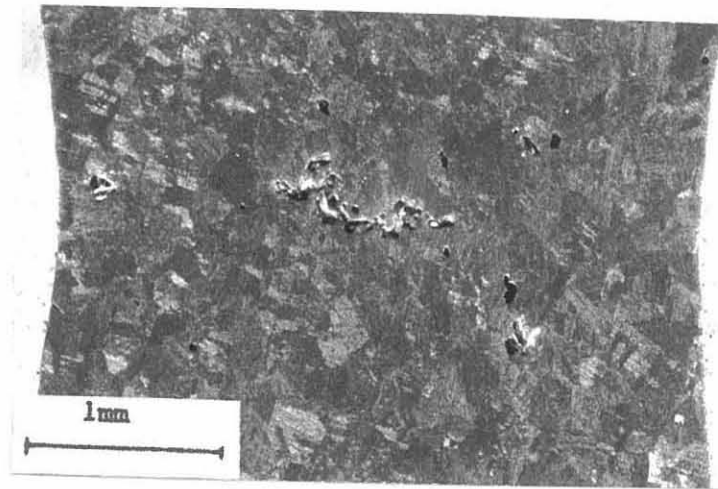
(a)



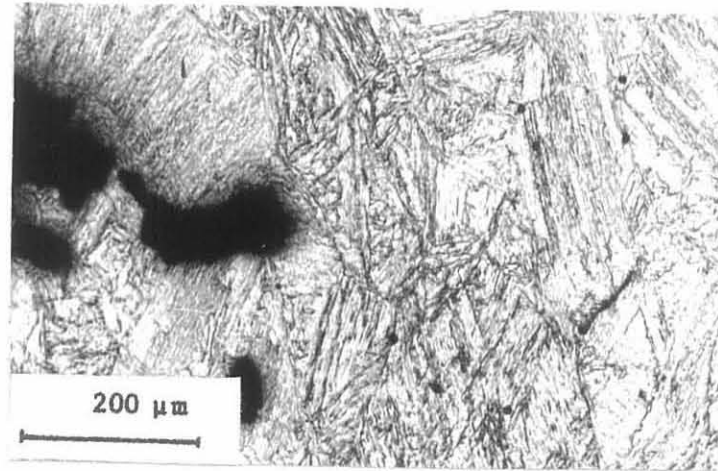
(b)

Figure 30. Tensile mechanical properties of samples A and B as a function of prior austenite grain size.

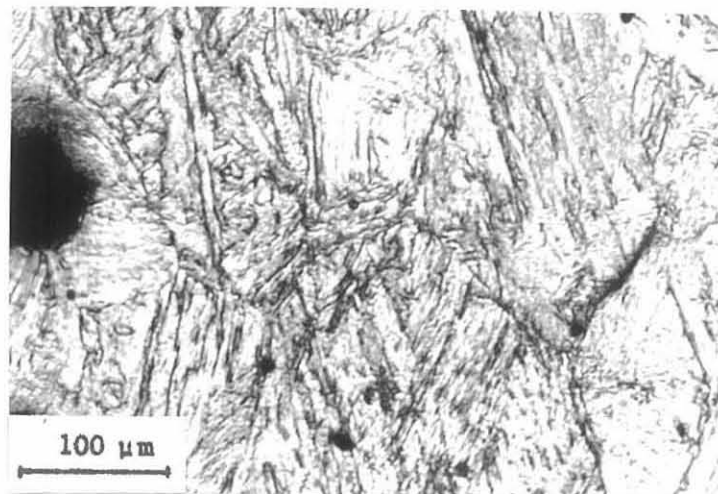
- (a) At 500° C
(b) At 550° C



(a)



(b)



(c)

Figure 31. Formation of intergranular cavitation in association with ductile void growth and coalescence, in sample B (solution treated at 1200°C for one hour) deformed at 400°C.

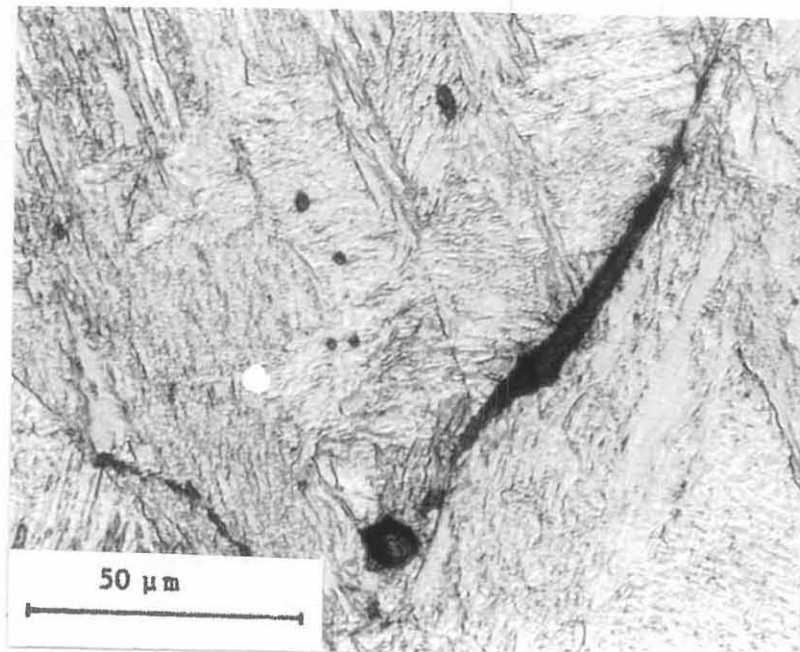
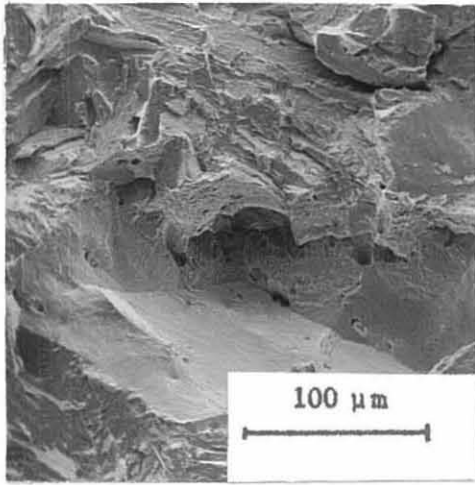
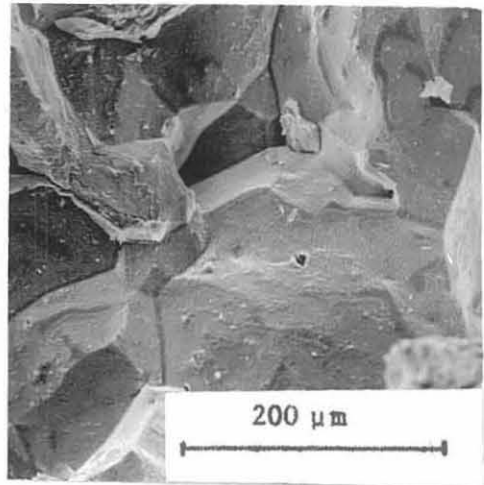


Figure 32. Intergranular cavitation in sample B
(solution treated at 1200°C for one hour)
at 400°C during deformation at a nominal
applied strain rate of $7.5 \times 10^{-4} \text{min}^{-1}$.
(Tensile axis vertical)

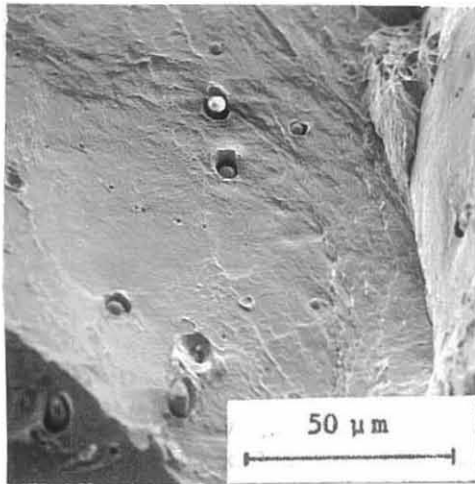
Figure 33. Cavitated boundaries in specimens of sample B (single solution treated at 1200°C for one hour); (a), (b), and (c) boundaries in a specimen deformed at 450°C; (d), (e), and (f) boundaries in a specimen deformed at 700°C.



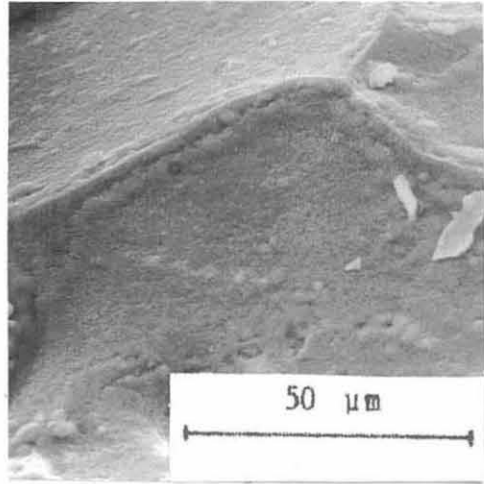
(a)



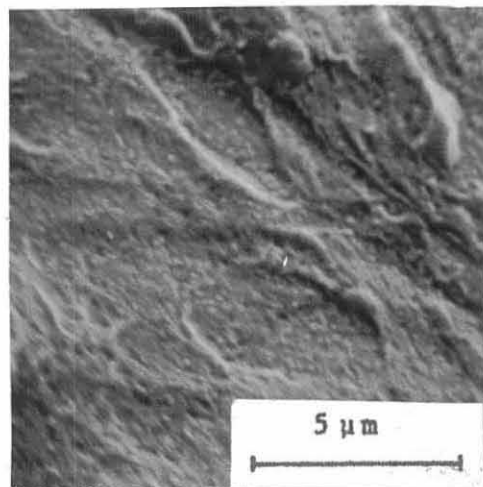
(d)



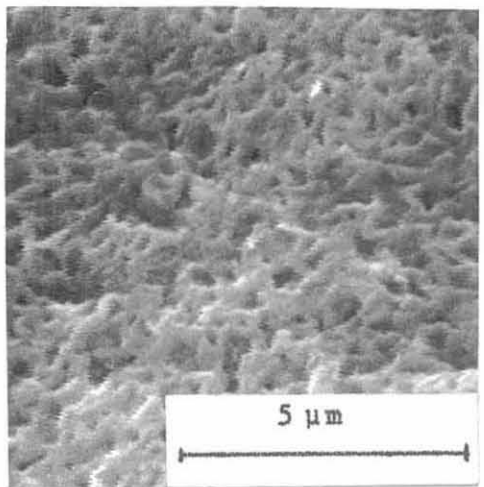
(b)



(e)



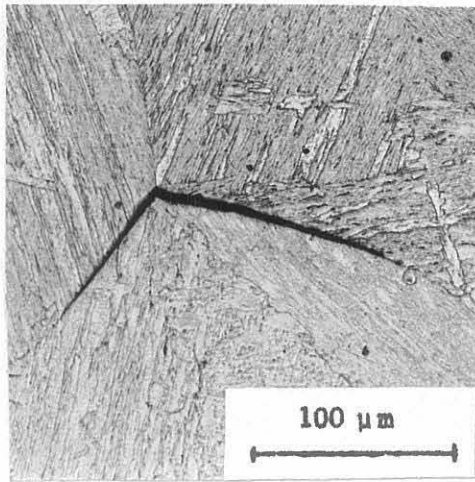
(c)



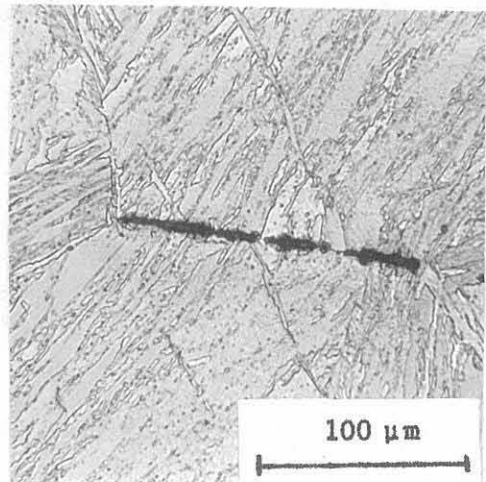
(f)

Figure 33

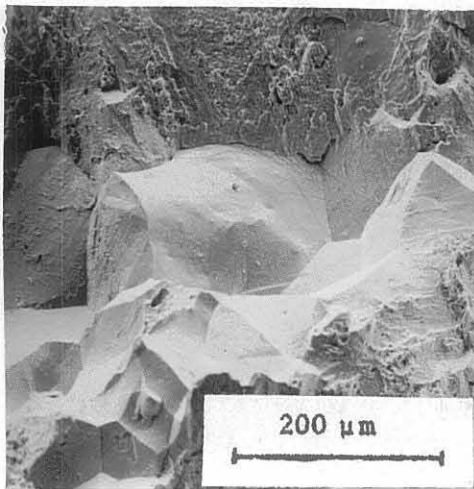
Figure 34. Cavitated boundaries in specimens of sample A (single solution treated at 1200°C for one hour); (a), (b) and (c) boundaries in a specimen deformed at 500°C; (d), (e) and (f) boundaries in a specimen deformed at 700°C.



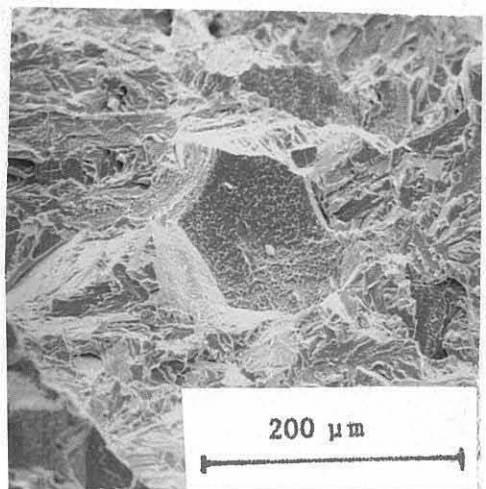
(a)



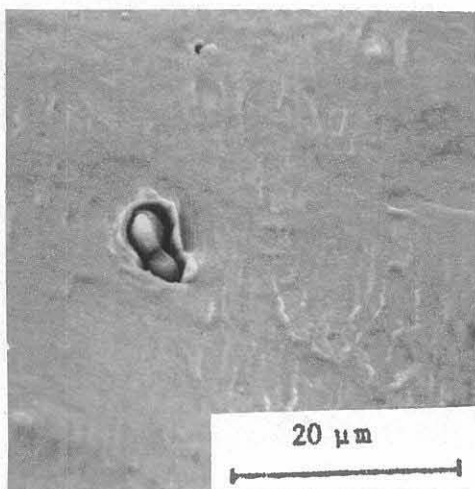
(d)



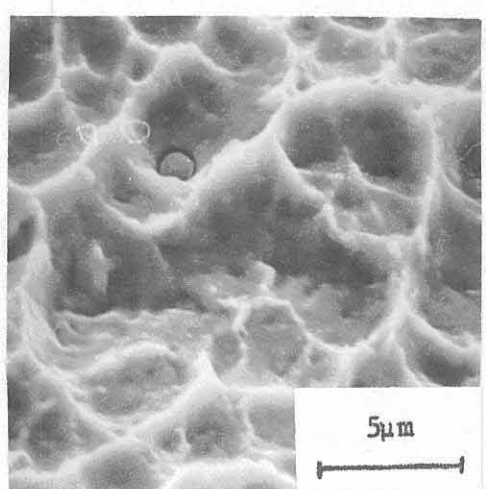
(b)



(e)



(c)



(f)

Figure 34.

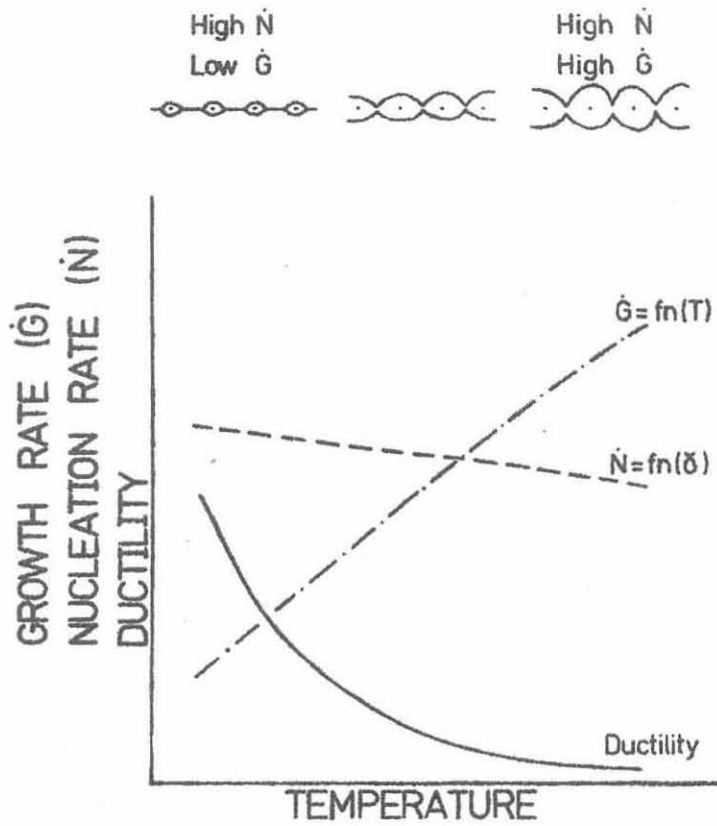
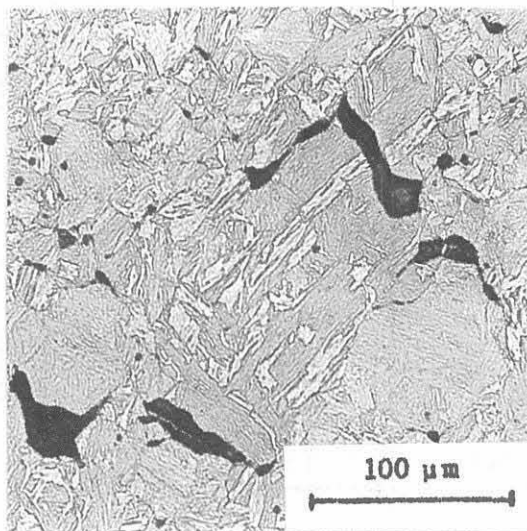


Figure 35. Schematic illustration of the way in which high rates of cavity nucleation at high temperatures might promote reduced ductility and the absence of ductility minimum.

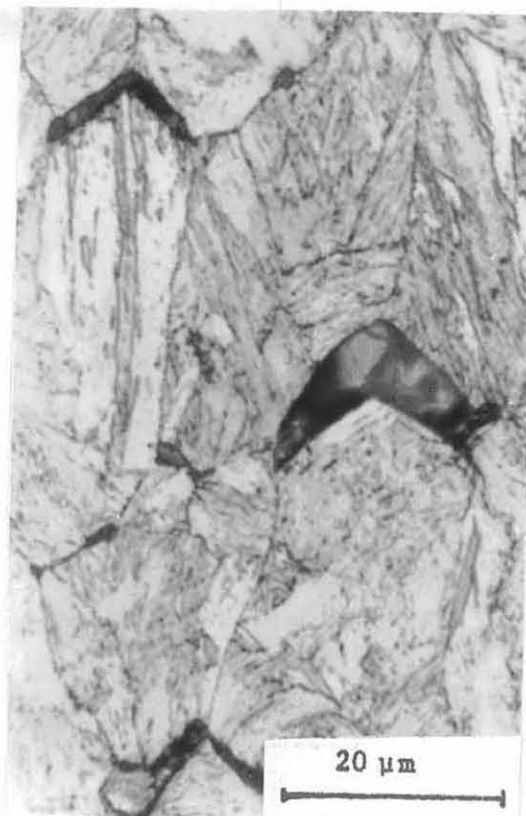


(a)

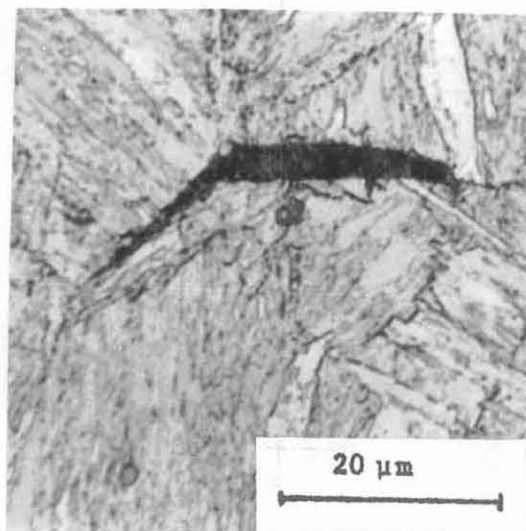


(b)

Figure 36. Cavitation in sample A solution treated at 1000°C for one hour.
(a) General cavitation along gauge length
(b) Large cavity opening close to final fracture in a specimen deformed at 700°C .
(Tensile axis vertical)



(a)



(b)

Figure 37. Cavitation in samples A and B after solution treatment at 1000°C for one hour, both specimens deformed at 600°C.

(a) $\frac{1}{2} | \frac{1}{2} | \frac{1}{4}$ A

(b) $\frac{1}{2} | \frac{1}{2} | \frac{1}{4}$ B

(Tensile axis vertical)

CHAPTER IV

Tensile Strain Rate Sensitivity Effects in Commercial
'susceptible' and 'non-susceptible' $\frac{1}{2}\text{Cr}$ $\frac{1}{2}\text{Mo}$ $\frac{1}{4}\text{V}$ Steel
at Elevated Temperatures

4.1 Background

The general relationship between flow stress and strain rate as proposed by Zener and Holloman¹⁷⁴ for conditions of constant temperature and strain is given by:

$$\sigma = C(\dot{\epsilon})^m \Big|_{\epsilon, T} \quad (4.1)$$

where m is the strain rate sensitivity as defined in figure 20. Dieter¹⁷³ further defines the strain rate sensitivity as the ratio of the incremental change in $\log \sigma$ to the resultant change in $\log \dot{\epsilon}$, at a given strain and temperature. He had in mind the situation in which the value of m was obtained from a test where the strain rate is rapidly changed from one value ($\dot{\epsilon}_1$) to another ($\dot{\epsilon}_2$) such that:

$$m = \frac{\log \left(\frac{\sigma_2}{\sigma_1} \right)}{\log \left(\frac{\dot{\epsilon}_2}{\dot{\epsilon}_1} \right)} \quad (4.2)$$

This approach is clearly most applicable to the situation in which m is reasonably high, so as to allow a measurable change in flow stress for the step changes of strain rate that are possible using conventional tensile testing machines. As will be shown for the present work, a change of four orders of magnitude of strain rate produced only a small change in the measured flow stress values. Therefore, in order to make a crude estimation of the strain rate sensitivity of the commercial samples,

the 0.2% flow stress was plotted against the applied nominal strain rate (for individual tests) on a log-log basis, and the slope calculated by the method of least squares. The form of equation (4.1) is very similar to that of equation (3.1) viz:

$$\sigma_t = \sigma_o \epsilon_t^n \quad (3.1)$$

It may be understood, therefore, that values of m and C in equation (4.1) can be generated in a similar manner to n and σ_o of equation (3.1) (see figure 27).

Following the work of Hart^{162,172} dealing with the theory of the tensile test, recent work¹⁷⁵ has analysed the stability of tensile creep deformation for both constant load and constant stress tests. Basically the work examined stability in terms of the requirement:

$$m + n > 1 \quad (4.3)$$

for stable flow. It is clear that this inequality is consistent with other well known results for necking and unstable flow. For the special case of a solid exhibiting only strain hardening, plastic flow in tension would be stable if:

$$\frac{d\sigma}{d\epsilon} > \sigma \quad (4.4)$$

This result, which has been attributed to Considère¹⁷⁶, follows from equation (4.3) by setting m equal to zero. Similarly, it may be shown that for a solid that exhibits no strain hardening,

$$m > 1 \quad (4.5)$$

for stable flow in tension. This is consistent with the usual observation that linearly viscous materials, in which m is equal

to unity, can be drawn to great lengths without necking.

Concerning the analysis of creep testing¹⁷⁵, it was shown that deformation becomes unstable prior to the onset of secondary creep and it was proposed that all 'steady-state' creep experiments conducted in tension are therefore unstable. In the present work a simple attempt to examine the degree of instability (which will promote the rapid onset of strain localisation) was made by evaluating the parameter $(m + n)$ for various conditions of temperature and prior austenite grain size.

Further work discussed in this chapter relates to the possible strain rate effects in hot hardness measurement. By using the values of n and m determined by uniaxial tensile testing it has been possible to estimate a representative strain and strain rate for the indentation process at elevated temperatures.

4.2 Experimental Results

Tensile tests were carried out upon specimens from both commercial samples as described in chapter three. A range of crosshead velocities was employed for each series and the various flow and ductility parameters were thus obtained at a range of nominal strain rates. The value of nominal strain rate quoted were calculated according to:

$$\dot{\epsilon}_E = \frac{d\epsilon_E}{dt} = \frac{d\left(\frac{l-l_0}{l_0}\right)}{dt} = \frac{1}{l_0} \frac{dl}{dt} = \frac{V}{l_0} \quad (4.6)$$

where V = crosshead velocity

l_0 = original specimen gauge length

Figures 38 and 39 compare the measured flow stresses for samples A and B after single solution treatment as a function of

temperature. Two main points are apparent:

- (i) Strain rate hardening for both samples is significant only at temperatures in excess of 400°C .
- (ii) The effect is not large even for a change in applied nominal strain rate of four orders of magnitude.

The comparison of the mechanical properties of the samples after equivalent solution treatment ignores the important effects of grain size. Accordingly, specimens of both samples were double solution treated as previously described to achieve a range of prior austenite grain sizes with an ostensibly similar degree of solution of vanadium carbide throughout. Tensile tests were carried out at 550°C , at applied nominal strain rates of $7.5 \times 10^{-4} \text{ min}^{-1}$, $3.0 \times 10^{-3} \text{ min}^{-1}$ and $1.2 \times 10^{-2} \text{ min}^{-1}$. The variation of the various flow and ductility parameters σ_0 , U.T.S., 0.2% P.S., n , % R.A. and % Elon. with grain size and strain rate are shown in figure 40 for both samples A and B.

The flow stress of sample A as measured by σ_0 , U.T.S. and 0.2% P.S. appears to be slightly higher than that of sample B, as observed previously. The work hardening behaviour of the two samples is similar except for the observation that in the coarsest grain size condition, the value of n for sample B increases with decrease of strain rate. As the strain rate is increased the n values for the various grain size conditions converge. The n value for the coarse grain specimens of sample B, however, remains slightly greater at higher strain rates than for finer grain sizes. This observation is therefore consistent with the previous discussion of work hardening behaviour of sample B as a

function of grain size. The observed reduction of work hardening exponent in the coarse grained specimens with increased strain rate is indicative of the rate dependence of the matrix hardening phenomena in this sample at 550°C. It may be likened to a dynamic strain aging effect which, while it does not produce the serrated yielding of the Portevin-Le Châtelier effect, allows a strain rate sensitive hardening to be observed since at the lower strain rates, dislocation velocities will become comparable with diffusion rates of atoms like vanadium and carbon. This point is discussed further in the next chapter. The data of figure 40 underline the importance of grain size in this context since it would appear that the above-mentioned effect is marked only in coarse grained specimens of sample B. Presumably, for the other finer grain sizes of sample B and sample A the degree of grain boundary sliding acts to mask the effect as measured during conventional tensile testing.

The ductility behaviour illustrated in figure 40 shows that while the effect of increased grain size in reducing ductility is reduced for sample A (i.e. the values for %R.A. converge at the higher strain rate), it is exaggerated for sample B (i.e. the values for %R.A. converge at the lower strain rate). Overall, the ductility is observed to increase with increased strain rate. The final failure mode of all specimens within this strain rate range and at 550°C involved the formation of intergranular cavities. The lowest grain size of sample B (110 µm) lies within the range of grain sizes for sample A (35 - 125 µm). It is significant therefore that the ductility

behaviour of fine grained sample B is similar to that of sample A in that %R.A. approaches 40% for a strain rate of $1.2 \times 10^{-2} \text{ min}^{-1}$.

The combined effect of grain size and strain rate upon measured ductility for intergranular failure of samples A and B during conventional tensile testing is summarised in figure 41. It is clear that the behaviour of sample B is essentially an extension of that of sample A at increased grain sizes. This figure therefore underlines the importance of coarse prior austenite grain size in promoting low ductilities at elevated temperatures during failure by intergranular cavitation.

4.3 Estimation of Strain Rate Sensitivity and Associated 'degree of instability' of Tensile Deformation

Following the method outlined in section 4.1, values for the strain rate sensitivity, m , of samples A and B were determined as the slope of a log-log plot of 0.2% flow stress against nominal strain rate. Figure 42 illustrates typical plots for samples A and B at 550°C . The estimated values of m and C are quoted with these data. This procedure was repeated for values of flow stress at the various nominal applied strain rates over the range of temperature 400°C to 700°C . Figure 43 compares the variation of m and C with temperature for samples A and B (in the single solution treated condition).

Three main points are apparent:

- (i) Specimens which had been solution treated at 1000°C for one hour generally show increased values of m and C over those exhibited by specimens which had been

solution treated at 1200°C for one hour.

- (ii) A marked increase in strain rate sensitivity occurs consistently at the higher temperatures.
- (iii) These crude estimates for m and C are ostensibly similar for the two samples A and B.

Using the data of figure 40, estimates of m and C were made as a function of prior austenite grain size at 550°C. Figure 44 illustrates the form of the variation of m and C with prior austenite grain size for samples A and B. It appears that fine grained specimens of both samples exhibit increased values of both m and C .

In order to examine the 'degree of instability' as assessed through the parameter $(m + n)$, values of n as described in chapter three were combined with values of m determined under equivalent conditions of temperature and prior austenite grain size. Figure 45 compares the variation of $(m + n)$ with testing temperature for samples A and B (in the single solution treated condition).

Several main points are apparent:

- (i) For the highest temperatures it is clear that m dominates, so that $(m + n)$ becomes comparatively large (i.e. reduced 'degree of instability').
- (ii) A minimum in the value of $(m + n)$ occurs within the temperature range 450°C to 600°C for both specimens. The notable exception to this behaviour being that exhibited by sample A after single solution treatment at 1000°C.

- (iii) In this respect the form of the temperature response of $(m + n)$ is very similar to the ductility responses of the two samples, since the deformation behaviour would appear to be most unstable in the region of the ductility minima associated with final failure, by intergranular cavitation. The 'degree of instability' being least in those specimens which were observed to exhibit the highest values of ductility.

The importance of high strain rate sensitivity in promoting stable superplastic flow with enhanced ductility was discussed in chapter one. The work of Fleck et al.¹³⁰ also refers to the importance of high m values in promoting stable plastic flow at high temperatures during the deformation of an industrial copper based alloy. In particular, they observed a change in the mode of formation of intergranular cavities with grain size (as discussed previously and illustrated schematically in figure 8). The intergranular void sheet mechanism, which they propose occurs for the fine grain materials, involves multiple nucleation of many cavities on the many grain boundaries present (viz. figure 36) followed by void growth resulting from plastic strain concentrations in the region of the void. As discussed previously, the authors contend that the ductility is controlled by the plastic coalescence of the voids through the formation of internal necks as in ductile failure at ambient temperature. They propose therefore that the significance of a high m value is that the failure of the internal necks will be restricted through increased stability of deformation. The parameter m is usually increased by

a decrease in grain size for a given temperature and strain rate, (as illustrated in figures 43 and 44).

The authors¹³⁰ give no details of estimation of m or n in their system but propose that at high temperatures and fine grain sizes, m will be more dominant than n . As mentioned previously, the effect of reduced n should be similar to that of reduced m in the failure of the internally necked regions. The observation of the minimum values of $(m + n)$ in the region of the ductility minima would appear to support this contention. To further examine the possible control which this 'degree of instability' exerts upon the ductility during final failure by intergranular cavitation, values of $(m + n)$ for both samples at 550°C were plotted as a function of grain size. It may be recalled that 550°C is close to the temperature of the ductility minimum in each case. The results are presented in figure 46. Several important points should be noted:

- (i) The response of the parameter $(m + n)$ to variation in grain size at this temperature is very similar to that observed for ductility as a function of grain size (figure 41).
- (ii) In this respect, the deformation behaviour of sample B is once again recognised as being essentially an extension of that of sample A at larger grain sizes.
- (iii) The observed correlation between the form of the ductility behaviour and that of $(m + n)$ suggests that the ductility observed during final failure by intergranular cavitation is to some extent controlled

by the 'degree of instability' of tensile deformation.

- (iv) Extending the arguments of Fleck et al.¹³⁰, it would appear that the 'intergranular void sheet' mode of final failure is associated in this instance with a decreased 'degree of instability' (i.e. increased value of $(m + n)$).

These latter remarks cast serious doubts upon the total validity of theoretical treatments of failure by intergranular cavitation (like those¹¹⁰⁻¹¹⁶ discussed in chapter one) in which the ductility at final failure is thought to be essentially independent of any strain localisation effects and associated rupture mode.

4.4 The Relationship between Elevated Temperature Flow Stress and Hot Hardness

In chapter two it was shown that values of the Vickers Pyramid Hardness of the two commercial samples at elevated temperatures were substantially the same. In chapter three it was further illustrated that values of the 0.2% flow stress of the two samples measured at a strain rate of $7.5 \times 10^{-4} \text{ min}^{-1}$ were also substantially the same. It would appear possible, therefore, to make a direct correlation between elevated temperature flow stress and hot hardness.

Extensive work by Tabor¹⁵² has established that at ambient temperatures:

$$(H_V)_r = 3.0 \sigma_r \text{ (kg. mm}^{-2}\text{)} \quad (4.7)$$

where σ_r is the representative yield stress measured in kg. mm^{-2}

and $(H_V)_r$ is the corresponding Vickers Pyramid Hardness in kg. mm^{-2} . For a work hardening material it was further established that the representative yield stress was that measured at an offset strain of 8.0%. In this way equation (4.7) may be modified thus:

$$(H_V)_r = 0.306 \sigma_0 (0.08)^n \quad (\text{kg. mm}^{-2}) \quad (4.8)$$

where σ_0 and n are as defined in equation (3.1) and σ_0 is measured in units of MN m^{-2} .

Values of $(H_V)_r$ were calculated according to equation (4.8) and compared with measured values, H_V , by plotting the ratio $(H_V)_r / H_V$ as a function of temperature. The results are shown in figure 47a. Two main points are to be noted:

- (i) Within the range of scatter, the ratio of calculated hardness to measured hardness follows ostensibly the same trend for both materials.
- (ii) The deviation of the calculated values of hardness from the measured values appears to be greatest in the ranges 400°C to 500°C and above 600°C .

The significance of this latter observation is that for the lower temperature range the deformation is essentially controlled by work hardening, whereas at the highest temperatures the data discussed earlier in this chapter has suggested that the deformation is rather more strain rate sensitive. In order to make allowance for variation in the representative yield stress through strain rate hardening, as well as strain hardening equation (4.7) was further modified (see Appendix II) to give:

$$(H_V)_r = 0.306 \sigma_y \Big|_{\epsilon \dot{\epsilon}} 10^{(Am + Bn)} \quad (\text{kg. mm}^{-2}) \quad (4.9)$$

where $\sigma_y \Big|_{\epsilon, \dot{\epsilon}}$ is the value of the proof stress determined at certain values of ϵ and $\dot{\epsilon}$ (in MN m^{-2})

$$A = \log\left(\frac{\dot{\epsilon}_r}{\dot{\epsilon}}\right) \quad (4.10)$$

in which $\dot{\epsilon}_r$ is the representative strain rate for the hardness indentation.

$$B = \log\left(\frac{\epsilon_r}{\epsilon}\right) \quad (4.11)$$

in which ϵ_r is the representative strain for the hardness indentation.

m, n as defined previously.

Different values of $\dot{\epsilon}_r$ and ϵ_r were used during the solution of equation (4.9) until the deviations shown in figure 47a were minimised. The results are shown in figure 47b. It would appear that, for the present work the value of hot hardness, in the range 400°C to 700°C , is best related to the tensile flow properties through a representative yield stress calculated at a strain of 0.5% and a strain rate of $5 \times 10^{-2} \text{ min}^{-1}$.

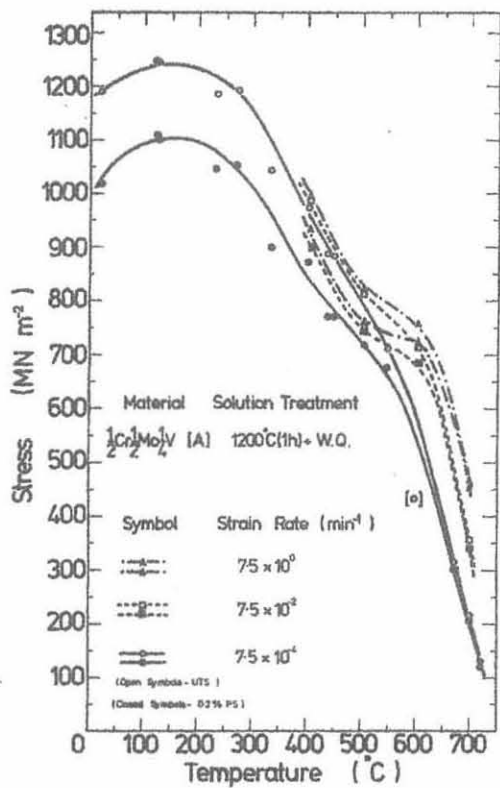
4.5 Conclusions

The work described in this chapter has established:

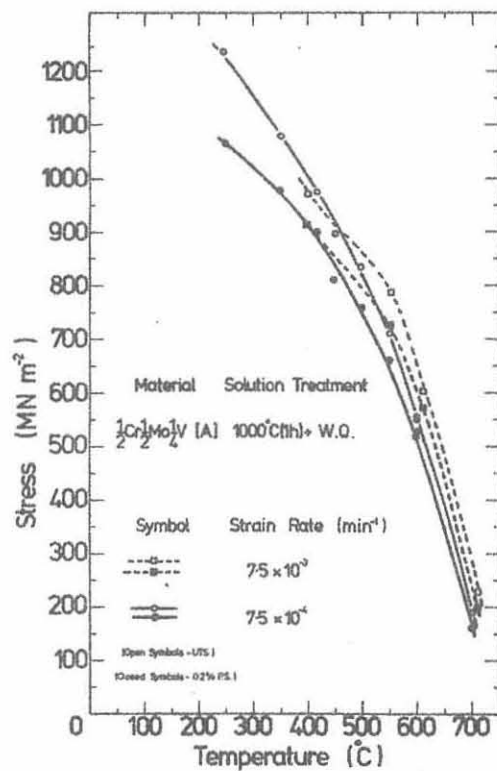
- (i) That at 550°C the deformation and ductility behaviour of the 'susceptible' sample B is essentially an extension of that of sample A at coarser grain size.
- (ii) That the increased ductility of sample A deformed at 550°C and a nominal strain rate of $7.5 \times 10^{-4} \text{ min}^{-1}$ appears to be associated with an increase in the value of the parameter $(m + n)$ at finer grain sizes.
- (iii) That the value of hardness in the range 400°C to 700°C

is best related to the tensile flow properties through a representative yield stress calculated at a strain of 0.5% and a strain rate of $5 \times 10^{-2} \text{ min}^{-1}$.

Furthermore it would appear that the association between increased ductility and decreased 'degree of instability' at finer grain sizes is consistent with the observation that final unstable rupture of specimens in this condition occurs as a result of strain localisation in the intercavity regions.



(a)

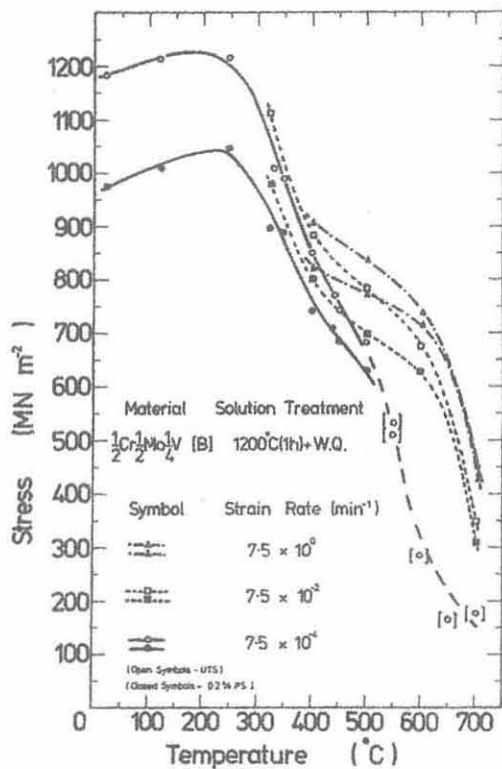


(b)

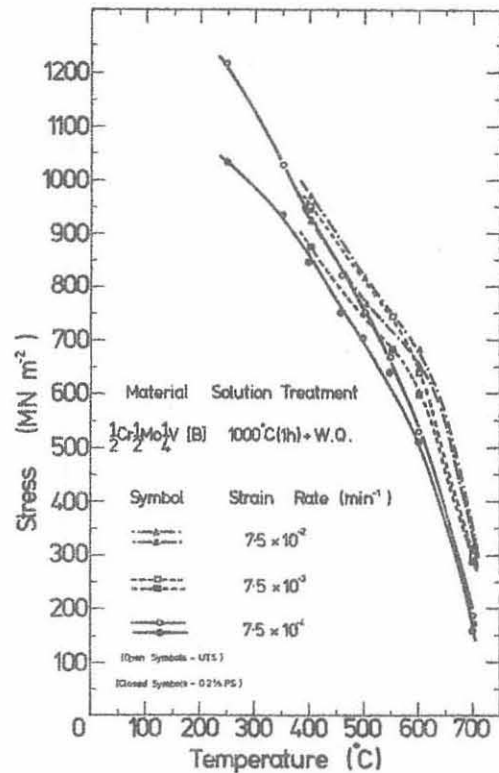
Figure 38. Comparison of measured flow stress values for sample A at various nominal applied strain rates.

(a) After single solution treatment at 1200°C for one hour.

(b) After single solution treatment at 1000°C for one hour.

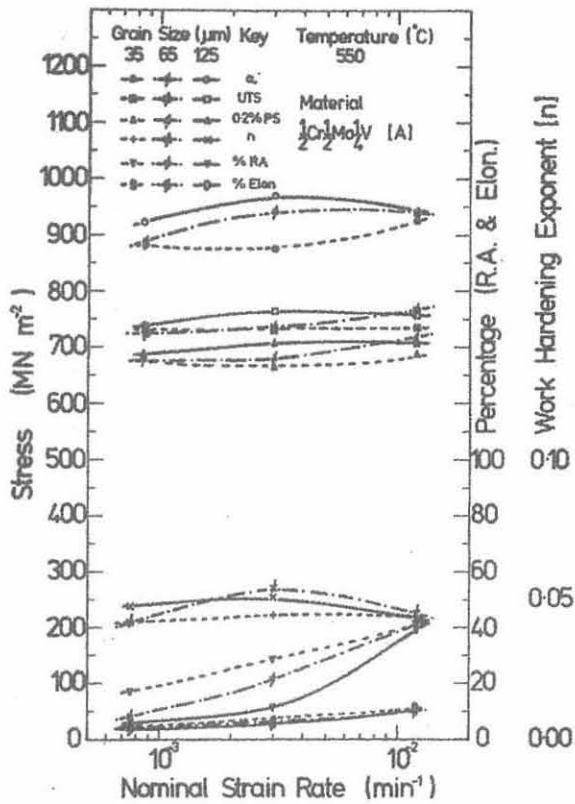


(a)

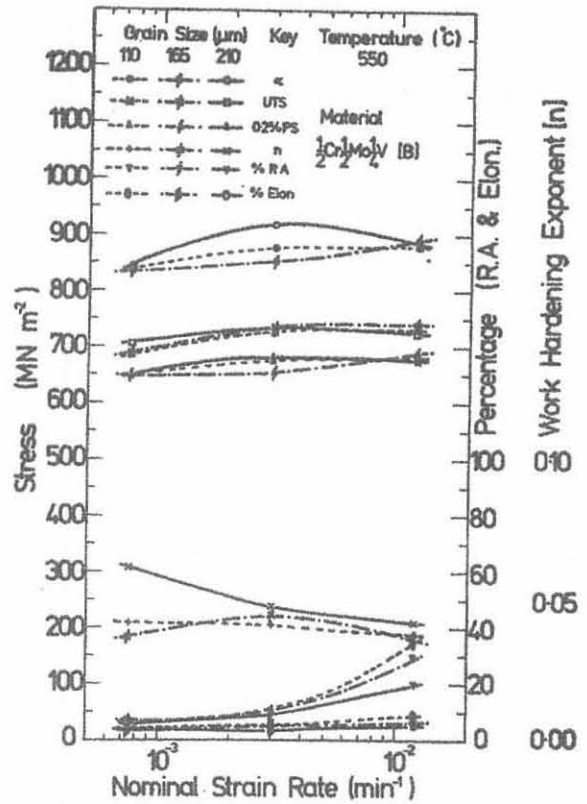


(b)

Figure 39. Comparison of measured flow stress values for sample B at various nominal applied strain rates.
 (a) After single solution treatment at 1200°C for one hour.
 (b) After single solution treatment at 1000°C for one hour.



(a)



(b)

Figure 40. Comparison of various flow and ductility parameters for the deformation of samples A and B having various prior austenite grain sizes, as a function of nominal applied strain rate.

(a) $\frac{1}{2}\text{Cr}\frac{1}{2}\text{Mo}\frac{1}{4}\text{V}$ A

(b) $\frac{1}{2}\text{Cr}\frac{1}{2}\text{Mo}\frac{1}{4}\text{V}$ B

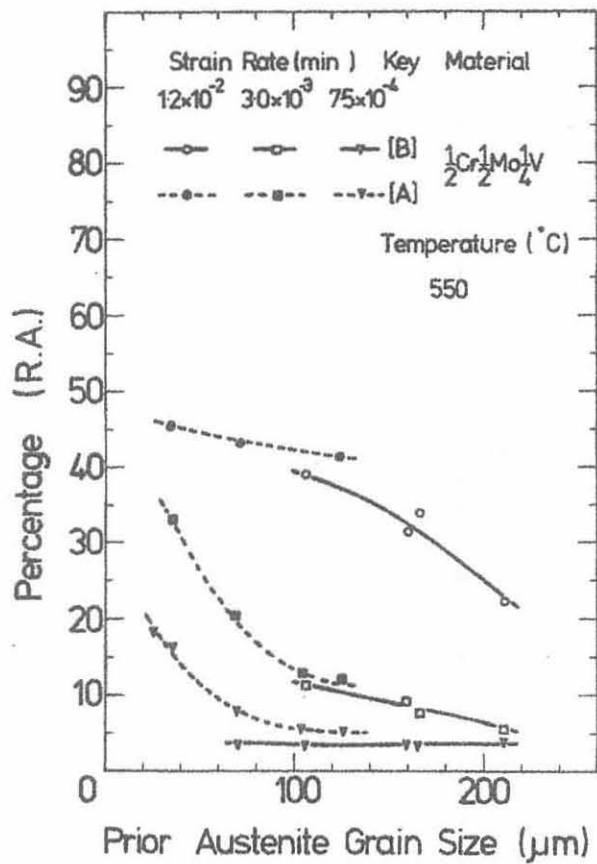
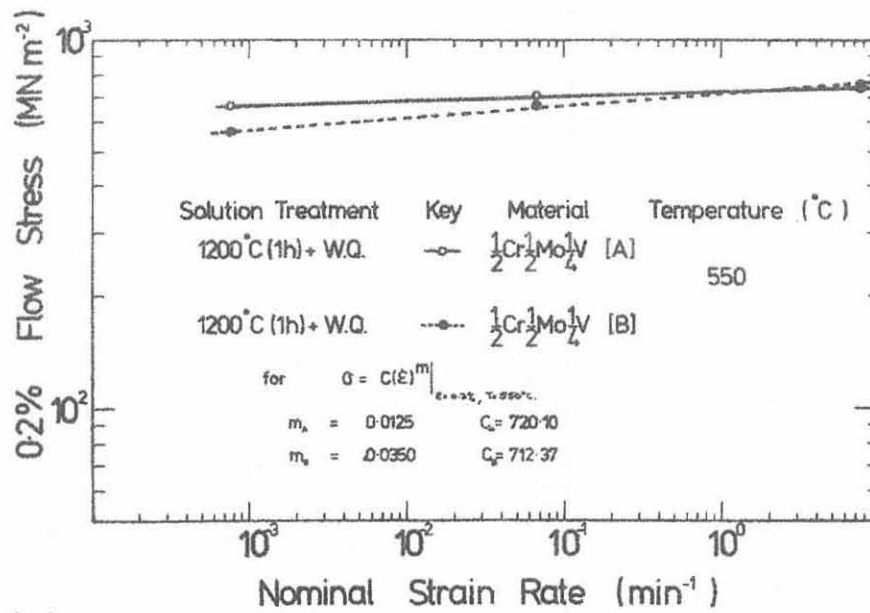
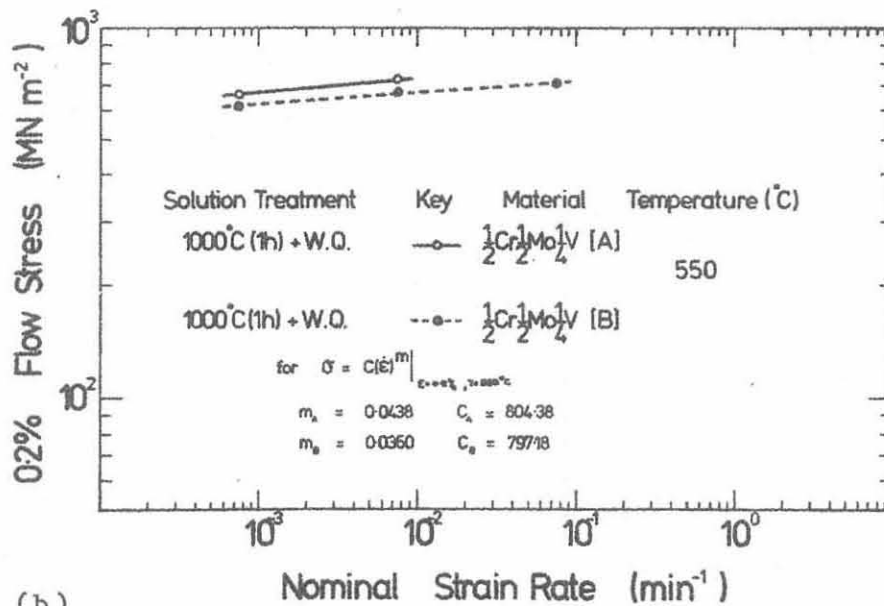


Figure 41. Ductility of samples A and B for various nominal applied strain rates as a function of prior austenite grain size.



(a)

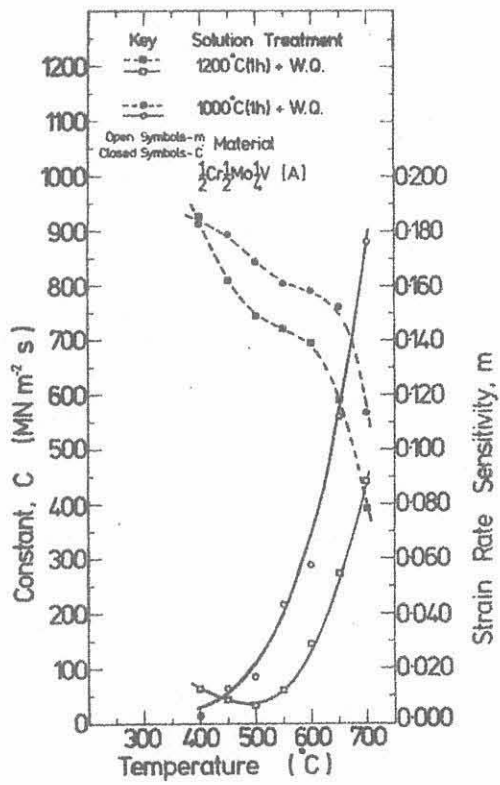


(b)

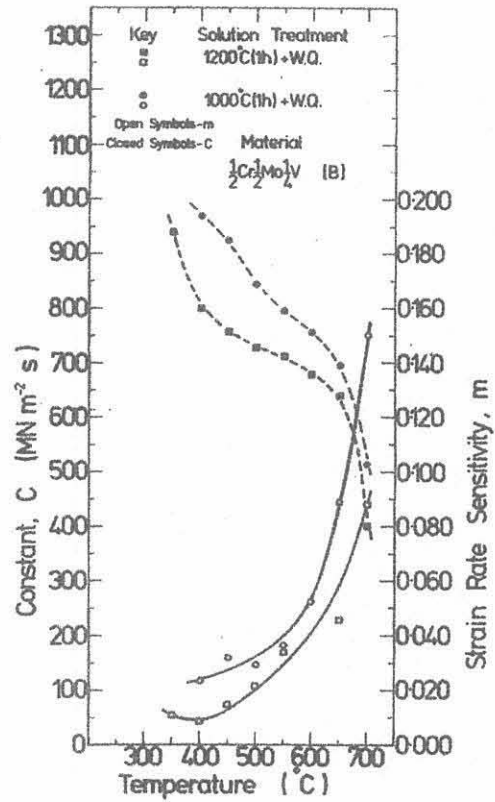
Figure 42. Plots of 0.2% flow stress versus nominal strain rate for samples A and B on a log-log scale, at 550 $^{\circ}\text{C}$.

(a) After solution treatment at 1200 $^{\circ}\text{C}$ for one hour.

(b) After solution treatment at 1000 $^{\circ}\text{C}$ for one hour.



(a)



(b)

Figure 43. Strain rate sensitivities of samples A and B, after single solution treatment at 1200°C for one hour and 1000°C for one hour, as a function of temperature.

(a) $\frac{1}{2}\text{Cr}|\frac{1}{2}\text{Mo}|\frac{1}{4}\text{V}$ A

(b) $\frac{1}{2}\text{Cr}|\frac{1}{2}\text{Mo}|\frac{1}{4}\text{V}$ B

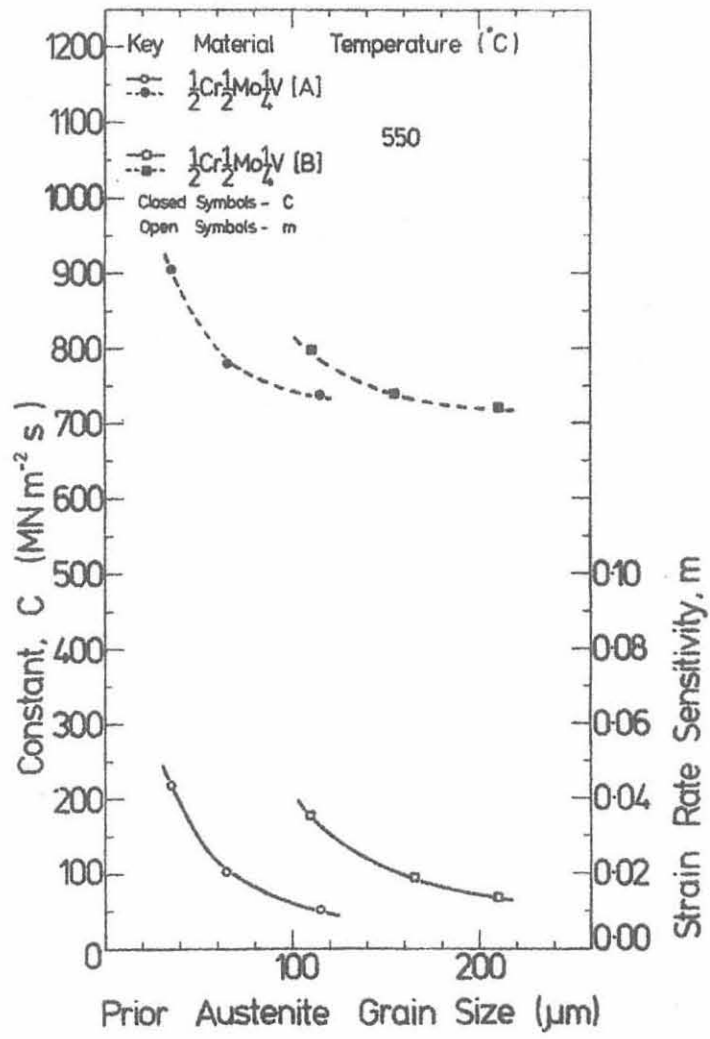
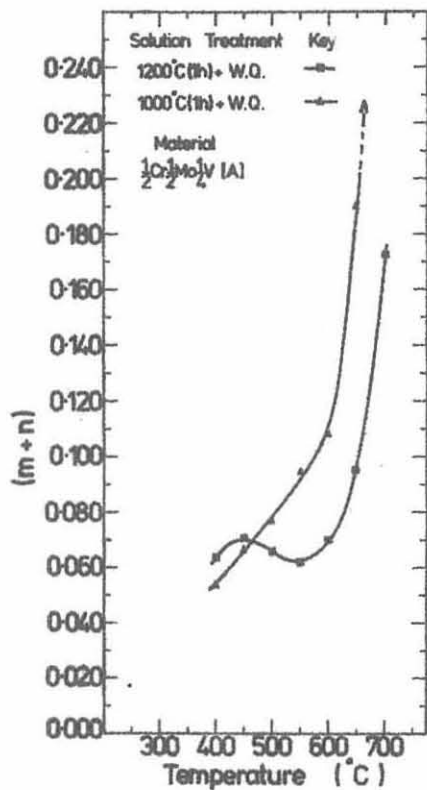
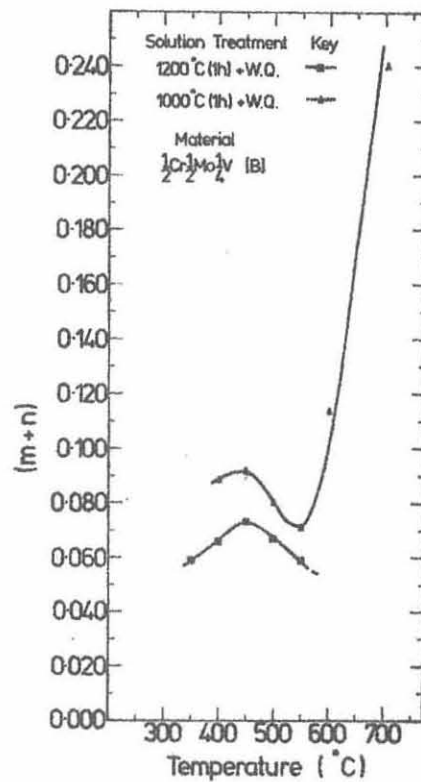


Figure 44. Variation of parameters m and C with prior austenite grain size during deformation of samples A and B at 550°C.



(a)



(b)

Figure 45. Examination of the approach to stable tensile deformation in samples A and B through inspection of the response of $(n+m)$ as a function of temperature. (n values determined at a nominal strain rate of $7.5 \times 10^{-4} \text{ min}^{-1}$)

(a) $\frac{1}{2} | \frac{1}{2} | \frac{1}{4}$ A

(b) $\frac{1}{2} | \frac{1}{2} | \frac{1}{4}$ B

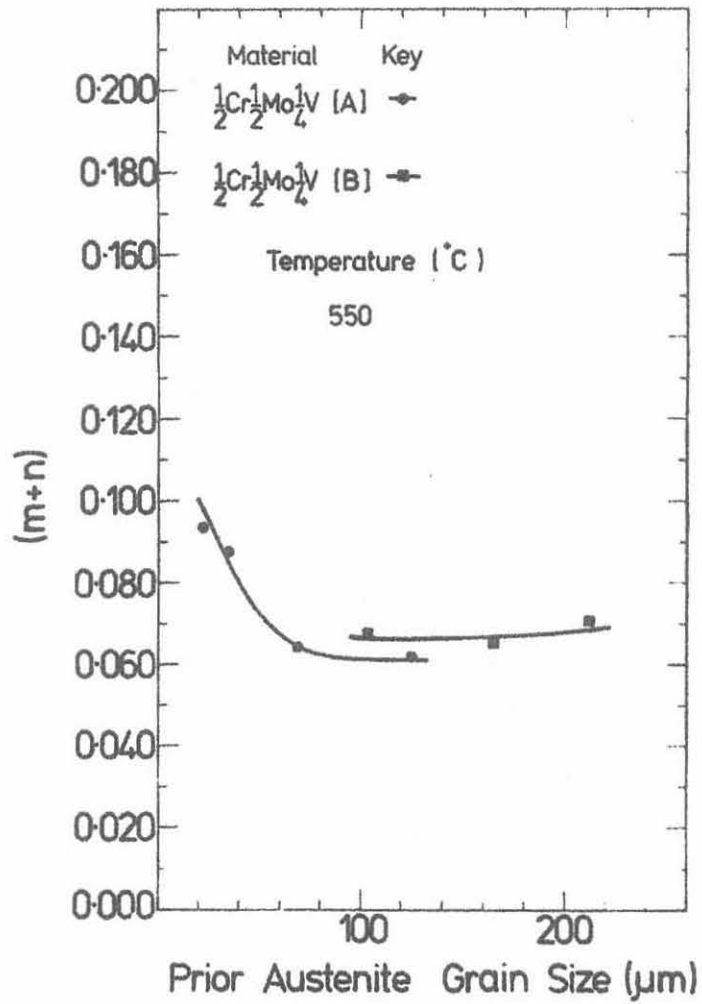
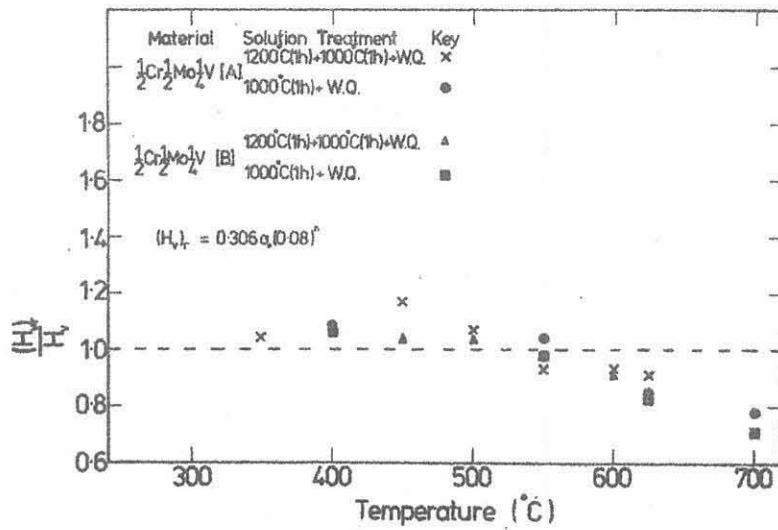
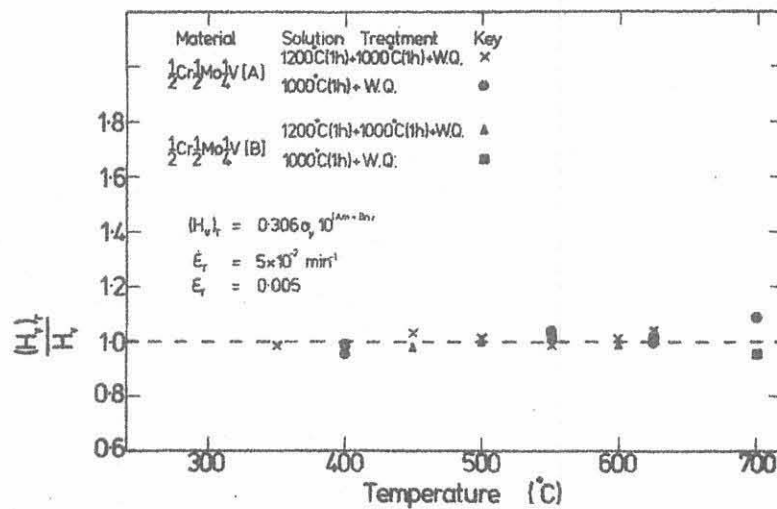


Figure 46. Variation of parameter (m+n) with prior austenite grain size during deformation of samples A and B at 550°C.



(a)



(b)

Figure 47. (a) Comparison of measured hot hardness with that calculated according to equation (4.8)

(b) Comparison of measured hot hardness with that calculated according to equation (4.9), with $\epsilon_r = 0.005$ and $\dot{\epsilon}_r = 5 \times 10^{-2} \text{ min}^{-1}$.

CHAPTER V

The Anisothermal Stress Relaxation Behaviour of Commercial
'susceptible' and 'non-susceptible' $\frac{1}{2}\text{Cr } \frac{1}{2}\text{Mo } \frac{1}{4}\text{V}$ Steel

5.1 Introduction

In stress relief heat treatments, the heating time is comparable with the soaking time, and it has been established¹⁸² that significant stress relief may occur during the heating cycle. The work described in this chapter was carried out in an attempt to assess the conditions of stress, temperature and strain rate under which intergranular failure similar to that observed in the weld HAZ of figure 1, might occur during a thermal stress relief heat treatment. The investigation described consists basically of the monitoring of the stress relaxation behaviour of smooth tensile specimens which are held at a constant strain, while being heated at a constant rate of $50^{\circ}\text{C h}^{-1}$ from ambient to 700°C . Previous work¹⁷¹⁻¹⁸² employing the anisothermal stress relaxation test has examined the effectiveness of post weld heat treatment as a means of reducing levels of residual stress in welded structures. Little or no attention was paid to the possibility of cracking during these studies.

The total imposed strain rate during tensile testing may be divided into elastic and plastic components, thus:

$$\dot{\epsilon}_T = \dot{\epsilon}_e + \dot{\epsilon}_p \quad (5.1)$$

where $\dot{\epsilon}_T$ = total strain rate;
 $\dot{\epsilon}_e$ = elastic strain rate;
 $\dot{\epsilon}_p$ = plastic strain rate.

For the condition $\dot{\epsilon}_T = 0$

$$\dot{\epsilon}_p = -\dot{\epsilon}_e = -\frac{\dot{\sigma}}{K} \quad (5.2)$$

where $\dot{\sigma}$ = measured stress rate

K = appropriate elastic coefficient for
both specimen and machine.

The specimen thus continues to undergo plastic straining due to the residual elastic strain in the specimen and the load measuring cell.

Analytical^{162,172} and experimental^{183,184} work by Hart and his co-workers has established the usefulness of isothermal stress relaxation testing in the investigation of the deformation behaviour of materials that lack substantial ductility. In particular, this work established that after plotting the variation of stress and strain rate, monitored during a stress relaxation test, on a log-log basis then the strain rate sensitivity, at a particular strain rate, is given by the slope of the curve at that point. This observation is consistent with figure 20 in which:

$$\left. \frac{d \log \sigma}{d \log \dot{\epsilon}} \right|_{\epsilon, T} = m \quad (5.3)$$

The isothermal stress relaxation test thus accomplishes, by a continuous variation, what is usually attempted by the discrete strain rate or load change tests.

For the anisothermal stress relaxation test there are two major complications, viz:

- (i) E , and therefore K , varies with variation of temperature
- (ii) The constantly increasing temperature precludes any

description of the process in terms of 'steady-state' deformation.

It is likely that an accurate analysis may be achieved by considering the process as a series of very short time isothermal tests. In the present investigation no attempt was made to deal with the second (possibly the most important) factor. A very simple approach was adopted to allow for the first. It is summarised in figure 48a. It was found that for conditions of loading employed, K was approximately equal to E (see figure 52). In this way, an estimate of the strain rate experienced by a specimen at a particular stress and temperature was made simply by dividing the measured stress rate ($\dot{\sigma}$) by the value of Young's Modulus for $\frac{1}{2}\text{Cr } \frac{1}{2}\text{Mo } \frac{1}{4}\text{V}$ at that temperature. The data was then presented as plots of stress versus temperature and strain rate versus temperature.

5.2 Experimental

For isothermal stress relaxation it is usually only necessary to preload the specimen to a predetermined level and then monitor the load relaxation after the crosshead movement has been stopped¹⁸⁵. For anisothermal stress relaxation, it is necessary to compensate for the thermal expansion of both the loading train and the specimen so that the observed relaxation of stress occurs only through deformation of the specimen. Previous work¹⁷⁷⁻¹⁸² has employed a variety of mechanical compensation systems. For the present investigation a MAND electro-servo hydraulic universal testing machine was employed in closed loop strain control mode to maintain the specimen strain constant during the heating cycle.

The system is illustrated schematically in figure 48b. Temperature variation along the specimen gauge length was maintained within $\pm 3^{\circ}\text{C}$ for temperatures above 200°C .

The control of heating rate was achieved by replacing the set point potentiometer of an SKL 12 amp proportional temperature controller by a Beckman high precision 10 turn helical potentiometer (of the same value). This potentiometer could be turned at various rates by a small 10-speed motor. In this way the set point temperature could be adjusted linearly at rates varying from 5°C/hr up to 300°C/hr . The tests were conducted with an applied heating rate of 50°C/hr . This system operated satisfactorily at temperatures above 200°C . Due to the inadequate compensation of furnace power at low temperatures, there was found to be an offset of 180°C between the set point temperature and the measured specimen temperature as shown schematically in figure 49. Above 200°C , measured heating rates fell within $50^{\circ}\text{C} \pm 1^{\circ}\text{C/hr}$.

The extensometers used were made from stainless steel. To check differential thermal expansion that was introduced as a result of their being of different composition from the specimen, the lower loading pin was removed so that the loading system was simply suspended from the load cell. The system was then heated at a rate of 50°C/hr and the signal from the LVDT's* plotted against specimen temperature using an X-Y plotter. The results are shown in figure 50. It appeared that for heating during this off load condition, the displacement as measured by the LVDT's decreased

*

Linear voltage - displacement transducers

initially as the temperature was raised in the range ambient to 200°C . Above this temperature the displacement remained constant to within $\pm 7.5 \times 10^{-3}$ mm. On the control gauge length of 50.8 mm this corresponds to strain control within $\pm 0.015\%$ above 200°C .

The load cell was connected to a MAND solid state resistance bridge and amplifier module. The amplifier gain was set such that 250 KN gave an output of 10 V. The load signal was fed to one channel of a Rikadenka two channel chart recorder. By employing a ten step voltage back-off unit, it was possible to arrange the chart recorder sensitivity so that a load of 40 KN caused a full scale recorder deflection of 250 mm. During a test the specimen temperature was recorded on the other channel. The load and load rate at a particular temperature were estimated directly from the record as shown in figure 51. The variation of Young's Modulus for $\frac{1}{2}\text{Cr } \frac{1}{2}\text{Mo } \frac{1}{4}\text{V}$ steel with temperature was taken from the data of Date¹⁸⁶. Values calculated from load-displacement curves made during the present work at ambient temperature and at 700°C are compared with those of Date¹⁸⁶ on figure 52. It would appear that the approximation of $K = E$ is fairly well justified. The specimens used were some 120 mm overall length having a parallel guage length of 55 mm, and a guage diameter of 12.7 mm. They were machined prior to heat treatment and checked for distortion and initial hardness prior to testing. After insertion into the loading rig the specimens were loaded at a nominal strain rate of 0.12 min^{-1} . Initial stresses in the range 200 to 850 MN m^{-2} were employed. In this way the maximum strain applied to a specimen was of the order of 0.1%.

5.3 Anisothermal Stress Relaxation Behaviour of 'non-susceptible' Commercial $\frac{1}{2}\text{Cr } \frac{1}{2}\text{Mo } \frac{1}{4}\text{V}$ Steel

A two part testing program was used to assess the separate effects of solution treatment and prior austenite grain size upon the anisothermal stress relaxation of the commercial $\frac{1}{2}\text{Cr } \frac{1}{2}\text{Mo } \frac{1}{4}\text{V}$ samples. In the first part, samples which had been single solution treated at 1200°C and 1000°C respectively for one hour, were loaded to initial stresses in the range 200 to 850 MN m^{-2} and then subjected to the testing procedure outlined. In the second, samples which had been double solution treated to produce a range of prior austenite grain sizes were loaded to an initial stress of 550 MN m^{-2} and then stress relieved.

Figure 53 compares the stress - temperature response of single solution treated specimens of the non-susceptible sample (A). The numbers in parentheses identify the specimen used in a particular test. They are also shown on the strain rate - temperature response curves of figure 55. All of the stress curves showed an increase in the stress level as the temperature was initially increased from ambient to about 150°C . This effect may be due to specimen shrinkage as carbon comes out of the solution to form carbides. However, in view of the evidence of figures 49 and 50, suggesting that uneven heating of extensometers and specimen in this temperature region leads to contraction at the LVDT control position, it would appear that some of the observed increase in stress arises from the way in which the testing machine attempts to maintain constant strain by pulling the specimen to keep the signal from the LVDT's unchanged.

No evidence of cavitation was found in any of the specimens which had been solution treated at 1000°C for one hour. Figure 54 illustrates cavitation typical of the type found in specimen #3 and #14, which had been stress relieved from the highest stress levels in the series of tests upon specimens solution treated at 1200°C for one hour. Comparison with figure 34 would suggest that this cavitation of figure 54 had occurred in the latter stages of the test at temperatures in excess of 600°C.

Figure 55 compares the strain - rate temperature response of the same batch of specimens. Two major observations are immediately apparent from the form of the curves:

- (i) For all the tests there are two marked strain - rate troughs.
- (ii) The position of these troughs would appear to correspond to that of the ductility minima observed during tensile testing.

To investigate the nature of the rate controlling processes associated with the occurrence of these strain rate minima a simple Arrhenius Rate Law analysis was performed by modifying the familiar Arrhenius Rate Equation in which:

$$\text{rate} \propto \exp \frac{-\Delta H}{RT} \quad (5.4)$$

to the form:

$$\dot{\epsilon}_{\min} = \text{constant} \times \exp \frac{-\Delta H}{RT_{\dot{\epsilon}_{\min}}} \quad (5.5)$$

where: R = gas constant

ΔH = apparent activation energy

Values of minimum strain rate versus the reciprocal of the absolute

temperature at which the minimum occurred were plotted on a log-linear graph. Only results from the series of tests made on specimens solution treated at 1000°C for one hour are presented since the occurrence of cavitation in the other series would require that analysis of the additional contribution to the strain rate through cavitation be made. Figure 56 illustrates the form of these 'Arrhenius Plots' and indicates apparent activation energies of 52.75 kcal mol⁻¹ and 18.61 kcal mol⁻¹ for the upper and lower temperature troughs respectively.

These values are similar to those (59.0 kcal mol⁻¹ and 19.0 kcal mol⁻¹) reported³ in an investigation of the dependence of strain rate sensitivity minima on strain rate and testing temperature for $\frac{1}{2}\text{Cr } \frac{1}{2}\text{Mo } \frac{1}{4}\text{V}$ steam pipe material subject to uniaxial tensile testing. The value of 19 kcal mol⁻¹ for the lower temperature minimum is comparable with the activation energy for the diffusion of carbon in ferrite while that for the upper temperature minimum is comparable with the activation energy for the diffusion of vanadium in ferrite of 57 kcal mol⁻¹ 187. In the present context it would appear reasonable to attribute the lower temperature trough to a carbon-dislocation interaction and the upper temperature trough to a vanadium-carbon-dislocation interaction, consistent with the previous work³.

Despite the complications involved in the characterisation of stress - strain rate behaviour from anisothermal stress relaxation tests, as outlined in the first section of this chapter, an attempt was made to investigate the stress - strain rate relationship through the method illustrated in figure 42. Figure 57

shows the stress dependence of strain - rate at various temperatures plotted on a log-log basis. It is clear from the values of the slopes (m') of these plots that the stress - strain rate dependence determined under these conditions does not correspond to that determined isothermally in the tensile testing investigation. There are two major reasons why this should be so:

- (i) The stresses to produce various strain rates were not measured at the same strain, only at the same temperature.
- (ii) The temperature at which the stress and strain rate for a particular data point were measured was itself changing so that, in effect, the slope should be measured in stress - strain rate - temperature space, rather than just in stress - strain rate space.

For the first condition, it is impossible to achieve conditions of constant strain and constant temperature simultaneously from data derived during anisothermal testing. For the lower stresses, in the condition of lower strain, it is reasonable to suppose that the measured strain rates would be higher than if they had been determined at the same value of strain as those at higher stresses¹⁷². This would lead to a higher observed slope of the stress - strain rate response. For the second condition, the situation may be likened to one in which the initial transient isothermal deformation behaviour of the material is assessed during each small increment of temperature increase. According to the work of Hart¹⁸⁴ an important contribution to this transient behaviour may arise through the relaxation of stress by anelastic

deformation. The relative contribution to the strain rate through anelastic relaxation will be greatest at the lower levels of strain. Once again, this would lead to a higher observed slope of the stress - strain rate response. The values of m' are consistently observed to be greater than those of m determined from isothermal uniaxial tensile testing.

Figure 58 illustrates the stress - strain rate response of specimens of sample A which had been tested under conditions of isothermal stress relaxation at 50°C and 700°C . The measured values of the slopes appear to be quite close to those values of m determined from isothermal tensile testing, supporting the analyses of Hart^{162,172}. The fact that the stress - strain rate behaviour observed for anisothermal stress relaxation did not correspond to that observed for isothermal testing conditions casts some doubt on the reliability of predictions of anisothermal stress relaxation behaviour from creep and tensile data determined in isothermal tests (e.g. see ref.182).

The results of the second part of the program of tests on sample A are shown in figures 59 and 60. Figure 61 illustrates the variation of strain rate with prior austenite grain size at various temperatures. The observed decrease of strain rate with increase in grain size at 550°C is consistent with an increased contribution to the deformation process through grain boundary sliding⁸¹, at this temperature. The strain rate at 350°C and 450°C appears to be only slightly dependent upon the prior austenite grain size.

In summary, for the conditions of testing employed,

two troughs in the strain rate versus temperature response of $\frac{1}{2}\text{Cr } \frac{1}{2}\text{Mo } \frac{1}{4}\text{V}$ steel are observed. The lower temperature trough appears to be associated with a carbon - dislocation interaction but only slight grain boundary sliding. The upper temperature trough appears to be compatible with a vanadium - carbon - dislocation interaction and a much increased contribution to the observed deformation arising from grain boundary sliding.

Some evidence of cavitation in this 'non-susceptible' sample of $\frac{1}{2}\text{Cr } \frac{1}{2}\text{Mo } \frac{1}{4}\text{V}$ steel was found in specimens which had been heat treated to achieve both high degree of solution of vanadium carbide and coarse prior austenite grain size. The nature of this cavitation suggested that it had formed at temperatures in excess of 600°C .

5.4 Anisothermal Stress Relaxation Behaviour of 'susceptible' Commercial $\frac{1}{2}\text{Cr } \frac{1}{2}\text{Mo } \frac{1}{4}\text{V}$ Steel

The deformation behaviour of the 'susceptible' sample B under conditions of anisothermal stress relaxation investigated using the same two part program as described for sample A.

Figure 62 compares the stress - temperature response of the single solution treated specimens. The form of the curves appears ostensibly similar to that observed (figure 53) for the 'non-susceptible' sample A. However, they differ in one major respect in that for some specimens the stress appears to have undergone sudden reduction. In particular, specimens #15 and #4 show marked stress drops at about 350°C .

Macro-examination of these specimens, after sectioning and polishing, revealed that they had both suffered extensive

cracking perpendicular to the stress axis as shown in figure 63.

The micrographs of figures 64 and 65 illustrate that -

- (i) the failure was intergranular;
- (ii) little plastic deformation had occurred;
- and (iii) where blunting had occurred it was usually in association with inclusions.

Furthermore it is clear from figure 65 that the stresses associated with the growth of these cracks were high enough to cause the inclusions to be broken. Little evidence of cracking away from the main fracture was found. It would seem reasonable to suppose that such rapidly growing cracks were formed during the observed stress drops at about 350°C . Both specimens show further rapid stress drop behaviour at higher temperatures. It is most likely that further growth of the cracks formed at 350°C was occurring at temperatures in the region of 550°C to 600°C .

Figure 66 compares the strain rate - temperature response of specimens of sample B after single solution treatments at 1200°C and 1000°C for one hour. Although the detailed strain rate behaviour of sample B is complicated by the extensive cavitation, the strain rate troughs are again apparent. Figure 67 compares the stress - strain - rate response of specimens in the two conditions of prior solution treatment at various temperatures. Once again the values of m' are greater than values of m determined during the tensile testing investigation.

Figures 68 and 69 illustrate the stress - temperature and strain rate - temperature response respectively in specimens of sample B double solution treated to produce a range of prior austenite grain sizes. Figure 70 shows the strain rate variation as a

function of prior austenite grain size. Once again it appears that the observed strain rates at 350°C and 450°C are only slightly dependent upon grain size, while at 550°C the observed decrease of strain rate at increased grain size is consistent with an increased contribution to the deformation process through grain boundary sliding.

5.5 Discussion

It is clear that the anisothermal stress relaxation behaviour of the 'susceptible' sample $\frac{1}{2}\text{Cr } \frac{1}{2}\text{Mo } \frac{1}{4}\text{V B}$ differs from that of sample A in one major respect. That is in the formation of extensive intergranular cracking. Comparison of figures 63 and 65 with figure 1 (reproduced again in this chapter) suggests that this cracking behaviour is similar to that observed in weld HAZ's which have suffered stress relief cracking. The conditions under which such cracking arises have been identified as being associated with a trough in the strain rate - temperature response of $\frac{1}{2}\text{Cr } \frac{1}{2}\text{Mo } \frac{1}{4}\text{V}$ which itself appears to be controlled by a carbon - dislocation interaction mechanism³. The work of Glen¹⁵ in which intergranular failure was observed to occur during a 'transition of creep rate' would appear to be directly comparable.

An important question which arises, concerns the temperature at which the cracking was observed to occur. Why, one may ask, did the specimens of sample B, heat treated under similar conditions, not fail in a similar manner when deformed at 350°C in the rising load tensile tests described in chapter three? This question is important not only because it focuses attention upon the mechanism by which SRC occurs, but also because it highlights the inadequacy of the interpretations of SRC discussed in chapter

one which essentially attribute the phenomena to an alloy carbide strengthening effect apparently associated with the promotion of intergranular cavitation at temperatures in excess of 500°C as observed in uniaxial tensile testing.

The extremely brittle nature of the cracking illustrated in figures 63, 64 and 65 suggests that the cracks, once nucleated have grown rapidly under the action of the high applied stress. The model of Smith and Barnby¹⁰⁵ for the nucleation of grain boundary cavities may be described by an equation of the form:

$$\sigma^2 = \frac{2\gamma E\pi c}{d^2(1-\nu^2)} \quad (5.6)$$

where:

- σ = stress
- $2d$ = distance between barriers along boundary
- $2c$ = barrier thickness
- E = Young's modulus
- γ = surface energy term
- ν = Poisson's ratio

Recalling equation (1.3) in which:

$$r_c = \frac{2\gamma}{\sigma} \quad (1.3)$$

and making the following assumptions:

- (i) barrier thickness equals critical nucleus size,
(i.e. $r_c = c$);
- (ii) distance between barriers equals that estimated at 450°C
(i.e. $\bar{r}_{450} = d$);
- (iii) $\nu = 0.3$;

it is then possible to solve equations (5.6) and (1.3) simultaneously for the conditions of the observed stress drops in specimens

#4 and #15, at 350°C. Taking the value for Young's Modulus at 350°C from figure 52 to be $18 \times 10^4 \text{ MN m}^{-2}$, and the measured stresses at the beginning of the stress drops as 410 MN m^{-2} and 350 MN m^{-2} for specimens #15 and #4 respectively, then values of r_c and γ may be calculated as:

(i) for specimen #15

$$r_c = 87 \times 10^{-10} \text{ m}$$

$$\gamma = 1.8 \text{ J m}^{-2}$$

(ii) for specimen #4

$$r_c = 81 \times 10^{-10} \text{ m}$$

$$\gamma = 1.4 \text{ J m}^{-2}$$

The values for r_c appear to be rather small, certainly particles $160 \times 10^{-10} \text{ m}$ in diameter would not be easily seen by SEM⁷⁵. The values of γ are about an order of magnitude lower than the values of 'effective surface energy' quoted¹⁶⁵ for steels. However, these estimations of critical nucleus size and surface energy do indicate that nucleation should be relatively easy under these conditions of stress and temperature.

To understand why growth of intergranular cavities under these same conditions was not observed during tensile testing it is necessary to recall that the work hardening rate and strain rate sensitivity of the material at 350°C were both observed to be low. Furthermore, even if some cavity growth occurred during the rising load tensile test it would not be accompanied by any marked reduction of stress level. In this way it is possible to envisage a situation in which a growing cavity becomes rapidly blunted as a result of strain localisation. The observation

of a blunted boundary cavity formed at 400°C in sample B (see figure 32) is clear support for this idea.

The conditions of loading in the anisothermal stress relaxation test differ in that they allow crack propagation to occur in association with stress reduction. It was observed that little plastic deformation was associated with the cracks. Furthermore, the fact that the failure occurred in association with a strain rate trough and little grain boundary sliding, indicates that the condition of the material was such that resistance to initial matrix flow was high. In this situation, crack tip blunting will be inhibited until extensive crack growth has occurred.

In chapter three it was observed that the nucleation of intergranular cavities at temperatures above 400°C appeared to be easier in sample B than in sample A. One possible reason for this behaviour was believed to be the increased impurity content of sample B. Once again, in view of the magnitude of the estimated surface energy associated with the stress relief cracks it is tempting to relate the ease of nucleation and propagation to an impurity segregation effect. This possibility is discussed in greater detail in chapters six and seven.

The foregoing observations and discussion underline the inadequacy of the currently available theories of failure by intergranular cavitation. In particular, the situation in which cavity growth rates are assumed to be slower at low temperatures and final unstable failure is assumed to occur only after a certain proportion of the grain boundaries have become cavitated is seen to be unrealistic. *Furthermore, the understanding of*

SRC as a problem of low rupture strain is now seen as one in which failure occurs at low strains because it is essentially nucleation controlled.

It is felt therefore that much of the confusion which has arisen in connection with the assessment of susceptibility to SRC is the result of adopting test procedures or microstructural conditions which allow failure to occur in a growth controlled manner, so that, as observed in chapter three, for example, the rising load tensile test normally imposes deformation conditions upon the specimen, which preclude the development of low strain intergranular failure at intermediate temperatures and high stresses. It would appear that any loading situation involving the application of either constant tensile stress or load will impose the same limitation¹⁷⁵ due to the rapid development of conditions of unstable deformation even in the absence of any cavitation. In this way it has formerly been found difficult to differentiate realistically between materials, all of which fail by intergranular cavitation, in terms of their susceptibility to SRC.

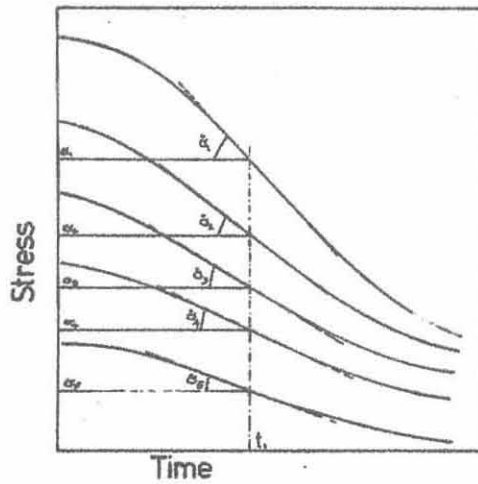
5.6 Conclusions

The foregoing simple analysis of the anisothermal stress relaxation behaviour of $\frac{1}{2}\text{Cr } \frac{1}{2}\text{Mo } \frac{1}{4}\text{V}$ steel has established:

- (i) The presence of two strain - rate troughs arising from (a) formation of carbon-dislocation interaction in the temperature range 300°C to 400°C ; and (b) formation of vanadium - carbon - dislocation - interaction in the temperature range 500°C to 600°C .
- (ii) That for the conditions of loading used, grain boundary

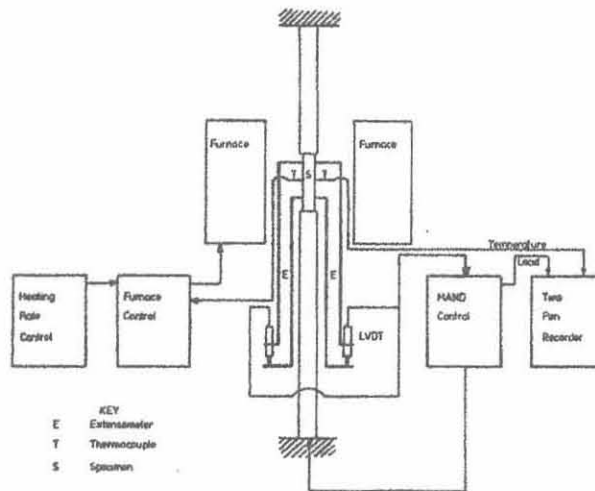
sliding is limited in the lower temperature trough, but active in the higher temperature trough.

- (iii) That failure of a material susceptible to SRC occurs in the region of the lower temperature strain rate trough due in the first instance to the way in which the loading conditions allow rapid crack propagation under the action of the high unrelieved stresses.
- (iv) That the mode of failure of a material susceptible to SRC is nucleation controlled intergranular cavitation and is therefore favoured by conditions of high stress, coarse grain size, high resistance to matrix flow and contaminated boundaries.
- (v) That even in the absence of adequate theoretical description, the anisothermal stress relaxation testing of smooth tensile specimens allows the production of reproducible observations of the conditions under which unstable intergranular cavitation occurs at very low strains.
- (vi) That SRC in $\frac{1}{2}\text{Cr } \frac{1}{2}\text{Mo } \frac{1}{4}\text{V}$ steel is not associated with a grain strengthening effect promoted by the formation of a fine dispersion of V_4C_3 .



Specimens having a range of initial stresses are heated at the same rate. After time t_i , each should be at the same temperature (T_i). At T_i , stress relaxation is occurring at various rates, depending on the current stress. Under these conditions, plastic strain rate $\dot{\epsilon}_p = -\frac{\dot{\sigma}}{E}$.

(a)



SPECIMENS LOADED AT ROOM TEMPERATURE, UNDER CLOSED LOOP STRAIN CONTROL, SIMULATING A RESIDUAL STRESS SITUATION. AS THE TEMPERATURE IS INCREASED, STRESS RELAXATION IS MONITORED.

(b)

Figure 48. (a) Outline of method used to estimate strain rate during anisothermal stress relaxation. (b) Block diagram of system used.

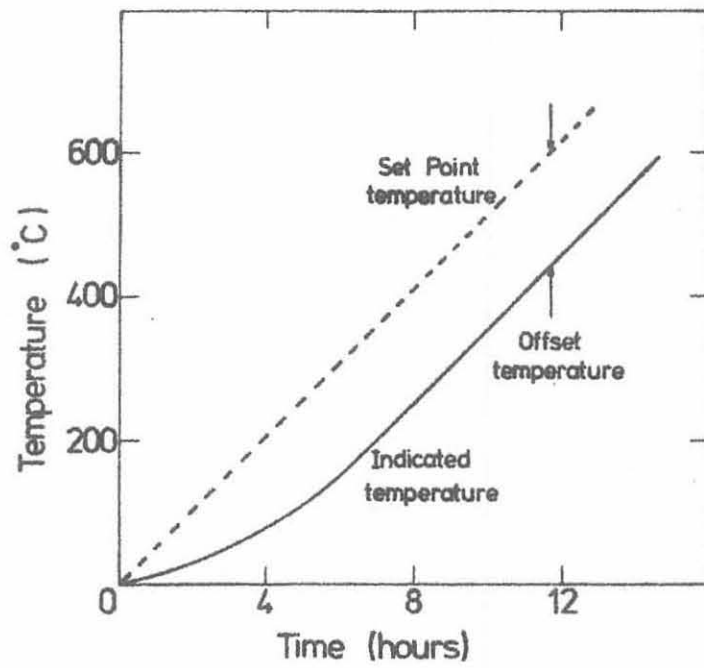


Figure 49. Schematic representation of the heating response of the specimen.

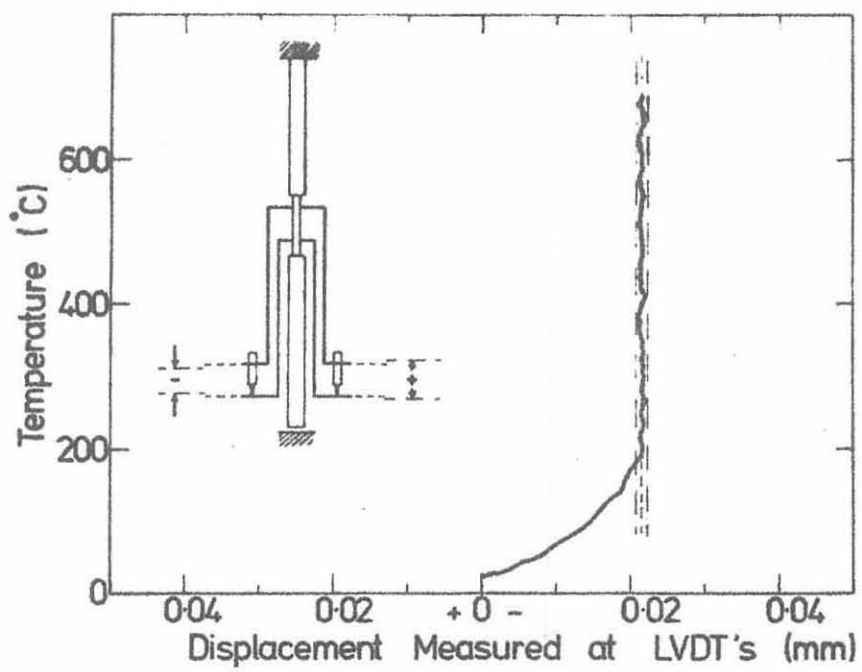


Figure 50. Off-load displacement as a function of temperature for a heating cycle similar to that illustrated in Figure 49.

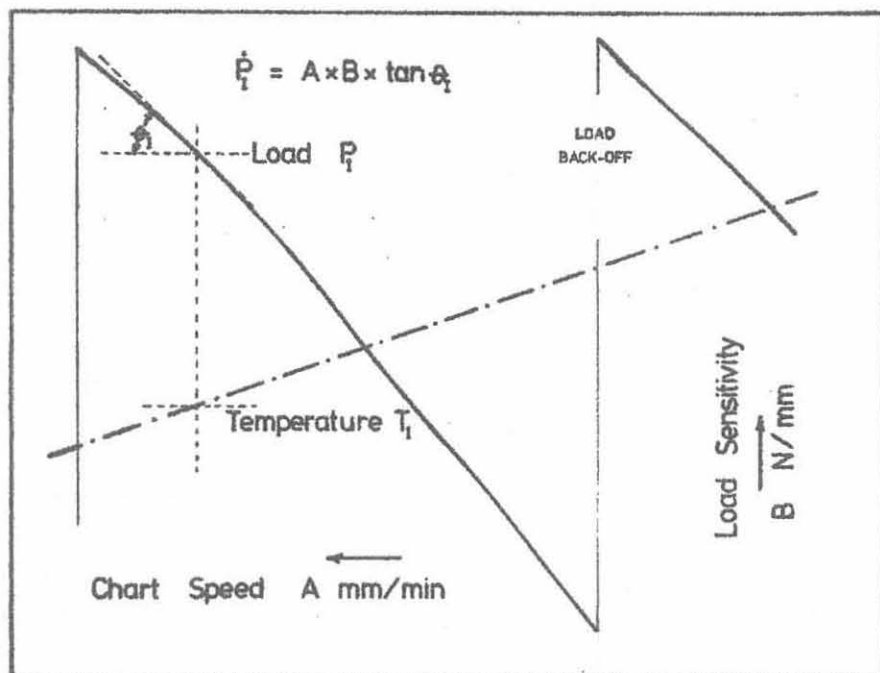


Figure 51. Schematic illustration of interpretation of load - time records.

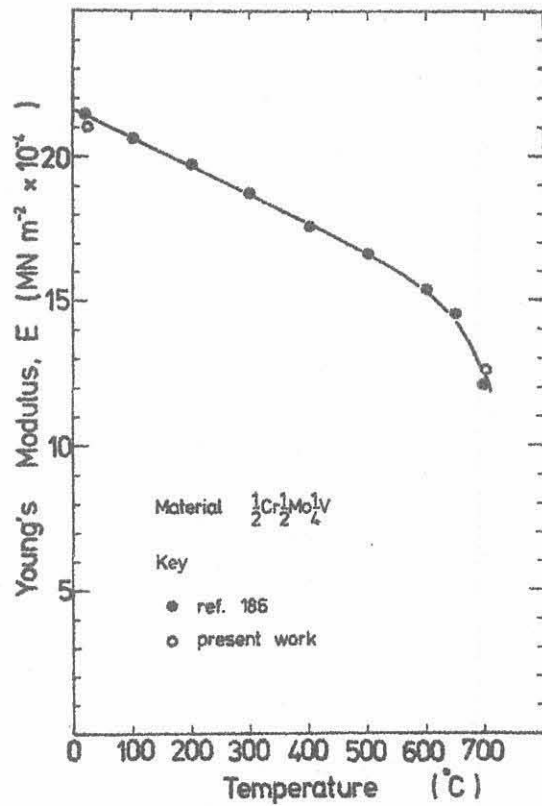
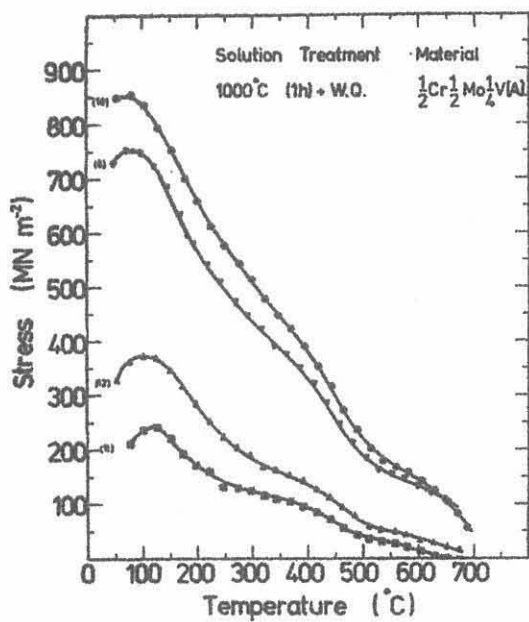
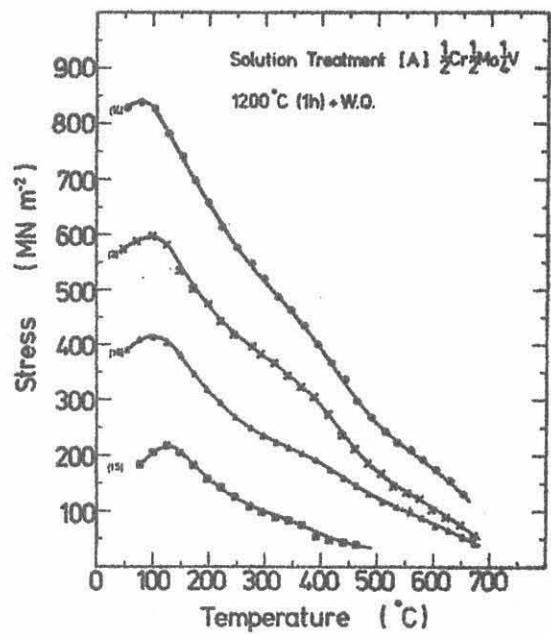


Figure 52. Variation of Young's Modulus with temperature. (186)



(a)

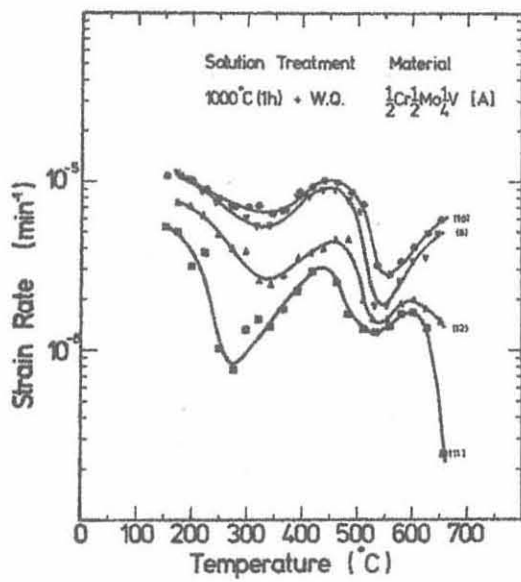


(b)

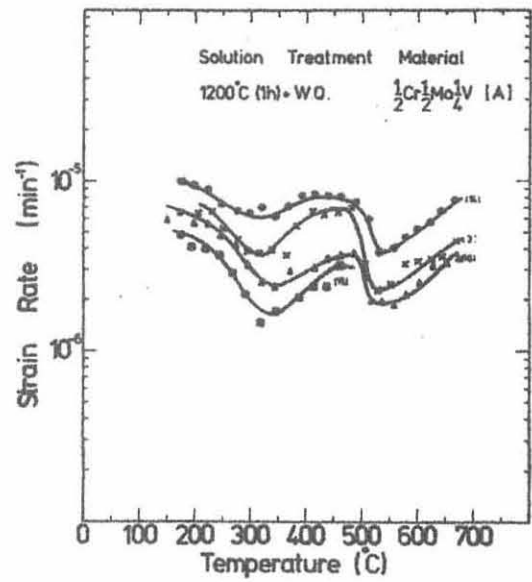
Figure 53. Stress - temperature response for $\frac{1}{2}\text{Cr} \frac{1}{2}\text{Mo} \frac{1}{4}\text{V} \text{ A}$
 (a) Solution treated at 1000° C for one hour
 (b) Solution treated at 1200° C for one hour.



Figure 54. Cavitation in specimen #3
(Tensile axis vertical)



(a)



(b)

Figure 55. Strain-rate - temperature response for $\frac{1}{2}\text{Cr} \frac{1}{2}\text{Mo} \frac{1}{4}\text{V}$ A
 (a) Solution treated at 1000°C for one hour
 (b) Solution treated at 1200°C for one hour.

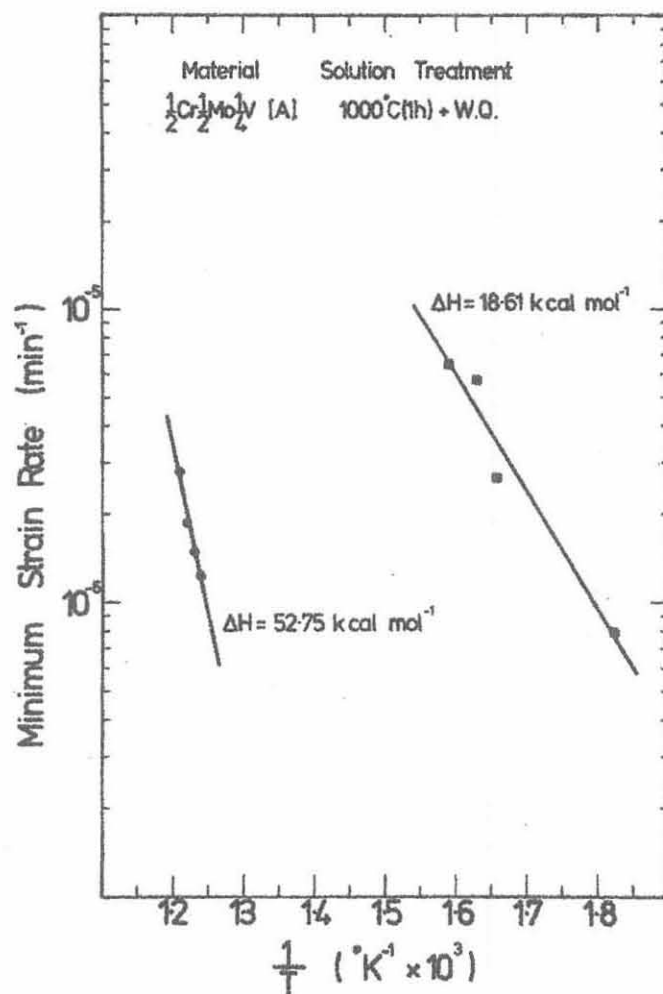
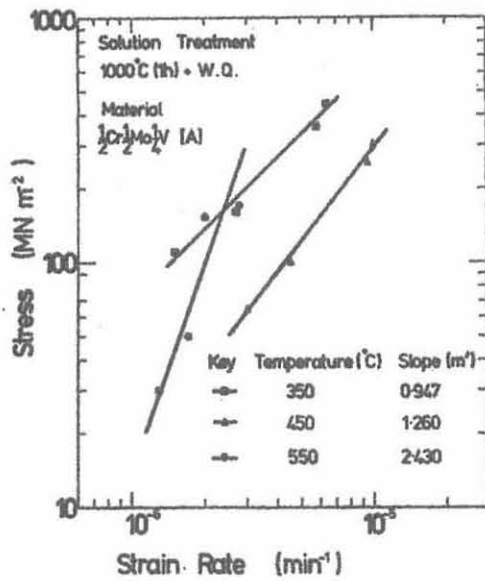
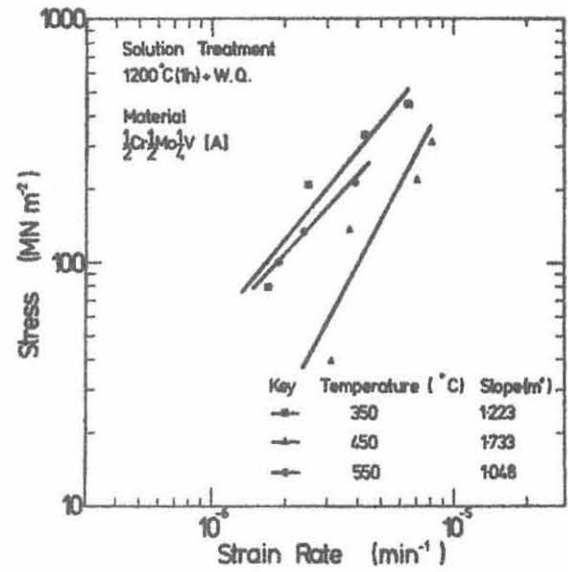


Figure 56. 'Arrhenius' plots for minimum strain rate conditions in $\frac{1}{2}\text{Cr} \frac{1}{2}\text{Mo} \frac{1}{2}\text{V}$ A.



(a)



(b)

Figure 57. Stress - Strain-rate plots at various temperatures. Data taken from anisothermal results.
 (a) $\frac{1}{2}\text{Cr} \frac{1}{2}\text{Mo} \frac{1}{4}\text{V}$ A solution treated at 1000°C
 (b) $\frac{1}{2}\text{Cr} \frac{1}{2}\text{Mo} \frac{1}{4}\text{V}$ A solution treated at 1200°C

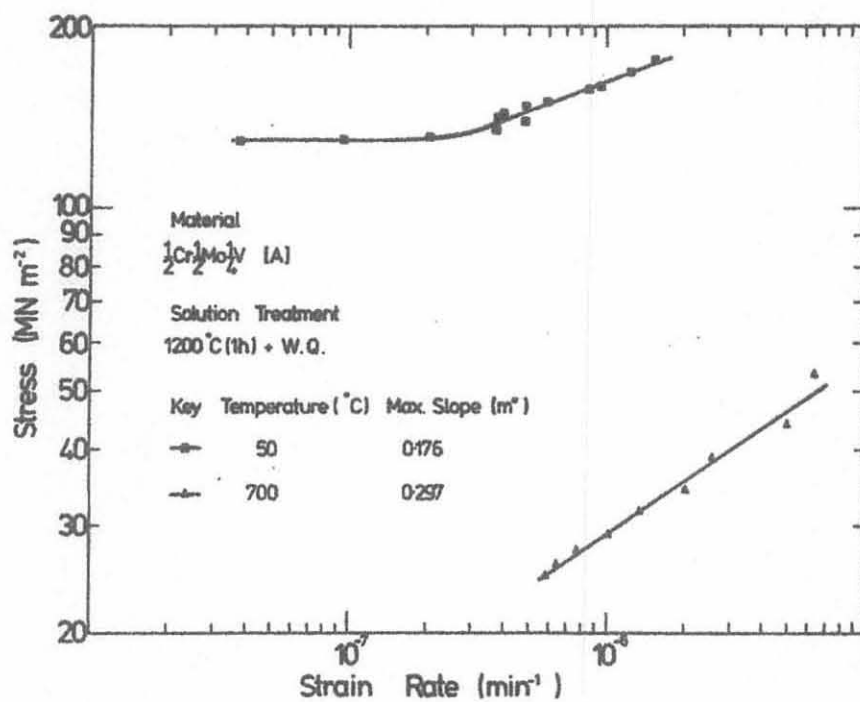


Figure 58. Isothermal stress - strain rate plots derived from isothermal stress relaxation of $\frac{1}{2}\text{Cr} \frac{1}{2}\text{Mo} \frac{1}{4}\text{V}$ A solution treated at 1200°C for one hour.

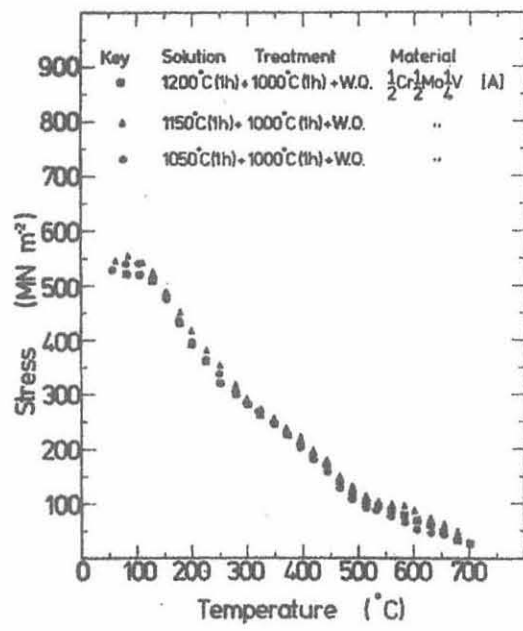


Figure 59. Stress - temperature response for $\frac{1}{2}\text{Cr} \frac{1}{2}\text{Mo} \frac{1}{4}\text{V}$ A after various solution treatments.

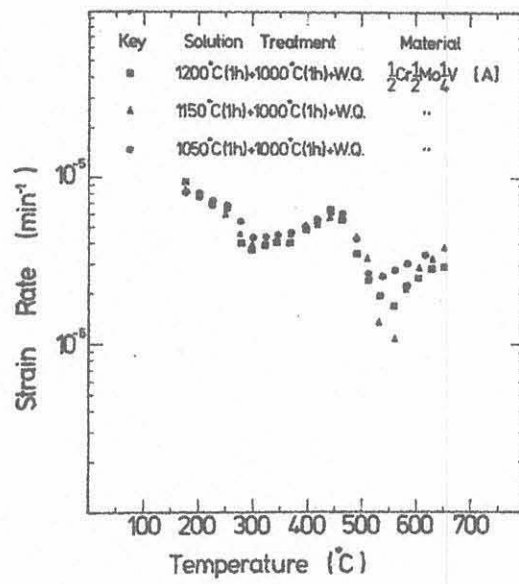


Figure 60. Strain - rate - temperature response for $\frac{1}{2}\text{Cr}-\frac{1}{2}\text{Mo}-\frac{1}{4}\text{V}$ A, after various solution treatments.

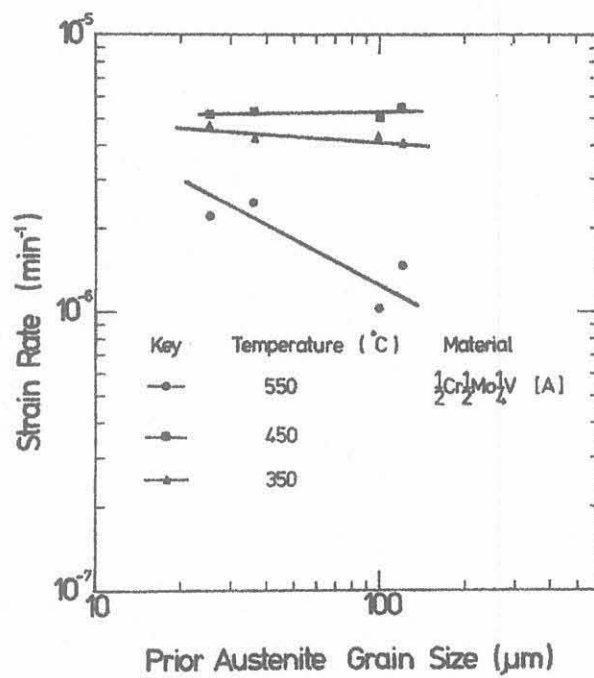
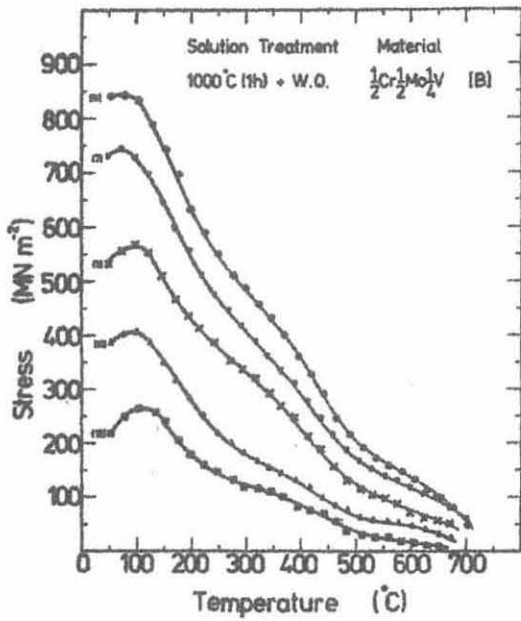
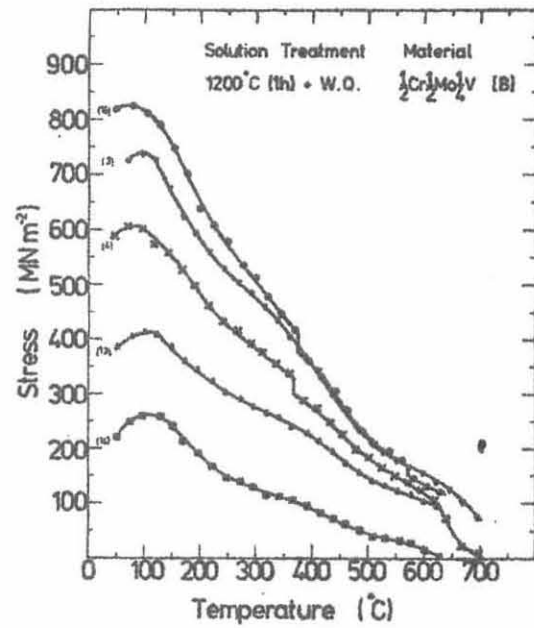


Figure 61. Strain - rate as function of prior austenite grain size at various temperatures.

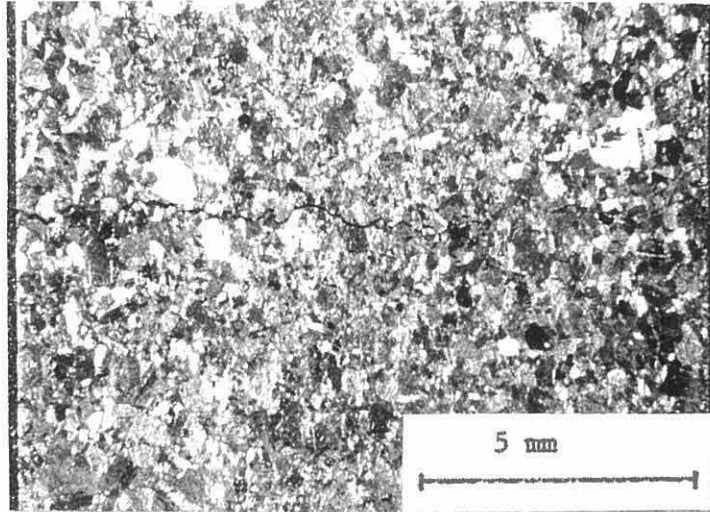


(a)

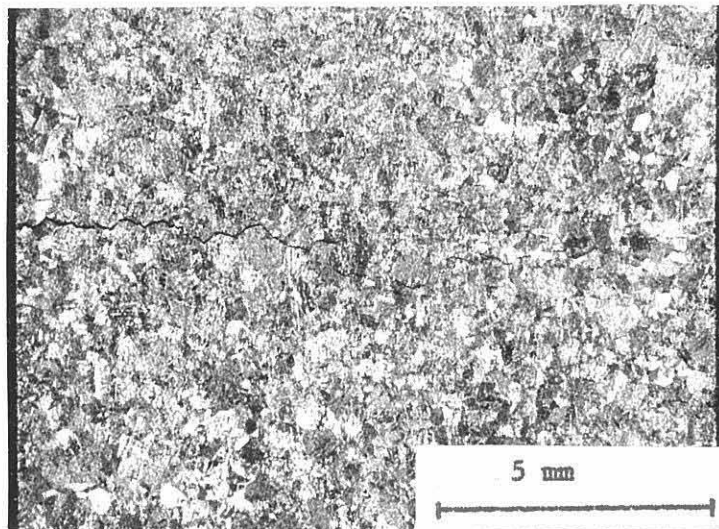


(b)

Figure 62. Stress - temperature response for $\frac{1}{2}\text{Cr} \frac{1}{2}\text{Mo} \frac{1}{4}\text{V}$ B
 (a) After solution treatment at 1000°C for one hour
 (b) After solution treatment at 1200°C for one hour



(a)



(b)

Figure 63. Gross cracking in $\frac{1}{2}\text{Cr } \frac{1}{2}\text{Mo } \frac{1}{4}\text{V B}$
during anisothermal stress relaxation.
(a) Specimen # 15
(b) Speciman # 4



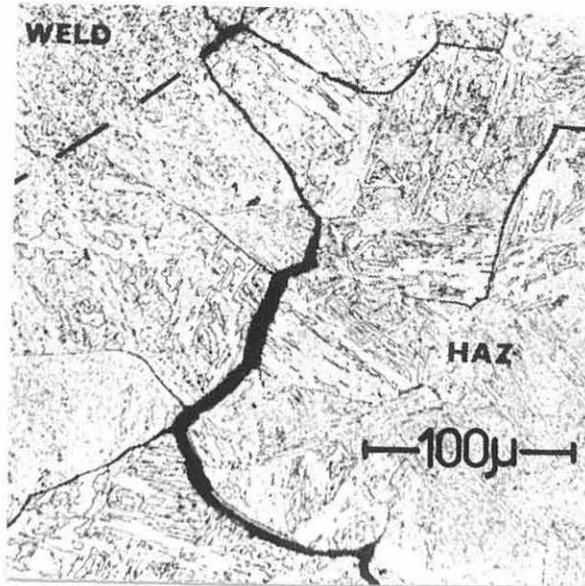
(a)



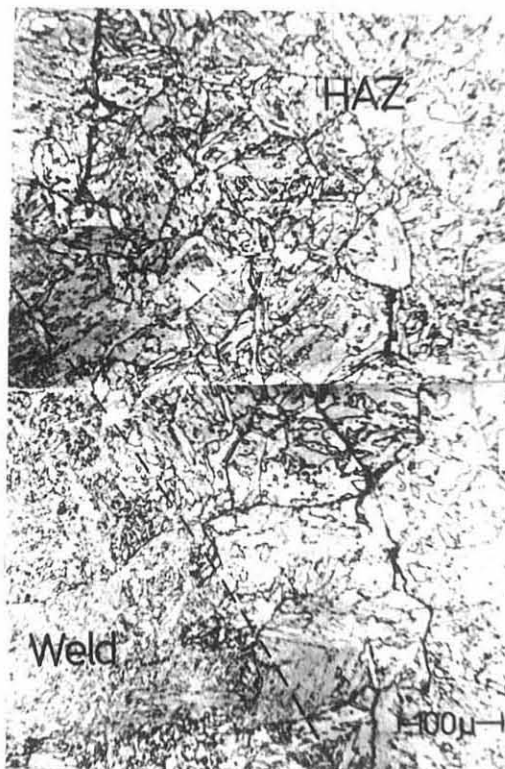
(b)

Figure 64. Details of cracking shown in Figure 63

(a) $\frac{1}{2}\text{Cr}$ $\frac{1}{2}\text{Mo}$ $\frac{1}{4}\text{V}$ B specimen # 4
(b) $\frac{1}{2}\text{Cr}$ $\frac{1}{2}\text{Mo}$ $\frac{1}{4}\text{V}$ B specimen # 15



(a)

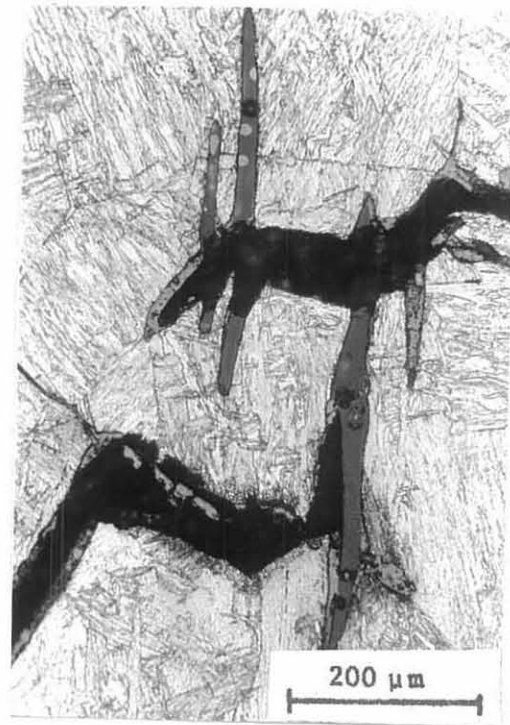


(b)

Figure 1. (a) HAZ cracking in A517F (Ref. 64)
(b) HAZ cracking in $\frac{1}{2}\text{Cr } \frac{1}{2}\text{Mo } \frac{1}{4}\text{V}$ (Ref. 50)
(N.B. A517F composition is basically 0.5%Cr 0.5%Mo 0.1%V)

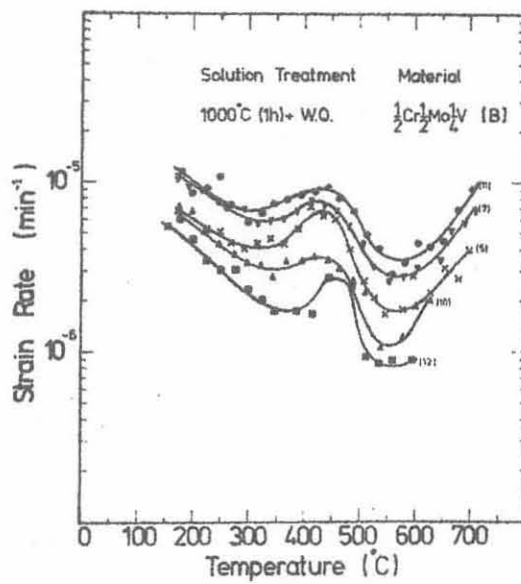


(a)

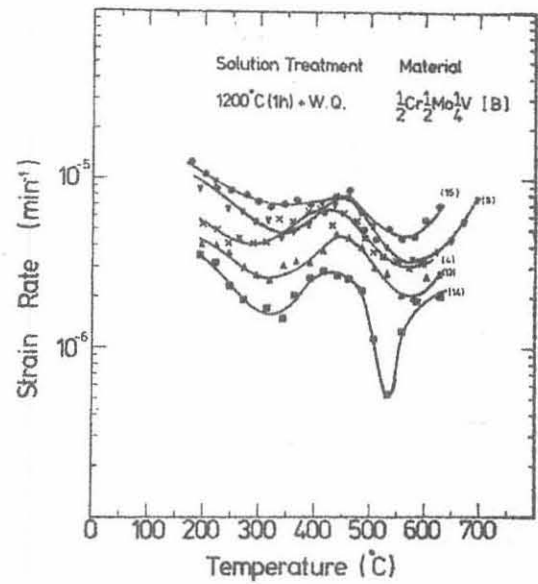


(b)

Figure 65. Details of cracking shown in Figure 63 illustrating fracture of inclusions intersecting main crack path.
(a) Specimen # 4
(b) Specimen # 15

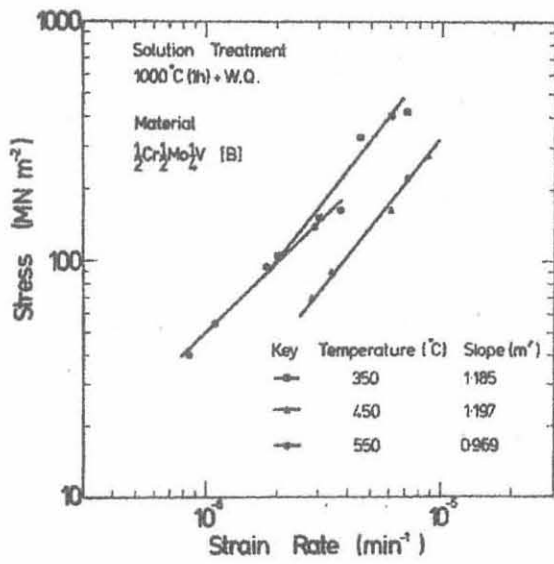


(a)

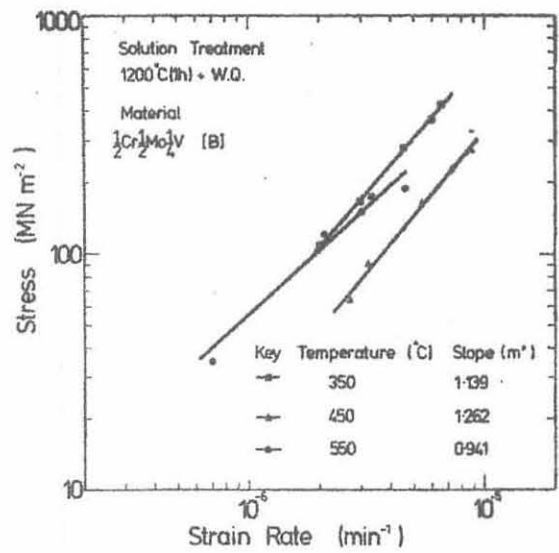


(b)

Figure 66. Strain - rate - temperature response of $\frac{1}{2}\text{Cr} \frac{1}{2}\text{Mo} \frac{1}{4}\text{V B}$
 (a) After solution treatment at 1000°C for one hour
 (b) After solution treatment at 1200°C for one hour



(a)



(b)

Figure 67. Stress - Strain-rate plots at various temperatures.

(a) $\frac{1}{2}\text{Cr} \frac{1}{2}\text{Mo} \frac{1}{4}\text{V}$ B solution treated at 1000°C

(b) $\frac{1}{2}\text{Cr} \frac{1}{2}\text{Mo} \frac{1}{4}\text{V}$ B solution treated at 1200°C

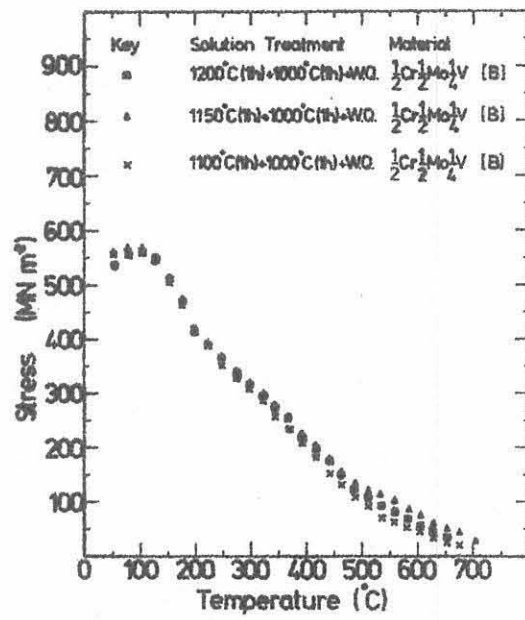


Figure 68. Stress - temperature response of $\frac{1}{2}\text{Cr} \frac{1}{2}\text{Mo} \frac{1}{4}\text{V}$ B after various solution treatments.

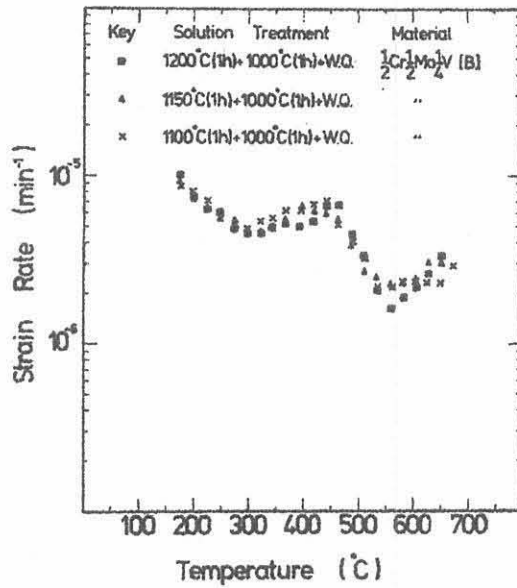


Figure 69. Strain - rate - temperature response of $\frac{1}{2}\text{Cr} \frac{1}{2}\text{Mo} \frac{1}{4}\text{V}$ B after various solution treatments.

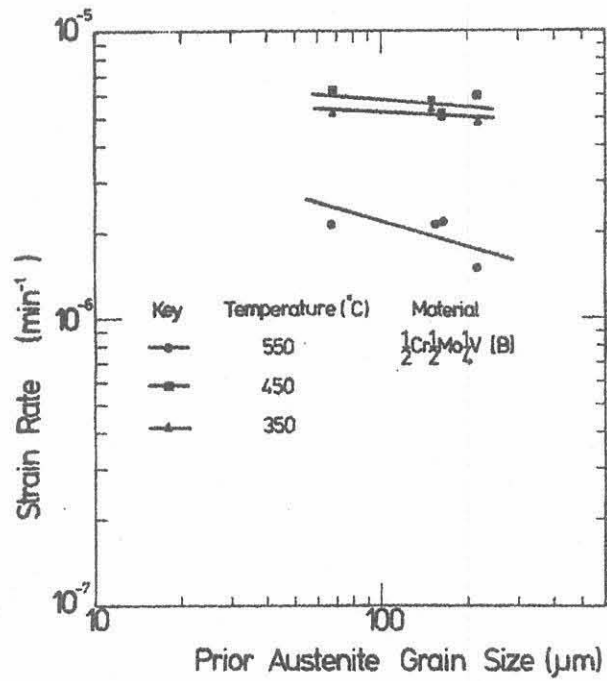


Figure 70. Strain rate as a function of prior austenite grain size for $\frac{1}{2}\text{Cr} \frac{1}{2}\text{Mo} \frac{1}{4}\text{V}$ B, at various temperatures.

CHAPTER VI

Intergranular failure of Commercial 'susceptible' and
'non-susceptible' $\frac{1}{2}\text{Cr}$ $\frac{1}{2}\text{Mo}$ $\frac{1}{4}\text{V}$ Steel at low temperatures6.1 Introduction

In chapter one of this thesis it was explained that SRC is commonly understood as a problem in which the cohesive strength of the prior austenite grain boundaries become limiting, in a situation in which the strength of the grains is increased. In chapter two it was shown that there was no marked strength increase within the grains as assessed by the hot micro-hardness test. However, the investigations described in chapters three and five pointed to the possibility of unstable intergranular cavitation failure occurring in an 'nucleation controlled' manner associated with very little matrix deformation. The conditions required for this mode of failure were understood to include:

- (i) High resistance to initial matrix flow.
- (ii) High probability of crack initiation upon a boundary.

The first requirement appears to be controlled by the amount of carbon or vanadium in solution in the martensitic matrix. The second requirement appears to depend upon the prior austenite grain size for the rapid build up of stress concentration on the grain boundary at low strains.¹⁷⁰ In addition, it was inferred that a further controlling factor for the second requirement might involve a lowering of the cohesive strength of the boundary as a result of impurity contamination⁷⁵.

The effects of impurity contamination in promoting intergranular failure through reduced boundary cohesion have been

extensively studied in connection with the phenomenon of temper embrittlement in steels^{189,190}. The work described in this chapter does not give a complete description of the kinetics and form of temper embrittlement in $\frac{1}{2}\text{Cr } \frac{1}{2}\text{Mo } \frac{1}{4}\text{V}$ steels, because this would be a separate study in itself. Instead it was designed simply to compare the propensity of the two commercial samples of $\frac{1}{2}\text{Cr } \frac{1}{2}\text{Mo } \frac{1}{4}\text{V}$ steel to fail in an intergranular manner at low temperatures, with the hope of producing a qualitative assessment of the relative cohesive strengths of the prior austenite grain boundaries. The work is complementary to that described in earlier chapters which have concentrated on the effect of matrix condition and microstructure.

6.2 Estimation of Fracture Toughness at 77°K in as quenched Material

The study of temper embrittlement in steels has identified the impurity elements responsible for the reduction of grain boundary cohesion as belonging to Groups IV, V and VI in the periodic table¹⁹¹. However, the way in which these elements segregate to the grain boundaries has not yet been completely established. While it would appear that segregation occurs during tempering of the steel in the range 350°C to 600°C¹⁹¹, it has also been observed¹⁹² that elements such as phosphorus and perhaps tin and antimony may segregate to austenite grain boundaries below a temperature of about 1150°C during austenitisation, and be retained in the boundaries when the steel is quenched.

Since solution temperature in excess of 1150°C have been used in the present work, it seemed appropriate to test the

latter possibility. The method used¹⁹² to assess this austenitic segregation employed fracture toughness testing (at 77°K) of specimens solution treated at various temperatures in the range 1000°C to 1350°C*. A marked reduction in the fracture toughness was observed for specimens solution treated below 1150°C. In the present investigation standard three point bend fracture toughness specimens²⁰² of both samples were single solution treated in the range 1000°C to 1200°C for one hour, water quenched and then tested at 77°K. Each specimen broke without any measurable deviation from linearity of the load-deflection record. Crack lengths of the failed specimens were measured using a travelling microscope and values of fracture toughness were calculated using the recommended²⁰² K-calibration for three point bend specimens.

The results are presented in figure 71 as fracture toughness versus prior austenite grain size. At first sight, the results of figure 71 would appear to be consistent with impurity segregation during austenitisation, since the fracture toughness of the most coarse grained sample B (solution treated at 1200°C for one hour) appears to be above that of specimens of the same sample that have been solution treated at lower temperatures. Furthermore, the fracture toughness of sample A appears to show a maximum at an intermediate grain size, which behaviour might be interpreted as representing the conflicting factors of grain size (in reducing the boundary impurity content at fine grain sizes¹⁹³)

*The exact procedure involved a double solution treatment program, with lower temperatures in the range 1000°C to 1300°C in order that prior austenite grain sizes of the specimens should be substantially the same.

and solution treatment temperature (in decreasing the segregation at high temperatures). However, a detailed examination of the fracture surfaces, by scanning electron microscopy failed to reveal evidence of grain boundary rupture in any of these tests. The form of the results of figure 71 must then be explained in terms of the microstructural features associated with cleavage failure in these materials¹⁶⁵. In the present context it was not established that any boundary weakening occurred as a result of impurity segregation during austenitisation of commercial $\frac{1}{2}\text{Cr } \frac{1}{2}\text{Mo } \frac{1}{4}\text{V}$ steels.

6.3 Observations of Tensile Mechanical Properties of Tempered $\frac{1}{2}\text{Cr } \frac{1}{2}\text{Mo } \frac{1}{4}\text{V}$ at 77°K

Temper embrittlement is usually observed to occur after tempering in the region 350°C to 600°C. The embrittlement kinetics usually exhibit a "C"-curve behaviour^{193,194} similar to that shown in figure 4, such that tempering at a temperature close to the nose may be expected to produce rapid embrittlement. The investigation in the present work was limited to the variation of tempering temperature. Hounsfield No.13 tensile specimens cut from samples A and B were single solution treated at 1200°C and 1000°C respectively, followed by a water quench. They were then tempered isothermally in tube furnaces for one hour at temperatures in the range ambient to 700°C and then water quenched once again, before testing.

These variously solution treated and tempered specimens were then pulled to failure at 77°K. The nominal applied strain rate was 10^{-2} min^{-1} . Figure 72 compares the low temperature tensile mechanical properties of specimens taken from samples A and B,

tempered in the range 400°C to 700°C after prior solution treatment at 1000°C . The flow stress levels for specimens from both samples are nominally similar, showing a peak after tempering at 615°C for one hour, consistent with the hardening behaviour reported in chapter two. However, there is a significant difference in the measured values of ductility and fracture stress between the samples, A and B. Figure 73 illustrates a series of scanning electron micrograph taken upon specimens fractured in this series of tests. It is clear that the fracture surfaces of the specimens of sample A contain more areas of ductile failure than those of sample B. There was no evidence of any intergranular failure in any of the specimens.

Figure 74 compares the low temperature tensile mechanical properties of variously tempered specimens of samples A and B, after single solution treatment at 1200°C . The flow stress variation for the two samples in this state of prior solution treatment differs in two respects, viz:

- (i) The occurrence of a trough in specimens of sample B tempered in the region 250°C to 350°C .
- (ii) An increase in the maximum values of flow stress in specimens of sample A tempered at 615°C over those observed for similarly heat treated specimens of sample B.

The ductility of both samples, under these conditions of heat treatment and testing, is very low. It is notable that while values of tensile %Elon and %R.A. for specimens solution treated at 1200°C are significantly lower than those measured in specimens

solution treated at 1000°C , the values of fracture toughness shown in figure 71 were ostensibly unaltered. Examination of the scanning electron micrographs of figures 75 and 76 gives some indication of the possible reasons for this behaviour.

It is clear that the failure behaviour of both samples, in the temperature range of 270°C to 430°C , involves the formation of intergranular cracks along prior austenite grain boundaries. The extent of grain boundary failure in both samples was limited to about 1% of the fracture surface area. It is probable that the decreased ductility of sample B, during the formation of intergranular cracks, arose through the effect of sample B having a coarser prior austenite grain size than sample A, for the same condition of prior solution treatment¹⁹⁵.

As explained previously, the kinetics of embrittlement associated with intergranular failure usually exhibits a "C"-curve behaviour, with minimum times for complete embrittlement of the order of a few minutes¹⁹⁴, or a few hours¹⁹³, depending upon the details of alloy composition and heat treatment. It is quite possible, therefore, that this limited survey has not truly assessed the severity and range of embrittlement associated with reduced cohesion at prior austenite grain boundaries in these alloys. Nevertheless, it has been possible to identify the basic requirements for failure by this mode in these alloys, viz:

- (i) Coarse prior austenite grain size (presumably to allow more intense impurity segregation at grain boundaries).
- (ii) Tempering in the range 270°C to 430°C for one hour.
- (iii) High matrix strength, achieved through low temperature testing.

With respect to the latter requirement it is significant that no intergranular failure was observed in association with the 'secondary hardening' peak in the measured values of flow stress. The tempering temperature of 615°C at this peak is outside the range of temperatures over which this embrittlement is normally experienced¹⁹¹. Indeed, it is widely accepted¹⁹⁰ that tempering an "embrittled" material at this temperature causes a reversible de-embrittlement to occur, so that the once weakened boundaries are made to appear strong. It would appear, therefore, that the observed intergranular failure at low temperatures is the result of an impurity segregation effect. It is not possible, at this stage to identify precisely the elements involved. However, considering the tempering temperature range in which the intergranular failure was observed, it seems most likely²⁰³ that relatively light atom of phosphorus is responsible for the observed effect.

These observations have an important bearing upon those made in the previous chapters concerning the occurrence of intergranular cavitation at elevated temperatures. In particular, attention is drawn to the conditions which promoted the unstable intergranular crack growth in sample B during the stress relaxation experiments. It is significant that the failures were shown to have occurred rapidly at about 350°C , under conditions in which matrix flow was restricted and in which the high applied stress and coarse prior austenite grain size served to allow nucleation controlled growth.

It is not clear that exactly the same conditions prevailed in the low temperature testing. It would appear that the

principal growth mode for cracks was by cleavage (in the instances where intergranular failure was found). Clearly for the failure at 350°C the principal growth mode was along prior austenite grain boundaries, as shown in figure 64. This behaviour arises, we may assume, because of the variation of matrix toughness with temperature. At 77°K the crack propagates under the action of a very high applied stress, such that it may pass easily from transgranular to intergranular mode with little branching, as shown in figure 77. However, during stress relaxation at 350°C the applied stress is lower and the matrix toughness is higher as exemplified by the high ductilities observed during tensile testing (fig. 23), such that easy crack propagation is best achieved along prior austenite grain boundaries, consistent with the crack-tip blunting argument of chapter five.

It is proposed, therefore, that the evidence so far discussed would suggest that the nucleation of failure of sample B during stress relaxation is in some respects similar to that which may be induced to occur at low temperatures after tempering at temperatures in the region at which the stress relaxation cracking occurred. The association of intergranular failure in both instances with boundary particles may well be resolved by consideration of the application of McMahon's carbide rejection model¹⁹¹ to both situations.

The importance of the trace elements in promoting stress relief cracking is therefore underlined. However, it is further noted that the detailed observations of earlier chapters have shown that the deformation behaviour of sample B at elevated temperatures is essentially an extension of that of sample A at

coarser grain size. Moreover, the observation that low temperature intergranular failure occurred in both samples must imply that the promotion of SRC involves the tipping of a delicately balanced set of conditions towards the promotion of unstable intergranular crack propagation.

6.4 The Effect of Tempering at 350°C in Promoting Intergranular Failure in the Region of the Ductile - brittle impact transition Temperature

Much of the early work which has studied temper embrittlement has employed the technique of measuring the shift in the ductile - brittle impact transition temperature as a means of assessing the "degree of embrittlement"¹⁸⁹. This method has recently been criticised¹⁹³ on the grounds that by measuring the fracture process at different temperatures it precludes any absolute measurement of the development of embrittlement due to failure along prior austenite grain boundaries. Furthermore, it would appear possible to confuse the relative contributions of fracture mode (viz. cleavage ductile, intergranular) to the observed transition behaviour. However, in view of the discussion of the previous section it is perhaps not surprising that increasing use of the impact transition temperature measurements is being made in the assessment of a material to SRC².

In the present work, the effect of tempering at 350°C upon the impact properties of samples A and B, after single solution treatment at 1200°C for one hour, and double solution treatment at 1200°C for one hour plus 1000°C for one hour, was assessed using the Hounsfield balanced impact machine. Solution treatment was carried out in batches as described previously. Tempering was

carried out by heating similar batches of specimens in a fluidised bed at 350°C for one hour.

Figures 78 to 81 illustrate the impact energy curves and specimens for samples A and B in these various conditions of prior heat treatment. It is clear that the behaviour of sample B after tempering at 350°C gives a larger shift in transition temperature than sample A for equivalent prior solution treatment. However, there are several points of confusion arising from the detailed interpretation of these impact transition curves. First is the variation in form with prior solution treatment. Those specimens which have been double solution treated show a sharp transition, whereas the single solution treated specimens showed a steady increase in energy absorbed during impact testing with increase of temperature. Furthermore, in the case of the double solution treated samples, it would appear that while the shift in impact transition temperature for sample B as a result of tempering at 350°C is greater than that of sample A, *the actual transition temperatures for sample A are higher than those of sample B even after tempering.*

A detailed examination of fracture surfaces of specimens produced in this experiment failed to show any evidence of intergranular failure in the region of any of the transition temperatures. However, isolated facets were found (figure 82) in specimens of sample B which had been single solution treated, tempered and then broken at -85°C and -60°C. The photographs of figure 83 illustrate that the impact transition is controlled essentially by a change in fracture mode from cleavage to ductile void coalescence. The single solution treated specimens would be

expected to contain more carbon in solution than the double solution treated specimens. In this way, variation of the yield stress temperature response of the samples in the region of the transition temperatures as a result of different prior solution treatment might explain the differing form of the curves. This point was not investigated experimentally.

It is clear that the criticisms levelled against the impact transition temperature test¹⁹³, concerning the shift of balance between matrix and boundary strengths with temperature, are particularly applicable to the present work in which the formation of ductile failure serves to complicate the situation where only a small amount of low temperature intergranular failure has been observed. In this respect, the assessment of susceptibility to SRC by the inspection of impact transition temperature shift, after appropriate tempering treatment, would seem to be unreliable, since the observed shift may not be directly associated with intergranular cracking.

6.5 Conclusions

This attempt to assess the relative cohesive strengths of prior austenite grain boundaries in both samples A and B, under the possible influence of boundary contamination has established the following limited conclusions:

- (i) No boundary weakening as a result of impurity segregation during austenitisation was observed.
- (ii) About 1% intergranular failure in the fracture surfaces of smooth tensile specimens from both samples A and B broken at 77^oK, was found in specimens tempered

in the range 270°C to 430°C.

- (iii) The loss of ductility associated with this mode of failure was greatest in sample B, solution treated at 1200°C for one hour.
- (iv) It would appear that the segregation of phosphorus along prior austenite grain boundaries may be reasonably associated with the occurrence of this low temperature intergranular failure.
- (v) The conditions of boundary contamination, and high applied stress promoting the nucleation of intergranular failure in the smooth tensile specimens at 77°K appeared to be similar to those prevailing during the initiation of cracks during stress relaxation at about 350°C.
- (vi) The variation of growth mode in these two situations could have resulted from variation in the matrix toughness as the temperature was increased.
- (vii) Measurements of the shift in ductile-brittle impact transition temperature are very difficult to interpret in terms of the effects reduced boundary cohesion in promoting intergranular failure, particularly when these effects are small.

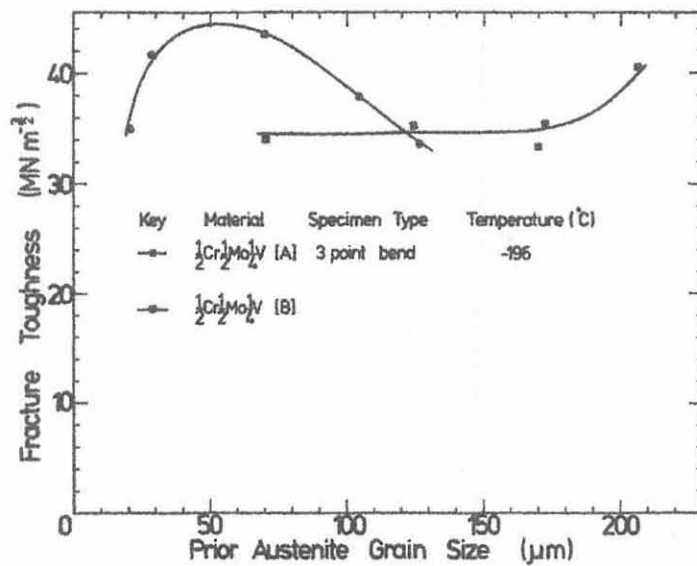
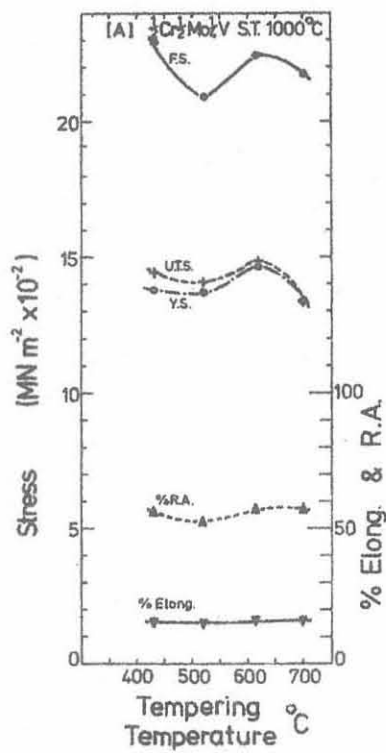
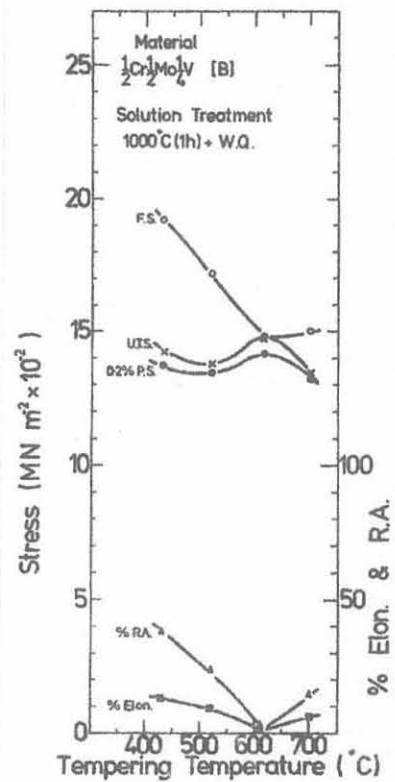


Figure 71. Fracture toughness of as quenched alloys at -196°C as a function of prior austenite grain size.



(a)



(b)

Figure 72. Low temperature tensile properties of quenched and tempered alloys after solution treatment at 1000°C for one hour.

(a) $\frac{1}{2}\text{Cr } \frac{1}{2}\text{Mo } \frac{1}{4}\text{V}$ A

(b) $\frac{1}{2}\text{Cr } \frac{1}{2}\text{Mo } \frac{1}{4}\text{V}$ B

Figure 73. Scanning Electron Micrographs of alloys A and B broken at -196°C

(a),(b),(c) - $\frac{1}{2}\text{Cr}$ $\frac{1}{2}\text{Mo}$ $\frac{1}{4}\text{V}$ A

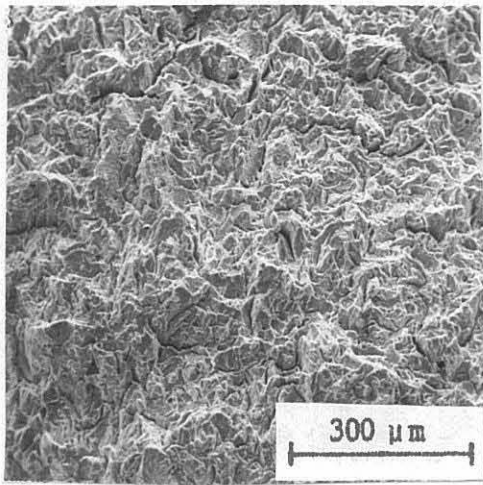
(d),(e),(f) - $\frac{1}{2}\text{Cr}$ $\frac{1}{2}\text{Mo}$ $\frac{1}{4}\text{V}$ B

(a),(d) - tempered at 430°C for one hour

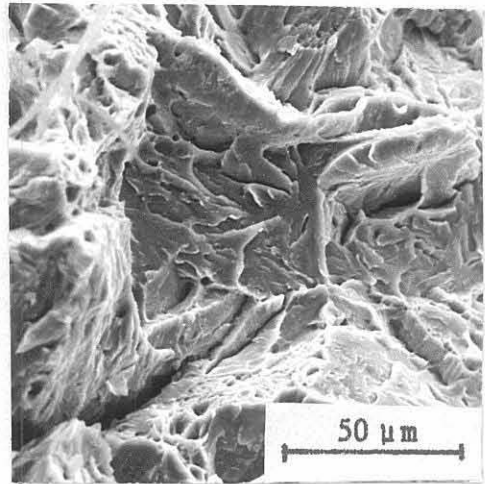
(b),(e) - tempered at 520°C for one hour

(c),(f) - tempered at 615°C for one hour

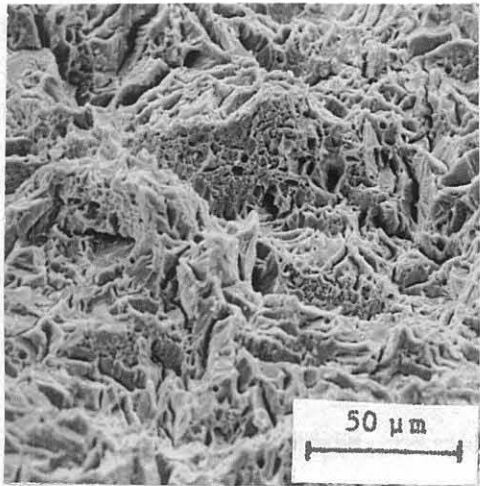
All specimens solution treated at 1000°C for one hour.



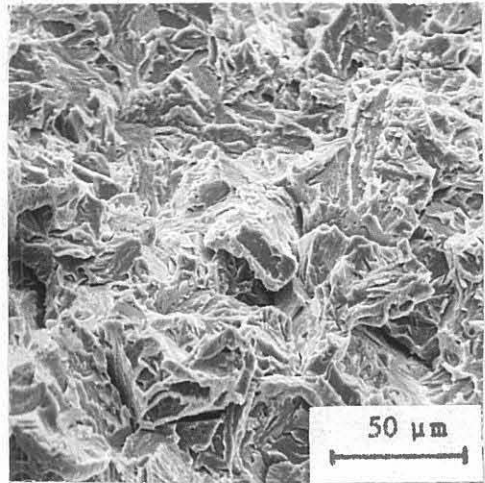
(a)



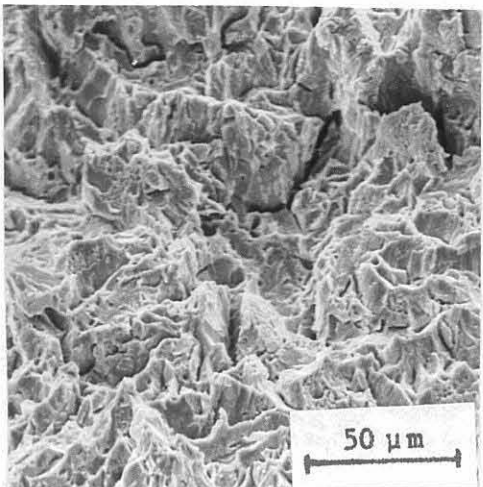
(d)



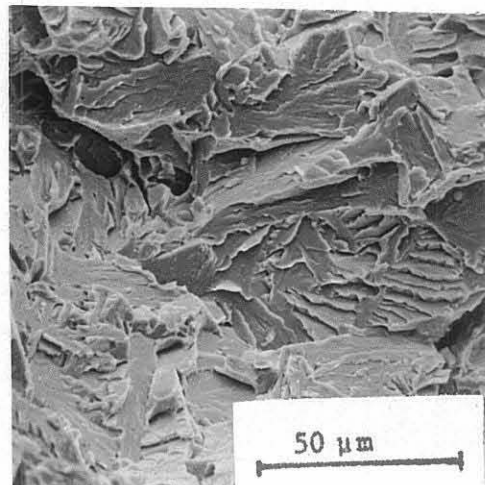
(b)



(e)

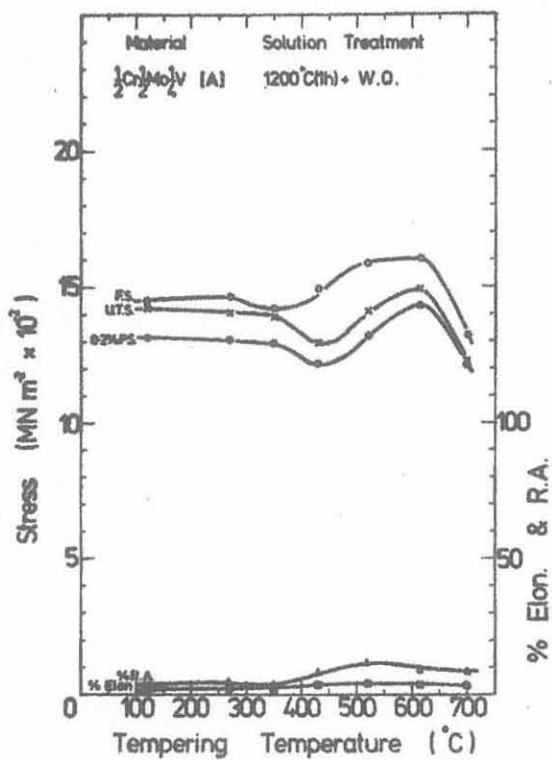


(c)

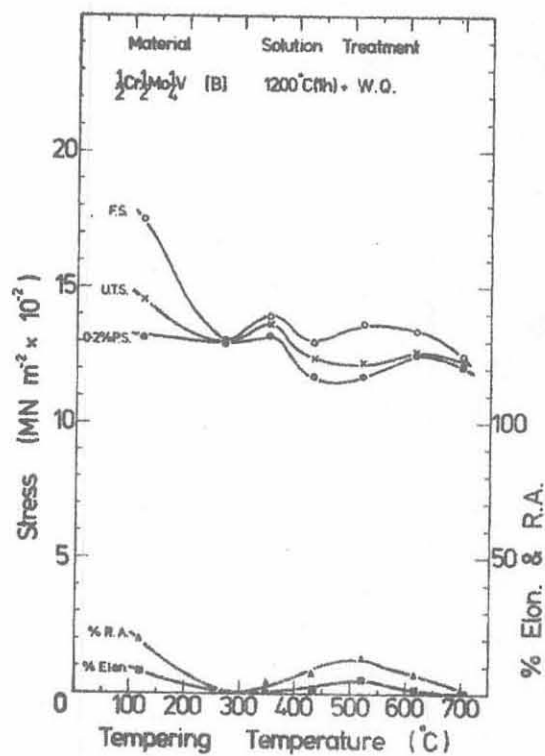


(f)

Figure 73.



(a)



(b)

Figure 74. Low temperature tensile properties of quenched and tempered alloys after solution treatment at 1200°C for one hour.

(a) $\frac{1}{2}\text{Cr} \frac{1}{2}\text{Mo} \frac{1}{4}\text{V}$ A

(b) $\frac{1}{2}\text{Cr} \frac{1}{2}\text{Mo} \frac{1}{4}\text{V}$ B

Figure 75. Scanning Electron Micrographs of alloys A and B broken at -196°C

(a),(b),(c) - $\frac{1}{2}\text{Cr}$ $\frac{1}{2}\text{Mo}$ $\frac{1}{4}\text{V}$ A

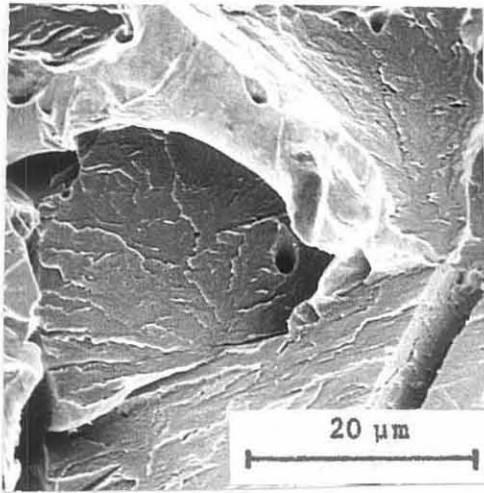
(d),(e),(f) - $\frac{1}{2}\text{Cr}$ $\frac{1}{2}\text{Mo}$ $\frac{1}{4}\text{V}$ B

(a),(d) - tempered at 120°C for one hour

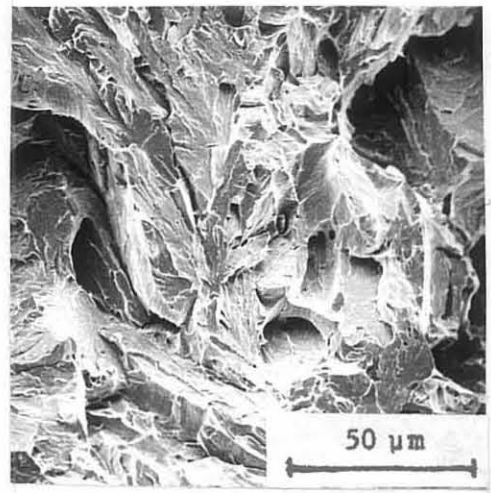
(b),(e) - tempered at 270°C for one hour

(c),(f) - tempered at 350°C for one hour

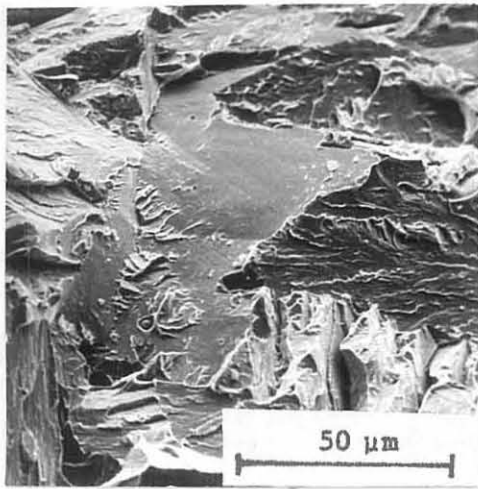
All specimens solution treated at 1200°C for one hour.



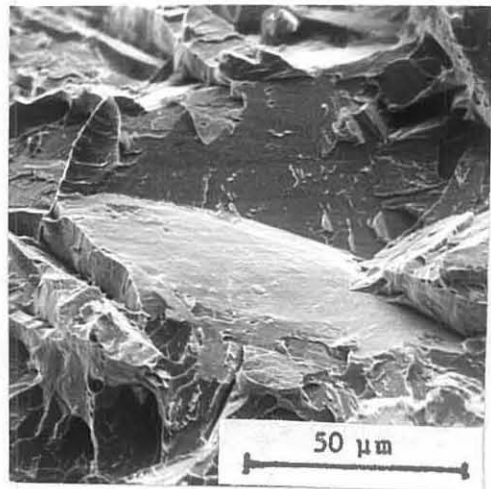
(a)



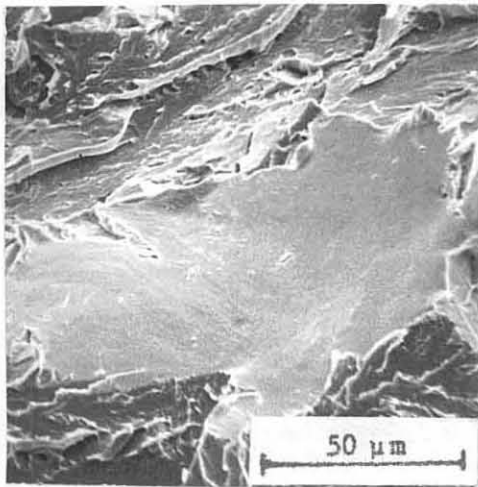
(d)



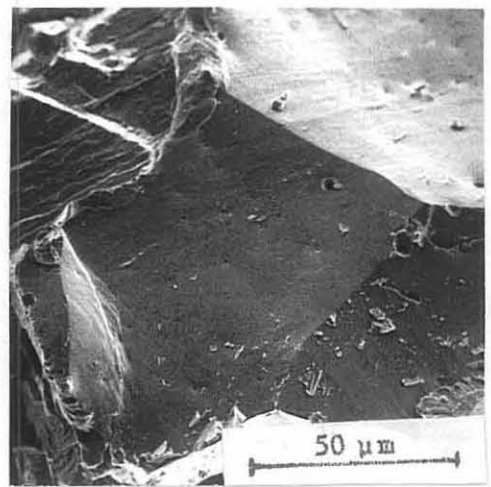
(b)



(e)



(c)



(f)

Figure 75.

Figure 76. Scanning Electron Micrographs of
alloys A and B broken at -196°C

(a),(b),(c) - $\frac{1}{2}\text{Cr } \frac{1}{2}\text{Mo } \frac{1}{4}\text{V}$ A

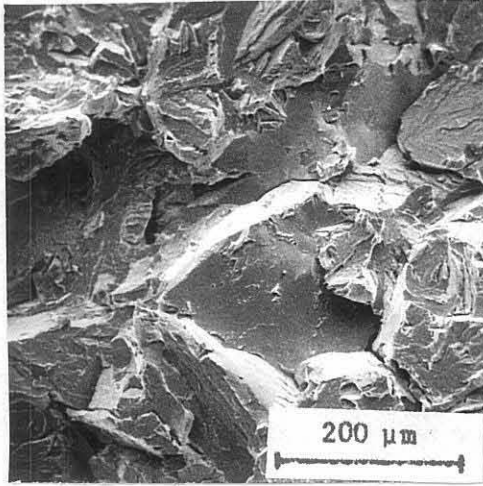
(d),(e),(f) - $\frac{1}{2}\text{Cr } \frac{1}{2}\text{Mo } \frac{1}{4}\text{V}$ B

(a),(d) - tempered at 430°C for one hour

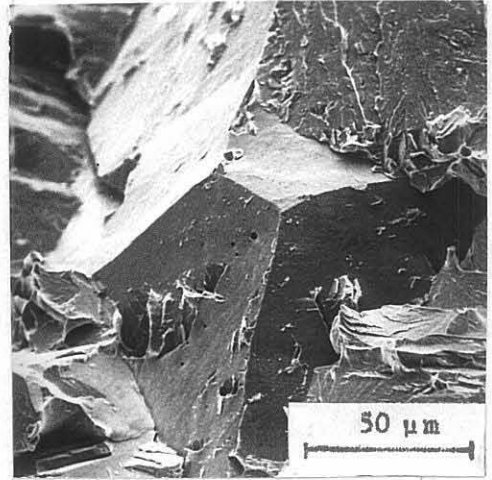
(b),(e) - tempered at 530°C for one hour

(c),(f) - tempered at 700°C for one hour

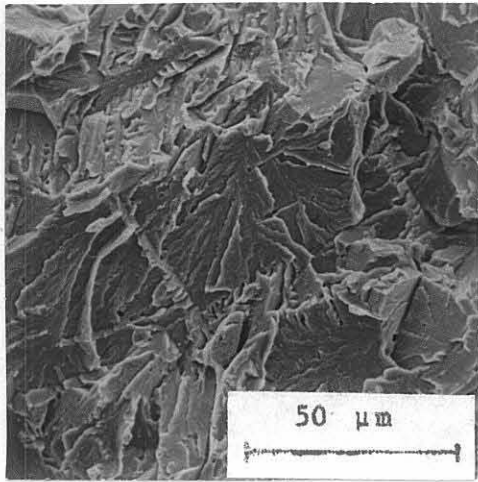
All specimens solution treated at 1200°C
for one hour.



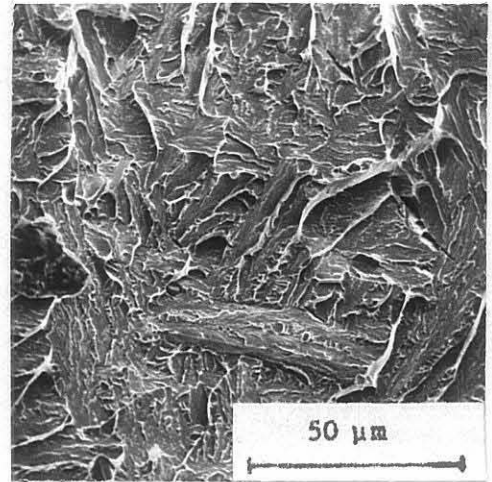
(a)



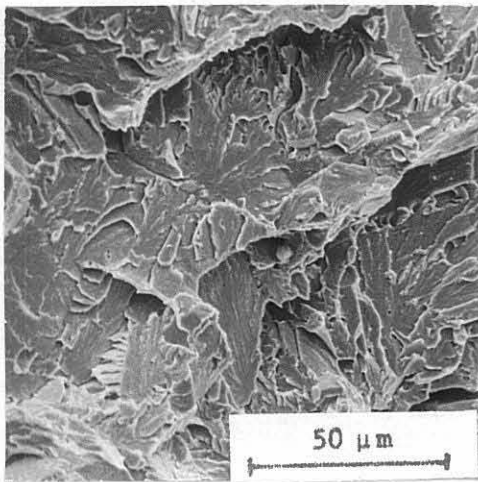
(d)



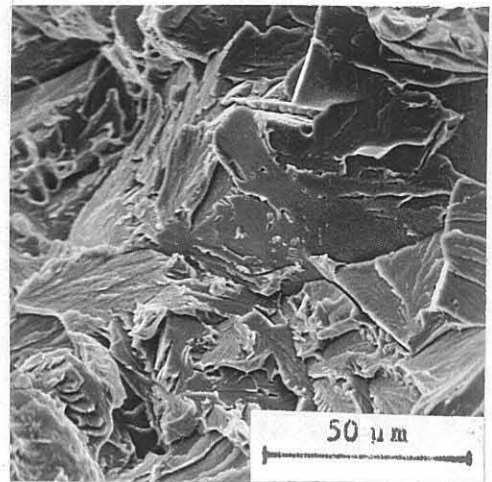
(b)



(e)



(c)



(f)

Figure 76.

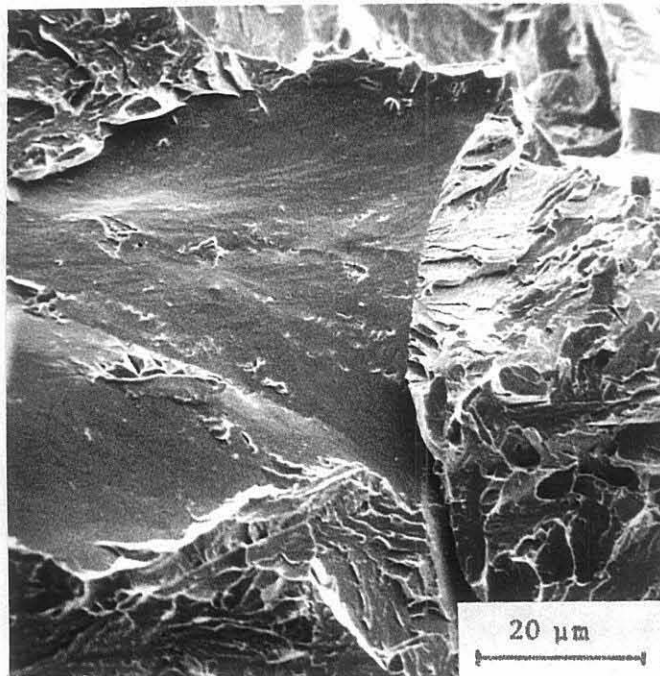
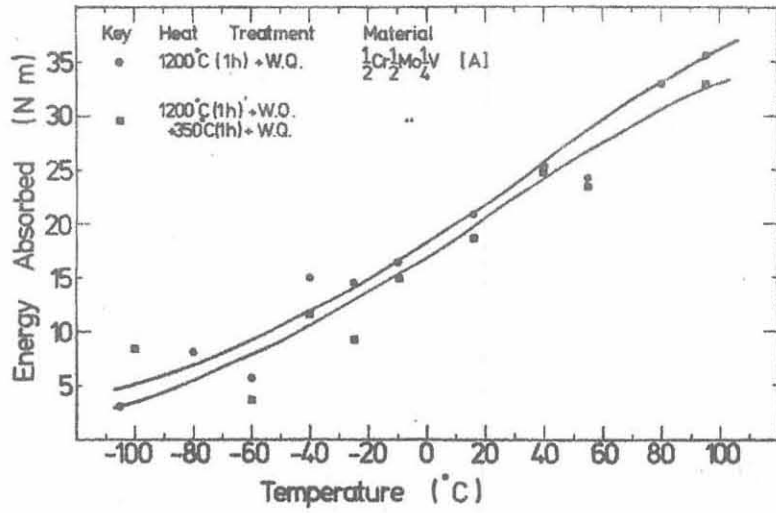
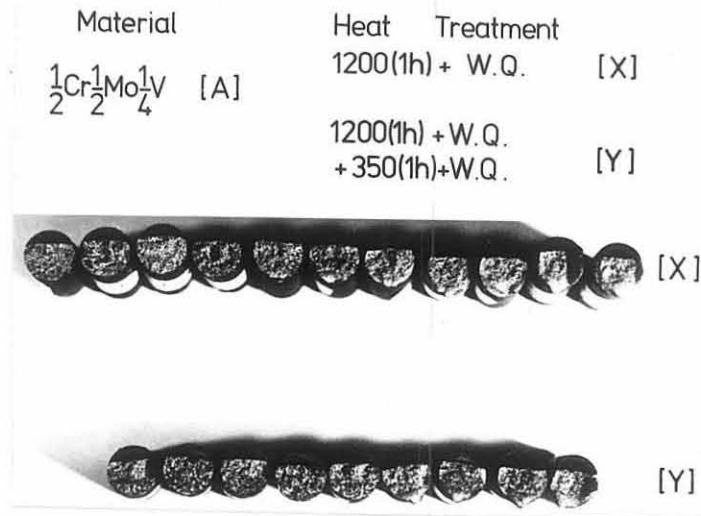


Figure 77. Failure of sample B at -196°C after solution treatment at 1200°C for one hour and tempering at 220° for one hour. Note the sharp transition from intergranular mode of crack propagation.

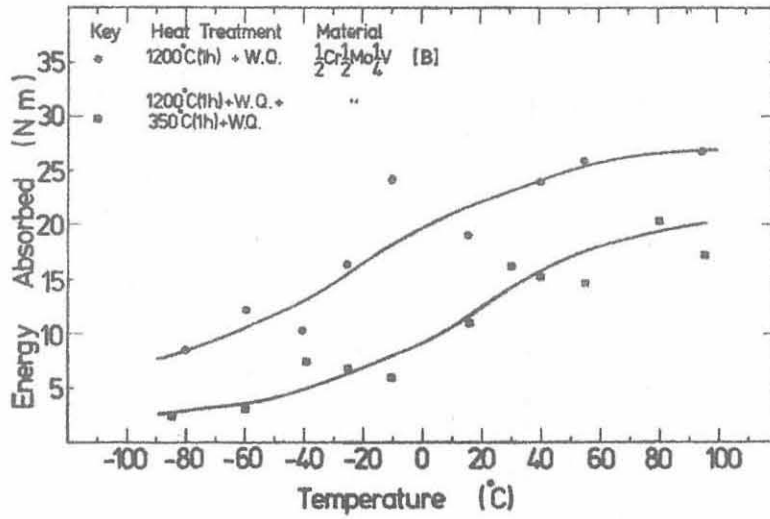


(a)

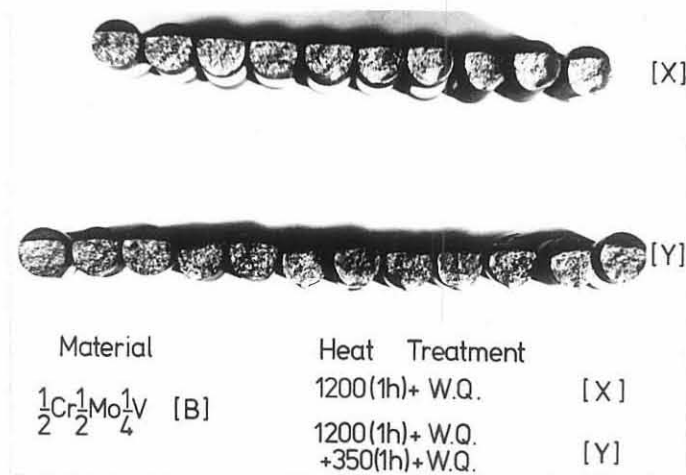


(b)

Figure 78. Impact behaviour of sample A solution treated at 1200°C and solution treated at 1200°C plus tempering at 350°C.
 (a) Energy - temperature transition
 (b) Fracture appearance.

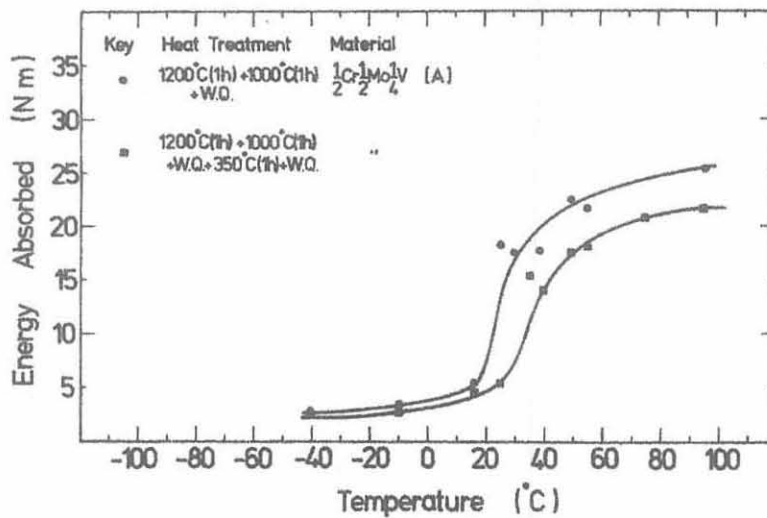


(a)

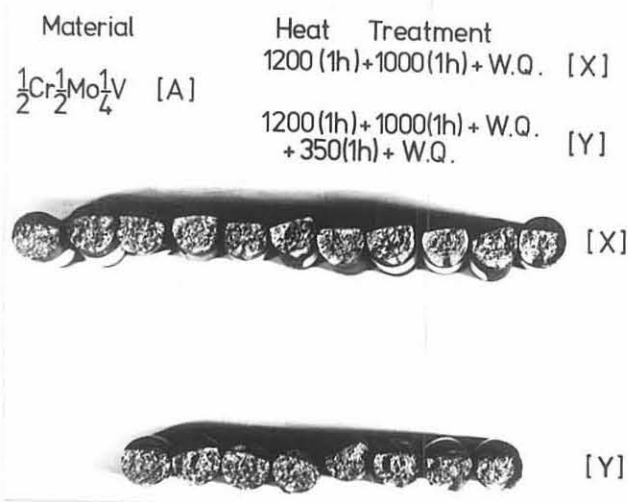


(b)

Figure 79. Impact behaviour of sample B solution treated at 1200°C, and solution treated at 1200°C plus tempering at 350°C.
 (a) Energy - temperature transition
 (b) Fracture appearance



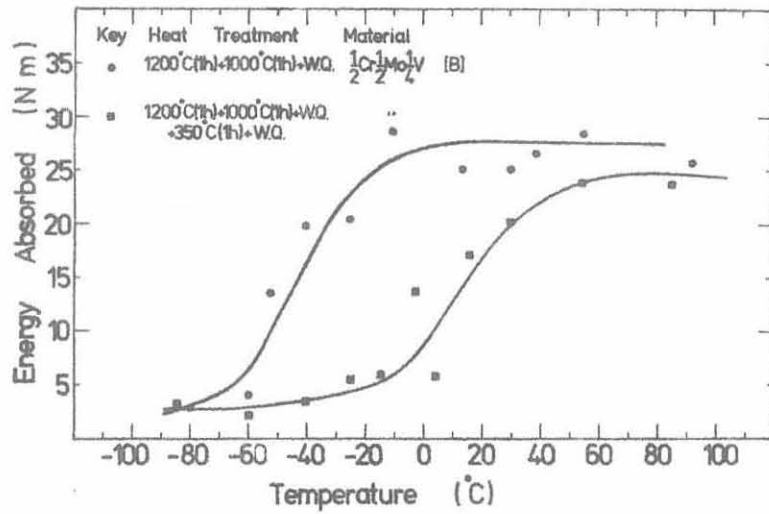
(a)



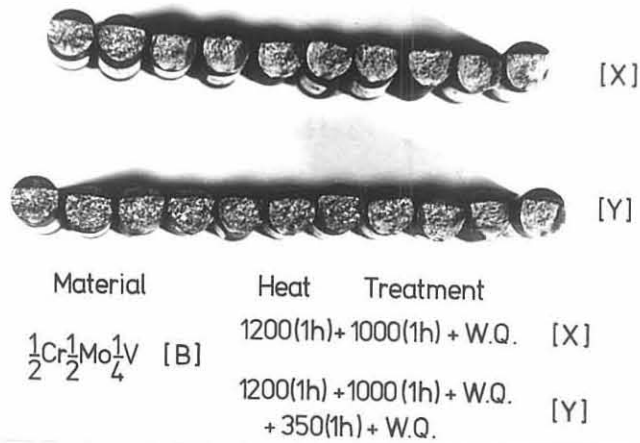
(b)

Figure 80. Impact behaviour of sample A solution treated at 1200°C (1h) plus 1000°C (1h) and also solution treated as above plus tempering at 350°C.

(a) Energy - temperature transition
 (b) Fracture appearance.



(a)

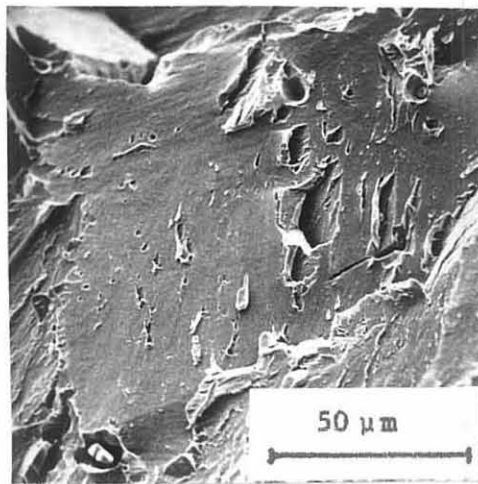


(b)

Figure 81. Impact behaviour of sample B solution treated at 1200°C (1h) plus 1000°C (1h) and also solution treated as above plus tempering at 350°C.

(a) Energy - temperature transition

(b) Fracture appearance.

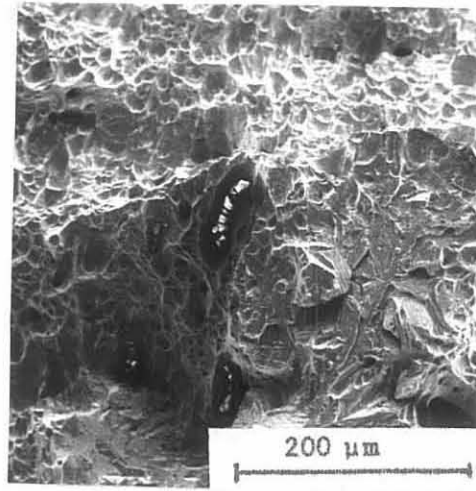


(a)

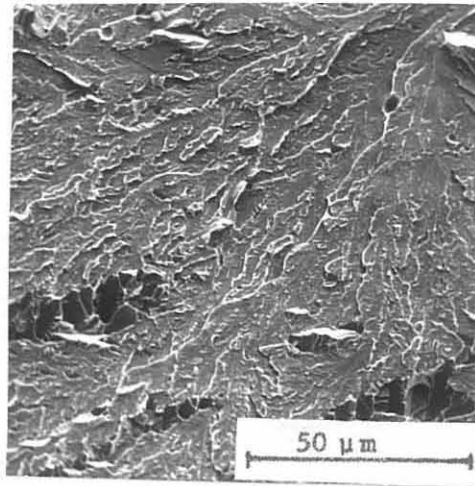


(b)

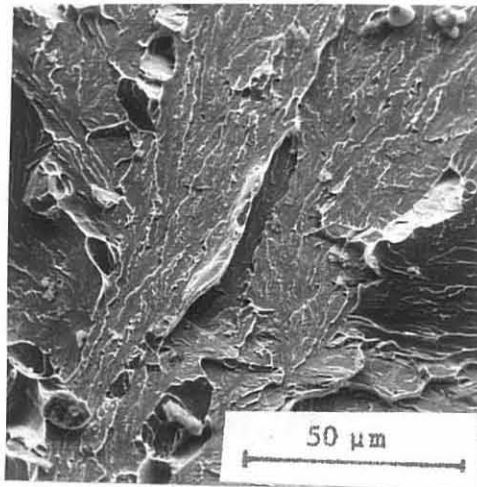
Figure 82. Examples of isolated intergranular facets found in sample B after single solution treatment and tempering at 350°C.
(a) Broken at -60°C (Impact energy 3 Nm)
(b) Broken at -85°C (Impact energy 2 Nm)



(a)



(b)



(c)

Figure 83. Typical examples of fracture behaviour during impact testing of alloys A and B
 (a) $\frac{1}{2}\text{Cr } \frac{1}{2}\text{Mo } \frac{1}{4}\text{V B}$ solution treated at 1200°C (1h) + 1000°C (1h) and broken at -25°C with an energy of 20 Nm
 (b) Ditto, broken at -80°C with an energy of 2 Nm
 (c) $\frac{1}{2}\text{Cr } \frac{1}{2}\text{Mo } \frac{1}{4}\text{V A}$ solution treated at 1200°C (1h) + 1000°C (1h) and broken at -40°C with an energy of 2 Nm

CHAPTER VII

The Tensile Mechanical Properties of High Purity $\frac{1}{2}\text{Cr } \frac{1}{2}\text{Mo } \frac{1}{4}\text{V}$ and $2\frac{1}{4}\text{Cr } 1\text{Mo}$ Steel at Elevated Temperatures7.1 Introduction

This chapter describes the results of a small study carried out on two samples of high purity low-alloy steel. The chemical analyses of these samples were given in Table II (chapter two). In essence, the work described chapters three and four is further examined from two standpoints, viz:

- (i) The effect of sample purity; and
- (ii) the effect of sample base composition,

upon the promotion of low ductility at elevated temperatures during unstable failure by intergranular cavitation. The former factor is considered by comparing the behaviour of the commercial samples of $\frac{1}{2}\text{Cr } \frac{1}{2}\text{Mo } \frac{1}{4}\text{V}$ steel with that of the high purity sample, while for the latter the behaviour of the high purity $2\frac{1}{4}\text{Cr } 1\text{Mo}$ steel is compared with that of the $\frac{1}{2}\text{Cr } \frac{1}{2}\text{Mo } \frac{1}{4}\text{V}$ series of steels.

$2\frac{1}{4}\text{Cr } 1\text{Mo}$ steel is widely used in creep resisting situations, equivalent to those in which $\frac{1}{2}\text{Cr } \frac{1}{2}\text{Mo } \frac{1}{4}\text{V}$ steel is used¹⁶³. Indeed it is often preferred because of its apparently reduced susceptibility to SRC^{58,65}. The usual explanation for this observation is that the absence of precipitation of V_4C_3 in $2\frac{1}{4}\text{Cr } 1\text{Mo}$ steel allows stress relaxation to occur without the promotion of grain strengthening and concomitant intergranular failure.⁶⁵

7.2 The Variation of Prior Austenite Grain Size and Secondary Hardening as a Function of Prior Solution Treatment.

Both of the high purity samples were received in the form of 25 mm diameter round bars. These bars were cold rolled to approximately 10 mm diameter before being heat treated. Figure 84 illustrates the variation of prior austenite grain size as a function of prior solution treatment for the two samples of high purity steel. For the limited data presented, it would appear that the $\frac{1}{2}\text{Cr } \frac{1}{2}\text{Mo } \frac{1}{4}\text{V}$ (H.P.) sample achieves a coarser grain size than the $2\frac{3}{4}\text{Cr } 1\text{Mo}$ (H.P.) sample, after equivalent solution treatment.

Figure 85 illustrates the isothermal hardening response of the two high purity samples after tempering at 625°C. Four main observations are apparent:

- (i) The $2\frac{3}{4}\text{Cr } 1\text{Mo}$ (H.P.) sample undergoes considerably more softening than the $\frac{1}{2}\text{Cr } \frac{1}{2}\text{Mo } \frac{1}{4}\text{V}$ (H.P.) sample for equivalent heat treatment.
- (ii) The degree of softening in the $\frac{1}{2}\text{Cr } \frac{1}{2}\text{Mo } \frac{1}{4}\text{V}$ (H.P.) sample is similar to that observed in the commercial samples A and B.
- (iii) The behaviour of the $\frac{1}{2}\text{Cr } \frac{1}{2}\text{Mo } \frac{1}{4}\text{V}$ (H.P.) sample after double solution treatment is consistent with that observed for the commercial samples A and B, suggesting that V_4C_3 may be brought out of solution in austenite, by appropriate solution treatment.
- (iv) The behaviour of the $2\frac{3}{4}\text{Cr } 1\text{Mo}$ (H.P.) sample after

double solution treatment is not consistent with that observed for the $\frac{1}{2}\text{Cr } \frac{1}{2}\text{Mo } \frac{1}{4}\text{V}$ samples, but suggests, that some carbon may be brought out of solution at the lower austenitising temperatures.

The alloy carbide, Mo_2C , which is responsible for the secondary hardening of $2\frac{1}{4}\text{Cr } 1\text{Mo}$ is generally felt to be completely soluble in austenite¹⁴⁴. It is easy to understand why an examination of the tempering behaviour of $2\frac{1}{4}\text{Cr } 1\text{Mo}$ has led many authors^{196,197,49,163} to attribute the low occurrence of SRC in this alloy to the reduced grain strengthening which occurs during reheat-treatment after welding.

7.3 The Effect of Prior Solution Treatment on the Tensile Mechanical Properties of the High Purity Alloys at Elevated Temperatures

Hounsfield No.13 double shouldered were solution treated in batches as described in chapter three. Because of the small amount of material available, these heat treatments were restricted mainly to:

- (i) 1200°C (1h) + W.Q.
- (ii) 1200°C (1h) + 1000°C (1h) + W.Q.

Testing was confined mainly to temperatures in excess of 400°C since the work described in chapter three had indicated that failure by intergranular cavitation was not observed during rising load tensile testing below 400°C. A nominal applied strain rate of $7.5 \times 10^{-4} \text{ min}^{-1}$ was used for all the tests. Figure 86 compares the elevated tensile mechanical properties of the high purity samples after solution treatment at 1200°C for one hour.

Three main points are apparent:

- (i) For temperatures greater than 600°C , the strength of the $2\frac{3}{4}\text{Cr } 1\text{Mo}$ (H.P.) sample is lower than that of the $\frac{1}{2}\text{Cr } \frac{1}{2}\text{Mo } \frac{1}{4}\text{V}$ (H.P.) sample.
- (ii) For temperatures greater than 500°C the ductility of the $2\frac{3}{4}\text{Cr } 1\text{Mo}$ (H.P.) sample is greater than that of the $\frac{1}{2}\text{Cr } \frac{1}{2}\text{Mo } \frac{1}{4}\text{V}$ (H.P.) sample.
- (iii) The ductility of the $2\frac{3}{4}\text{Cr } 1\text{Mo}$ (H.P.) sample increases at the highest temperatures, while that of the $\frac{1}{2}\text{Cr } \frac{1}{2}\text{Mo } \frac{1}{4}\text{V}$ (H.P.) sample remains relatively low.

These observations tend to suggest that the formation of vanadium carbide in $\frac{1}{2}\text{Cr } \frac{1}{2}\text{Mo } \frac{1}{4}\text{V}$ steel might indeed promote reduced ductility through intergranular cavitation in association with increased grain strengthening at elevated temperatures. The effect is certainly not as marked as the ambient temperature hardening response might lead one to expect.

Figure 87 compares the elevated temperature tensile mechanical properties of the high purity samples after double solution treatment at 1200°C for one hour plus 1000°C for one hour. The flow stress levels for both samples are nominally similar to those measured in specimens which had received the single solution treatment. The data of figure 88 shows that the double solution treated specimens exhibit increased levels of ductility over those which had been single solution treated.

Figure 89 compares the work hardening behaviour of the two high purity samples in the various states of prior solution treatment. Figure 90 compares the effectiveness of equation (3.2) in predicting the value of U.T.S. for the high purity

samples from the work hardening data of figure 89. The equations of the best straight lines determined by the method of least squares for the data of figure 90 are:

(a) for $\frac{1}{2}\text{Cr } \frac{1}{2}\text{Mo } \frac{1}{4}\text{V}$ (H.P.)

$$(\text{Calc. U.T.S.}) = 1.014382 (\text{Expt. U.T.S.}) + 9.03 \text{ MNm}^{-2} \quad (7.1)$$

(correlation coefficient, $r = 0.998967$)

(b) for $2\frac{1}{4}\text{Cr } 1\text{Mo}$ (H.P.)

$$(\text{Calc. U.T.S.}) = 0.992328 (\text{Expt. U.T.S.}) + 22.27 \text{ MNm}^{-2} \quad (7.2)$$

(correlation coefficient, $r = 0.999640$)

As for the commercial samples, the results of figure 90 and equations (7.1) and (7.2) provide some measure of confidence for quantitative discussion of the temperature dependence of σ_0 and n shown in figure 99.

The limited amount of data for the high purity materials shows that the flow stress as assessed by σ_0 is not significantly altered by prior solution treatment in either sample. The behaviour of the work hardening exponent for the $2\frac{1}{4}\text{Cr } 1\text{Mo}$ sample shows the appearance of troughs at about 500°C for the single solution treated specimens and 600°C for the double solution treated specimens. Although neither of these troughs coincides with the observed ductility troughs at 550°C it appears that the values of n above 550°C for the double solution treated specimens are lower than those for the single solution treated specimens. When considered in conjunction with the observed elevated temperature flow stress behaviour and the ambient temperature secondary hardening response of the $2\frac{1}{4}\text{Cr } 1\text{Mo}$ (H.P.) sample, it would appear that the behaviour of the double solution treated specimens may not be easily explained in terms

of alloy carbide formation.

The work hardening behaviour of the $\frac{1}{2}\text{Cr } \frac{1}{2}\text{Mo } \frac{1}{4}\text{V}$ (H.P.) sample illustrates higher values of n for the double solution treated specimens consistent with the overall behaviour of the commercial samples. However, the limited data does not suggest any marked trough for either the single or double solution treated specimens of the high purity samples. Inspection of the data of figure 28 suggests that the n - temperature response of the commercial sample A, after single solution treatment at 1000°C for one hour, is relatively flat except for the much increased value of n at 700°C . No tests were carried out on the high purity samples at 700°C . The flat temperature response of the n values in the $\frac{1}{2}\text{Cr } \frac{1}{2}\text{Mo } \frac{1}{4}\text{V}$ (H.P.) sample in the region of the ductility minima as compared with the sharp trough-like response of n for the $2\frac{1}{4}\text{Cr } 1\text{Mo}$ sample is directly comparable with the observed ductility behaviour of both samples in this temperature region. This behaviour suggests that some control upon the ductility during failure by intergranular cavitation is exerted by the mode of deformation, as discussed in chapters three and four. Because of the limited amount of material available, no investigation of strain rate sensitivity of the high purity samples was made.

7.4 The Effect of Prior Austenite Grain Size upon the Tensile Mechanical Properties of the High Purity Samples at 500°C

In chapter three it was observed that prior austenite grain exerted an important influence upon the ductility of $\frac{1}{2}\text{Cr } \frac{1}{2}\text{Mo } \frac{1}{4}\text{V}$ material during failure by intergranular cavitation. A limited series of tests was conducted upon the high purity samples to

examine briefly the effects of variation of prior austenite grain size upon their respective mechanical properties at 500°C.

Tensile specimens were solution treated in the following manner:

- (i) 1200°C (1h) + 1000°C (1h) + W.Q.
- (ii) 1100°C (1h) + 1000°C (1h) + W.Q.
- (iii) 1000°C (1h) + W.Q.

and then pulled to failure at 500°C, at a nominal strain rate of $7.5 \times 10^{-4} \text{ min}^{-1}$. The results are presented in figure 91. The points in parentheses are those measured from specimens which had been single solution treated at 1200°C for one hour. It is clear that the values of the various flow stress parameters σ_0 , UTS, 0.2% P.S. for the $2\frac{1}{4}\text{Cr } 1\text{Mo}$ (H.P.) sample are consistently higher than those for the $\frac{1}{2}\text{Cr } \frac{1}{2}\text{Mo } \frac{1}{4}\text{V}$ sample. No explanation of this phenomena could be found in the literature, and in the absence of any detailed metallographic examination, none can be given here. This effect is unexpected in view of the observed secondary hardening behaviour of the two samples (figure 85) and further points to the absence of any direct association between the precipitation characteristics and the short term tensile mechanical properties of these steels at 500°C.

The mode of failure for all of those tests was by intergranular cavitation. The level of ductility observed in the $\frac{1}{2}\text{Cr } \frac{1}{2}\text{Mo } \frac{1}{4}\text{V}$ sample is considerably greater than that measured for the $2\frac{1}{4}\text{Cr } 1\text{Mo}$ sample and presumably results from the higher levels of flow stress in the latter sample. It is notable that the behaviour of the work hardening exponent as a function of grain size, for the $2\frac{1}{4}\text{Cr } 1\text{Mo}$ sample, closely resembles the response of the reduction of area, suggesting again some association between

the deformation mode and failure by intergranular cavitation in the material. The values of the work hardening exponent for the $\frac{1}{2}\text{Cr } \frac{1}{2}\text{Mo } \frac{1}{4}\text{V}$ sample are slightly greater than those for the $2\frac{1}{4}\text{Cr } 1\text{Mo}$ sample. Clearly the ductility behaviour of the $\frac{1}{2}\text{Cr } \frac{1}{2}\text{Mo } \frac{1}{4}\text{V}$ is in no way an extension of that of $2\frac{1}{4}\text{Cr } 1\text{Mo}$, as was inferred during the comparison of the behaviour of the commercial samples of $\frac{1}{2}\text{Cr } \frac{1}{2}\text{Mo } \frac{1}{4}\text{V}$ steel. However, it would appear that for the $\frac{1}{2}\text{Cr } \frac{1}{2}\text{Mo } \frac{1}{4}\text{V}$ (H.P.) the effect of increased grain size in reducing ductility is not seen until a relatively coarse grain size is employed. It is felt that this effect relies on the way in which boundary purity affects the growth of intergranular cavities. This point is further discussed in the next section.

7.5 Comparison of the Behaviour of Commercial and High Purity Materials

This section, attempts to place the limited data derived during the testing of the high purity samples in the broad general context of that obtained during the testing of the commercial purity samples. Most emphasis is laid upon the comparison of the behaviour of the three samples of $\frac{1}{2}\text{Cr } \frac{1}{2}\text{Mo } \frac{1}{4}\text{V}$ steel, because of the small amount of data available for the $2\frac{1}{4}\text{Cr } 1\text{Mo}$ sample.

Figure 92 compares the percentage reduction of area and measured values of 0.2% proof stress at 500°C for the four samples as a function of prior austenite grain size. The points shown in parentheses are those observed in specimens which had received a single solution treatment at 1200°C for one hour. Three main points are apparent:

- (a) For any particular sample, the ductility of a specimen which had received the 1200°C single solution treatment was lower than that for double solution treated specimens even at nominally similar grain size and proof strength levels.
- (b) For the $\frac{1}{2}\text{Cr}$ $\frac{1}{2}\text{Mo}$ $\frac{1}{4}\text{V}$ series there is a significant improvement in ductility in the high purity sample.
- (c) For the commercial purity samples, the main improvement in ductility would appear to be closely linked with the finer grain size achieved in sample A after equivalent solution treatment.

The effect of purity in the $\frac{1}{2}\text{Cr}$ $\frac{1}{2}\text{Mo}$ $\frac{1}{4}\text{V}$ series is further emphasized in figure 93 which illustrates the variation of 0.2% proof stress, work hardening exponent and ductility at 500°C in specimens of $\frac{1}{2}\text{Cr}$ $\frac{1}{2}\text{Mo}$ $\frac{1}{4}\text{V}$,¹⁸⁷ all having the same prior austenite grain size (~130 μm), with variation of the total impurity content of those elements usually associated with low temperature intergranular failure. It is clear that the arguments concerned with the possible association of work hardening exponent with ductility cannot explain the dramatic increase of ductility in the high purity sample.

Since the variation of proof stress and work hardening exponent at 500°C as a function of purity is low (and probably reflects the reduced alloy content of the high purity sample) it is felt that the explanation for the improved ductility of the high purity sample lies in the propensity of the intergranular cavities to be more easily blunted under these conditions. Figure 94 shows examples of blunted cavities found

in the high purity samples at 550°C. It is clear that the blunting is effected both along the boundary as well as at triple points. Figure 95 illustrates the formation of cavities in high purity $\frac{1}{2}\text{Cr } \frac{1}{2}\text{Mo } \frac{1}{4}\text{V}$ strained immediately prior to final failure at 500°C. The prior austenite grain size of this specimen was about 130 μm . Figure 96 shows a detail of the crack tip blunting which occurred during the failure of this specimen.

It is clear that the final failure of the high purity material having grain sizes less than about 130 μm is intimately associated with ductile failure of the intercavity regions to produce cavity coalescence. This process would appear to be very similar to that observed in the fine grained specimens of commercial sample A (figure 36) which behaviour was similarly associated with an increased ductility. The orientation of the major crack in figure 95a clearly suggests that the major growth of cavities in this specimen occurred in association with a shear band. This behaviour is very similar to the void sheet process proposed by Rogers^{196,197} for ductile failure by the plastic growth and coalescence of voids formed around inclusions. As discussed previously, this similarity has been referred to¹³⁰ in the context of cavitation failure of a commercial copper based alloy. However it has never been examined in high purity materials.

Figure 92 shows an apparently sharp drop in ductility of $\frac{1}{2}\text{Cr } \frac{1}{2}\text{Mo } \frac{1}{4}\text{V}$ (H.P.) for grain sizes in excess of about 130 μm . It is felt that this observation indicates a rapid shift of failure mode to the 'critical crack length' type as proposed by Taplin¹³⁰ and Soderberg¹³². Figure 97 illustrates a coarse grained specimen strained at 500°C. It shows a flatter mode of growth like that

observed for the coarse grained specimen of the commercial samples (figure 34).

Investigation of angular distribution of cavities has usually been concerned with the interpretation of cavity growth as controlled by grain boundary sliding or vacancy condensation.¹⁹⁸⁻²⁰⁰ Depending upon whether the distribution showed a tendency to peak around 45° or 90° , the cavity growth mechanism has been deduced to be based upon on grain boundary sliding or vacancy condensation respectively. Recent work²⁰¹ which examined the effect of grain size on the distribution of creep cavities in austenitic stainless steel showed a shift in the peak of the angular distribution from 90° towards 45° for a decrease in grain size. This behaviour was interpreted in terms of cavity growth in the coarser grain size specimens occurring primarily by the plastic tearing of boundary precipitate -matrix interfaces lying perpendicular to the applied stress. For the fine grained specimens, it was felt that such growth was influenced rather more by a shear controlled process.

Although no detailed examination of the angular distribution of cavities was made in this work, it would appear from comparison of figures 36 (fine grained sample A) and 95 (130 μm grain size $\frac{1}{2}\text{Cr}$ $\frac{1}{2}\text{Mo}$ $\frac{1}{4}\text{V}$ (H.P.) sample), and figures 34 (coarse grained sample A) and 97 (170 μm grain size $\frac{1}{2}\text{Cr}$ $\frac{1}{2}\text{Mo}$ $\frac{1}{4}\text{V}$ (H.P.) sample), that the transition from shear controlled growth to normal stress controlled growth with varying prior austenite grain size occurs in a manner directly comparable to the observed ductility behaviour. The reason for this behaviour is most easily explained in terms of a lower cohesive strength of the boundaries in the commercial samples such that growth occurs simply by pulling

them apart even at relatively fine grain sizes. The slow transition of failure mode in the commercial samples is presumably indicative of the competing action of the factors of low boundary cohesion and incidence of triple points in promoting crack tip blunting and associated shear controlled cavity growth. As observed in the third chapter this behaviour appears to be associated with increased stability of tensile deformation in the finer grained specimens. In the high purity sample these competing factors are not as marked so that the shear controlled failure mode is allowed to persist even at larger grain sizes. The sharp transition in ductility reflects the reduced resistance to cavity growth arising from the reduced number of triple points in the coarse grained material. The situation described above is summarised schematically in figure 98.

In conclusion it would appear that the data of figure 93 illustrates the effect of decreased sample purity in reducing boundary cohesion during failure by intergranular cavitation and thereby promoting low resistance to crack growth. The mechanism by which sample purity affects boundary strength under these conditions is by no means clear.

7.6 Conclusions

The work described in this chapter produced only a limited amount of data in an attempt to examine the effects of sample purity and base composition upon the intergranular failure mode of quenched low alloy steels at elevated temperatures. It has established four main points, viz:

- (i) That the behaviour of $2\frac{1}{4}\text{Cr } 1\text{Mo}$ steel is not directly comparable with that of $\frac{1}{2}\text{Cr } \frac{1}{2}\text{Mo } \frac{1}{4}\text{V}$ steel solely in

terms of the precipitation characteristics of the two materials.

- (ii) That the effect of reduced sample purity in $\frac{1}{2}\text{Cr}$ $\frac{1}{2}\text{Mo}$ $\frac{1}{4}\text{V}$ steel is to promote reduced boundary cohesion during failure by intergranular cavitation.
- (iii) That the final failure mode during intergranular cavitation of the $\frac{1}{2}\text{Cr}$ $\frac{1}{2}\text{Mo}$ $\frac{1}{4}\text{V}$ steel is dependent both upon prior austenite grain size and sample purity such that high ductility in the high purity sample is maintained even at relatively coarse grain size because of the operation of a shear controlled void sheet mechanism in the absence of reduced boundary cohesion.
- (iv) That the effect of increased boundary cohesion in the high purity sample is similar to that of reduced grain size in the commercial samples, in that it allows the promotion of cavity blunting and associated increased ductility.

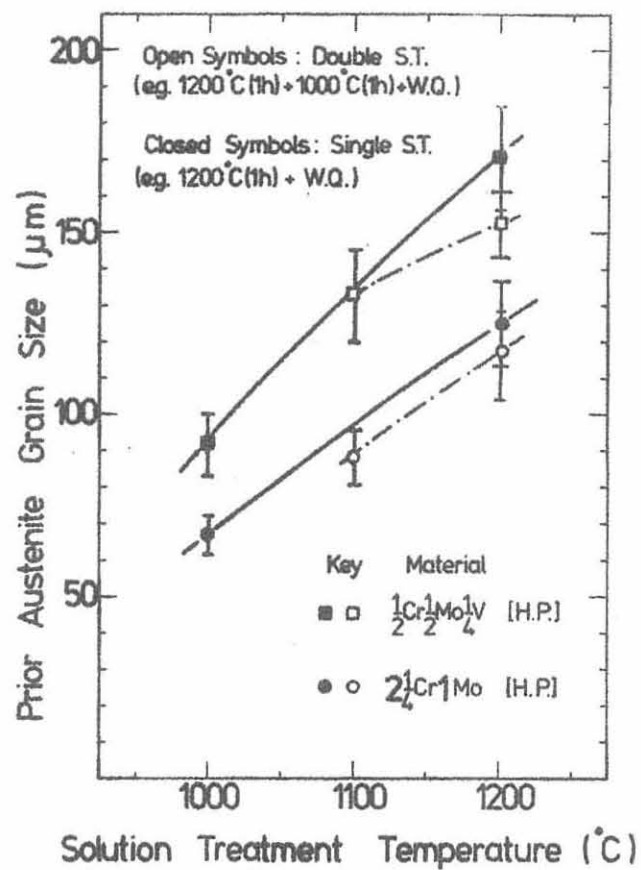


Figure 84. Variation of prior austenite grain size of high purity samples with different solution treatment temperatures.

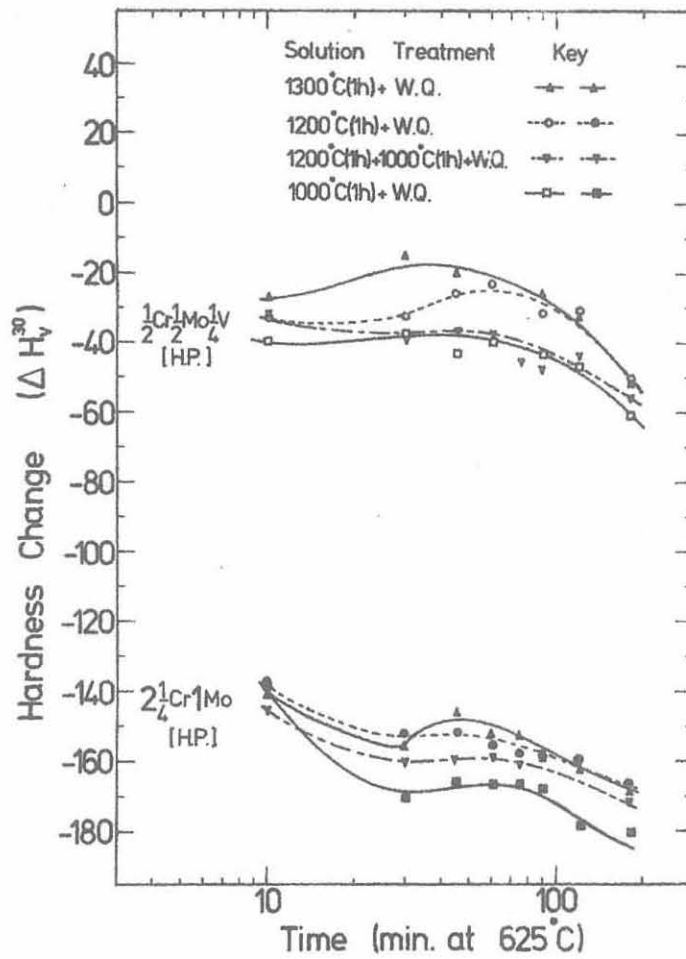


Figure 85. Secondary hardening of high purity samples after tempering at 625°C .

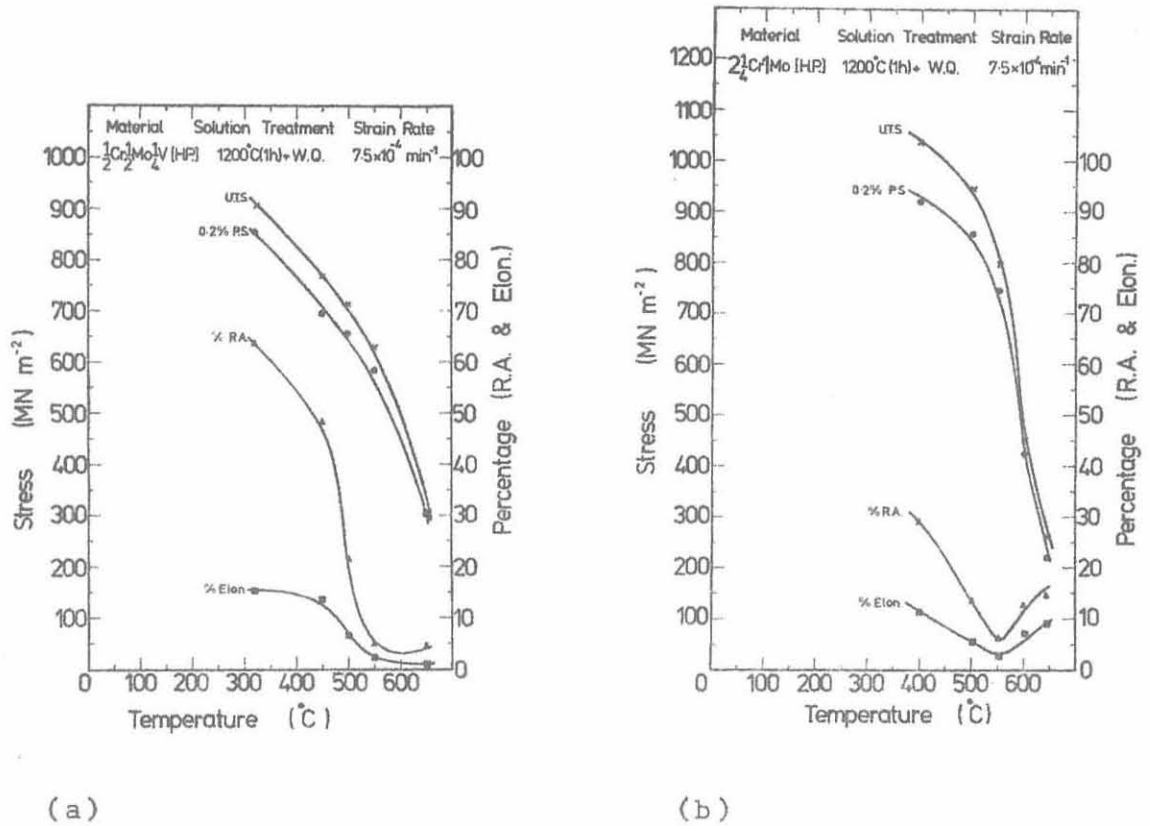
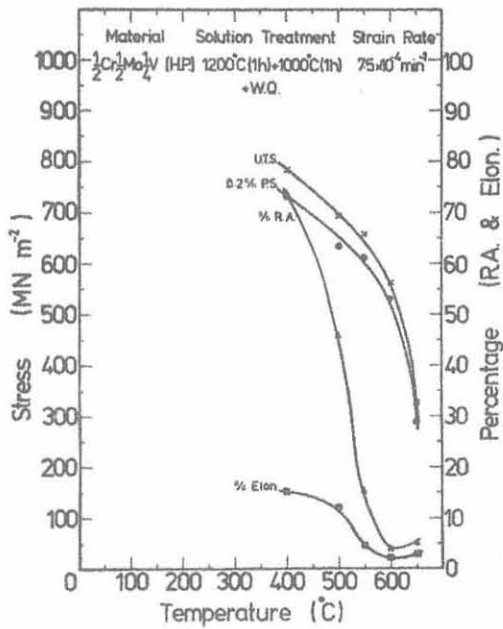
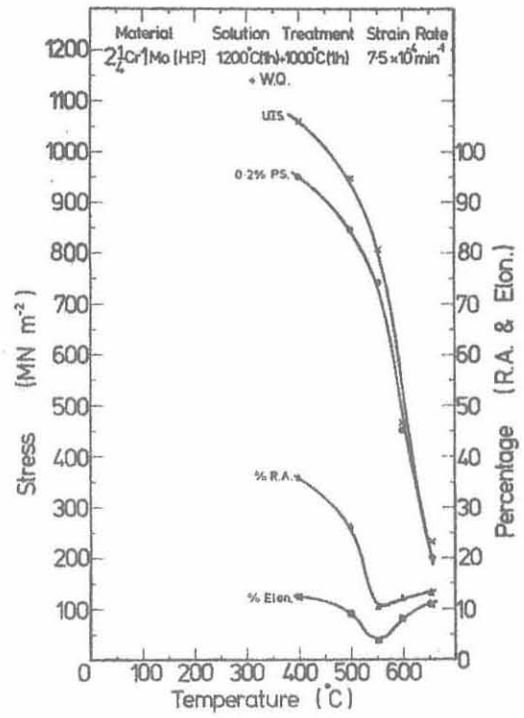


Figure 86. Elevated temperature tensile mechanical properties of high purity samples after solution treatment at 1200°C for one hour.
 (a) $\frac{1}{2}\text{Cr} \frac{1}{2}\text{Mo} \frac{1}{4}\text{V}$ H.P.
 (b) $2\frac{1}{4}\text{Cr} 1\text{Mo}$ H.P.



(a)

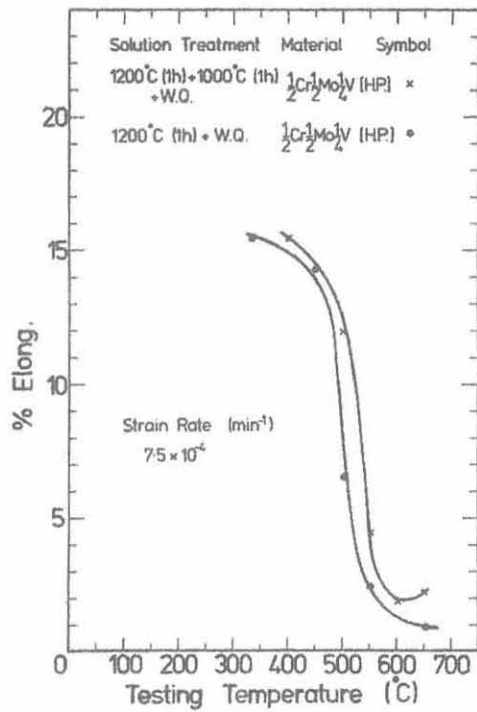


(b)

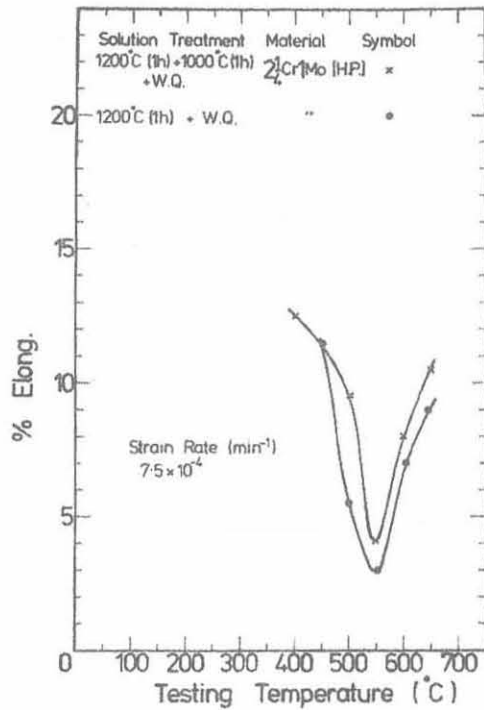
Figure 87. Elevated temperature tensile mechanical properties of high purity samples after double solution treatment.

(a) $\frac{1}{2}\text{Cr} \frac{1}{2}\text{Mo} \frac{1}{4}\text{V}$ H.P.

(b) $2\frac{1}{4}\text{Cr} 1\text{Mo}$ H.P.



(a)



(b)

Figure 88. Comparison of percentage elongation at elevated temperatures in high purity samples which have been both single and double solution treated.

(a) $\frac{1}{2}\text{Cr}\frac{1}{2}\text{Mo}\frac{1}{4}\text{V}$ H.P.

(b) $2\frac{1}{4}\text{Cr}1\text{Mo}$ H.P.

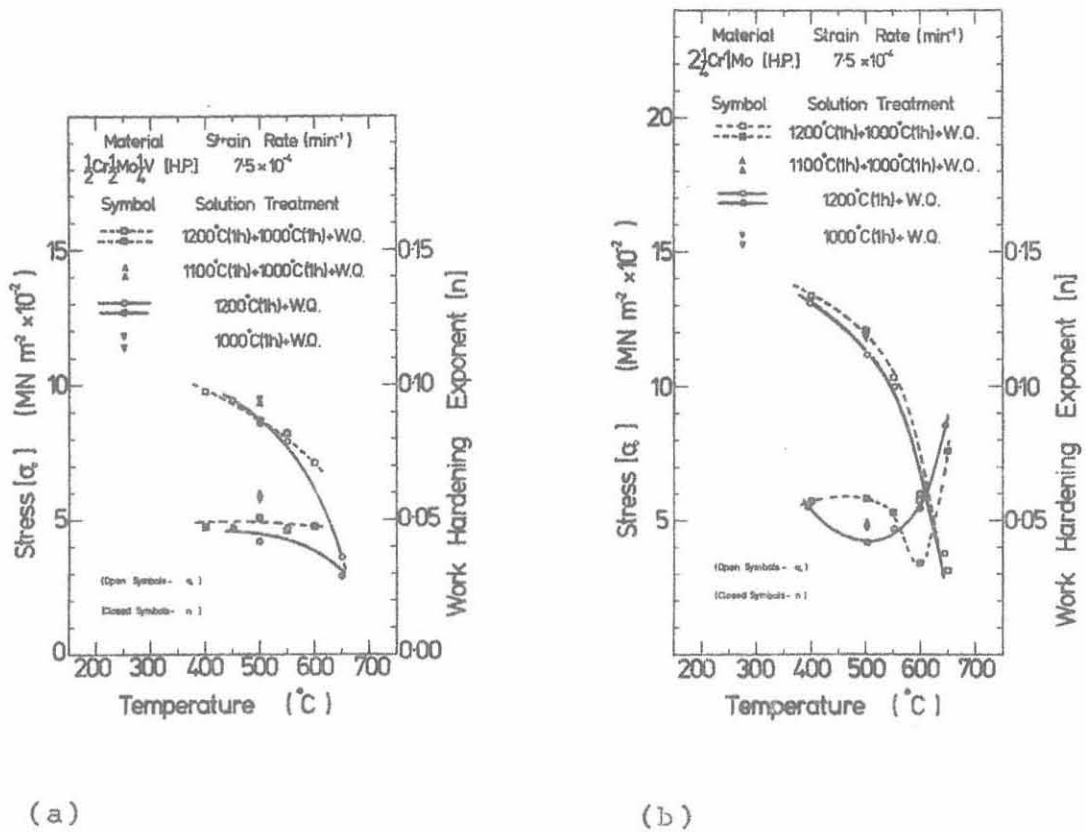
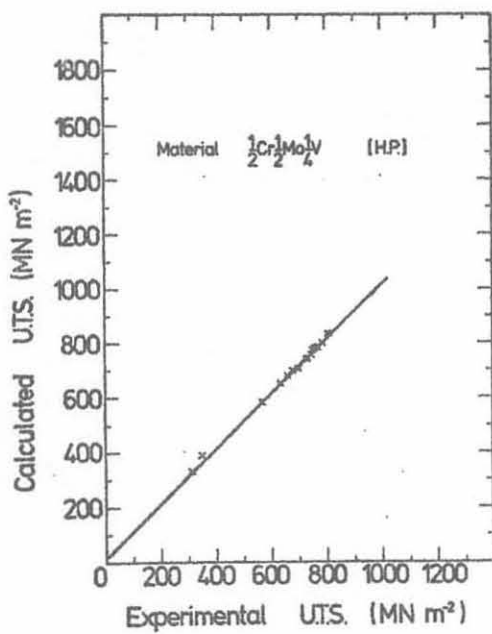


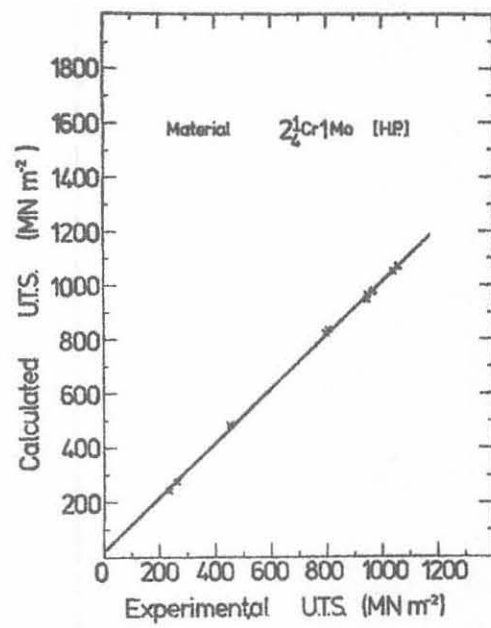
Figure 89. Work hardening behaviour of the high purity samples after various solution treatments.

(a) $\frac{1}{2}\text{Cr} \frac{1}{2}\text{Mo} \frac{1}{4}\text{V}$ H.P.

(b) $2\frac{1}{4}\text{Cr} 1\text{Mo}$ H.P.



(a)



(b)

Figure 90. Comparison of experimental values of UTS with those calculated from values of σ_0 and n .

(a) $\frac{1}{2}\text{Cr} \frac{1}{2}\text{Mo} \frac{1}{4}\text{V}$ H.P.

(b) $2\frac{1}{4}\text{Cr} 1\text{Mo}$ H.P.

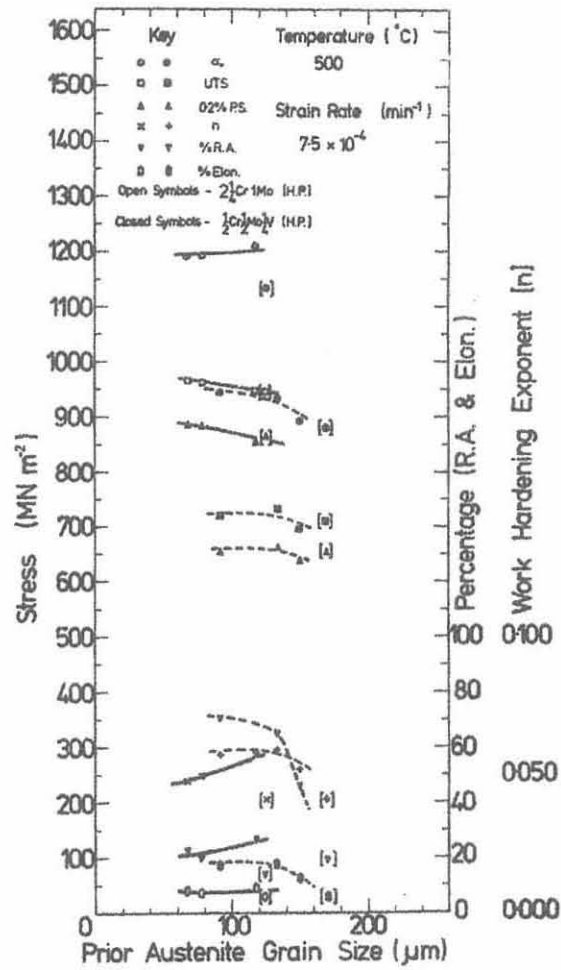


Figure 91. Tensile mechanical properties of high purity samples at 500°C as a function of prior austenite grain size.

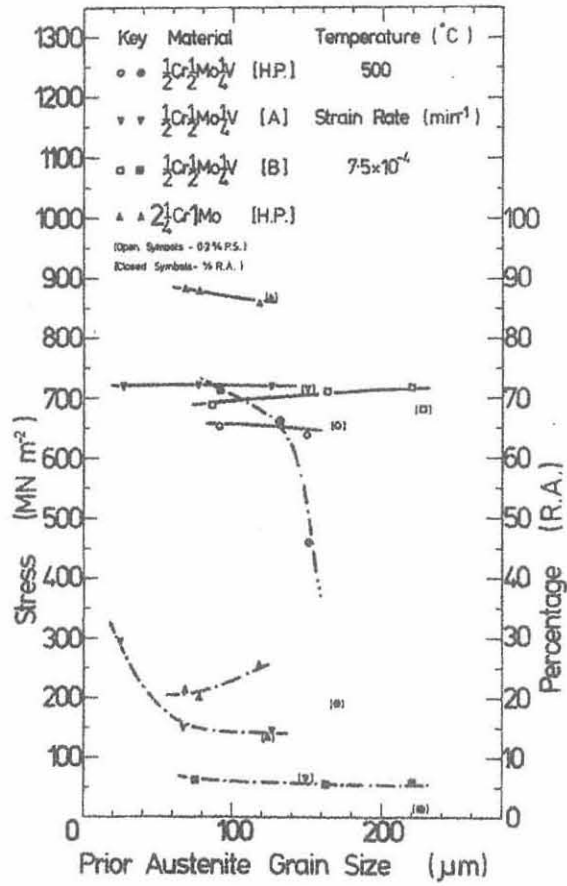


Figure 92. Comparison of strength and ductility of four samples studied at 500°C as a function of prior austenite grain size.

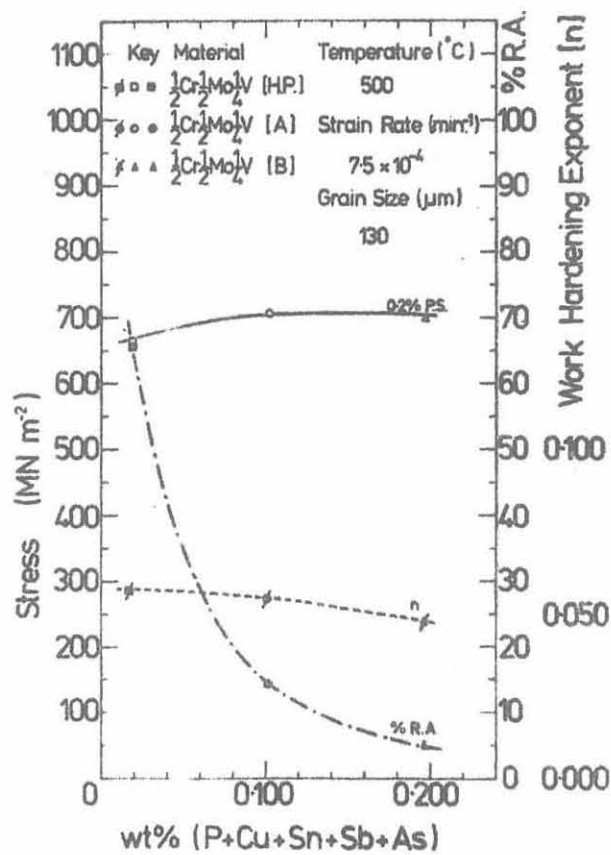


Figure 93. Variation of 0.2% proof stress, work hardening exponent and % reduction of area for $\frac{1}{2}\text{Cr} \frac{1}{2}\text{Mo} \frac{1}{4}\text{V}$ steel deformed at 500°C as a function of purity.



(a)



(b)

Figure 94. Cavitation in high purity samples occurring at 550°C.
(a) $\frac{1}{2}\text{Cr } \frac{1}{2}\text{Mo } \frac{1}{4}\text{V}$ H.P.
(b) $2\frac{1}{4}\text{Cr } 1\text{Mo}$ H.P.
(Tensile axis vertical)

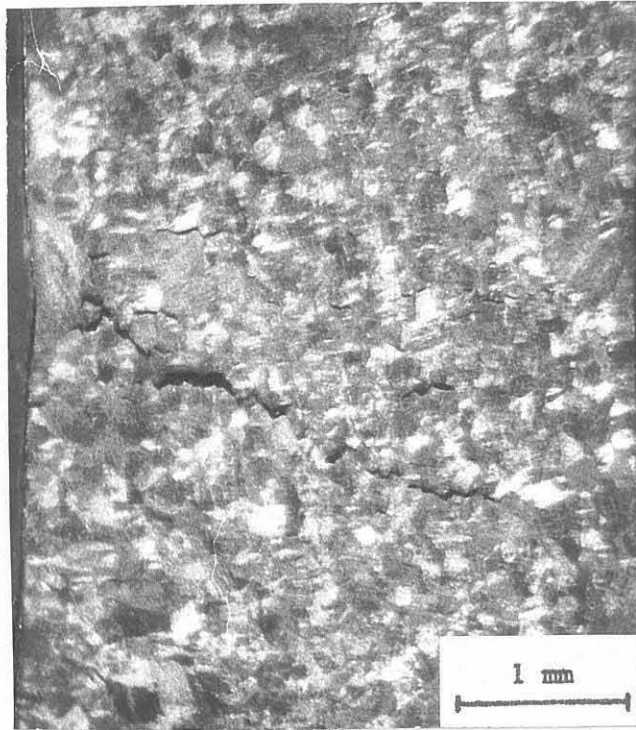


Figure 95. Cavitation in $\frac{1}{2}\text{Cr } \frac{1}{2}\text{Mo } \frac{1}{4}\text{V}$ H.P. Steel having a prior austenite grain size of approximately $130 \mu\text{m}$ and deformed at 500°C .

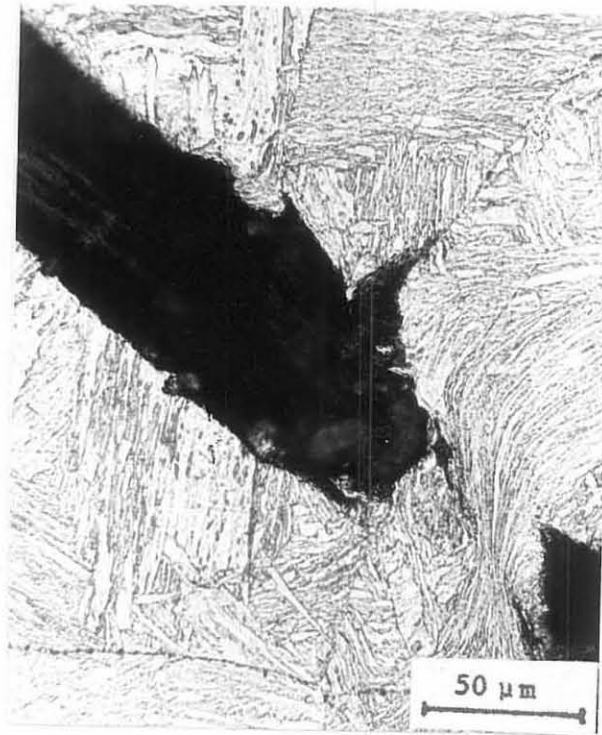


Figure 96. Detail of cavitation illustrated in figure 95 showing extensive crack tip blunting prior to final failure.

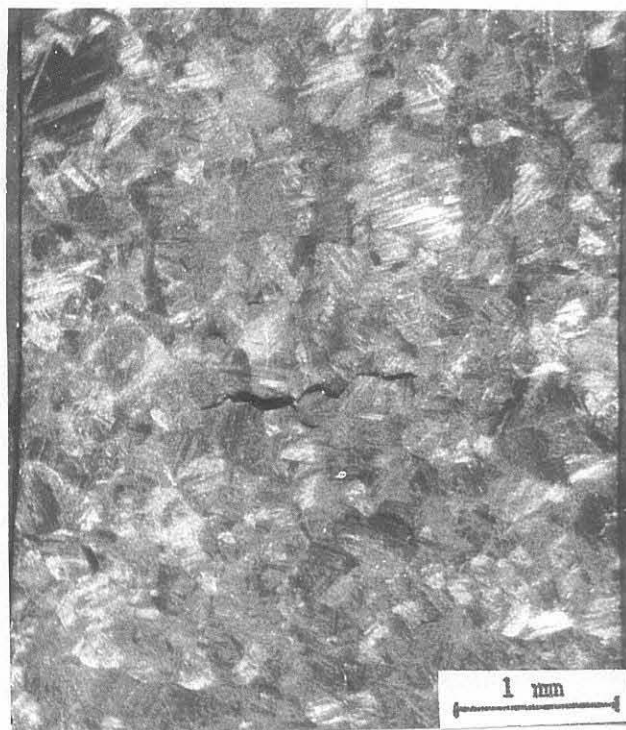


Figure 97. Cavitation in $\frac{1}{2}\text{Cr } \frac{1}{2}\text{Mo } \frac{1}{4}\text{V}$ H.P. Steel having a prior austenite grain size of approximately $170 \mu\text{m}$ and deformed at 500°C .

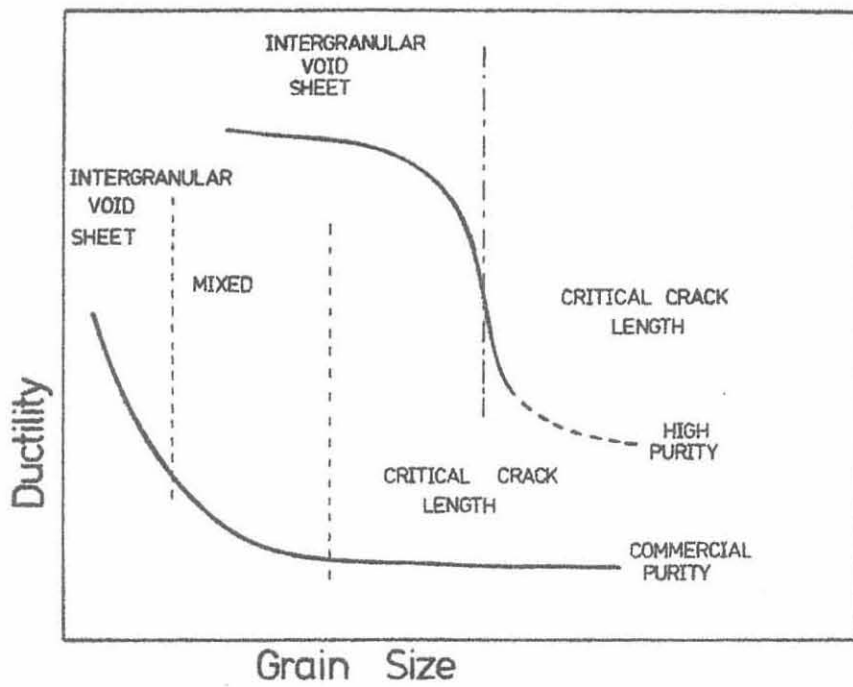


Figure 98. Schematic representation of the effect of purity upon the failure mode during intergranular cavitation.

CHAPTER VIII

Concluding Remarks8.1 The Mechanism of Stress Relief Cracking in
Cr-Mo-V Steels

In chapter five it was shown that extensive intergranular cracking occurred during the thermal stress relief of coarse grained sample B. In particular, it was clearly illustrated that the cracking occurred during the heating cycle of a stress relief heat treatment at about 350°C. Observations of the form of the cracking, as well as estimations of the critical nucleus size and surface energy associated with it, indicated that such stress relief cracking is effectively nucleation controlled unstable intergranular failure.

It is significant that the cracking described occurred at about 350°C for three major reasons:

- (i) This temperature is close to that of the lower of the two observed minima in strain-rate which are experienced during anisothermal stress relaxation.
- (ii) Tensile specimens tempered at this temperature (after equivalent solution treatment) and then broken at 77°K showed evidence of intergranular failure, as described in chapter six.
- (iii) Tensile specimens deformed at this temperature (after equivalent solution treatment) do not fail in a brittle intergranular manner, as shown in chapter three.

For the first, after comparison of the apparent

activation energies for the two strain-rate minima with published data, it appears reasonable to attribute the lower temperature strain-rate minimum to a carbon-dislocation interaction, and the upper temperature minimum to a vanadium-carbon-dislocation interaction. The cracking is therefore not associated with a creep strengthening effect due to the formation of a fine dispersion of alloy carbides. For the second, it is reasonable to attribute the boundary weakening observed after tempering at 350°C to an impurity segregation effect, most probably involving phosphorous. Considering the observations of chapters three, four and seven concerning sample purity, it is tempting to relate this effect to the observed ease of nucleation and growth of cavities during stress relaxation at 350°C. For the last, it is necessary to understand that the conditions of loading in the anisothermal stress relaxation test allow crack propagation to occur in association with stress reduction, but that this is not so for the rising load tensile test. Furthermore, it was noted in chapters three and four that both the work hardening exponent and the strain rate sensitivity of $\frac{1}{2}\text{Cr } \frac{1}{2}\text{Mo } \frac{1}{4}\text{V}$ steel are low for deformation at 350°C. It seems likely, therefore, that even when cavity nucleation occurs in a rising load tensile test at 350°C, subsequent growth is inhibited because the growing cavity rapidly becomes blunted as a result of strain localisation. For the anisothermal stress relaxation test, the conditions of loading allow such crack tip blunting to be inhibited until significant crack growth has occurred. Essentially, these are the conditions which exist in a weld HAZ during thermal stress relief.

Throughout the thesis the importance of prior austenite

grain size in promoting low ductility in association with intergranular failure has been emphasised. In this respect it is noted that the prior austenite grain size of sample B is about twice that of sample A after solution treatment at 1200°C. It has become apparent that this observation is significant for two major reasons:

- (i) For any boundary impurity segregation phenomena it is recognised that a larger grain size will allow more intense boundary coverage for a given bulk concentration of impurity, because of a reduced grain boundary area.
- (ii) Triple points are recognised as providing barriers to cavity growth such that a fine grain size will promote cavity blunting.

It appears, therefore that while both samples showed evidence of boundary weakness during failure at 77°K, the conditions of microstructure and loading during stress relaxation at 350°C were sufficient to cause nucleation controlled intergranular failure of sample B but not of sample A, consistent with their respective observed susceptibilities to stress relief cracking.

The mechanism of stress relief cracking in Cr-Mo-V steels may be summarised in the following three sentences:

- (i) SRC occurs in the first instance under loading conditions which allow rapid propagation of nucleation controlled intergranular failure.
- (ii) In Cr-Mo-V steels SRC is not associated with the creep strengthening of the grains as a result of the formation of a fine dispersion of alloy carbides.

- (iii) The susceptibility of commercial Cr-Mo-V steels to SRC depends largely upon the extent of austenite grain coarsening within a weld HAZ, and to some degree upon the segregation of impurities to the prior austenite grain boundaries.

8.2 The Significance of Current Theoretical Treatments of Intergranular Cavitation to the understanding of Stress Relief Cracking

In chapter one it was described how current theoretical treatments of intergranular cavitation have generally recognised three stages in the promotion of final failure, viz:

- (i) the nucleation of cavities;
- (ii) the stable growth of cavities;
- (iii) unstable fracture.

The mechanism of stress relief cracking described in the previous section of this chapter, has suggested that the intermediate stage involving stable cavity growth is largely eliminated during failure by SRC. As discussed in chapter one, the theoretical understanding of the final stage of unstable fracture is very limited. Furthermore, the understanding of the second stage is such that none of the currently available theories can predict the occurrence of unstable nucleation controlled cavity growth such as has been observed for SRC.

In chapter five it was implied that a major factor which acts to promote this mode of nucleation controlled intergranular failure was the propensity of a growing cavity to remain unblunted. Observations, described in chapters three and seven, of cavities formed during the rising load tensile testing

of commercial purity and high purity samples, have shown that cavities are blunted primarily at triple points but may also be blunted at positions along a prior austenite boundary. The requirement for this latter condition would appear to depend upon sample purity. A further condition which was inferred to promote cavity blunting was the propensity of the material to allow strain localisation through unstable tensile deformation in the region of the growing cavity.

This last condition allows one to understand more clearly the existence of two basic forms of final unstable failure during intergranular cavitation. These may be compared directly with the two categories of cracking and rupture as described by Knott¹⁶⁵ for the various micro-mechanisms of fracture at ambient temperature. In this way, the observed association of increased strain rate sensitivity and work hardening exponent with increased ductility during the failure of fine grained specimens at 550°C, is indicative of a rupture process in which the ductility at final failure is controlled by the deformation of the blunted intercavity regions. On the other hand when cavity blunting is inhibited, through conditions of loading, microstructure or composition, the mode of failure is more clearly brittle and crack-like and in this respect favoured by conditions of high applied stress, and ease of cavity nucleation.

This is not to say that the analogy with failure behaviour at ambient temperatures should be carried over in its entirety to the phenomenon of intergranular cavitation at elevated temperatures. The limited success which has been experienced at the present time²⁰⁴ by the many workers who have

attempted to apply LEFM* to the treatment of creep crack growth bears out this observation. However, it would appear that much of the present incompleteness of the theoretical treatments of intergranular cavitation arises as a result of the way in which inadequate account is made of the various possible micromechanisms of cavity growth.

8.3 The Possibility of Safer Thermal Stress Relief of Weld HAZ's

The work described in this thesis has identified the conditions under which failure by stress relief cracking may be expected to occur in Cr-Mo-V steels. However, at most it may only be regarded as a beginning in the solution of the wider problem involving the real welding situation. In this respect, there remains at least two major questions, viz:

- (i) What, if any, is the effect of pre-existing cracks, defects, inhomogeneity and stress concentration upon failure by nucleation controlled intergranular cavitation?
- (ii) What is the effect of mixed microstructure, such as may be produced within a weld HAZ, upon failure by nucleation controlled intergranular cavitation?

For the first it is desirable that a welding engineer be able to decide to thermally stress relieve a particular structure through knowledge of the 'defect tolerance' of a material for conditions of thermal stress relief. However, it is clear that assessment

*

Linear Elastic Fracture Mechanics

of such a parameter must take due account of the possibility of cavity blunting in materials having low strain rate sensitivity and rate of work hardening. It is possible to argue that an increase in stress concentration may in fact encourage cavity blunting and therefore reduce the extent to which nucleation controlled intergranular cavitation may occur. In this way, there may exist a critical range of stress concentration below which nucleation does not occur and above which growth is prevented because of cavity blunting. This idea may be investigated in the first instance by using blunt notched tensile specimens in an anisothermal stress relaxation experiment such as that described in chapter five. The use of fatigue pre-cracked specimens will present some major difficulties not least of which is the effect of oxidation at the crack tip during testing.

For the second question it is clearly important to assess the role of various weld HAZ microstructures with a view to optimising parameters like weld heat input, welding speed and electrode or filler composition, such that cavity blunting may be promoted during thermal stress relief. For the present, it would appear that significant progress in the assessment of a particular steel's susceptibility to stress relief cracking may be made simply by measuring the extent of prior austenite grain coarsening during welding.

Finally, with regard to stress relieving practice it would appear to be safer to adopt a stress relieving heat treatment which allows significant stress relaxation to occur at the lower temperatures where failure by nucleation controlled intergranular cavitation is not observed. After inspection of the data

of chapter five, it may be supposed that for Cr-Mo-V steels a suitable treatment is of the form:

- (i) heat at 50°C/h to a temperature in the range 270°C to 300°C ;
- (ii) hold for six hours;
- (iii) further heat at $50^{\circ}/\text{h}$ to a temperature in the range 690°C to 710°C ;
- (iv) cool at a rate 50°C/h to ambient.

Such a schedule will provide the added benefit of requiring less power for operation than the conventional treatments as described on page 15.

APPENDIX I

The Relationship between Ultimate Tensile Strength
and Work Hardening Behaviour

During uniaxial tensile testing, the true stress, σ_t is related to load, P, by

$$P = \sigma_t A$$

where A = current cross sectional area.

The U.T.S. is measured at the maximum load when

$$dP = \sigma_t dA + A d\sigma_t = 0 \quad (A1.1)$$

Plastic deformation is assumed to occur at constant volume, so that

$$\frac{dL}{L} = \frac{-dA}{A} = d\epsilon_t \quad (A1.2)$$

Transposing equation (A1.1) and substituting equation (A1.2) the condition at maximum load may be described by

$$\frac{d\sigma_t}{d\epsilon_t} = (\sigma_t)_u \quad (A1.3)$$

The subscript u denotes that this is the value of U.T.S. expressed in terms of true stress.

If the material deforms according to equation (3.1.)

viz:

$$\sigma_t = \sigma_o (\epsilon_t)^n$$

$$\frac{d\sigma_t}{d\epsilon_t} = n \sigma_o (\epsilon_t)^{n-1}$$

$$(\epsilon_t)_u = n$$

$$\therefore (\sigma_t)_u = \sigma_o n^n \quad (A1.4)$$

Now U.T.S. is measured experimentally in terms of engineering stress which may be related to true stress according to:

$$\begin{aligned}\sigma_t &= \sigma_e (1 + \epsilon_e) \\ \text{i.e. } (\sigma_e)_u &= \left(\frac{\sigma_t}{1 + \epsilon_e} \right)_u = \text{U.T.S.}\end{aligned}\quad (\text{A1.5})$$

The subscript e denotes engineering stress and strain. The relationship between true strain and engineering strain may be expressed as:

$$\begin{aligned}\epsilon_t &= \ln (1 + \epsilon_e) \\ \text{i.e. } \exp(\epsilon_t) &= 1 + \epsilon_e \\ \therefore (\epsilon_e)_u &= \exp(n) - 1\end{aligned}\quad (\text{A1.6})$$

Substituting equations (A1.4) and (A1.6) into equation (A1.5) yields:

$$\text{U.T.S.} = \frac{\sigma_0 n^n}{\exp(n)} \quad (3.2)$$

APPENDIX II

An Approximate Relationship between Tensile Flow Stress
and Vickers Pyramid Hardness at Elevated Temperatures

The following simple analysis attempts to incorporate strain-rate hardening as well as strain hardening effects into the correlation of tensile flow stress with Vickers Pyramid Hardness at elevated temperatures. The approach is summarised in figure 99. Essentially, it is assumed that:

- (i) m and n are independent of strain, strain-rate and each other;
- (ii) m and n are both small (< 0.1).

These gross assumptions seriously limit the general applicability of the analysis. However, the data of chapters three and four suggest that to a first approximation they are valid for the present work.

The work of Tabor¹⁵² established that in general, the relationship between VPN and tensile flow stress may be expressed as:

$$(H_V)_r = 3\sigma_r \quad (A2.1)$$

where the subscript r refers to 'representative' values of flow stress and VPN.

If (by convention) VPN is measured in units of kg.mm^{-2} and flow stress in units of MNm^{-2} , equation (A2.1) may be expressed as:

$$(H_V)_r = 0.306 \sigma_r \quad (A2.2)$$

The representative tensile flow stress, σ_r , is that value of tensile flow stress determined at certain representative values of strain, ϵ_r , and strain rate, $\dot{\epsilon}_r$, which satisfies equation (A2.2).

If the experimental value of tensile flow stress, σ_y , is determined at different values of strain, ϵ_y , and strain rate, $\dot{\epsilon}_y$, it is then necessary to estimate the value of σ_r through knowledge of m , n , $\dot{\epsilon}_r$ and ϵ_r .

Referring to figure 99, if the flow stress measured at constant strain, $\epsilon = \epsilon_y$, is equal to σ_1 at $\dot{\epsilon} = \dot{\epsilon}_r$, then:

$$m = \frac{\log \frac{\sigma_1}{\sigma_y}}{\log \frac{\dot{\epsilon}_r}{\dot{\epsilon}_y}} = \frac{\log \frac{\sigma_1}{\sigma_y}}{A} \quad (A2.3)$$

Similarly, if the flow stress measured at constant strain rate, $\dot{\epsilon} = \dot{\epsilon}_r$, is equal to σ_r at $\epsilon = \epsilon_r$, then:

$$n = \frac{\log \frac{\sigma_r}{\sigma_1}}{\log \frac{\epsilon_r}{\epsilon_y}} = \frac{\log \frac{\sigma_r}{\sigma_1}}{B} \quad (A2.4)$$

From equation (A2.3):

$$Am = \log \frac{\sigma_1}{\sigma_y}$$

From equation (A2.4):

$$Bn = \log \frac{\sigma_r}{\sigma_1}$$

Adding:

$$Am + Bn = \log \frac{\sigma_r}{\sigma_y}$$

$$\therefore \sigma_r = \sigma_y 10^{(Am+Bn)} \quad (A2.5)$$

Substituting equation (A2.5) into equation (A2.2) gives:

$$(H_v)_r = 0.306 \sigma_y 10^{(Am+Bn)} \text{ (kg.mm}^{-2}\text{)} \quad (A2.6)$$

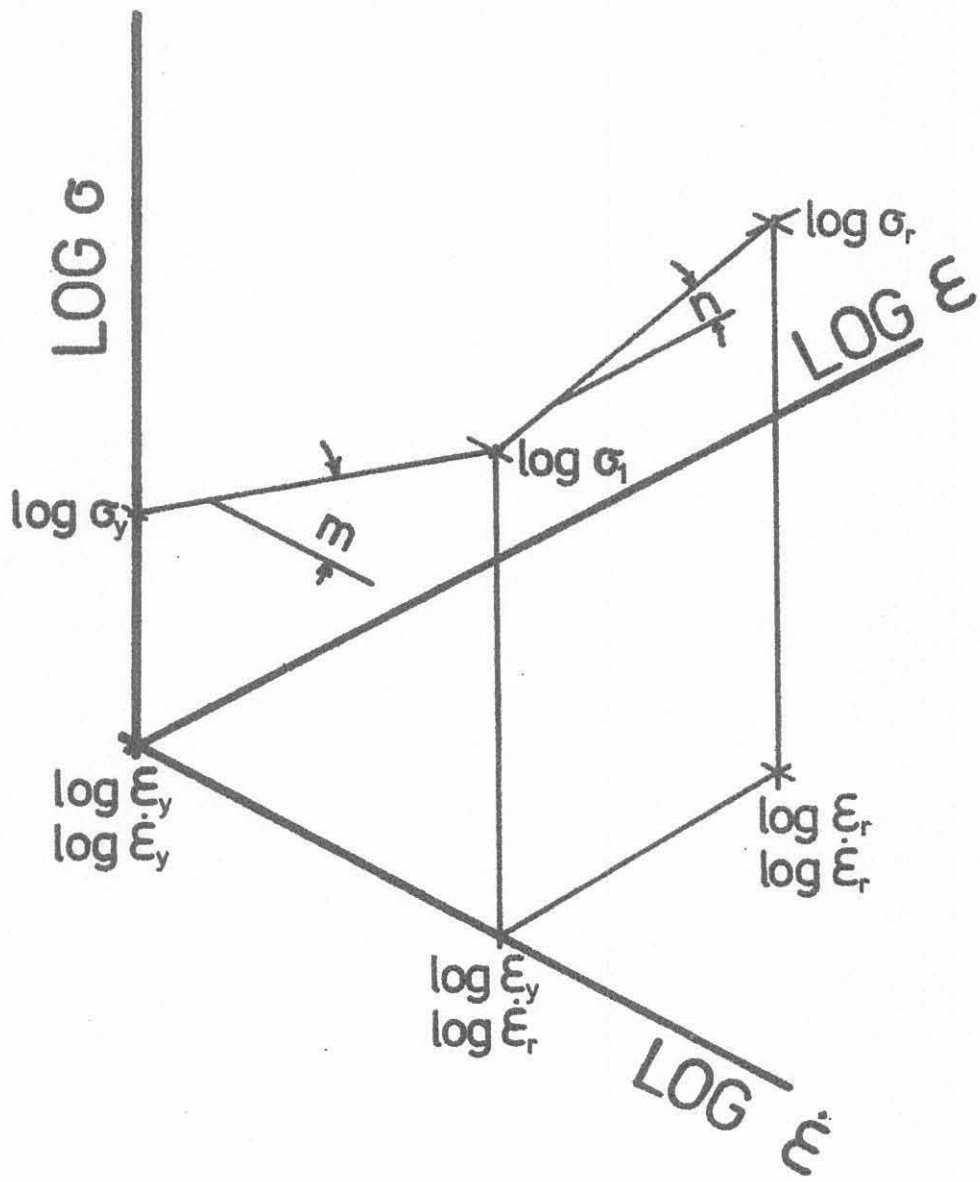


Figure 99. Schematic illustration of the relationship between σ_r and σ_y .

REFERENCES

1. R. W. Nichols, *Welding in the World*, (1969), 7, pp 244-260.
2. G. D. Joy and A. M. Sage, "Stress relief heat treatment of Vanadium steels", (1972), Highveld publication.
3. M. G. Gemmill, "The Merits and Demerits of Strengthening Mechanisms in Low-Alloy Steels", Climax Molybdenum Publ., Conference on Steel Strengthening Mechanisms, Zurich, (1969).
4. J. Barford and G. Willoughby, *Metal Science Journal*, (1971), 5, p 32.
5. E. Smith and J. Nutting, *Brit. J. Appl. Phys.*, (1956), 7, pp 214-217.
6. R. G. Baker and J. Nutting, *J.I.S.I.*, (1959), 189, pp 257-268.
7. E. Smith and J. Nutting, *J.I.S.I.*, (1957), 187, pp 314-329.
8. A. K. Seal and R. W. K. Honeycombe, *J.I.S.I.*, (1958), 188, pp 9-15.
9. J. J. Irani and R. W. K. Honeycombe, *J.I.S.I.*, (1965), 203, pp 826-833.
10. D. Raynor, Ph.D. Thesis Sheffield, (1967)
11. E. Tekin and P. M. Kelly, *J.I.S.I.*, (1965), 203, p.715.
12. D. Raynor, J. A. Whiteman and R.W.K. Honeycombe, *J.I.S.I.*, (1966), 203, p 349.
13. E. Smith, *Acta. Met.*, (1966), 14, p 583.
14. W. E. Stumpf and C. M. Sellars, in "The Mechanism of Phase Transformations in Crystalline Solids", *Inst. Metals, Monograph No.33*, London, (1969), p 120.

15. J. Glen, J.I.S.I., (1957), 186, pp 21-48.
16. J. Glen, J.I.S.I., (1958), 188, pp 30-39.
17. J. Glen, J.I.S.I., (1958), 188, pp 114-135.
18. J. Nutting and J. M. Arrowsmith, in "Structural processes in creep", I.S.I. Spec. Rep. 70, (1961), pp 147-165.
19. G. J. P. Buchi, J. H. R. Page and M. P. Sidey, J.I.S.I., (1965), 203, pp 291-298.
20. J. H. R. Page and G. J. P. Buchi, J.I.S.I., (1965), 203, p 485.
21. J. Barford and R. V. Day in "Discussion at the Autumn General Meeting, 1965", J.I.S.I., (1966), 204, pp 899-900.
22. H. G. A. Bates and K. A. Ridal in "Joint Conference on Creep" Inst. Mech. Eng. London, (1963), p 99.
23. J. H. Woodhead and A. G. Quarrel, J.I.S.I., (1965), 203, pp 605-620.
24. M. C. Murphy, D. Duval and A. Chitty, Metallurgia, (1965), 71, p 13.
25. M. C. Murphy and G. Branch, J.I.S.I., (1969), 207, p 1347.
26. J. Myers, G. Willoughby, R. K. Ham and J. Barford, Met.Sci.J., (1968), 2, p 209.
27. D. M. Schartz and B. Ralph, Phil. Mag., (1969), 19, p 1069.
28. G. L. Dunlop and P. J. Turner, Met.Sci.J., (1975), 9, pp 370-374.
29. A. T. Davenport and R. W. K. Honeycombe, Proc.Roy.Soc., (1971), A322, p 191.
30. A. D. Batte, Ph.D. Thesis, University of Cambridge, (1970).
31. G. L. Dunlop, Ph.D. Thesis, University of Cambridge, (1973).
32. R. W. Bailey, J.Jun.Inst.Eng., (1935), 46, pp 1-19.

33. P. A. Stone and J. D. Murray, J.I.S.I., (1965), 203,
pp 1094-1107.
34. D. McLean, J.I.S.I., (1965), 203, p 900.
35. T. Boniszewski, I.S.I. Conference, (Dec. 1971).
36. Y. Ito and M. Nakanishu, The Sumitomo Search No. 7, (1972),
pp 27-36.
37. P. Harris and K. E. Jones in "International Conference on
Welding Research related to Power Plant"., (1972).
38. G. V. Smith and E. J. Dulis, ASTM Proc. 49, (1949), p 584.
39. J. Glen, J.I.S.I., (1947), 155, p 501.
40. T. Yukitoshi and K. Nishida, Trans.ISIJ., (1972), 12,
pp 429-434.
41. D. Hall and G. H. J. Bennett, J.I.S.I., (1967), 205,
pp 304-314.
42. J. F. Ratliff and R. M. Brown, Trans.ASM. 60, (1967),
pp 176-186.
43. P. G. Stone and J. D. Murray, ISI Conference, (1966).
44. R. Bruscatto, Weld.Res.Suppl., (1970), pp 148-156.
45. B. E. Hopkins, H. R. Tipler and G. D. Branch, J.I.S.I.,(1971),
209, pp 745-746.
46. H. R. Tipler, in "International Conference on the Properties
of Creep Resistant Steels" Dusseldorf, May 1973.
47. B. B. Argent, M. N. van Niekerk and G. A. Redjèrn, J.I.S.I.,
(1970), 208, pp 830-843.
48. C. F. Bilsby and K. J. Barton, Metal Construction and Brit.
Weld. J., (1970), pp 167-170.
49. K. P. Bentley, Brit.Weld. J., (1964), 11, pp 507-515.
50. K. E. Jones, in "Welding of Creep Resisting Steels",
Weld. Inst. Conf., (1970), paper 5.

51. K. J. Irvine and F. B. Pickering, J.I.S.I., (1960), 194, pp 137-153.
52. R. A. Swift and H. C. Rogers, Welding Res.Suppl., (1971), pp 357-373.
53. W. D. Doty, Weld.Inst.Autumn Meeting, 1970.
54. A. T. Price and M. J. Siverns, Met.Constr. and Brit.Weld.J., (1970), pp 239-245.
55. L. Tall and J. A. Lambert, Welding J., (1964), 43, pp 10_S-23_S.
56. W. H. Busby, Brit.Weld.J., (1967), 14, pp 39-43.
57. T. R. Gurney, BWRA Bulletin, (1968), 9, pp 68-70.
58. J. D. Murray, Brit.Weld.J., (1967), 14, pp 447-456.
59. C. F. Meitzner and A. W. Pense, Welding Res.Suppl., (1969), pp 431-440.
60. R. W. Nichols, Welding Res.Abroad, (1970), pp 36-44.
61. R. N. Younger and R. G. Baker, Brit.Weld.J., (1961), 8, pp 579-587.
62. S. Weiss, W. P. Hughes and H. J. Mackee, Weld.Res., (1962), pp 17-22.
63. H. Nakaruma, T. Naiki and H. Okabayashi, Proc. 1st. Int. Conf. Fracture, Sendai, Japan, (1965), 2, pp 863-878.
64. C. F. Meitzner, D.Phil. Thesis, Lehigh University, (1968).
65. T. Boniszewski and N.F. Eaton, in "9th Commonwealth Mining and Metallurgical Congress", Inst.Min. and Met., London, (1969), paper 2.
66. J. Ruge, Private communication to Nichols, ref.40 cited in ref. 1.
67. B. A. Glossop, N. F. Eaton and T. Boniszewski, Met.Constr. and B.W.J., (1969), 1, pp 68-73.

68. R. O. L. Cadman, Discussion to reference 67, Met.Constr., (1969), 1, p 125.
69. R. A. Swift, Weld.Res.Suppl., (1971), pp 195-200.
70. E. Szabb, Brown Boveri Mitteilungen, (1966), pp 126-136.
71. B. Watkins, H. G. Vaughan and G. M. Lees, Brit.Weld.J., (1966), pp 350-356.
72. K. G. Richards, Oxelosund Steel Book, Sect.7, p 22.
73. G. G. Saunders, in "Third International Conference on Fracture", Munich, (1973), paper viii - 432.
74. D. V. Thornton, English Electric Rept. No.W/L1n9(C3), (1969).
75. T. Boniszewski and N. E. Eaton, Metal Sci.J., (1969), 3, pp 103-110.
76. T. Boniszewski, Discussion of Papers, Met.Constr. and Brit. Weld. J., (1969), 1, p 127.
77. R. L. Drinnan and P. Harris, GEC Power Eng. Ltd., Rept.No. T. P. R 12/106, (1970).
78. P. Greenfield and K. E. Jones, Private communication to G. D. Joy and A. M. Sage, ref.31 in reference 2.
79. Z. Jeffries, J.Am.Inst.Metals (1917) p 300.
80. D. A. Woodford and R. H. Goldhoff, Matls.Sci. and Eng., (1969), 5, pp 303-324.
81. A. J. Perry, Brown Boveri Research Report "Cavitation Creep", (1973).
82. D. McLean, J.Inst.Met., (1956), 85, pp 468-472.
83. D. M. R. Taplin, Private communication.
84. A. N. Stroh, Proc.Roy.Soc., (1954), A233, pp 404-414.
85. J. N. Greenwood, Bull.Inst.Met., (1952), 1, pp 104-105.
86. J. N. Greenwood, J.I.S.I., (1952), 171, p 380.

87. J. N. Greenwood, D. R. Miller and J. W. Suiter, *Acta.Met.*, (1954), 2, pp 250-258.
88. J. N. Greenwood, *J.I.S.I.*, (1954), 176, pp 268-269.
89. E. S. Machlin, *Trans. AIME.*, (1956), 206, pp 106-111.
90. N. J. Grant, in "Fracture" (John Wiley, New York), (1959), pp 562-578.
91. R. C. Boettner and W. D. Robertson, *TMS-AIME*, (1961), 221, pp 613-622.
92. R. W. Balluffi and L. L. Seigle, *Acta.Met.*, (1955), 3, pp 170-177.
93. R. D. Gifkins, *Acta.Met.*, (1956), 4, p 98
94. C. W. Chen and E. S. Machlin, *Acta. Met.*, (1956), 4, pp 655-656.
95. C. W. Chen and E. S. Machlin, *Trans.AIME*, (1957), 209, pp 829-835.
96. C. H. M Jenkins, E. H. Bucknall and E. A. Jenkinson, *J.Inst.Met.*, (1944), 70, pp 57-79.
97. A. H. Cottrell, in "Structural Processes in Creep", *I.S.I. and Inst.Met.*, London, (1961), pp 1-18.
98. R. Resnick and L. Seigle, *Trans.AIME.*, (1957), 209, pp 87-94.
99. P. W. Davies and B. Wilshire, *J.Inst.Met.*, (1961), 90, pp 470-472.
100. C. G. Bieber and R. F. Decker, *Trans.AIME.*, (1961), 221, pp 629-636.
101. C. W. Chen and E. S. Machlin, *TMS-AIME*, (1958), 212, pp 718-730.
102. H. R. Tipler, L. H. Taylor and B. E. Hopkins, *Met.Sci.J.*, (1970), 4, pp 167-170.
103. R. T. Ratliff and G. W. Greenwood, *Phil.Mag.*, (1965), 12, pp 59-69.

104. D. McLean, Rept.Prog. Phys., (1966), 29, p 1.
105. E. Smith and J. T. Barnby, Met.Sci.J., (1967), 1, pp 1-4.
106. R. W. Balluffi and L. L. Seigle, Acta.Met., (1957), 5,
pp 449-454.
107. R. D. Stacey, Metallurgia, (1958), 58, pp 125-128.
108. B. Burton and J. P. Barnes, Met.Sci.J., (1975), 9, pp 18-21.
109. D. Hull, and D. E. Rimmer, Phil.Mag., (1959), 4, pp 673-687.
110. G. W. Greenwood, Phil.Mag., (1963), 8, pp 707-709.
111. M. V. Speight and J. E. Harris, Met.Sci.J., (1967), 1, p 83.
112. R. P. Skelton, Met.Sci.J., (1968), 2, p 106.
113. R. P. Skelton, Met.Sci.J., (1975), 9, p 192.
114. J. E. Harris, M. O. Tucker and G. W. Greenwood, Met.Sci.J.,
(1974), 8, p 311.
115. M. V. Speight and W. Beere, Met.Sci.J., (1975), 9, p 190.
116. R. Raj and M. F. Ashby, Acta.Met., (1975), 23, pp 653-666.
117. M. F. Ashby and R. Raj, in "Mechanics and Physics of Fracture"
Inst.of Physics and Met.Soc., Cambridge, (1975),
paper 16.
118. E. S. Machlin, in "Fracture", (John Wiley, New York), (1959),
pp 623-626.
119. J. Intrater and E. S. Machlin, Acta.Met., (1959), 7, pp 140-143.
120. P. Bowring, P.W.Davies and B. Wilshire, Met.Sci.J., (1968), 2,
pp 168-171.
121. J. H. Hensler and G. V. Cullen, J.Australian Inst.Met., (1964),
9, pp 38-45.
122. D. M. R. Taplin and A. L. Wingrove, Acta.Met., (1967), 15,
pp 1231-1236.
123. D. M. R. Taplin, Phil Mag., (1969), 20, pp 1079-1082.

124. B. Wilshire, *Scripta. Met.*, (1970), 4, pp 361-366.
125. P. W. Davies and B. Wilshire, *Phil.Mag.*, (1965), 11,
pp 189-190.
126. Y. Ishida and D. Mclean, *Met.Sci.J.*, (1967), 1, pp 171-172.
127. D. M. R. Taplin, *Met.Eng.Quart.*, (1970), 10, pp 31-34.
128. R. Raj and M. F. Ashby, *Met.Trans.*, (1971), 2, pp 1113-1127.
129. J. A. Williams, *Phil.Mag.*, (1969), 165, pp 635-639.
130. R. G. Fleck, C. J. Beevers and D. M. R. Taplin, *Met.Sci.J.*,
(1975), 9, pp 49-54.
131. F. A. McClintock, in "Ductility", ASM, (1967), p 225.
132. R. Söderberg, *Met.Sci.J.*, (1975), 9, pp 275-279.
133. G. J. Davies, J. W. Edington, C. P. Cutler and
K. A. Padmanabhan, *J.Mat.Sci.*, (1970), 5, p 1091.
134. R. H. Johnson, *Met.Rev.*, (1970), 15, p 145.
135. S. Sagat, P. A. Blenkinsop and D. M. R. Taplin, *J.Inst.Metals*,
(1972), 100, p 268.
136. D. M. R. Taplin and S. Sagat, *Mat.Sci.Eng.*, (1972), 9, p 153.
137. A. R. Marder, *TMS-AIME*, (1969), 245, p 1337.
138. G. L. Dunlop, E. Shapiro, D. M. R. Taplin and J. Crane,
Met.Trans., (1973), 4, pp 2039-2044.
139. B. J. Cane and G. W. Greenwood, *Met.Sci.J.*, (1975), 9,
pp 55-60.
140. D. M. R. Taplin, Private communication.
141. L. A. Erasmus, *J.I.S.I.*, (1964), 202, pp 128-134.
142. K. J. Irvine, F. B. Pickering and T. Gladman, *J.I.S.I.*,
(1967), 205, pp 161-182.
143. T. Gladman and F. B. Pickering, *J.I.S.I.*, (1968), 206,
pp 653-664.

144. N. E. Hannerz and F. DeKazinczy, *J.I.S.I.*, (1970), 208, pp 475-481.
145. J. Barford and R. V. Day, CERL Rept. No. RD/L/R1515, (1968).
146. R. Dolby, Ph.D. Thesis, University of Cambridge, (1971).
147. C. J. McMahon, Private communication.
148. E. Tekin and P. M. Kelly, *J.I.S.I.*, (1965), 203, p 715.
149. D. Raynor and R. W. K. Honeycombe, *J.I.S.I.*, (1966), 204, p 349.
150. E. Smith, *Acta.Met.*, (1966), 14, p 583.
151. M. Tanino and J. Nishida, *Trans.J.I.M.*, (1968), 9, pp 103-110.
152. D. Tabor, "The hardness of metals", Clarendon, (1951).
153. H. D. Merchant, *J.I.S.I.*, (1972), 210, pp 442-446.
154. H. D. Merchant, G. S. Murty, S. N. Bahadur, L. T. Dwivedi, Y. Mehrotra, *J. Matls.Sci.*, (1973), 8, pp 437-442.
155. C. S. Tedman Jr. and J. H. Westbrook, *Trans.ASM*, (1967), 60, pp 442-449.
156. G. S. Mann and L. H. Van Vlack, *Met.Trans.*, (1972), 3, pp 2005-2006.
157. K. B. Gove, Ph.D. Thesis, University of Cambridge, (1973).
158. P. W. Bridgman, "Studies in Large Plastic flow and Fracture", (McGraw-Hill, New York), (1952).
159. F. A. McClintock and A. S. Argon, "Mechanical Behaviour of Materials", (Addison-Wesley, Massachusetts), (1966).
160. J. F. Knott, "Fundamentals of Fracture Mechanics", (Butterworths, London), (1974).
161. A. Nadai and M. J. Manjoine, *J.Appl.Mech.*, (1941), A77, p 8.
162. E. W. Hart, *Acta.Met.*, (1967), 15, pp 351-355.
163. W. Barr and M. J. Siverns, *Brit.Weld.J.*, (1967), 14, pp 238-243.

164. R. Pilkington, G. Willoughby and J. Barford, *Met.Sci.J.*, (1971), 5, pp 1-8.
165. J. F. Knott, in "Mechanics and Physics of Fracture", Inst. of Physics and Met.Soc., Cambridge (1975), paper 9.
166. T. Gladman, B. Holmes and F. B. Pickering, *J.I.S.I.*, (1970), 208, pp 172-183.
167. M. F. Ashby, *Acta.Met.*, (1972), 20, p 887.
168. H. J. Frost, Ph.D. Thesis, Harvard University, (1974).
169. F. W. Crossman and M. F. Ashby, *Acta.Met.*, (1975), 23, pp 425-440.
170. G. L. Dunlop and D. M. R. Taplin, *Scripta.Met.*, (1969), 3, pp 641-644.
171. A. Nadai, "Theory of Flow and Fracture of Solids", (McGraw-Hill, New York), (1950), 1, pp 74-75.
172. E. W. Hart, *Acta.Met.*, (1970), 18, pp 599-610.
173. G. E. Dieter, "Mechanical Metallurgy", (McGraw-Hill, New York), (1961), pp 255-256.
174. C. Zener and J. H. Holloman, *J.Appl.Phys.*, (1944), 15, pp 22-32.
175. M. A. Burke and W. D. Nix, *Acta.Met.*, (1975), 23, pp 793-798.
176. A. Considère, *Ann.Ponts Chaussées*, (1885), 6, p 574.
177. J. C. Ritter and R. McPherson, *J.I.S.I.*, (1970), 208, p 935.
178. J. C. Ritter and R. McPherson, *J.I.S.I.*, *Austral.Weld.Res.*, (1970), 7, p 1.
179. M. Caubo, *Welding J.*, (1963), 42, p 282_S.

180. D. F. T. Roberts et al. in "Joint Int.Conf. on Creep",
Inst.Mech.Engrs., London, (1963), paper 63.
181. G. Murry and A. Constant, Rev.Met., (1965), p 127.
182. J. C. Ritter and R. McPherson, J.I.S.I., (1973), 211,
pp 123-128.
183. D. Lee and E. W. Hart, Met.Trans., (1970), 2, pp 1245-1248.
184. E. W. Hart and H. D. Solomon, Acta.Met., (1973), 21,
pp 295-307.
185. F. W. Noble and D. Hull, Acta.Met., (1964),12, pp 1089-1092.
186. E. H. F. Date, J.I.S.I., (1969), 207, p 988.
187. C. J. Smithells, "Metals Reference Book", 4th Ed.
(Butterworths, London),(1967).
188. W. W. Gerberich, C. E. Hartbower and P. P. Cummins,
Welding Res.Suppl., (1968), 10, pp 433_S-443_S.
189. B. C. Woodfine, J.I.S.I., (1953), 173, p 229.
190. C. J. McMahon Jr., in "Temper Embrittlement in Steel",
A.S.T.M. (S.T.P. 407), (1968), p 127.
191. C. J. McMahon Jr., in "Mechanics and Physics of Fracture",
Inst.of Physics and Met.Soc., Cambridge,(1975) paper 20.
192. G. Clark, R. O. Ritchie and J. F. Knott, Nature Physical
Sciences, (1972), 239, p 104.
193. L. C. E. Geniets and J. F. Knott, Met.Sci.J., (1972), 6,
p 69.
194. H. C. Feng, E. A. Wilson and C. J. McMahon Jr., in
"The Microstructure and Design of alloys", Inst.of
Metals, Cambridge, (1973), paper 26.
195. J. M. Capus, J.I.S.I., (1962), 200, pp 922-927.

196. H. C. Rogers, Acta.Met., (1959), 7, p 750.
197. H. C. Rogers, TMS-AIME, (1960), 218, p 498.
198. D. M. R. Taplin, Met.Eng.Quart., (1970), p 103.
199. A. Gittins and J. A. Williams, Scripta Met., (1969) 3, p 209.
200. P. W. Davies et al., Phil. Mag., (1968), 18, p 197.
201. P. Rama Rao et al., J.I.S.I., (1973), 211, p 801.
202. "Methods for Plane Strain Fracture Toughness (K_{IC}) Testing",
B.S.I. Draft for Development 3 - 1971.
203. J. Q. Clayton, Private communication.
204. D. R. Hayhurst, D. A. Kelly, A. R. S. Ponter,
"Prediction of component life at high temperatures -
a summary of papers", Metals and Materials, (1976),
2, pp 44-45.